The Efficient and Selective Catalytic Oxidation of Terpenoids and Aromatic Hydrocarbons by the P450 Monooxygenase CYP101B1

Emma Ashleigh Hall

Supervisors:
Dr Stephen Bell
Associate Professor Hugh Harris

August 2015

Thesis submitted for the degree of Master of Philosophy

SCHOOL OF PHYSICAL SCIENCES

THE UNIVERSITY of ADELAIDE

Contents

Abstract

CYP101B1, from the bacterium *Novosphingobium aromaticivorans*, has been shown to bind and oxidise β-ionone to 3-hydroxy-β-ionone and camphor to 5-*exo*-hydroxycamphor.[1] Whole-cell reactions of CYP101B1 have been observed to turn blue, which suggests indole oxidation to indigo.[1–3] Therefore, CYP101B1 has the potential to act as a biocatalyst for the oxidation of a broad range of substrates.

β-Ionone and other similar norisoprenoids were initially tested to determine which structural features were important for binding to CYP101B1. Small adjustments to the β-ionone structure indicated the butenone side chain was important for tight substrate binding to CYP101B1. The cyclohexene component of β-ionone is also a better fit for the active site than linear or aromatic analogues. Further testing of aromatic substrates, such as indole, phenylcyclohexane and *p*-cymene, indicated that CYP101B1 binds substituted aromatics such as phenylcyclohexane and could produce products in a reasonable yield. Smaller aromatics, such as *p*-cymene, could still bind and react with CYP101B1, but the activities and product levels generated were lower than the larger two-ring aromatics.

CYP101B1 oxidation of camphor and other terpenoid based substrates was studied. However, these substrates had large dissociation constants and low product formation rates due to a larger proportion of the NADH being used to reduce oxygen to hydrogen peroxide or water instead of products. Multiple oxidation products were formed with these substrates, which was most likely due to their poor fit in the CYP101B1 active site. This was not an ideal outcome, so the substrates or enzyme require modification to improve the reactivity and selectivity of the biocatalyst.

Terpenoid substrates were modified to include an acetate side chain, resulting in a structure more similar to the norisoprenoids. This greatly improved the binding and activity with CYP101B1, and resulted in production of a single oxidation product in the *in vitro* turnovers. The ketone moiety of the acetate group leads to better binding to CYP101B1 and results in more desirable catalytic properties.

The affinity of CYP101B1 for aromatic structures was determined using a range of biphenyl and naphthalene derivatives. These structures exhibited reasonably tight binding; however, moderate NADH consumption rates, product formation rates and coupling between the substrate and CYP101B1 were observed. Therefore, the CYP101B1 active site favours more polar sub-

strates. Activity for hydrophobic substrates could be increased by modifying CYP101B1 to remove specific contact between a hydrophilic amino acid side chain and the ketone group, which is important in the binding of norisoprenoids and monoterpenoid acetate substrates. The turnovers had high product selectivity and, in most cases, only a single product was generated. The drug, diclofenac, was reacted with CYP101B producing the metabolite, 4`-hydroxydiclofenac, in reasonable yield.

CYP101B1 is a useful biocatalyst for selective C−H bond oxidation of norisoprenoids and terpenoid acetates. It also shows potential for other substrates if CYP101B1 is modified or with the addition of an ester protecting group onto the target molecule.

Statement

I certify that this work contains no material which has been accepted for the award of any other degree or diploma in my name, in any university or other tertiary institution and, to the best of my knowledge and belief, contains no material previously published or written by another person, except where due reference has been made in the text. In addition, I certify that no part of this work will, in the future, be used in a submission in my name, for any other degree or diploma in any university or other tertiary institution without the prior approval of the University of Adelaide and where applicable, any partner institution responsible for the joint-award of this degree.

I give consent to this cop of my thesis, when deposited in the University Library, being made available for loan and photocopying, subject to the provisions of the Copyright Act 1968.

I also give permission for the digital version of my thesis to be made available on the web, via the University's digital research repository, the Library Search and also through web search engines, unless permission has been granted by the University to restrict access for a period of time.

Signed: Date:

Acknowledgments

I would like to thank Stephen Bell for being a extremely helpful supervisor over the two years of my project. Thanks goes to Hugh Harris who also provided help whenever I asked.

The Bell group and Pyke group also deserve thanks for all their support and friendship during my masters which meant I always enjoyed my time in the lab.

I would also like to thank my family and friends for always encouraging me to be the person I can be and to preform to the best of my abilities.

Special thanks to Michael, who put up with proof reading my thesis and all the other ups and downs associated with doing a research degree and writing a thesis.

Chapter 1

Introduction to Cytochrome P450 enzymes and CYP101B1

1.1 General Overview of P450s

Cytochrome P450 enzymes (P450s or CYPs) are heme monooxygenase proteins that can insert one atom of molecular oxygen into a C−H bond (Equation 1.1).[4] P450s are present in most living organisms as they can metabolise compounds and may be involved in biosynthetic reactions. Different forms can oxidise a wide range of compounds, which leads to potential uses as biocatalysts. The oxidation reaction of a P450 occurs at the active site, which has a heme cofactor consisting of a porphyrin ring with an iron centre (Figure 1.1). A cysteine ligand is bound to the iron at the proximal side of the heme. P450s use this iron centre to activate dioxygen to catalyse the regio- and stereoselective formation of a hydroxy bond.

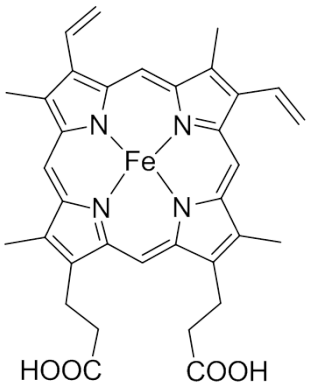

Figure 1.1: Structure of a heme cofactor

$$\mathrm{RH + NAD(P)H + H^+ + O_2 \longrightarrow NAD(P)^+ + H_2O + ROH} \qquad (1.1)$$

The ferrous form of P450s, when bonded to carbon monoxide, gives the characteristic absorbance at 450 nm which gives the P450 family its name (P is derived from pigment due to its red colour). Within the P450 super-

family, enzymes are classified into families and subfamilies based on amino acid sequence similarity. Families are classified with a numerical identifier, such as 101, and a letter to classify a further subfamily, such as A. A second number, such as 1, catalogues the enzyme within the subfamily. Combining these examples gives CYP101A1, which is the first enzyme identified in the A subfamily of the 101 family.[5]

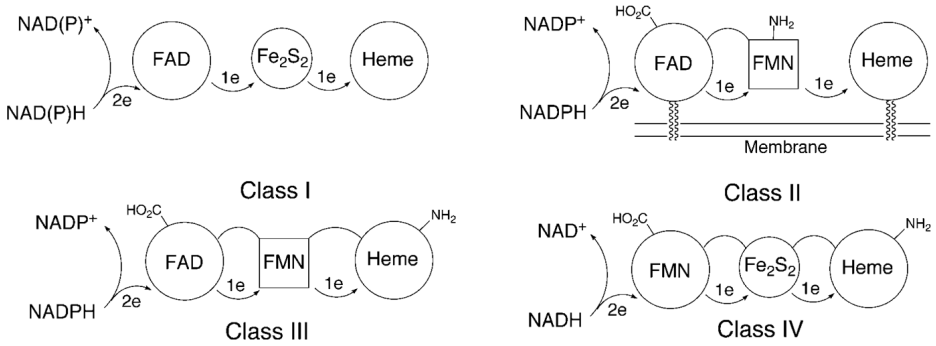

Figure 1.2: The different classes of electron transfer proteins used by P450s

Several different electron transfer systems have been shown to support P450 activity (Figure 1.2). These proteins transfer electrons from NAD(P)H one at a time to the P450 when required. The class I electron transfer system is comprised of two electron transfer proteins. The electron acceptor is a flavin adenine dinucleotide (FAD) containing protein, while the protein which transfers the electron to the P450 is generally an iron sulphur ferredoxin. This electron transfer system is most commonly found in bacterial and mammalian mitochondrial P450 systems. The class II electron system is a single protein which contains both a FAD and a flavin mononucleotide (FMN) cofactor. This is commonly found in eukaryotic systems where both the reductase and the P450 protein are bound to the cell membrane. The class III electron transfer system has the electron transfer components fused to the P450 protein. The electron transfer partners are similar to the class II electron transfer system. The final electron transfer system is the class IV; this system is fused to the P450 and contains FMN and an iron sulphur electron transfer cofactor.[6] Both class III and IV systems are found in bacteria.

The catalytic cycle of P450 enzymes is believed to be consistent for all members of the superfamily (Figure 1.3).[7–9] In its resting state, the ferric iron centre is bound to a water oxygen (I). This water molecule is then displaced by the substrate binding (II). The substrate binding can be monitored by UV-Vis spectrometry as the enzyme shifts from a low spin state at 420 nm

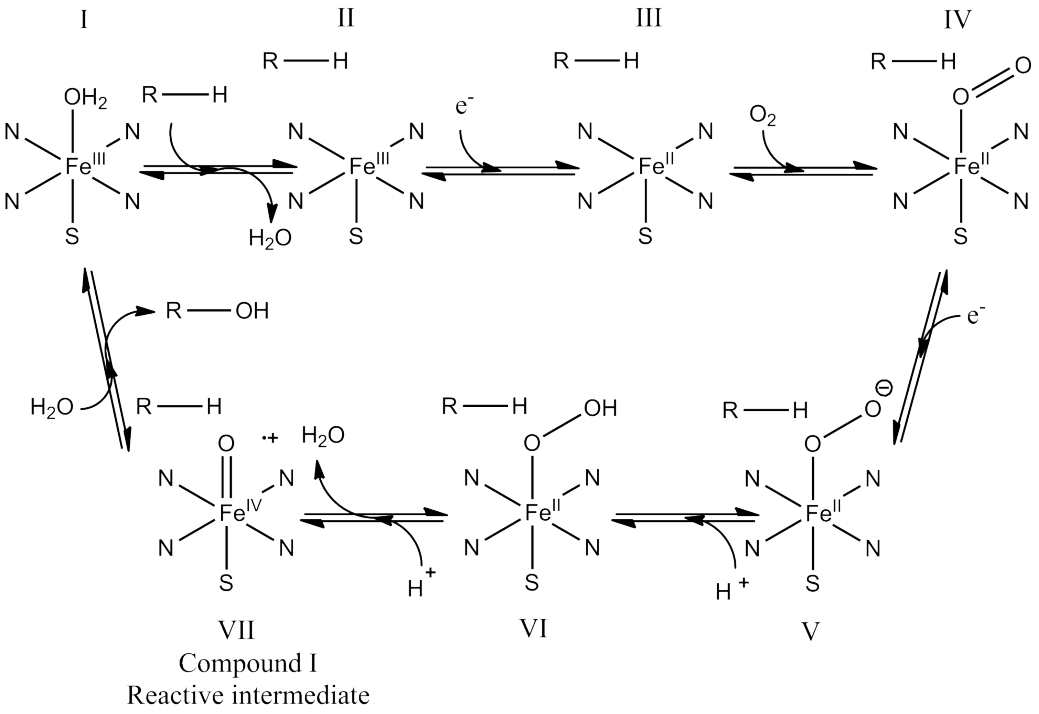

Figure 1.3: The catalytic cycle of P450 enzymes

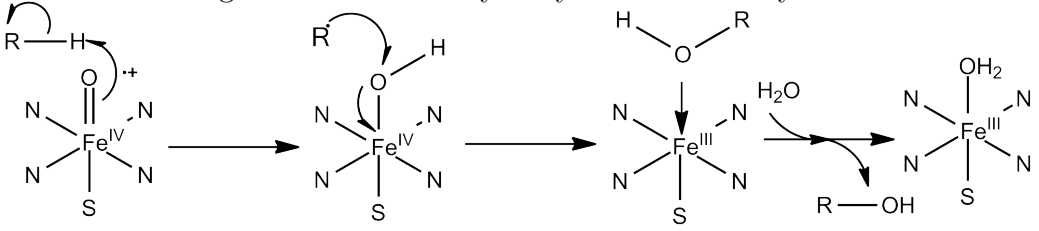

Figure 1.4: The radical recombination mechanism of P450 enzymes

to a high spin state at 390 nm as the enzyme goes from six to five coordinate (Section 2.4). The dissociation constant, a measure of how tightly the substrate binds to the enzyme, can also be determined using UV-Vis spectrometry (Section 2.5). Both these experiments give an indication of the substrate-enzyme active site fit.

The high spin ferric P450 enzyme (II) then accepts an electron. After electron transfer (III), oxygen can bind to the ferrous iron complex (IV). The ferrous iron complex undergoes several transformations involving the addition of a second electron (V) and protonation of the oxygen further from the iron (VI) which leads to O−O bond cleavage. This results in formation of the highly reactive radical cation intermediate (VII, compound I) which

extracts a hydrogen atom from the substrate (Figure 1.4). This generates a substrate radical which extracts the OH from the intermediate. This radical reacts with the alcohol group now attached to the enzyme and forms the oxidised product. The product now moves away from the enzyme and a water molecule binds again returning the enzyme to its resting state.

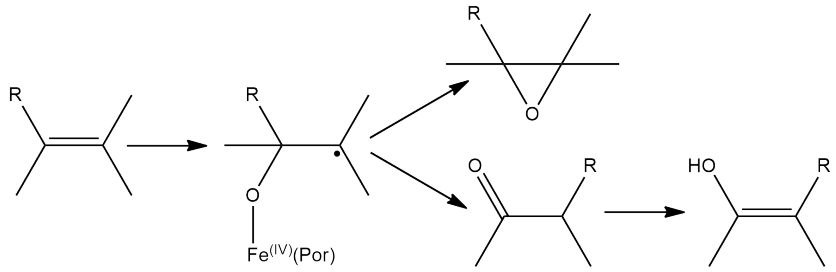

Figure 1.5: Epoxidation and group migration reactions

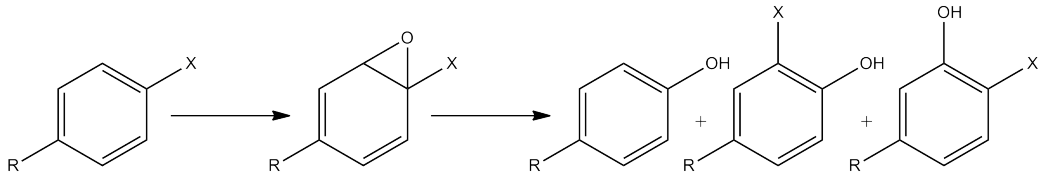

Figure 1.6: Aromatic oxidation by the NIH shift

The high selectivity for C−H bond oxidation arises from the ability of the enzyme to bind the substrate in an orientation which results in only one C−H bond in close proximity to compound I. This high selectivity is not normally possible when performing this reaction using conventional chemistry, due to the difficulty in forming the alcohol product from the strong C−H bond and the reactive nature of chemicals involved. In addition, P450s are capable of catalysing other reactions such as heteroatom release, heteroatom oxidation, desaturation, dehydrogenation, and C−C bond cleavage, amongst others.[7–9] Further oxidation can also occur on products; these can produce ketones, aldehydes and carboxylic acids. Epoxidation involves compound I reacting with one carbon of an alkene group; the remaining carbon produces a radical group which is then attacked by the oxygen to form an epoxide. However, this could also produce group mirgration as the R group bonded to the initial carbon could bind to the radical group instead (Figure 1.5).[7–9] Oxidation of the C−H bond on an aromatic ring occurs by a different mechanism which involves epoxide formation on the aromatic ring, most likely via a radical or carbonium ion intermediate compound. This epoxide reacts to form an

alcohol via an NIH shift which involves migration of a ring substituent to the *ortho* position (Figure 1.6).[7–9]

The turnover of the catalytic cycle can be assayed by UV-Vis spectrometry (Section 2.6). By monitoring the absorbance of NADH (A_{340nm}), the rate of enzyme turnover can be be determined (Figure 2.2a). If the substrate binds reasonably well to the P450, a high NADH consumption rate is expected. The product formation rate and coupling can be determined by measuring the amount of product formed in the turnover. However, if water is still present in the active site from a poor substrate fit, uncoupling reactions can occur which decrease these values. There are two main uncoupling pathways which result in the production of either hydrogen peroxide or water (Figure 1.7).[7–9] Hydrogen peroxide is formed from species VI when the second proton binds to the oxygen bound to the iron. This can occur when water is still present in the active site. Water is formed from compound I (VII) when two further protons are added to the oxo oxygen. This can occur if the substrate is too far away from the heme iron centre for C−H bond oxidation to occur.[7–9]

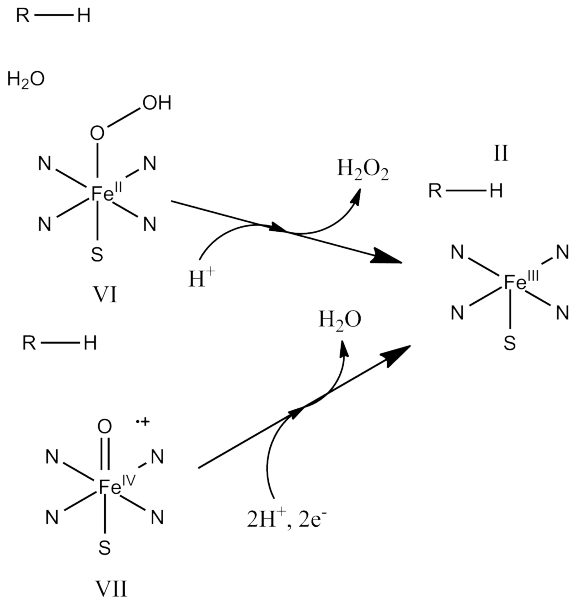

Figure 1.7: Two main uncoupling reactions of P450s

There has been extensive research into the application of bacterial P450s as biocatalysts, due to their ease of production and high substrate and product selectivity. They are easier to handle as the enzyme is not bound to the cell membrane as the P450s of plants and animals are. This makes production

and purification easier and bacterial enzymes often catalyse reactions with high activity.[4] Another advantage of using an enzyme is that it falls in a relatively new area of green chemistry. The reaction requires only water, oxygen, one proton and an electron source, and is performed under ambient conditions.[10,11]

While using enzymes as biocatalysts is attractive, there are some issues to consider before they can be utilised on a large scale. The P450 enzyme requires addition of the expensive cofactor NAD(P)H to supply electrons. This needs to be regenerated *in vitro* or the reaction can be conducted in a whole-cell reaction in which the cell is able to regenerate the reducing equivalents.[12,13] Whole-cell reactions require the substrates and products be able to enter and leave the cell; either of these can be toxic to cells. This results in death of the cells, thus breaking the catalytic cycle.[12,13] The solubility of the substrate in water is also an important consideration, as most organic substrates are not very soluble in aqueous solution. Another problem with enzymes is that they may be particularly unstable under the reaction conditions. The tertiary structure of the enzyme unfolds when the aqueous solvent is removed, the enzyme is heated or the P450 is exposed to too much organic solvent. Electron transfer is often the rate limiting step of the reaction and there is often a need to improve the speed and efficiency of this step. The best solution is to use the physiological electron transfer partners if they are known and available.[12,13]

1.2 The CYPome of *Novosphingobium aromaticivorans*

The oligotrophic bacterium *Novosphingobium aromaticivorans* contains sixteen P450 enzyme encoding genes. These enzymes are distributed across several families such as CYP101, CYP108 and CYP111.[1] It has been shown that several of these enzymes can bind a large range of substrates, including terpenes, aromatics and linear alkanes. One possible explanation of why this bacterium is able to act on such a broad range of compounds is that it is able to catabolise a large number of substrates. This allows it to survive in environments which offer little support for life.[14] The four CYP101 (B1, C1, C1 and D2) and CYP111 family enzymes from *N. aromaticivorans* use a class I electron transfer system, comprising a ferredoxin and ferredoxin reductase. These systems are highly active in converting terpenoid substrates to products with activity of 39–91 s^{-1}.[6]

CYP111A2 converts linalool to 8-hydroxylinalool.[1,15] This indicates that the enzyme can bind linear terpene-based structures and, due to its structure being a long carbon chain, also alkane-based structures.

CYP108D1 from the same bacterium is not supported by the class I electron transfer system. However, it binds a range of organic compounds, such as phenylcyclohexane, *p*-cymene, naphthalene, α-terpineol, fluorene and valencene. Phenylcyclohexane produced trans-4-phenylcyclohexanol (97%) and cis-4-phenylcychexanol (2%) and a further oxidation product of 4-phenylcyclohexanone (1%). *p*-Cymene reacted to form 4-isopropylbenzyl alcohol (94%) and *p*-α,α-trimethyl alcohol (6%). Naphthalene was reacted to form 1-naphthol. α-Terpineol was reacted to form the only product of 7-hydroxy-α-terpineol. These reactions showed a high degree of selectivity without need for modification of the P450, a desirable feature for a potential biocatalyst.[15,16]

CYP101D1 and CYP101D2 both catalyse camphor hydroxilation yielding 5-*exo*-hydroxy-camphor as the major product (99%).[15,17] Therefore, CYP101D1 and CP101D2 are similar in behaviour to the archetypal CYP101A1 ($P450_{cam}$) which also reacts similarly with camphor with high productivity and stereospecificity.[18]

The reactivity of CYP101C1 has been determined using α-ionone, β-ionone and β-damascone as substrates. β-Ionone was oxidised to two products by CYP101C1, the major product 4-hydroxy-β-ionone (yield 75%) and the minor product 3-hydroxy-β-ionone (yield 25%).[1,19] α-Ionone was oxidised to three different products, the major, trans-3-hydroxy-α-ionone (54%). β-Damascone produced one major product with a further five minor products being observed. 4-hydroxy-β-damascone was the major product (yield 73%).[19]

The aim of this thesis is to investigate the potential of CYP101B1 as a catalyst for fine chemical synthesis or drug metabolite production. This required developing a greater understanding of CYP101B1 binding and activity. This will involve testing a range of compounds including aromatic, terpene and drug based molecules with CYP101B1. The testing will involve binding experiments using spin-state shifts and dissociation constants, and activity experiments using *in vivo* reactions, *in vitro* reactions and NADH consumption rates.

Currently, the reactivity of CYP101B1 has been determined using β-ionone and camphor as substrates. β-Ionone was oxidised to two products by CYP101B1; a minor product, 4-hydroxy-β-ionone (10.5%), and a major prod-

uct, 3-hydroxy-β-ionone (89.5%).[1] Camphor has been reported to produce 5-*exo*-hydroxy-camphor as the major product, alongside three other products.[1] CYP101B1, when incorporated in a whole-cell oxidation system, has also been observed to turn cell media blue. This indicates that aromatic oxidation of indole has occurred, followed by dimerization to indigo.[1–3] Initially, substrates which were similar to those previously studied with CYP101B1 would be investigated.[1,15] CYP101B1 would be treated with α-ionone, β-ionone, ionone analogues, phenylcyclohexane, *p*-cymene and indole to determine the products formed. This would produce data which could be used as a benchmark in further studies with new substrates.

CYP101B1 will be screened with terpenoid substrates. This will determine in detail the substrate parameters required for efficient substrate binding. It will provide valuable information on the selectivity of product formation on different terpenoid structural frameworks. Aromatic substrates will be screened for CYP101B1 binding and activity. This will test which hydrophobic substrates can bind to CYP101B1. These aromatic compounds are often parent structures for drug molecules or toxic chemicals such as polychlorinated biphenyls (PCBs). In the future, this information may be used to generate drug metabolites from aromatic drug compounds related to these substrates. This research could help determine the side-effects of drug compounds. Such research is required before a drug can be approved.

Chapter 2

Experimental

2.1 General

Substrates, laboratory solvents and reagents were purchased from Sigma-Aldrich, Tokyo Chemical Industry and Alfa-Aesar. Biological chemicals, such as antibiotics, detergents, dithiothreitol (DTT) and isopropyl β-D-1-thiogalactopyranoside (IPTG) were purchased from Astral Scientific.

The media solutions used for cell growth were as follows. In 1 litre of Super Optimal broth with Catabolite repression (SOC):

- tryptone (20 g);
- yeast extract (5 g);
- $MgCl_2$ (1 g);
- NaCl (0.5 g);
- KCl (0.2 g); and
- 0.2 % w/v glucose.

In 1 litre of Lysogeny Broth (LB):

- tryptone (10 g);
- yeast extract (5 g); and
- NaCl (10 g).

In 1 litre of 2 x YT broth;

- tryptone (16 g);
- yeast extract (10 g); and
- NaCl (5 g).

In 1 litre of trace elements solution:

- Na_2EDTA (20.1 g);
- $FeCl_3(6H_2O)$ (16.7 g);
- $CaCl_2(H_2O)$ (0.74 g);
- $CoCl_2(6H_2O)$ (0.25 g);
- $ZnSO_4(7H_2O)$ (0.18 g);
- $MnSO_4(4H_2O)$ (0.132 g); and
- $CuSO_4$ $(5H_2O)$ (0.10 g).

In 1 litre of *E. Coli* minimal media (EMM):

- K_2HPO_4 (7 g);
- KH_2PO_4 (3 g);
- $(NH_4)_2SO_4$ (1 g);
- Na_3Citrate (0.5 g);
- $MgSO_4$ (0.1 g); and
- 20 % glucose (20 mL).

In LB and 2 x YT the necessary antibiotics were added to their working concentrations: for ampicillin (amp), 100 μg/ mL and for kanamycin (kan), 30 μg/ mL. For EMM, half the working concentration was added of both amp and kan.

Analytical High Pressure Liquid Chromatography (HPLC) was performed on an Agilent 1260 infinity pump equipped with an auto injector connected to an Agilent Eclipse Plus C18 column (250 mm x 4.6 mm, 5 μm). The products were separated using a gradient between 20:80 and 95:5 acetonitrile/water (0.1 % trifluoroacetic acid (TFA)). Separation occurred at a rate of 1 mL min^{-1} over 30 minutes, after holding the concentration of acetonitrile at 20 % for 5 minutes. Gas Chromatography-Mass Spectrometry (GC-MS)

data were collected on a Shimadzu GC-17A using a QP5050A GC-MS detector and a DB-5 MS fused silica column (30 m x 0.25 mm, 0.25 μm). The injector and interface were maintained at a constant temperature of 250°C and 280°C. For the monoterpenoid and monoterpenyl acetates, the GC-MS method used an initial oven temperature of 80°C for 3 min then increasing by 10°C per min until the maximum temperature of 220°C which was held for 3 min. All other compounds were analysed on the GC-MS using a program with an initial oven temperature of 120°C for 3 min, increasing by 10°C per minute until the maximum temperature of 220°C which was held for a further 7 minutes. UV/Vis spectrometry was performed on a Varian Cary 5000 or a Agilent Cary 60 spectrophotometer at 30 ± 0.5°C.

2.2 Whole-cell turnovers

The DNA vectors pETDuet containing the ferredoxin reductase (ArR) and ferredoxin (Arx) genes and pRSFDuet containing CYP101B1 and Arx genes were transformed into BL21(DE3) (40 μL) and cooled on ice for 1 h.[1] The sample was then heat shocked for 1 min at 42°C and then placed back on ice for 2 minutes. SOC (200 μL) media was added to the sample which was shaken at 37°C at 200 rpm for 1 h. The solution was then spread onto an $LB_{amp/kan}$ antibiotic plate and heated at 37°C overnight. A single colony was removed and grown in 3 mL of $LB_{amp/kan}$ at 37°C at 150 rpm for 4 h. The 3 mL of cells were added to a 2 x $YT_{amp/kan}$ (500 mL) supplemented with trace metal solution (1.5 mL) and grown at 37°C with 120 rpm for 4 h. Gene expression was induced with 100 μM IPTG stock solution and grown at 25°C at 120 rpm overnight. The cells were harvested from the supernatant by centrifugation (5000 g, 10 min) and the cells were resuspended in EMM (1 L). The resuspended cells (200 mL) were transfered into separate 2 L baffled flasks and substrate was added (2 mM). The flasks were shaken at 30°C and 150 rpm for 6 h. Further additions of substrate (2 mM) and glucose (4 mL of a 20 % solution) were made after 6 h and the reaction continued overnight. The supernatant was separated from the cells by centrifugation (5000 g, 10 min).

Where authentic samples of potential products were available, they were used to identify the products via co-elution experiments via analytical HPLC and GC-MS. When required, products were extracted from the supernatant by liquid-liquid extraction using ethyl acetate (3 x 100 mL), washed with brine (100 mL) and dried with magnesium sulphate. The products were purified on silica using a gradient from 80:20 to 50:50 hexane to ethyl acetate

using 2.5 % increases every 100 mL. The solvent was removed under reduced pressure and the products analysed by NMR in chloroform-d with tetramethylsilane (TMS), dimethyl sulfoxide-d_6 or acetone-d_6. The spectra were obtained on either Varian Inova-600 spectrometer operating at 600 MHz for ^{1}H and 151 MHz for ^{13}C or Agilent DD2 spectrometer operating at 500 MHz for ^{1}H and 126 MHz for ^{13}C.

2.3 Enzyme Purification

2.3.1 Purification of CYP101B1

The CYP101B1 gene cloned in the pET28 vector was transformed into BL21 (DE3) (40 μL) as described above using an LB_{kan} antibiotic plate. Colonies were added to 2 x YT_{kan} (4 x 500 mL) which were grown at 37°C with 120 rpm for 5 h. Protein production was induced by adding 100 μL IPTG (from a 0.5 M stock solution) in each flask with further shaking at 25°C and 120 rpm for 72 h. The cells were harvested by centrifugation and stored before purification at -20°C. The cells were resuspended in 50 mM Tris buffer (pH 7.4, 250 mL) containing 1 mM DTT (buffer T) and then lysed by sonication (Auto tune CV334, Sonics and Materials, US) using 80 x 20 s pulses with 40 s intervals. The resulting solution was centrifuged to remove cell debris and the pellet discarded (40 000 rpm, 25 min, 4°C).

Ammonium sulphate was added gradually to the supernatant containing the P450 until the solution reached 25 % w/v. The resulting solution was centrifuged to remove any precipitate, which was discarded (30 000 g, 30 min, 4°C). The concentration of ammonium sulphate was then increased to 50 % and the precipitated P450 collected as a pellet by centrifugation (30 000 g, 30 min, 4°C). The protein was resuspended in 100 mL of buffer T and desalted with Sephadex G-25 Coarse grain column (250 mm x 40 mm) using buffer T. The protein was then purified using an ion exchange DEAE Sepharose column (XK50, 200 mm x 40 mm, GE Healthcare) using a gradient from 0 to 250 mM KCl in buffer T at 8 mL/min. The fractions with $A_{419}/A_{280} > 1$ were collected and concentrated using an ultrafiltration cell with a 30 kDa exclusion membrane until the P450 reached approximately 10 mL. The solution was then centrifuged (5000 g, 10 min) to remove any debris.

An equal volume of 80 % glycerol was added before filtration through a 0.22 μm syringe filter, and stored at -20°C. Before use, glycerol and salts

were removed from the P450 using a 5 mL gel filtration column (PD-10, GE Healthcare) using 50 mM Tris (pH 7.4) buffer.

2.3.2 Purification of ArR

The ferredoxin reductase, ArR, was produced using the DNA vector pET26-ArR by transformation into BL21(DE3) (40 μL) and grown on an LB_{kan} antibiotic plate. Four colonies were added to four separate 2 x YT_{kan} (500 mL) solutions and grown at 37°C at 120 rpm overnight. Protein production was induced using 100 μM IPTG and the growth continued at 25°C and 120 rpm for 72 h. The cells were collected by centrifugation, resuspended in buffer T, then lysed by sonication. The resulting solution was centrifuged to remove any cell debris and the yellow protein containing supernatant retained (40 000 rpm, 25 min, 4°C).

The protein was purified using an ion exchange DEAE Sepharose Column using a gradient from 100 mM to 400 mM KCl in buffer T at 8 mL/min. The yellow fractions containing the protein were collected and concentrated using Vivacell 100 (Sartorius Stedium) with a 10 kDa exclusion membrane and centrifugation (2300 g, $\sim$ 2 h). To desalt the solution 50 mL of buffer T was added twice and concentrated to 20 mL in volume each time. The protein was purified further on a Source-Q column (XK26, 80 mm x 30 mm, GE Healthcare) using a gradient from 8 % to 30 % of 1 M KCl in buffer T at 6 mL/min over 400 mL. The protein-containing fractions with $A_{280}/A_{458} < 8$ were collected and concentrated using Vivacell 100 and centrifugation (2300 g, $\sim$ 2 h) until the ArR reached approximately 10 mL in volume. The solution was then centrifuged (5000 g, 10 min) to remove any precipitate. The resulting solution of ArR was then diluted with glycerol and stored at -20°C.

2.3.3 Purification of Arx

The ferredoxin, Arx, was produced using the DNA vector pRSFDuet-Arx which was transformed into BL21(DE3) (40 μL) and grown on an LB_{kan} plate. A single colony was then removed and grown in LB_{kan} solution (50 mL) at 37°C with 120 rpm overnight. 5 mL of cells were added to 500 mL 2 x YT_{kan} x 8 containing trace metal solution (1.5 mL) and grown at 37°C at 120 rpm for 5 h. Protein production was induced using 100 μM IPTG and the growth continued at 25°C and 120 rpm for 72 h. The cells were harvested by centrifugation and stored before purification at -20°C. The cells were resuspended

in 10 mM Tris buffer (pH 7.4, 300 mL) containing 2 mM DTT, 10% glycerol, β-mercaptoethanol (3 mL) and Tween (1 mL). Lysozyme (300 mg) was added and the resulting solution was stirred for 30 min on ice. The cells were then lysed by sonication. The resulting solution was centrifuged to remove the cell debris (40 000 g, 25 min, 4°C).

The supernatant was applied to an ion exchange DEAE Sepharose Column and the protein was eluted using a gradient of 100 mM to 400 mM KCl in 50 mM Tris (pH 7.4) with 2 mM DTT (buffer T2) at 6 mL/min. The brown fractions containing the protein were collected and concentrated using Vivacell 100 and centrifugation (2300 g, $\sim$ 2 h). Salt was removed from the protein using a Sephadex G-25 medium grain column (250 mm x 40 mm) using buffer T2. The protein was further purified on a Source-Q column using a gradient from 10 % to 35 % of 1.5 M KCl in buffer T2 at 6 mL/min. The fractions with $A_{325}/A_{280} > 0.6$ were collected and concentrated using Vivacell 100 and centrifugation (2300 g, $\sim$ 2 h) until the Arx reached approximately 10 mL in volume. The solution was then centrifuged (5000 g, 10 min), the supernatant collected, diluted with glycerol and filter sterilised and stored at -20°C. Arx was desalted and the glyerol removed using a PD-10 column before use.

2.4 Spin-State Shifts

CYP101B1 was diluted with 50 mM Tris (pH 7.4) until the concentration was $\sim 3\,\mu$M and the resulting solution was used to determine the spin-state shift. The absorbance from 700 nm to 250 nm was recorded using the UV-Vis spectrophotometer. CYP101B1 (500 μL) was combined with 1 μL of substrate (0.1 to 0.5 M stock solution in dimethyl sulfoxide or ethanol) and the spectra were recorded again. Further additions of substrate were made until there was no visible change to the spectra. The percentage of the high spin state formed was estimated by comparison of the peak at 390 nm relative to the initial low spin peak at 419 nm with the spectra of the spin states of camphor-bound $P450_{cam}$ (Figure 2.1).

2.5 Dissociation constants

To determine how tightly different substrates bind to CYP101B1, a series of different spectra were recorded between 600 nm and 300 nm. CYP101B1 (2.5 mL) was combined with increasing 1 - 2 μL aliquots of a 1 mM stock

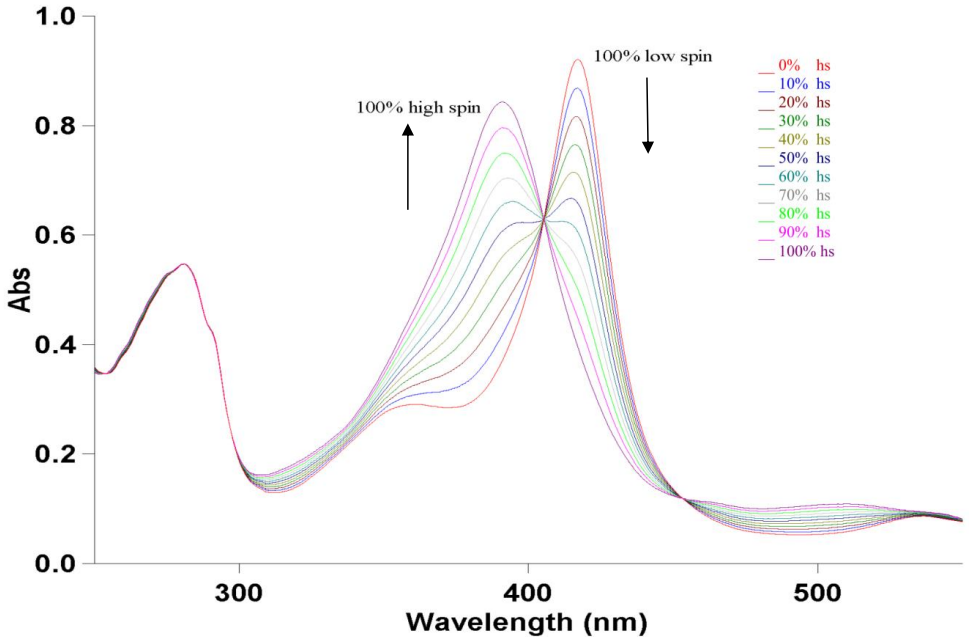

Figure 2.1: The spin state shifts of $P450_{cam}$ induced by camphor binding used to determine spin state shift of substrate-bound CYP101B1.

solution of substrate and the spectra were recorded. After 10 μL of substrate was added aliquots of a 10 mM stock solution and finally aliquots of 100 mM stock solution were added until the peak (420 nm) to trough (390 nm) difference did not change. To determine the dissociation constant of the substrate, the peak to trough difference was plotted against the substrate concentration and fitted to the function:[20,21]

$$\Delta A = \frac{\Delta A_{max}\ [S]}{K_d + [S]} \tag{2.1}$$

where ΔA represents the peak to trough difference, ΔA_{max} represents the maximum peak to trough difference, [S] is the substrate concentration and K_d is the dissociation constant.

If the dissociation constant is less than five times enzyme concentration, the assumption used to derive equation (2.1) is invalid. Rather, the tight binding equation must be used to determine the dissociation constant (2.2).[22]

$$\frac{\Delta A}{\Delta A_{max}} = \frac{[E] + [S] + K_d - \sqrt{([E] + [S] + K_d)^2 - 4\ [E]\ [S]}}{2[E]} \tag{2.2}$$

where ΔA represents the peak to trough difference, ΔA_{max} represents the maximum peak to trough difference, [E] is the concentration of CYP101B1, [S] is the substrate concentration and K_d is the dissociation constant.

To ensure the correct dissociation constant is obtained, three sets of data are collected and a curve is fitted to all three sets. The error in K_d is based on the range of values produced from this curve of best fit.

2.6 *In-vitro* turnovers and NADH consumption rates

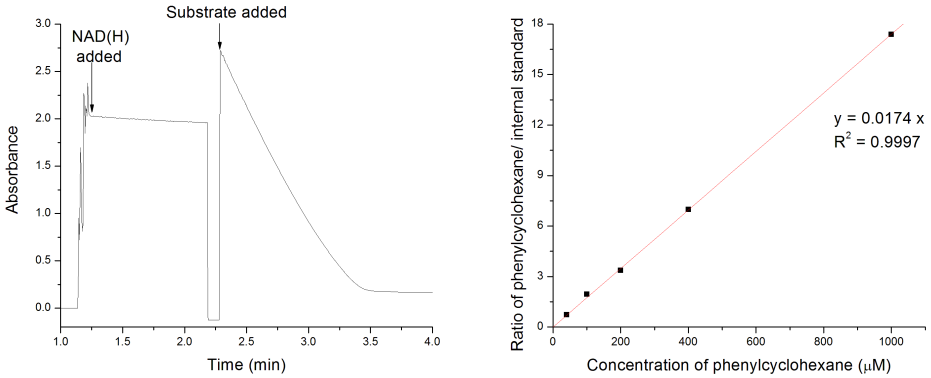

(a) Methyl ionone *in vitro* turnover (b) Calibration of phenylcyclohexane

Figure 2.2: An example of a NADH turnover assay

CYP101B1 (0.5 μM), Arx (5 μM) and ArR (1 μM) were added to oxygenated Tris buffer (50 mM, pH 7.4) in a total volume of 1.2 mL in a cuvette and allowed to reach 30°C. NADH was added to an A_{340} of ~ 2 ($\sim 320\,\mu$M) and the absorbance at 340 nm was recorded for the remainder of the experiment (Figure 2.2a). After a minute, substrate (1 mM) was added, the solution mixed and the decrease in A_{340} recorded. The rate of consumption of NADH was calculated from the gradient of the absorbance at 340 nm versus time using the extinction coefficient, $\epsilon = 6.22\,\text{mM}^{-1}\ \text{cm}^{-1}$.

To determine the product formation rate, the samples with an internal standard (500 μM) were analysed via GC-MS and HPLC. The total area of products/ internal standard ratio was used to calculate the concentration of the products. This value, when divided by the concentration of NADH (calculated from the absorbance at 340 nm), gave the coupling. The coupling when multiplied by the NADH rate of consumption, gave the product formation rate.

Products at different concentrations (20 μM to 500 μM) were combined with an internal standard (500 μM) and these were also analysed via GC-MS or HPLC. A calibration curve was made of product/ internal standard area versus concentration (Figure 2.2b). Where possible, this calibration was made with a product standard of the oxidation reaction. If that was impossible, an isomer or the starting material was used. This was used to calculate the amount of product in the completed turnover mixture.

Chapter 3

Assessing the Substrate Range of CYP101B1

3.1 Introduction

β-Ionone had been previously reported to be efficiently turned over with CYP101B1.[1,23] It was decided to begin testing CYP101B1 with similar molecules. This will provide more detailed information on the structural components required for favourable binding of substrates to CYP101B1, as well as the important features which determine the reactivity and the selectivity of oxidation (Figure 3.1).

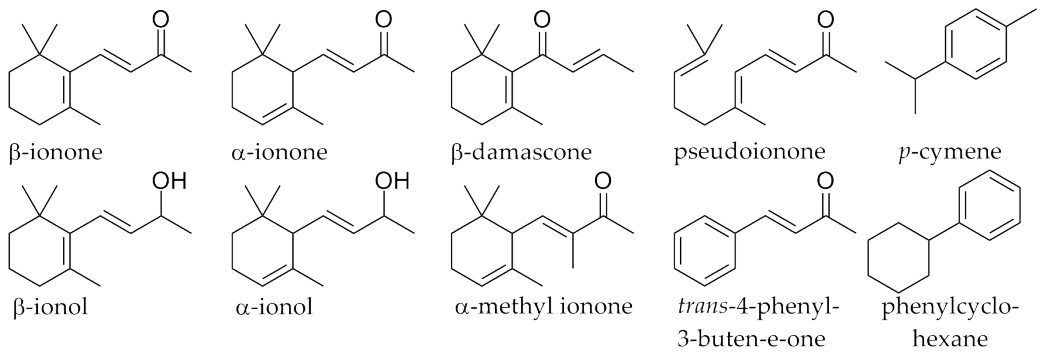

Figure 3.1: Aromatics, Norisoprenoids and related substrates

3.2 Norisopreniod Results

β-Ionone induces a type I spin-state shift of $\geq 95\,\%$ and binds tightly to CYP101B1 with $K_d = 0.23 \pm 0.1\mu M$.[1,6,15] The NADH consumption rate ($1600 \pm 100\,min^{-1}$), product formation rate ($1010 \pm 60\,min^{-1}$) and coupling (63 %) were high, indicating the substrate was held tightly in the active site close to the heme-iron and was efficiently oxidised. This indicates that β-ionone might be closely related to the natural substrate for CYP101B1.[1,6,15] The *in vitro* turnover of CYP101B1 with β-ionone was found to give two products, the major product, 3-hydroxy-β-ionone (90 %, m/z 208.2 AMU), and the minor product, 4-hydroxy-β-ionone (10 %, m/z 208.2 AMU) (Figure 3.2).[1,23] The *in vivo* turnover was found to give the same two main products with some minor products which were not identified, but were thought to be the ketones of the above mentioned alcohols, due to the m/z of 206.2 AMU observed via GC-MS. Our results, presented here, agree with what had already been reported for CYP101B1.[1,23]

Table 3.1: Substrate binding, steady state kinetic data and coupling data for norisoprenoids and the initial aromatics with CYP101B1. Steady state turnover activities were measured using a ArR:Arx:CYP101B1 concentration ratio of 1:10:1 (0.5 μM CYP enzyme, 50 mM Tris, pH 7.4). Coupling is the percentage efficiency of NADH utilization for the formation of products. Rates are reported as mean $\pm$ S.D.($n \geq 3$) and given in nmol(nmol-CYP)$^{-1}$min^{-1}.

CYP101B1/ substrate	%HS heme	K_d (μM)	NADH consumption rate (min^{-1})	Product formation rate (min^{-1})	Coupling %
β-ionone	≥ 95	0.2 ± 0.1	1600 ± 100	1010 ± 60	63
α-ionone	≥ 95	0.25 ± 0.04	1400 ± 100	660 ± 60	48
β-damascone	80	8.3 ± 0.9	931 ± 13	562 ± 12	60
pseudoionone	90	5.4 ± 0.1	180 ± 33	8.6 ± 1.9	5
trans-4-phenyl-3-buten-2-one	55	-	71 ± 28	-	-
α-methyl ionone	90	0.8 ± 0.01	1270 ± 1	958 ± 77	75
α-ionol	70	11.4 ± 0.5	1030 ± 50	764 ± 76	75
β-ionol	90	7.4 ± 0.2	1030 ± 55	670 ± 84	65
phenylcyclohexane	20	7.8 ± 0.9	293 ± 9	141 ± 17	48
p-cymene	5	23 ± 3	197 ± 27	25 ± 6	13

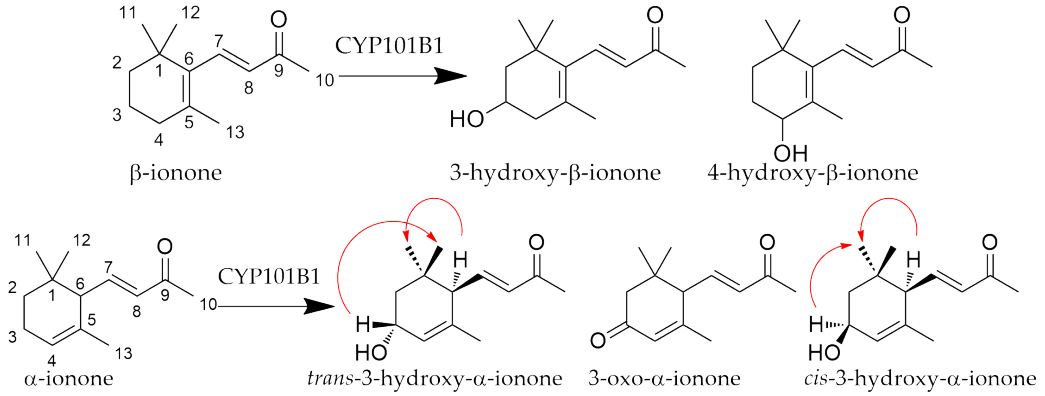

Figure 3.2: The products from the α-ionone and β-ionone *in vivo* turnovers. Red indicates the ROESY correlation used to assign the *cis* and *trans* isomers.

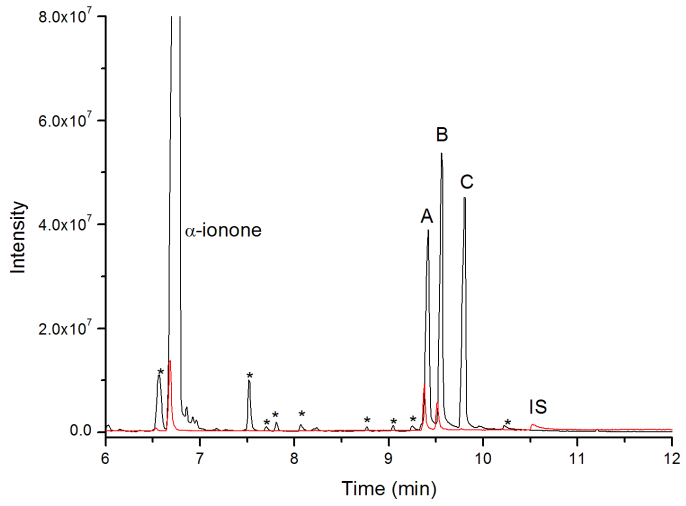

Figure 3.3: GC-MS analysis of CYP101B1 turnovers of α-ionone, *in vivo* (black), *in vitro* (red), *cis*-3-hydroxy-α-ionone (A), *trans*-3-hydroxy-α-ionone (B), 3-oxo-α-ionone (C), internal standard (IS) and impurities (*). Impurities are from the substrate or the extraction process.

α-Ionone has a similar overall structure to β-ionone; however, the alkene on the cyclohexene ring is in a different position (Figure 3.1). This would be expected to alter the conformation of the cyclohexene ring and the positions of the C−H bonds closest to the heme group. The spin state shift for α-ionone was similar to β-ionone ($\geq 95\,\%$) and it bound almost as tightly ($K_d = 0.25 \pm 0.04\,\mu M$) (Figure 3.4(a)(b)). However, the NADH consumption rate ($1400 \pm 100\,min^{-1}$), product formation rate ($660 \pm 60\,min^{-1}$) and coupling ($48\,\%$) were lower than those found for β-ionone. α-Ionone *in vitro* oxidation produced two products which, after column chromatography, were identified via NMR as the *cis* isomer ($60\,\%$) and the *trans* isomer ($40\,\%$) of 3-hydroxy-α-ionone (Figure 3.2). The signals at 4.27 ppm and 4.25 ppm in the ^{1}H NMR indicated the formation of the *trans* isomer and *cis* isomer respectively . The correlation in the ROSEY spectra between the H3 and H6 signals, through the C11 methyl, indicated which isomer was formed (Figure 3.2). Whole-cell turnovers also produced the 3-oxo-α-ionone from the *cis* isomer which was determined from the C3 signal at 198.20 ppm in ^{13}C NMR, the GC-MS mass of 206.2 AMU and the lack of the hydrogen signal in the alcohol region of the ^{1}H NMR spectrum (Figure 3.3 and Appendix F.2). This further oxidation may occur in the whole-cell turnovers due to the concentration of substrate exceeding that of the product. Another possible reason for further oxidation was that, since the products were more soluble than the substrate, it may be easier for them to enter the cell. As a result, the products may be present in local concentrations higher than the substrate. As 3-oxo-α-ionone formed from the *cis* isomer it suggests that this isomer more readily coverts to the ketone than the *trans* isomer. No epoxidation of the double bond of α-ionone was observed.

β-Damascone is an isomer of β-ionone, except the alkene and ketone on the butenone side chain switch positions (Figure 3.1). This testing will provide information about how important the position of alkene and ketone are for substrate binding. β-Damascone had a lower spin state shift of $80\,\%$ and the dissociation constant was larger at $8.3 \pm 0.9\,\mu M$ when compared with the ionones (Figure 3.4(c)(d)). This indicates the position of the ketone and alkene are important for substrate binding in CYP101B1. In all likelihood, there is an amino acid present in CYP101B1 akin to tyrosine 96, which, in CYP101A1, binds to the ketone of camphor.[19] The NADH consumption rate ($930 \pm 13\,min^{-1}$) and product formation rate ($562 \pm 12\,min^{-1}$) were lower than the values for the ionone substrates, though the coupling was comparable to that of β-ionone ($60\,\%$). β-Damascone oxidation results in a product profile similar to that of β-ionone, with the major product being 3-hydroxy-β-damascone ($88\,\%$) and the minor product being 4-hydroxy-β-damascone

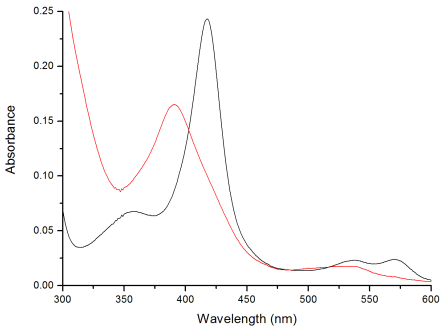

(a) α-ionone

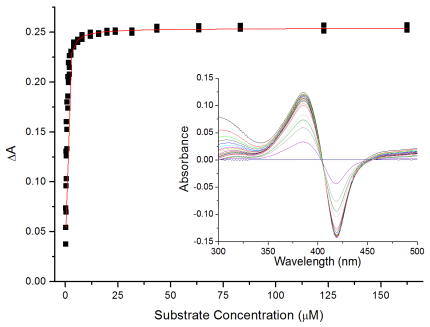

(b) α-ionone

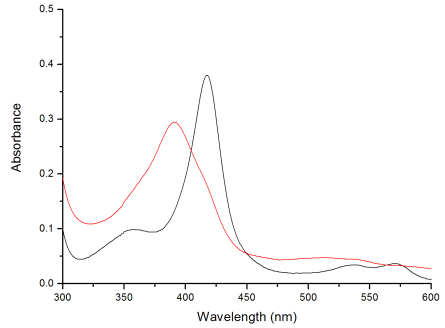

(c) β-damascone

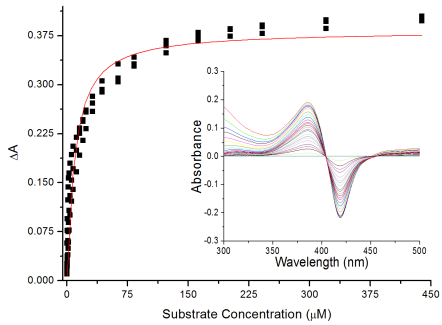

(d) β-damascone

Figure 3.4: Spin state shifts and dissociation constants for α-ionone and β-damascone. Spin state shift of α-ionone (a), dissociation constant of α-ionone (b), spin state shift of β-damascone (c) and dissociation constant of β-damascone (d).

(10 %) (Figure 3.5). These were identified by NMR from the coupling pattern of the chemical shifts of H3 and H4 signals (Appendix F.3). There were minor unidentified single oxidation products in both the *in vivo* and *in vitro* turnovers with a mass of 208.2 AMU (2 %) (Figure). Despite the shift of the ketone and alkene in this compound and weaker binding, β-damascone was held in an orientation over the heme centre within the active site of the enzyme similar to that of β-ionone.

Further investigation into other ionone-like structures with functional group modifications was made with the following compounds: α-methyl ionone, α-ionol, β-ionol, pseudoionone and *trans*-4-phenyl-3-buten-2-one (Figure 3.1). Pseudoionone is a linear analogue of β-ionone and will indicate whether CYP101B1 can tolerate linear norisoprenoids. Pseudoionone was found to give a high spin state shift of 90 % (Figure 3.8(d)) and reasonably tight

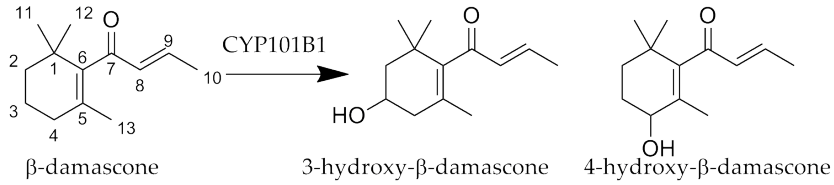

Figure 3.5: The products produced from the β-damascone turnovers

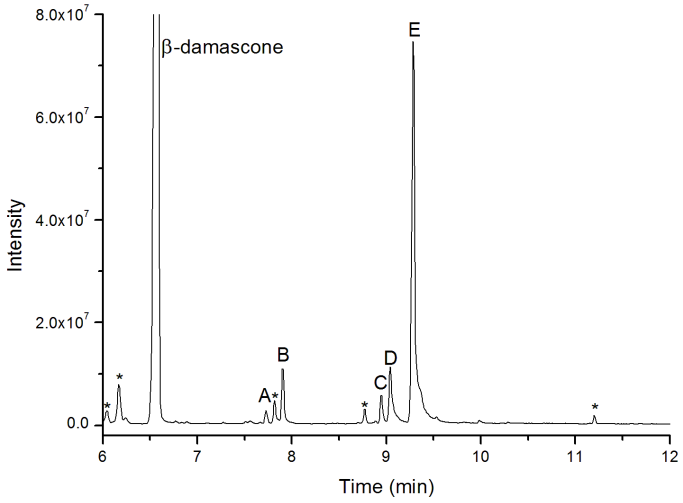

Figure 3.6: GC-MS analysis of CYP101B1 *in vivo* turnover of β-damascone, unidentified single oxidation products (A), (B) and (C), 4-hydroxy-β-damascone (D), 3-hydroxy-β-damascone (E) and impurities (*).

binding with a dissociation constant of $5.4 \pm 0.1\,\mu$M (Figure 3.10(d)). However, the NADH consumption rate ($180 \pm 33\,\mathrm{min}^{-1}$), product formation rate ($8.6 \pm 1.9\,\mathrm{min}^{-1}$) and coupling (5 %) were lower when compared to ionones and β-damascone. The products were not produced in a significant yield and could not be separated by silica chromatography, making identification impossible. However, pseudoionone is a mixture of two isomers and only two main products were identified in the turnover with a m/z of 208.2 AMU (Figure 3.7). The GC-MS fragmentation patterns of both isomers were similar, indicating the two products were oxidation products at the same C−H bond of the two different pseudoionone isomers. *trans*-4-Phenyl-3-buten-2-one replaces the substituted cyclohexene ring with a planar aromatic one. *trans*-4-Phenyl-3-buten-2-one gave a lower spin state shift of about 55 %. The NADH consumption rate ($71 \pm 28\,\mathrm{min}^{-1}$) was low compared to the other

ionone-like structures. In addition, no product was isolated from the *in vitro* and *in vivo* turnover. This may be due to the aromatic ring being held in a less favourable position in the active site for oxidation via the NIH shift mechanism.

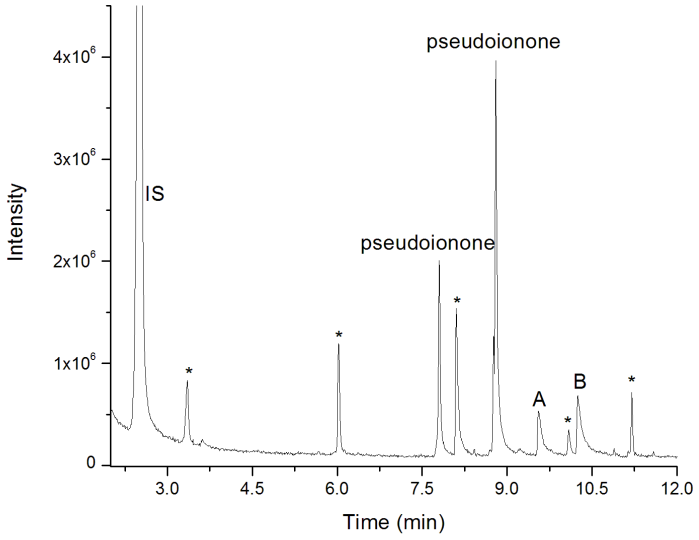

Figure 3.7: GC-MS analysis of CYP101B1 *in vitro* turnover of pseudoionone, unidentified single oxidation products (A) and (B), internal standard (IS) and impurities (*).

α-Methyl ionone has an extra methyl group on the butenone side chain (Figure 3.1). As it was previously found that this side chain was important for binding, it would be interesting to see the effects of making this side chain more bulky. Initial tests for binding with CYP101B1 gave a slightly decreased spin state shift (90 %) (Figure 3.8(c)) and a higher dissociation constant (0.83 $\pm$ 0.01μM) than previous ionone results (Figure 3.10(c)). However, binding was significantly tighter than that of β-damascone. The addition of the methyl group seemed to have a relatively minor negative effect on the binding of the substrate, indicating there is tolerance of larger side chain groups within the protein binding site. The NADH consumption rate (1270 $\pm$ 1 min^{-1}) and product formation rate (958 $\pm$ 77 min^{-1}) were both comparable to the values found for the ionones. Interestingly, coupling (75 %) was higher than previously reported for the ionones, which indicated more NADH was being used for the formation of products of α-methyl ionone than for uncoupling side reactions. The reaction with α-methyl ionone gave

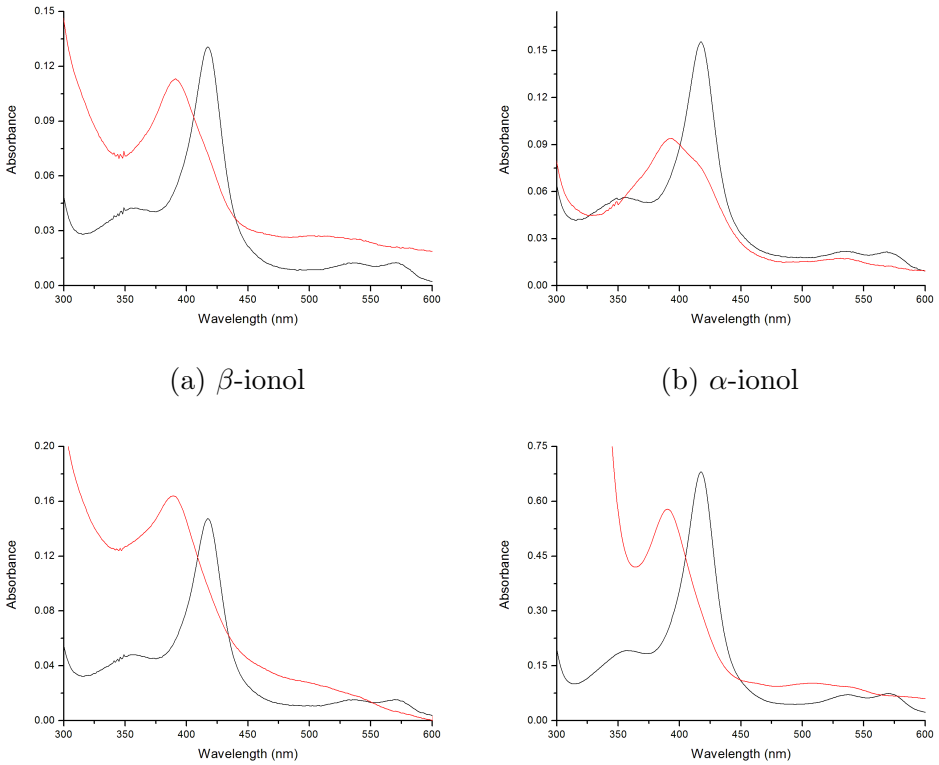

(a) β-ionol

(b) α-ionol

(c) α-methyl ionone

(d) pseudoionone

Figure 3.8: Spin state shifts for selected norisoprenoid compounds

similar products to α-ionone. The main products were *trans*-3-hydroxy-α-methyl-ionone and *cis*-3-hydroxy-α-methyl-ionone, with 3-oxo-methyl-ionone appearing in the *in vivo* turnover (Figure 3.9). Minor products were observed due to the presence of some β-methyl ionone (<10 %) in the starting material. The α-methyl ionone products could be assigned in a similar way to those of α-ionone (Appendix F.4). The *cis* and *trans* isomers were assigned by comparison with the α-ionone NMR and GC-MS spectra. Overall, the addition of the methyl group did not change the selectivity of the reaction and only seemed to make the binding to the P450 slightly worse than that of α-ionone.

The ionols (α- and β-) were chosen to further probe the role of the ketone in substrate binding to CYP101B1. The initial binding tests were conducted and both spin state shifts (70 % for α-ionol and 90 % for β-ionol, Figure 3.8(a) and (b)) were lower than the ionone equivalent. The dissociation constants were at least an order of magnitude higher than their ionone counterparts: 11.4 $\pm$ 0.5 μM for α-ionol and 7.4 $\pm$ 0.2 μM for β-ionol. β-Ionol is a better

substrate than α-ionol and the alcohols significantly reduced the affinity of the binding to CYP101B1 compared to the ketones. The NADH consumption rate for α-ionol and β-ionol were similar ($1030 \pm 50\,\mathrm{min}^{-1}$ and $\pm 55\,\mathrm{min}^{-1}$, respectively)(Figure 3.10(a)(b)). α-Ionol had a higher product formation rate ($764 \pm 76\,\mathrm{min}^{-1}$ compared to $670 \pm 84\,\mathrm{min}^{-1}$) and coupling (75 % compared to 65 %) than β-ionol. This was the opposite to that observed with the ionones. α-Ionol formed *cis*-3-hydroxy-α-ionol and *trans*-3-hydroxy-α-ionol as well as 3-oxo-α-ionol in the *in vivo* turnover (Figure 3.9). The H4 signals of both 3-hydroxy-α-ionol isomers were both singlets, which was a result of the bond angle being approximately 45° producing minimal coupling. β-Ionol formed 3-hydroxy-β-ionol as the major product and 4-hydroxy-β-ionol as the minor product (Figure 3.9). These products were all identified by NMR using the similar characteristic coupling patterns as their corresponding ionone compounds after purification on a semi-prep HPLC (Appendix F.5 and Appendix F.6). Overall, both ionol compounds did not bind as well as the ketone counterparts; having a ketone seems to be optimal for binding to CYP101B1. However, presence of an oxygen, even in the alcohol form, results in relatively high activity and a similar product profile. This indicates the substrates are held in a similar orientation in the active site of CYP101B1.

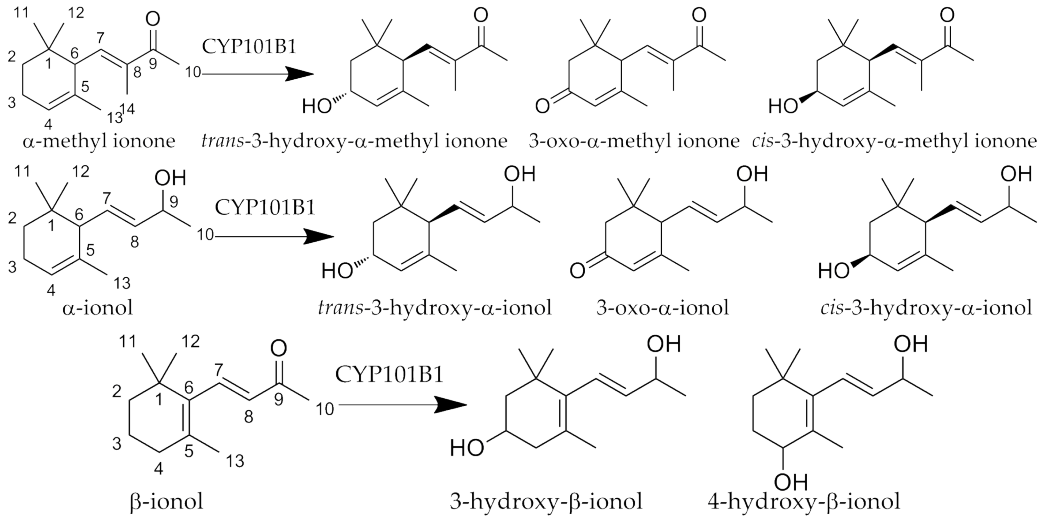

Figure 3.9: Products of α-methyl ionone, α-ionol and β-ionol

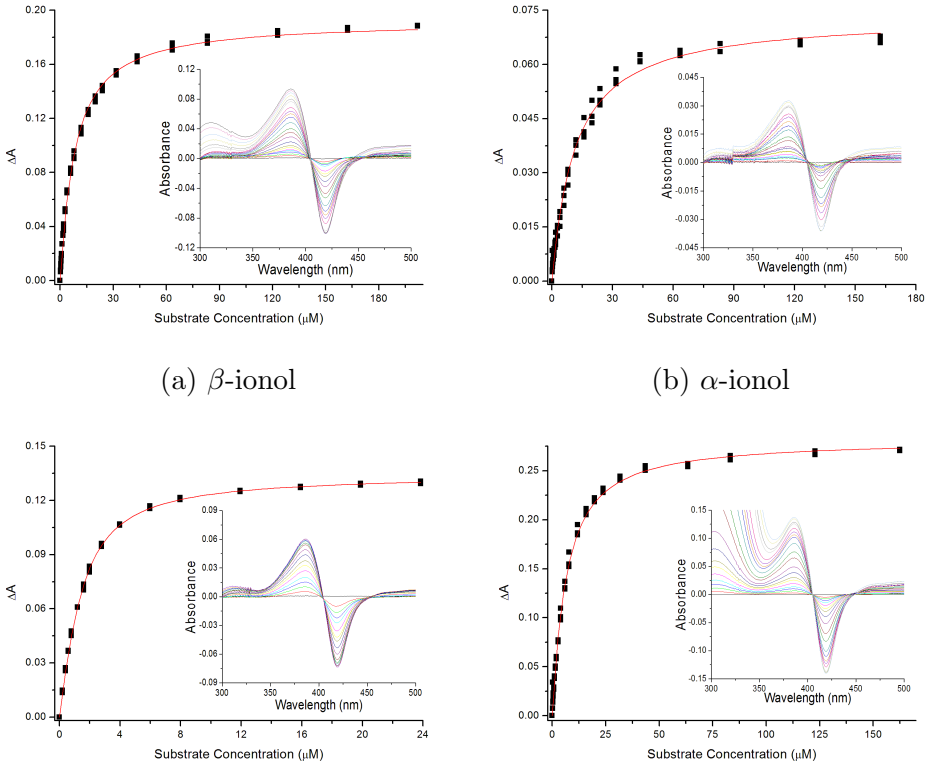

(a) β-ionol

(b) α-ionol

(c) α-methyl ionone

(d) pseudoionone

Figure 3.10: Dissociation constants for selected norisoprenoid compounds

3.3 Norisoprenoid Discussion

Results obtained with the ionone-type substrates indicate the substrates are being held in the active site, with the C3 position held closest to the heme iron and the C4 position close enough for competing allylic oxidation to occur, but not epoxidation in the α-ionone analogues. Oxidation of ionones with other P450 enzymes has been investigated. Self sufficient P450, CYP102A1 ($P450_{Bm3}$), selectively oxidised β-ionone at the C4 position.[11] CYP102A1 mutants have been reported to catalyse stereoselective oxidation at C3 for the different enantiomers of α-ionone.[24] These mutants were able to selectively produce (3*S*,6*S*)-hydroxy-α-ionone and (3*R*,6*R*)-hydroxy-α-ionone with a diastereomeric excess above 71 %. One mutant produced (3*S*,6*R*)-hydroxy-α-ionone with diastereomeric excess of 90 %. The best CYP102A1 mutants with (*R*)-α-ionone and (*S*)-α-ionone had lower product formation rates (152 min^{-1} and 98 min^{-1}) and coupling (39 % and 44 %) than CYP101B1.[24] Further in-

vestigation of CYP101B1 and the different enantiomers of α-ionone was not possible, as only racemic α-ionone was commercially available.

CYP101C1, also from *N. aromaticivorans*, which uses the same electron transfer partners as CYP101B1, rapidly oxidises β-ionone to give the major product 4-hydroxy-β-ionone (75 %) and the minor product 3-hydroxy-β-ionone(25 %) (product formation rate $\sim 2000\,\mathrm{min}^{-1}$).[1,19] CYP101C1 oxidises β-damascone to a mixture of 3- and 4-hydroxy-β-damascone and other further oxidation products, with 4-hydroxy-β-damascone as the major product.[19] However, it oxidises α-ionone very slowly (product formation rate $\sim 220\,\mathrm{min}^{-1}$) at the C3 position.[1,19] This is probably due to CYP101C1 favouring oxidation at the C4 position, as seen with β-ionone and damascone. This differs from the results obtained for CYP101B1. The differences between the active site of these two enzymes alters the binding and, as a result, the products generated.

The C4 oxidation of β-ionone is catalysed by the P450 enzymes CYP105A1 and CYP105B1 from *Streptomyces griseolus* and SYP105D1 from *Streptomyces griseus*.[25] CYP109B1 from *Bacillus subtilis* also oxidised β-ionone to form 4-hydroxy-β-ionone.[26] Conversely, CYP264B1 from *Sorangium cellulosum* So ce56 reacted with β-ionone at only the C3 position and CYP264B1 oxidised α-ionone at the C3 position.[27] CYP109B1, CYP109D1 oxidise α-ionone at the C3 position, but their physiological electron transfer partners are not available and the activities are very low using alternative systems.[26,28,29] CYP101B1 is therefore an excellent candidate for biocatalysis of β-ionone and norisoprenoids; the only other P450s comparable in terms of activity are CYP101C1 and CYP102A1. However, oxidation by CYP101B1 occurs at the C3 position instead of the C4 position.

3.4 Aromatic Substrate Results

N. aromaticavorans and other *Novosphingobium* species are known to degrade polycyclic aromatics. CYP108D1 from *N. aromaticavorans* has been shown to react with aromatics such as indole, phenanthrene, naphthalene and biphenyl. CYP101B1 also may have this application, as previous whole-cell

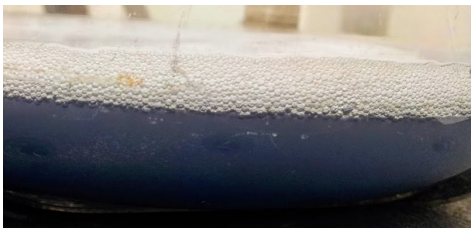

Figure 3.11: A whole-cell turnover after the addition of indole

turnovers have turned blue after the addition of IPTG, as tryptophan breaks down to indole.[1,3,16] To test this, a simple colorimetric experiment was conducted with indole, to determine whether aromatics are oxidised by CYP101B1. P450 enzymes can oxidise indole and then form indigo, turning the reaction blue (Figure 3.12).[1,2] When indole was added to the CYP101B1 *in vivo* turnover, the solution clearly turned blue (Figure 3.11) and *in vitro* tests with indole indicated it did bind to CYP101B1, with a 15 % shift to the high spin form observed. This indicated CYP101B1 is able to oxidise aromatic substrates. It was therefore decided to investigate other molecules containing aromatic ring components to get a better idea of which of these substrates can bind to CYP101B1. Phenylcyclohexane and *p*-cymene were chosen as test substrates.

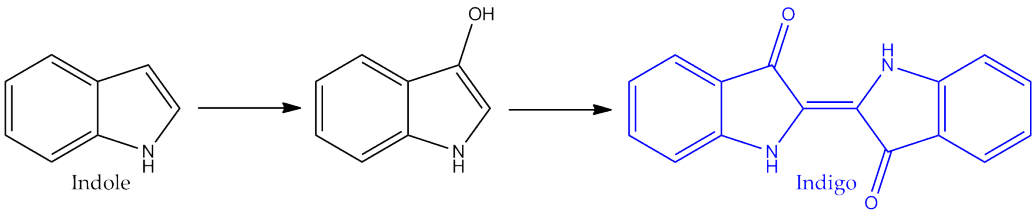

Figure 3.12: Conversion of indole to indigo mediated by P450

Phenylcyclohexane is larger than indole and contains an aliphatic cyclohexane ring, so will test the size of the CYP101B1 binding site and the preference of the aliphatic versus aromatic C−H bond oxidation. Phenylcyclohexane gave a spin state shift of 20 %; however, the dissociation constant (7.8 ± 0.9 μM) was comparable to β-damascone, which indicates relatively tight binding (Figure (a)(b). The NADH consumption rate (293 ± 9 min^{-1}), product formation rate (141 ± 17 min^{-1}) and coupling (48 %) were reasonable considering it is a large non-polar compound with little similarity to the norisoprenoids. Phenylcyclohexane oxidation resulted in a single product *in vitro* and *in vivo*, which was identified as *trans*-4-phenylcyclohexanol by NMR (Figure 3.4), due to the triplet of triplets signal at 3.70 ppm and the coupling of the molecule (Appendix F.7).

p-Cymene is a smaller molecule than phenylcyclohexane. *p*-Cymene induced a minimal shift in the spin state (5 %) and the dissociation constant was 23 ± 3 μM (Figure (c)(d)). This indicates *p*-cymene does not bind to CYP101B1 as well as phenylcyclohexane. The NADH consumption rate (197 ± 27 min^{-1}), product formation rate (25 ± 6 min^{-1}) and coupling (13 %) were all lower than values found for phenylcyclohexane and significantly lower than values found for the norisoprenoids. Turnovers of *p*-cymene with CYP101B1 produced two

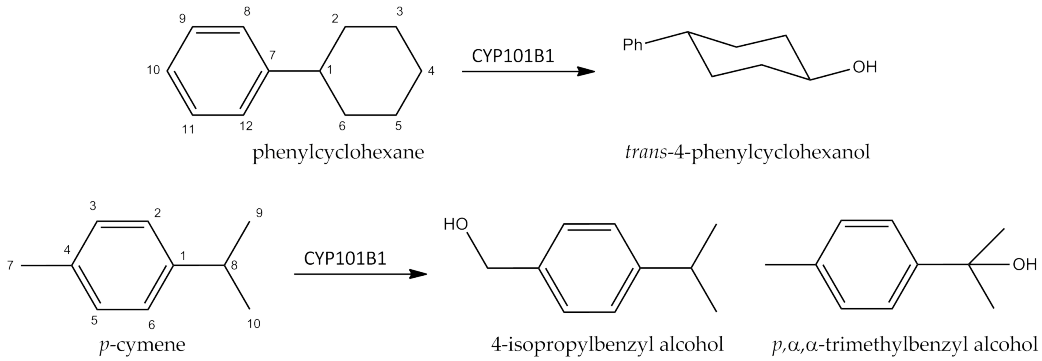

Figure 3.13: The reactions of Phenylcyclohexane and *p*-cymene with CYP101B1

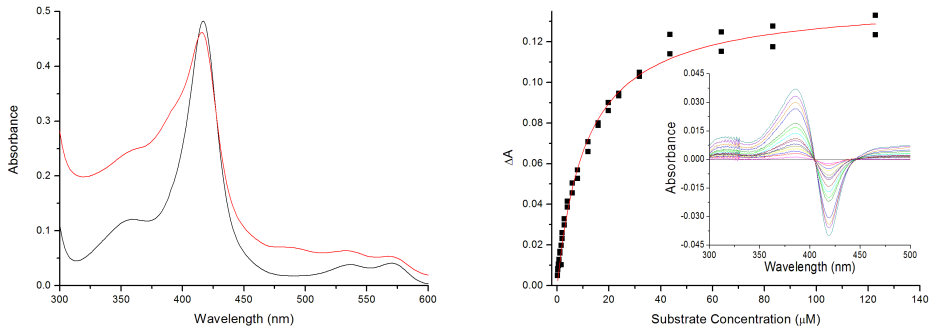

(a) phenylcyclohexane (b) phenylcyclohexane

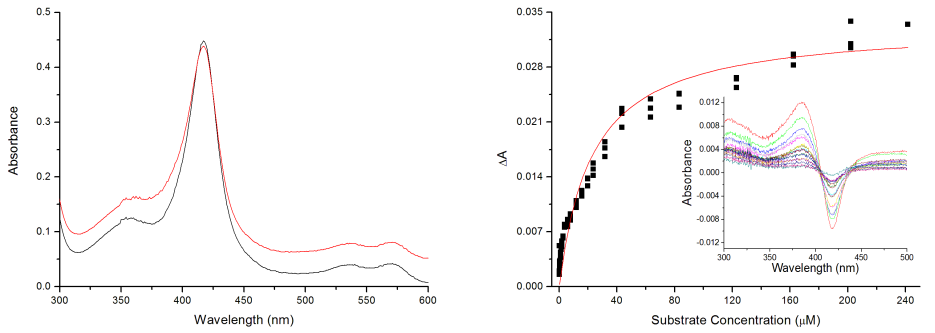

(c) *p*-cymene (d) *p*-cymene

Figure 3.14: Spin state shifts and dissociation constants for phenylcyclohexane and *p*-cymene. Spin state shift of phenylcyclohexane (a), dissociation constant of phenylcyclohexane (b), spin state shift of *p*-cymene (c) and dissociation constant of *p*-cymene (d)

products which were identified as p,α,α-trimethylbenzyl alcohol (25 %) and 4-isopropylbenzyl alcohol (75 %) by GC-MS co-elution experiments (Figure and 3.15). Overall, p-cymene was not as good a substrate for CYP101B1 as phenylcyclohexane. This was probably a result of p-cymene being a smaller molecule than phenylcyclohexane.

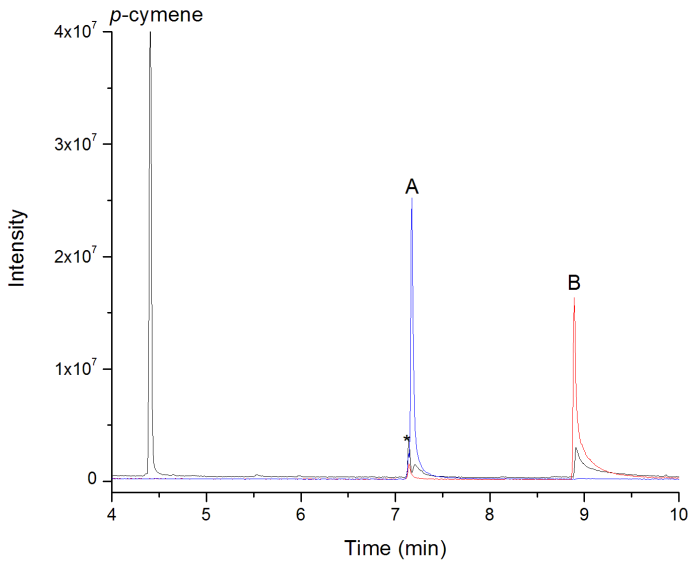

Figure 3.15: GC-MS analysis of *in vitro* CYP101B1 turnover of p-Cymene (black), p, α, α-trimethylbenzyl alcohol standard solution (blue), 4-isopropylbenzyl alcohol standard solution (red), α, α-trimethylbenzyl alcohol (A), 4-isopropylbenzyl alcohol (B) and impurities (*).

3.5 Aromatic Substrate Discussion

Phenylcyclohexane oxidation to *trans*-4-phenylcyclohexanol was not as active as the norisoprenoids but was reasonably well coupled to NADH consumption, which was comparable to α-ionone. Mutants of CYP101A1 have been found to oxidise phenylcyclohexane predominantly at the C4 position, but with lower activity than CYP101B1.[30–32] Selective mutations of CYP101A1 did result in oxidation at other positions; however, these were not regioselective and multiple products formed.[30–32] The mutants resulted in oxidation to *cis*-4-phenylcyclohexanol and *cis*-3-phenylcyclohexanol as well as *trans*-4-phenylcyclohexanol.[30–32] CYP108D1 can tightly bind phenylcyclohexane and

oxidise it to *trans*-4-hydroxyphenylcyclohexane. However, CYP108D1 has low activity due to the absence of native electron transfer partners.[16] So far, CYP101B1 seems to be the best P450 for forming *trans*-4-phenylcyclohexanol from phenylcyclohexane in terms of activity and selectivity.

3.6 Summary

Initial screening of CYP101B1 with a range of both norisoprenoid and aromatic substrates was successful in identifying compounds which react to varying degrees. The optimal substrate for CYP101B1 biocatalysis contains a ketone on a side chain of the substrate. By comparing β-ionone and α-ionone, it can be determined that the position of the alkene bond on the cyclohexane ring does not significantly affect binding. The main difference was in the selectivity of the C−H bond oxidation. Epoxidation was not observed in α-ionone, α-methyl ionone or α-ionol, suggesting the C3 position is being held more directly over the active site, with C3 pseudoequatorial and pseudoaxial C−H bonds being held closest to the heme iron. Changing the position of the alkene and ketone on the butenone side chain, in β-Damascone, resulted in weaker binding compared to β-ionone. The positions of the ketone or alkene are, therefore, important for efficient substrate binding and selectivity. α-Methyl ionone introduces a methyl group to the butenone side chain causing a reduction in binding efficiency. Ionols were examined to determine the effect of replacing the ketone with an alcohol. It was discovered that the ketone is important for binding and probably interacts with a specific amino acid residue in the active site of CYP101B1. However, these modifications do not significantly alter the selectivity of product formation.

The norisoprenoid structures were preferred over the aromatic molecules; however, phenylcyclohexane oxidation was regioselective. The binding of phenylcyclohexane to CYP101B1 was reasonably tight, suggesting the substrate binding pocket may also be lined with hydrophobic residues. The cyclohexane ring of phenylcyclohexane must bind more closely to the heme iron than the aromatic ring. As a result, CYP101B1 prefers to insert the oxygen into the non-aromatic C−H bond. However, CYP101B1 can still react and turnover compounds that contain aromatic rings, such as indole.

β-Ionone remains the best substrate in terms of binding and reactivity with CYP101B1. CYP101B1 had better rates of reaction than all previously reported P450s with α-ionone and phenylcyclohexane and was highly selective for the oxidation of these two compounds. Given the promising biocatalytic

properties observed with CYP101B1 with norisoprenoids and phenylcyclohexane, its activity with monoterpenoids (Chapter 4) and two-ring containing aromatic compounds (Chapter 6) will be further investigated.

Chapter 4

Analysis of Terpenoids as Substrates for CYP101B1

4.1 Introduction

The results of Chapter 3 indicate that CYP101B1 has a preference for compounds containing a ketone moiety over an alcohol and a cyclohexane over a benzene ring. With this in mind, it was decided to further test the substrate range of this enzyme by examining some smaller monoterpenoid substrates. (1*R*)-(+)-Camphor has been reported to interact with CYP101B1, although an in-depth analysis of its activity and selectivity has not been conducted (Figure 4.2).[15] Other monoterpenoids with a cyclic structure and a ketone group or oxygen present were chosen (Table 4.1). (+)-Sclareolide is a sesquiterpenoid and larger than norisoprenoids, and will test how CYP101B1 tolerates bulky substrates.

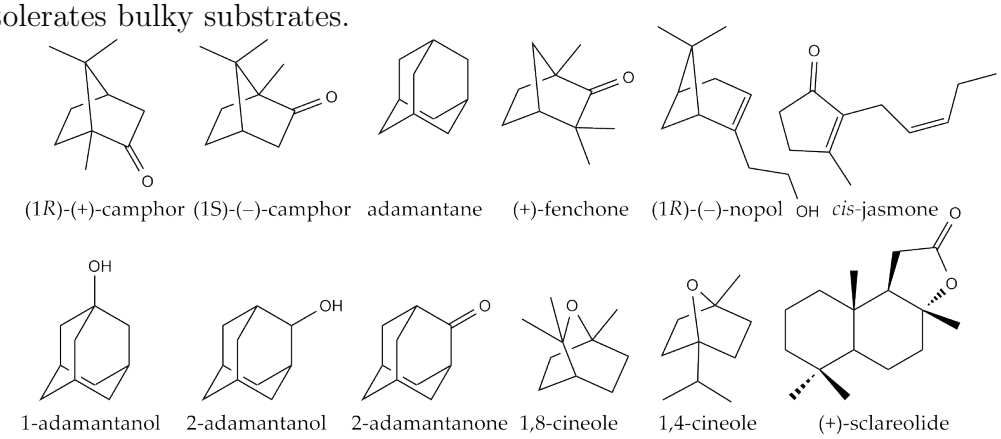

Figure 4.1: The terpenoid substrates tested with CYP101B1

4.2 Results

(1*S*)-(−)-Camphor was also chosen to observe any difference between enantiomers (Figure 4.1). Both enantiomers of camphor induced a spin state shift of 55 %, and had high dissociation constants ($330 \pm 10\,\mu$M for (1*R*)-(+)-camphor and $260 \pm 8\,\mu$M for (1*S*)-(−)-camphor). The NADH consumption rates were high ($1040 \pm 9\,\text{min}^{-1}$ for *R* and $1260 \pm 87\,\text{min}^{-1}$ for *S*); however, the product formation rate ($153 \pm 24\,\text{min}^{-1}$ for *R* and $157 \pm 44\,\text{min}^{-1}$ for *S*) and coupling (15 % for *R* and 13 % for *S*) were moderate. There was a high proportion of uncoupling occurring with these substrates, which most likely arose from a non-ideal fit in the active site. There were four different major oxidation products in the *in vitro* turnover of (1*R*)-(+)-camphor, which were identified by GC-MS co-elution or column chromatography. These were 6-*exo*-hydroxycamphor (15 %, m/z 168.1 AMU), 5-*exo*-hydroxycamphor (45 %, m/z 168.1 AMU), 5-*endo*-hydroxycamphor (25 %, m/z 168.1 AMU) and 9-hydroxycamphor (15 %, m/z 168.1 AMU). 9-Hydroxycamphor was identified by column chromatography and NMR analysis (Figure 4.2 and 4.3).[33] The remaining camphor products were identified by GC-MS co-elution with camphor products from a reaction with CYP176A1 and CYP101A1 by James de Voss at the University of Queensland.[15,34] The *in vivo* turnover showed further oxidation products that were not identified (m/z 166.1 AMU). (1*S*)-(−)-Camphor also gave a mixture of four main oxidation products. These were 6-*exo*-hydroxycamphor (30 %), 5-*exo*-hydroxycamphor (45 %), 5-*endo*-hydroxycamphor (5 %) and 9-hydroxycamphor (25 %) (Figure 4.2 and 4.3). The *in vivo* turnover showed some further oxidation products present which could not be purified in a yield sufficient for identification (m/z 166.1 AMU).

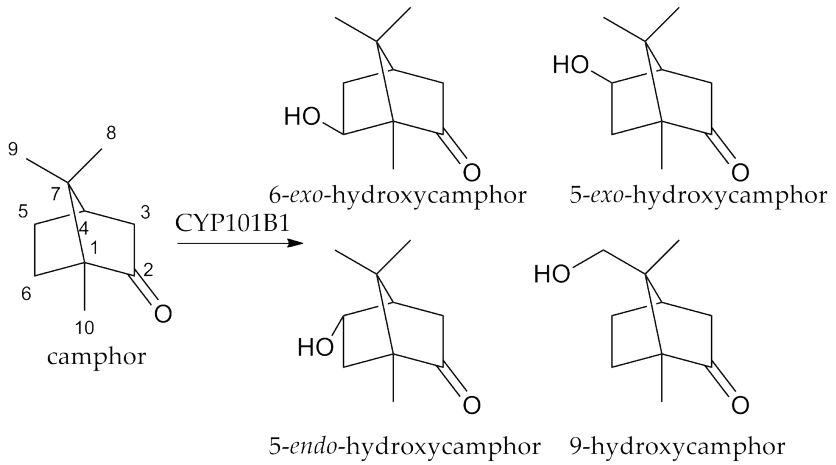

Figure 4.2: Products from the turnovers of the camphor isomers

Table 4.1: Terpenoid substrate binding, steady state kinetic data and coupling with CYP101B1. Steady state turnover activities were measured using a ArR:Arx:CYP101B1 concentration ratio of 1:10:1 (0.5 μM CYP enzyme, 50 mM Tris, pH 7.4). Coupling is the percentage efficiency of NADH utilization for the formation of products. Rates are reported as mean $\pm$ S.D.($n \geq 3$) and given in nmol(nmol-CYP)$^{-1}$min^{-1}.

CYP101B1/ substrate	%HS heme	K_d (μM)	NADH consumption rate (min^{-1})	Product formation rate (min^{-1})	Coupling %
(1*R*)-(+)-camphor	55	330 ± 10	1040 ± 9	153 ± 24	15
(1*S*)-(−)-camphor	55	260 ± 8	1260 ± 87	157 ± 44	13
(+)-fenchone	50	540 ± 20	1110 ± 78	198 ± 23	18
1,8-cineole	75	580 ± 15	938 ± 2	355 ± 12	38
1,4-cineole	50	610 ± 25	419 ± 35	42 ± 12	10
(1*R*)-(−)-nopol	50	60 ± 2	553 ± 87	165 ± 32	30
cis-jasmone	35	470 ± 20	133 ± 2	28 ± 11	21
adamantane	30	-	144 ± 10	0.16 ± 0.14	0.11
1-adamantanol	60	710 ± 30	415 ± 55	11 ± 4	3
2-adamantanol	55	-	349 ± 100	7 ± 3	2
2-adamantanone	35	550 ± 20	669 ± 7	104 ± 9	16
(+)-sclareolide	50	20 ± 4	-	-	-

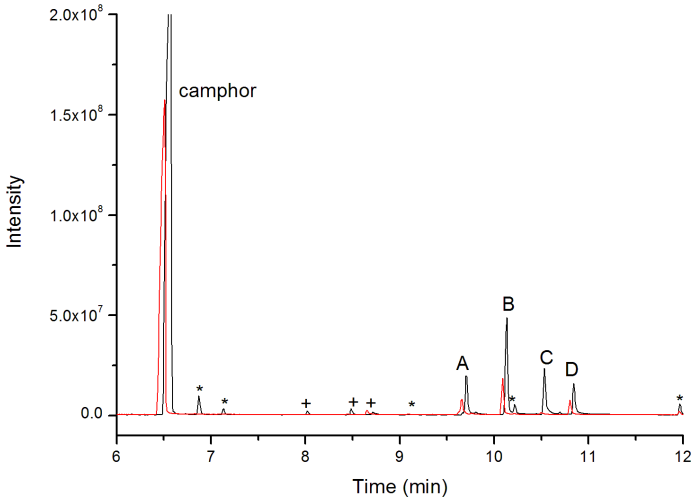

Figure 4.3: GC-MS analysis of CYP101B1 turnovers of (1*R*)-(+)-camphor and (1*S*)-(−)-camphor. (1*R*)-(+)-Camphor (black), (1*S*)-(−)-camphor (red), 6-*exo*-hydroxycamphor (A), 5-*exo*-hydroxycamphor (B), 5-*endo*-hydroxycamphor (C), 9-hydroxycamphor (D), further oxidation products (+) and impurities (*).

(+)-Fenchone is a bicyclic monoterpenoid with a similar structure to camphor, but the two methyl groups are located at carbon 3 rather than carbon 7 (Figure 4.1). It will be interesting to see the effects of this change on the reactivity of the substrate. (+)-Fenchone binding induced a spin state shift of 50 % that was much the same as camphor; however, the dissociation constant ($540 \pm 20\,\mu$M) was almost twice as large. The NADH consumption rate ($1110 \pm 78\,\text{min}^{-1}$) was comparable to camphor, but the product formation rate ($198 \pm 23\,\text{min}^{-1}$) and coupling (18 %) were slightly higher. (+)-Fenchone oxidation was more selective than the camphor substrates as the major product in both the *in vitro* and *in vivo*, 5-*exo*-hydroxyfenchone, made up 75 % of the products produced (m/z 168.1 AMU) (Figure 4.4). The remaining 25 % consisted of two unidentified single oxidation products that were not purified by column chromatography in sufficient yield to identify by NMR. Both had m/z of 168.1 AMU, indicating they were single monooxygenation products. 5-*exo*-Hydroxyfenchone was identified by NMR by the distinctive coupling between H5 at 4.37 ppm and H4 at 2.14 ppm, and the W coupling between H5 and H7b at 1.74 ppm (Figure 4.5, Appendix F.11). Shifting those methyl groups seems to modify substrate binding and increase selectivity of the reaction.

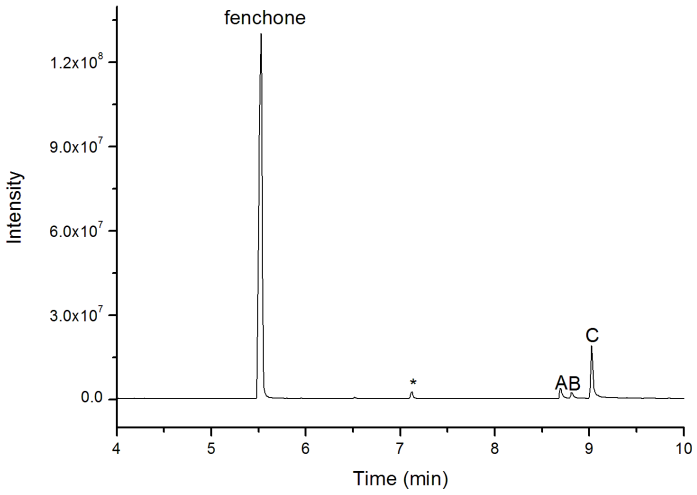

Figure 4.4: GC-MS analysis of CYP101B1 *in vivo* turnover of (+)-fenchone (black), unidentified single oxidation products (A) and (B), 5-*exo*-hydroxyfenchone (C) and impurities (*).

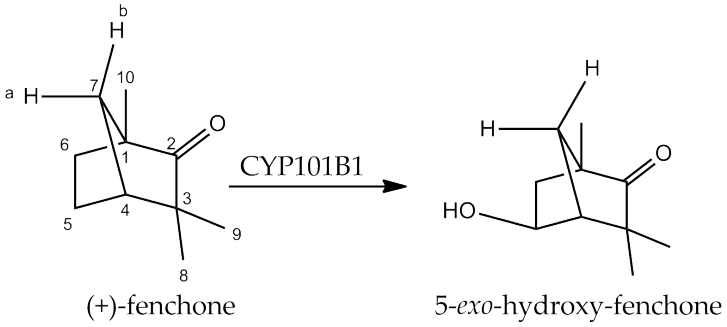

Figure 4.5: The *in vitro* turnover of (+)-Fenchone with CYP101B1

1,8-Cineole and 1,4-cineole are bicyclic monoterpenoids with an oxygen present in one of the rings, instead of as a ketone. 1,8-Cineole has the methyl groups next to the oxygen, which seemed to improve selectivity in (+)-fenchone (Figure 4.1). 1,4-Cineole has an isopropyl side chain and a smaller bridging group as it is now a [2.2.1] ring structure instead of the [2.2.2] ring structure of 1,8-cineole (Figure 4.1). 1,8-Cineole induced the largest spin state shift on binding (75 %) for all of the terpenoids; however, the dissociation constant was still large ($580 \pm 15\,\mu$M), indicating the binding was not tight. 1,4-Cineole had a similar spin state shift (50 %) to the other monoterpenoid compounds and a large dissociation constant ($610 \pm 25\,\mu$M). The NADH consumption rate for 1,8-cineole was $938 \pm 2\,\text{min}^{-1}$, which was double the rate for 1,4-cineole ($419 \pm 40\,\text{min}^{-1}$). For 1,8-cineole, 38 % of the NADH was used to convert substrate into products, resulting in a product formation rate of $355 \pm 12\,\text{min}^{-1}$. 1,4-Cineole was less productive, with only 10 % of the NADH used to form products, resulting in a product formation rate of $42 \pm 12\,\text{min}^{-1}$.

The *in vitro* turnover of 1,8-cineole gave a mixture of products, with the major product being 3-*endo*-hydroxy-1,8-cineole (90 %) and other unidentified single oxidation products (total 10 %, all with m/z 168.1 AMU). Whole-cell oxidation of 1,8-cineole resulted in large amounts of further oxidation products identified as 3-oxo-1,8-cineole (m/z 166.1 AMU) and 3-*endo*-hydroxy-5-oxo-1,8-cineole (m/z 182.1 AMU) (Figure ref18cineoleproducts). 3,5-*endo*-Dihydroxy-1,8-cineole was also obtained after column chromatography, but this was not observed in the GC-MS sample. The most logical conclusion is that this product was generated during the purification process from 3-*endo*-hydroxy-5-oxo-1,8-cineole (Figure 4.7).

3-*endo*-Hydroxy-1,8-cineole could be assigned from the signal at 4.46 ppm in the ^{1}H NMR and the coupling between H3 and H2, and H3 and H4. To determine the final position of the OH, the W coupling between H3 and H5

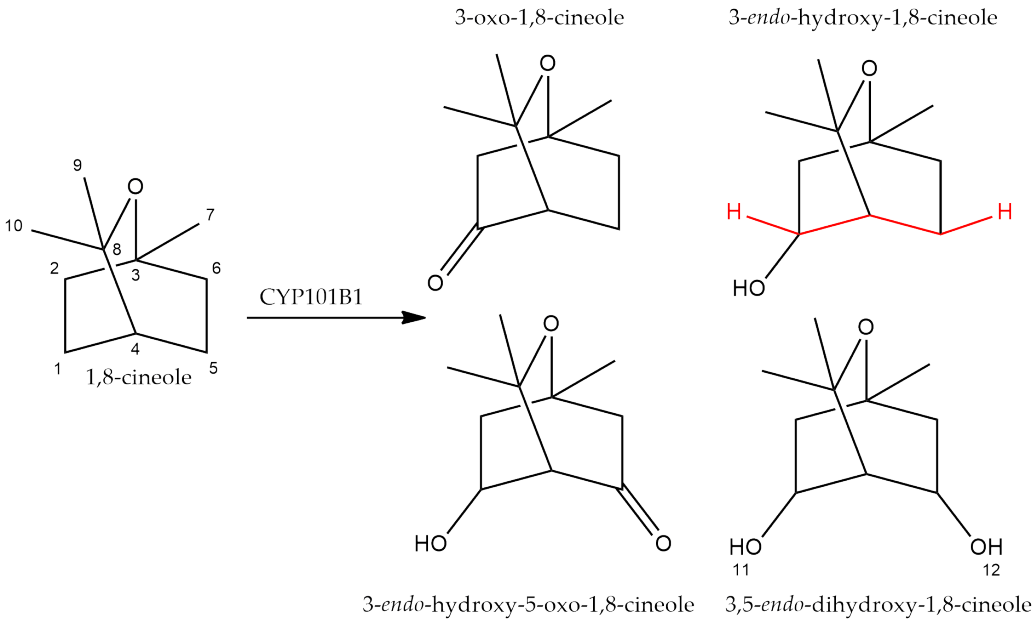

Figure 4.6: The products from the 1,8-cineole whole-cell turnover. The W shape which results in W coupling between the two exo hydrogen atoms is highlighted in red.

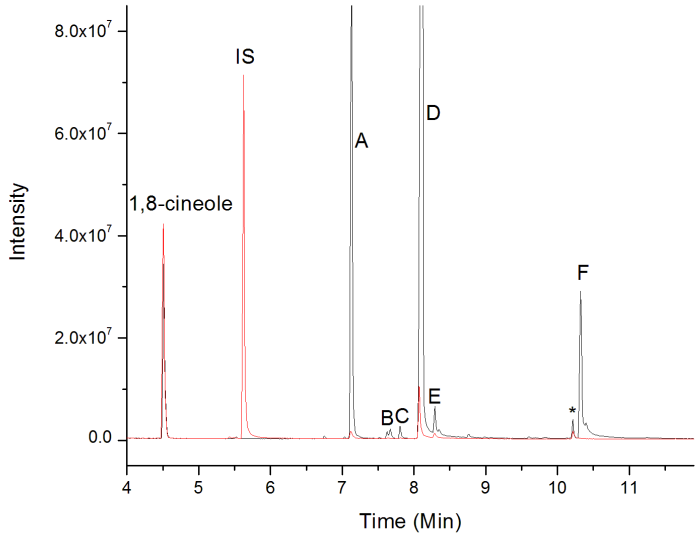

Figure 4.7: GC-MS analysis of CYP101B1 turnovers of 1,8-cineole, *in vivo* (black), *in vitro* (red), 3-oxo-1,8-cineole (A), unidentified single oxidation products (B), (C), and (E), 3-*endo*-hydroxy-5-oxo-1,8-cineole (D), 3-*endo*-hydroxy-5-oxo-1,8-cineole (F), internal standard (IS) and impurities (*).

was used which resulted in the the OH being assigned as *endo* (Appendix F.9). This W coupling is visible in the COSY NMR and indicates coupling between two hydrogens 4 bonds apart when the bonds form a W shape (Figure 4.6). However, further chiral analysis is required to determine which isomer was formed, as this product could also be 5-*endo*-hydroxy-1,8-cineole. The absence of H signal in the alcohol region of the ^{1}H NMR and the appearance of a signal at 213.2 ppm in the ^{13}C NMR indicated that 3-oxo-1,8-cineole had formed (Appendix F.9). The structure of 3-*endo*-hydroxy-5-oxo-1,8-cineole was determined from the H3 signal from 4.61–4.55 ppm in the ^{1}H NMR and the C5 signal at 210.5 ppm in the ^{13}C NMR (Appendix F.9). 3,5-*endo*-Dihydroxy-1,8-cineole was assigned using the symmetry of the molecule and the appearance of the doublet of doublets signal at 4.55 ppm of H3 and H5 and the two OH signals at 4.00 ppm (Appendix F.9). The unidentified products were not isolated in sufficient yield for determination by NMR.

Oxidation of 1,4-Cineole resulted in multiple products: the major product was 6-*endo*-hydroxy-1,4-cineole (60 %), with the remaining products unidentified (total 40 %) (Figure 4.8). These were either single oxidation products (m/z 168.1 AMU) or further oxidation products (m/z 166.1 AMU) (Figure 4.9). The major product was determined by NMR from the peak at 3.93 ppm and NOE correlation between H6 and H7 indicating the 6 position instead of the 5 position (Appendix F.10).

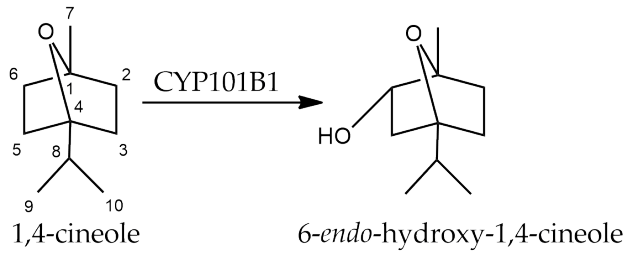

Figure 4.8: The identified product from the 1,4-cineole turnovers

Adamantane, 1-adamantanol, 2-adamantanol and 2-adamantanone were investigated as substrates (Figure 4.1). 1-Adamantanol and 2-adamantanol gave spin state shifts of 60 % and 55 %, respectively. The binding of the other substrates gave lower spin state shifts of 30 % (adamantane) and 35 % (2-adamantanone). Even though the alcohols induced a larger spin state shift than the ketone, the dissociation constant for 2-adamantanone was $550 \pm 20\,\mu$M compared with $710 \pm 30\,\mu$M for 1-adamantanol. The other dissociation constants could not be determined due to the low solubility and weak binding of adamantane and 2-adamantanol. The low solubility made

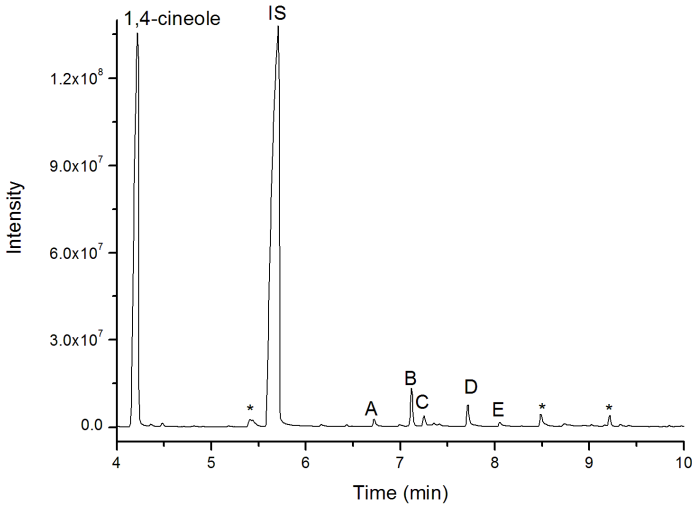

Figure 4.9: GC-MS analysis of CYP101B1 *in vitro* turnover of 1,4-cineole (black), unidentified products (A), (C), (D) and (E), 6-*endo*-hydroxy-1,4-cineole (B) internal Standard (IS) and impurities (*).

determining the NADH consumption rates and product formation rates for all these substrates more challenging. Adamantane performed the worst of all substrates tested, with a NADH consumption rate of $144 \pm 10\,\mathrm{min}^{-1}$ and a product formation rate of $0.16 \pm 0.14\,\mathrm{min}^{-1}$, due to a very low coupling (0.11 %) of the reducing equivalents to product formation. 1-Adamantanol and 2-adamantanol had similar NADH consumption rates ($415 \pm 55\,\mathrm{min}^{-1}$ for 1-adamantanol and $349 \pm 100\,\mathrm{min}^{-1}$ for 2-adamantanol), product formation rates ($11 \pm 4\,\mathrm{min}^{-1}$ for 1-adamantanol and 7 ± 3 min^{-1} for 2-adamantanol) and couplings (3 % for 1-adamantanol and 2 % for 2-adamantanol). The best substrate, however, was 2-adamantanone, with an NADH consumption rate of $669 \pm 7\,\mathrm{min}^{-1}$, product formation rate of $104 \pm 9\,\mathrm{min}^{-1}$ and coupling of 16 %. Adamantane gave two products: 1-adamantanol (90 %) and 2-adamantanol (10 %), which were identified by GC-MS co-elution experiments. Oxidation of 2-adamantanone resulted in 5-hydroxy-2-adamantanone (45 %) and 6-hydroxy-2-adamantanone (55 %) *in vitro* and *in vivo* (Figure 4.10). The *in vivo* oxidation of 2-adamantanol formed 6-hydroxy-1-adamantanol and 6-hydroxy-2-adamantanone (Figure 4.10). The *in vitro* turnover of 2-adamantanol produced 6-hydroxy-1-adamantanol (30 %) and 6-hydroxy-2-adamantanol (70 %).

6-Hydroxy-2-adamantanone was assigned from the appearance of the 4.08 ppm signal and the symmetry of the ^{13}C NMR (Appendix F.15). The signal at 67.3 ppm in the ^{13}C NMR indicated that 5-hydroxy-2-adamantanone was

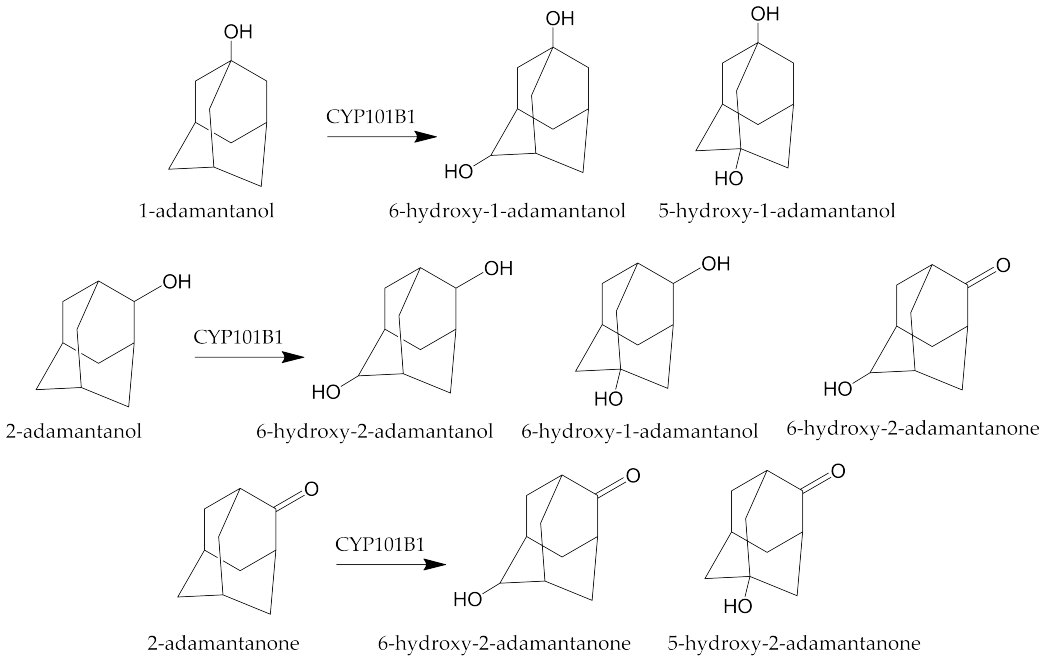

Figure 4.10: The products from the 1-adamantanol, 2-adamantanol and 2-adamantanone whole-cell turnovers

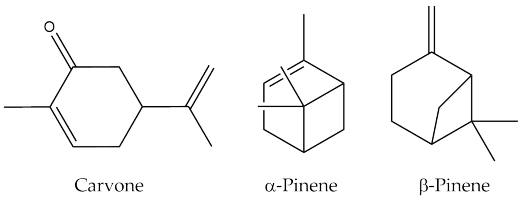

Figure 4.11: The structures of carvone, α- and β-pinene

formed (Appendix F.15). 6-Hydroxy-1-adamantanol was assigned from the single peak in the ^{1}H NMR at 3.74 ppm and the two peaks in the ^{13}C NMR at 73.2 ppm and 71.5 ppm (Appendix F.14). Turnovers of 1-adamantanol did not form enough products to determine their structures, but 6-hydroxy-1-adamantanol (90 %) was identified by co-elution with the product from the 2-adamantanol turnover (Appendix E.1). There was also an unidentified single oxidation product, which was most likely 5-hydroxy-1-adamantanol (10 %) as hydroxylation occurred at the 5 position in all other adamantane reactions (Figure 4.10).

Other substrates tested with CYP101B1 were carvone, α-(+)-pinene, α-(−)-pinene and β-(−)-pinene (Figure 4.11). Carvone and α-(−)-pinene gave spin

state shifts of <30 %. α-(+)-Pinene gave a spin state shift of 20 % and β-(−)-pinene 10 %. After these results were collected, an *in vivo* turnover was conducted for all the substrates. Unfortunately, minimal levels of products were observed for these substrates and testing was not continued. These substrates produced minimal products for different reasons: carvone due to its small structure and the pinene substrates due to their lack of an oxygen atom.

(1*R*)-(−)-Nopol is related to pinene, but it is larger, having twelve carbons rather than ten. It has some structural similarities to the norisoprenoids, as it has an alcohol-containing alkyl side chain (Figure 4.1). The spin state shift induced by (1*R*)-(−)-nopol was 50 %, but a noticeable difference was observed in the dissociation constant as this was much lower, at $60 \pm 2\,\mu$M, than the monoterpenoids. However, the NADH consumption rate ($553 \pm 87\,\text{min}^{-1}$) and product formation rate ($165 \pm 32\,\text{min}^{-1}$) were similar to those observed for the monoterpenoids, but the coupling was higher (30 %). The *in vitro* turnover for (1*R*)-(−)-nopol gave two oxidation products: 1-hydroxy-(1*R*)-(−)-nopol (90%) and 4-hydroxy-(1*R*)-(−)-nopol (10%) (Figure 4.13). 4-Hydroxy-(1*R*)-(−)-nopol was not purified by column chromatography from the *in vivo* reaction; however, 4-oxo-(1*R*)-(−)-nopol was isolated (Figure 4.12). It can be assumed that 4-hydroxy-(1*R*)-(−)-nopol was also formed, as it must for the further oxidation product to be generated. 1-Hydroxy-(1*R*)-(−)-nopol was identified as H5 couples to both H4 and H6 in the COSY NMR and the C1 ^{13}C NMR signal at 74.9 ppm along with the absence of a signal in the OH region. 4-Oxo-(1*R*)-(−)-nopol was assigned due to the coupling between H1, H5 and H6 and the C4 ^{13}C signal at 203.75 ppm and the absence of the H signal in the OH region (Appendix F.12).

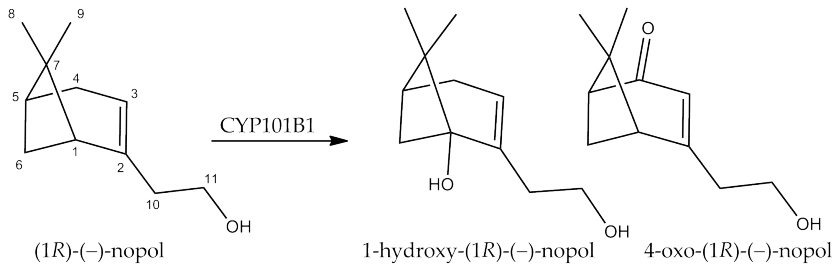

Figure 4.12: The products isolated from the (1*R*)-(−)-nopol *in vivo* turnover

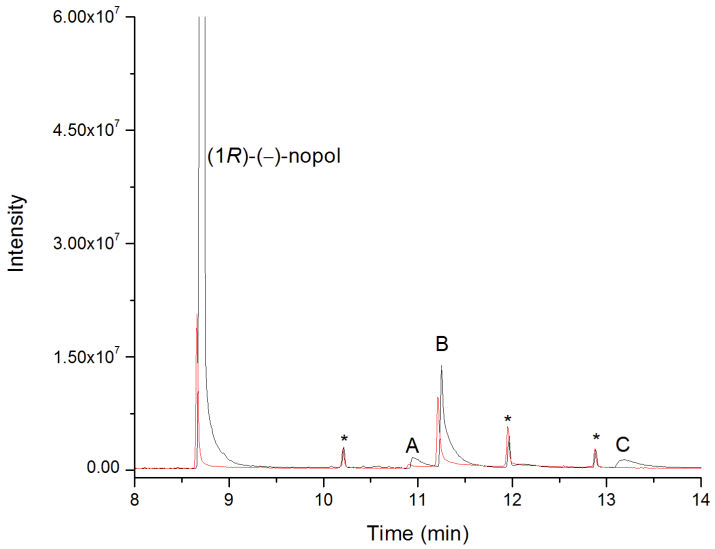

Figure 4.13: GC-MS analysis of CYP101B1 turnovers of (1*R*)-(−)-nopol. *in vivo* (black), *in vitro* (red), 4-hydroxy-(1*R*)-(−)-nopol (A) 1-hydroxy-(1*R*)-(−)-nopol (B), 4-oxo-(1*R*)-(−)-nopol (C) and impurities (*).

cis-Jasmone is a natural flavour and fragrance compound which also has twelve carbons; however, the ketone is on the pentene ring and the side chain is a non-polar cyclopentene chain (Figure 4.1). The ketone on the ring in *cis*-jasmone results in a spin state shift of 35 % and a dissociation constant of $470 \pm 20\,\mu$M. The NADH consumption rate ($133 \pm 2\,\text{min}^{-1}$), product formation rate ($28 \pm 11\,\text{min}^{-1}$) and coupling (21 %) were moderate. There were two products formed *in vitro* and *in vivo*, which were identified by NMR as 4-hydroxy-*cis*-jasmone (75 %) and 11-hydroxy-*cis*-jasmone (25 %) (Figure 4.14 and 4.15). 11-Hydroxy-*cis*-jasmone was identified by the 2H singlet at 4.58 ppm; 4-hydroxy-*cis*-jasmone was identified by the doublet signal at 4.71 ppm and the coupling between H4 and H3 and H4 and H11 in the COSY (Appendix F.13).

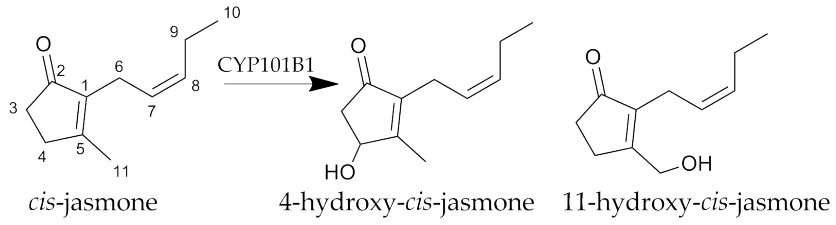

Figure 4.14: The products isolated from *cis*-jasmone oxidation

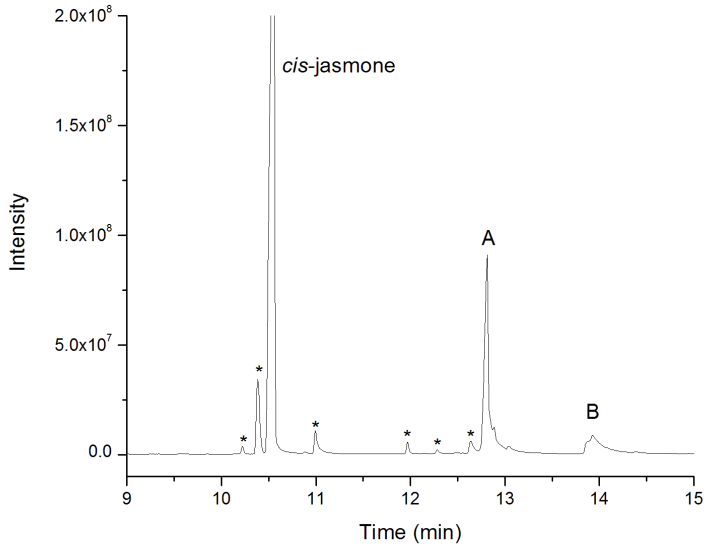

Figure 4.15: GC-MS analysis of CYP101B1 *in vitro* turnover of *cis*-jasmone. 4-hydroxy-*cis*-jasmone (A) 11-hydroxy-*cis*-jasmone (B) and impurities (*).

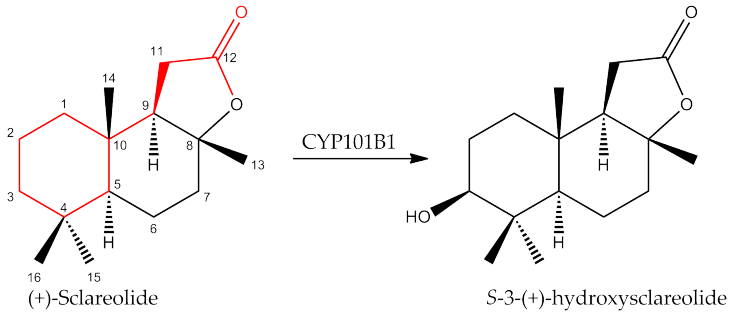

Figure 4.16: The single product isolated from (+)-sclareolide oxidation with the β-ionone-like backbone in red.

(+)-Sclareolide is a sesquiterpene lactone and was chosen as a substrate due to its β-ionone-like backbone (Figure 4.16). When compared to the norisoprenoids, it has additional bulk due to the extra carbon atoms and rings (Figure 4.1). This will indicate whether CYP101B1 tolerates larger substrates. (+)-Sclareolide gave a spin state shift of 50 % and a dissociation constant of $20 \pm 4\,\mu$M. This indicates the substrate was reasonably tightly bound in the active site of CYP101B1 when compared to other terpenoid compounds. However, the NADH consumption rate was not noticeably higher than the

rate in the absence of substrate and little or no product could be detected *in vitro*. A whole-cell turnover enabled the isolation of a single product, which was identified as (*S*)-3-(+)-hydroxysclareolide by NMR comparison to literature data (Appendix F.21, Figure 4.16).[35,36]

4.3 Discussion

Camphor has been tested with several different P450 enzymes. CYP101A1 ($P450_{cam}$) reacts with camphor stereoselectively to form 5-*exo*-hydroxycamphor with a product formation rate of 1080 min^{-1}, and 100 % coupling.[37,38] CYP101D1 and CYP101D2 both form 5-*exo*-hydroxycamphor with 99% selectivity. Both enzymes have a high coupling of >90%; product formation rates were high at $1758 \pm 36\,min^{-1}$ and $2010 \pm 102\,min^{-1}$, respectively.[1,6] CYP176A1 ($P450_{cin}$) from *Citrobacter braakii* catalysed the oxidation of both (1*R*)-(+)- and (1*S*)-(−)-camphor and formed a mixture of products. The selectivity was different from CYP101B1, with both enantiomers favouring the formation of 3-*exo*-hydroxycamphor (42 % and 39 %, respectively) over 5-*exo*-hydroxycamphor. The other products formed in decreasing yields were 5-*endo*-hydroxycamphor (32 % and 21 %, respectively), 6-*endo*-hydroxycamphor (14 % and 19 %, respectively), 3-*endo*-hydroxycamphor (7 % and 17 %, respectively) and 5-*exo*-hydroxycamphor (4 % and 5 %, respectively).[34] The coupling was 35 % for (1*R*)-(+)-camphor and 25 % for (1*S*)-(−)-camphor.[34] These enzymes all had higher product formation rates and coupling than CYP101B1 with the two camphor isomers, indicating the camphor isomers are not an ideal fit for the CYP101B1 active site.

1,8-Cineole is the natural substrate of CYP176A1. It selectively oxidises 1,8-cineole to (1*R*)-6-*exo*-hydroxy-1,8-cineole in high yield and with a high rate of oxidation.[34,39,40] This enzyme can be used for production of (1*R*)-6-*exo*-hydroxy-1,8-cineole in high yields, which can then be used for further synthesis.[34,40] CYP101B1 did not have as high a rate as CYP176A1, but it was highly selective (>90 %) for either 3-*endo*-hydroxy-1,8-cineole or 5-*endo*-hydroxy-1,8-cineole. CYP176A1 had a coupling of 80 %, which was much higher than the coupling observed with CYP101B1 (38 %).[34]

CYP101B1 had poor affinity for adamantane, 1- and 2-adamantanol but could bind 2-adamantanone more strongly. CYP101A1 can hydroxylate adamantane, forming 1-adamantanol (98 %) as the major product, with 2-adamantanol (2 %) as the remaining product.[37,38] CYP101A1 was mutated (Y96F–F193L) to improve its binding for adamantane which had the best

NADH rate of $333\,\mathrm{min}^{-1}$; the product formation rate was high at $98\,\mathrm{min}^{-1}$. However, this did lower the selectivity from 98 % for the WT enzyme to 95 % (1-adamantanol) with 2-adamantanol and even 2-adamantanone being formed.[38] CYP101D2 was mutated to suit more hydrophobic substrates, and had a much higher rate of product formation with adamantane than was obtained with CYP101B1 ($255 \pm 11\,\mathrm{min}^{-1}$).[17] Selectivity for 1-adamantanol was reduced from 98% to 95%.[16] CYP101B1 with adamantane gave a similar product distribution to other enzymes, with the major product being 1-adamantanol. However, CYP101B1 gave lower rates and coupling with adamantane, resulting in minimal product forming.

2-Adamantanone is a substrate for several other bacterial P450 enzmyes. CYP101D1 selectively oxidises 2-adamantanone to form 5-hydroxy-2-adamantanone with an NADH rate of $427 \pm 19\,\mathrm{min}^{-1}$, a product formation rate of $386 \pm 13\,\mathrm{min}^{-1}$ and a coupling of 90 %. These results were much higher than the values obtained for CYP101B1.[1] 5-Hydroxy-2-adamantanone was also formed from 2-adamantanone with CYP101A1.[37,41] CYP101B1 reacted with 2-adamantanone to form 5-hydroxy-2-adamantanone (45 %) and 6-hydroxy-2-adamantanone (55 %) but with a lower product formation rate (104 ± 9 min^{-1}) and coupling (16 %) than the other enzymes. This highlights the difference between CYP101B1 and the other related P450s, CYP101A1, CYP101D1 and CYP101D2 which despite being in the same family share <50 % sequence identity with each other.

Other examples of (+)-sclareolide oxidation have been conducted with mutants of CYP102A1 ($P450_{BM3}$). These gave (*S*)-3-(+)-hydroxysclareolide the same product as CYP101B1.[36]

Results from the monoterpenoid substrates indicate that, while the presence of a ketone increases reactivity, it does not always result in selective and efficient turnovers. The monoterpenoids had larger dissociation constants and lower rates of product formation and coupling compared to the norisoprenoids, as the substrates were potentially a poor fit for the active site. (1*R*)-(−)-Nopol and (+)-sclareolide showed the tightest binding, presumably due to their alcohol and ketone group, respectively. However, both had moderate product formation rates and coupling. Smaller substrates with low compatibility to the enzymes active site can bind in multiple orientations or can move around. This leads to a mixture of products and low selectivity. This was most evident with (1*R*)-(+)-camphor, which had four different products. However, selectivity was increased when changing (1*R*)-(+)-camphor to (+)-fenchone and further still when changing to 1,8-cineole. The best monoterpenoid substrate was 1,8-cineole, which contains an ether

oxygen within a ring and was oxidised with high selectivity. Further investigation into these types of structures could be instructive. The monoterpenoids could be modified by adding a protecting group to give them more structural similarity to the norisoprenoids, which could promote reactivity and improve selectivity.

Chapter 5

Oxidation of Monoterpenoid Acetates by CYP101B1

5.1 Introduction

In order to see whether modification of a monoterpenoid alcohol substrate to a more ionone-like substrate would improve the biocatalytic properties, available monoterpenoid acetates were examined (Figure 5.1). Fenchyl acetate, isobornyl acetate and bornyl acetate were chosen as they are related to fenchone and camphor, allowing for direct comparisons (Table 5.1). Other monoterpenoid acetate substrates were myrtenyl acetate, which is similar to (1*R*)-(−)-nopol, 5-norbornene-2-yl acetate, and α-terpinyl acetate which is related to α-terpineol (Table 5.1). Linear monoterpene acetates including neryl acetate, linalyl acetate and geranyl acetate were tested, which are the acetates of nerol, linalool and geraniol, respectively (Table 5.1).

5.2 Results

5-Norbornen-2-yl acetate is the smallest acetate compound tested and has an alkene group close to where the site of oxidation was likely to occur according to the products of camphor and (+)-fenchone. The binding of this substrate induced a spin state shift of 65 % and dissociation constant of $510 \pm 15\,\mu$M. This substrate had an NADH consumption rate of $139 \pm 5\,\text{min}^{-1}$ and a product formation rate of $75 \pm 18\,\text{min}^{-1}$. As a result, the coupling was 54 %, which was higher than all of the terpenoids analysed in Chapter 4. In the

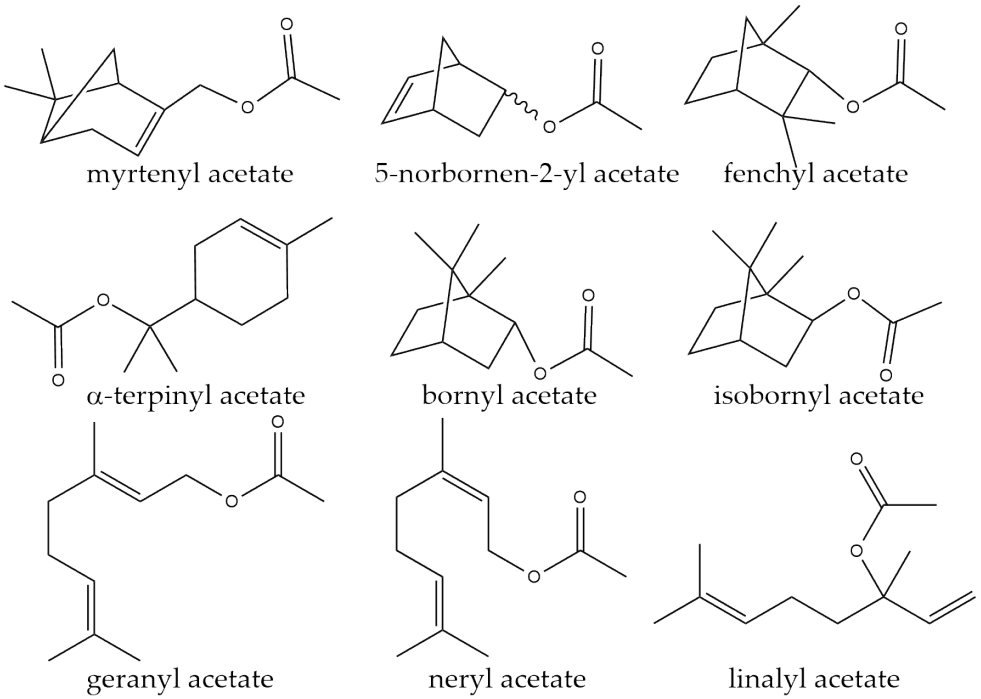

Figure 5.1: The monoterpenoid acetate substrates tested with CYP101B1

turnovers of substrate, the product formed was 5-epoxynorborane-2-yl acetate, assigned from the loss of the alkene peaks and the two new peaks at 3.35 ppm and 3.25 ppm (Appendix F.19). The NMR also indicated that the other epoxide isomer has been formed, but it was not isolated in enough yield to identify.

α-Terpinyl acetate had a higher spin state shift of 70 % compared to α-terpineol (10 % HS). However, the NADH consumption rate ($246 \pm 28\,\mathrm{min}^{-1}$) was low and no products were observed in the *in vitro* or *in vivo* turnovers. As a result of this, α-terpinyl acetate was not pursued further. Neryl acetate gave a spin state shift of 80 %, higher than that of nerol (25 % HS). The NADH consumption rate ($1070 \pm 70\,\mathrm{min}^{-1}$) was high and a single product was generated (m/z 212.1 AMU) (Figure 5.2). Geranyl acetate and linalyl acetate produced spin state shifts of 55 % and 35 % respectively, greater than those of geraniol (15 % HS) and linalool (25 % HS). The NADH consumption rates ($281 \pm 5\,\mathrm{min}^{-1}$ and $109 \pm 3\,\mathrm{min}^{-1}$, respectively) were not as high as that of neryl acetate. Several single oxidation products were formed for these substrates (m/z 212.1 AMU). The products were unable to be isolated in sufficient yield after chromatography. To fully characterise these products, a larger scale turnover and different purification methods would be required.

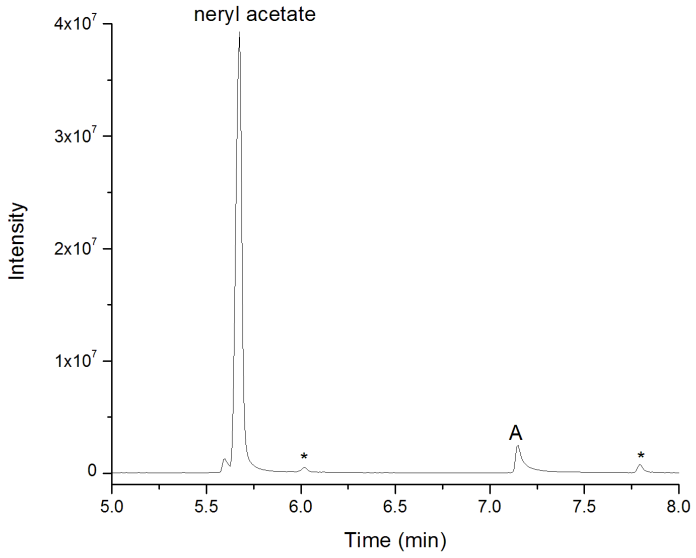

Figure 5.2: GC-MS analysis of CYP101B1 *in vivo* turnover of neryl acetate (black), unidentified single oxidation product (A) and impurities (*).

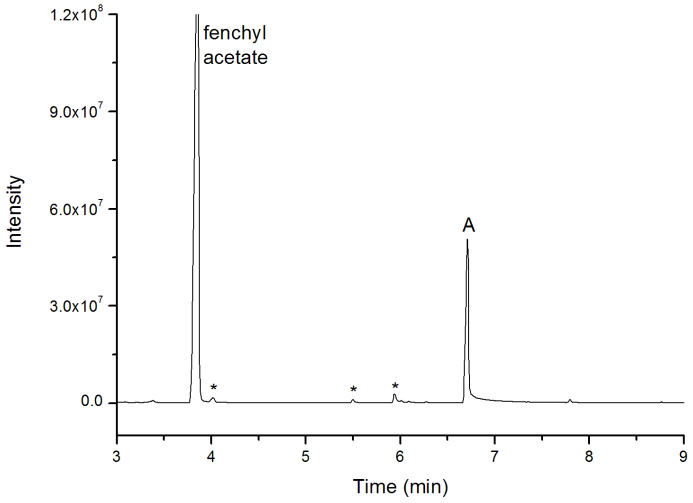

Figure 5.3: GC-MS analysis of CYP101B1 *in vivo* turnover of fenchyl acetate (black), 5-*exo*-hydroxy-fenchyl acetate (A) and impurities (*).

Fenchyl acetate has a similar structure to (+)-fenchone, replacing the ketone group with an acetate group. This makes fenchyl acetate more like the

norisoprenoids (Figure 5.1). Fenchyl acetate induced a spin state shift of 80 % (Figure 5.6a compared to Figure 5.6b) and was bound with a dissociation constant of $7.3 \pm 0.8\,\mu$M. Therefore, the spin state shift of CYP101B1 with fenchyl acetate is higher than that of (+)-fenchone, with a 74-fold increase in binding affinity. The NADH consumption rates were similar for the two substrates, with the fenchyl acetate activity being $1220 \pm 5\,\text{min}^{-1}$. However, a major improvement was observed for the product formation rate ($1110 \pm 26\,\text{min}^{-1}$), due to an increase in coupling (90 %). Selectivity for (+)-fenchone for the major product 5-*exo*-hydroxyfenchone was 75 %. Fenchyl acetate oxidation generated a single product identified as 5-*exo*-hydroxy-fenchyl acetate (Figure 5.4 and 5.3). This was determined from the NOESY correlation between H5 and H8 (Appendix F.16).

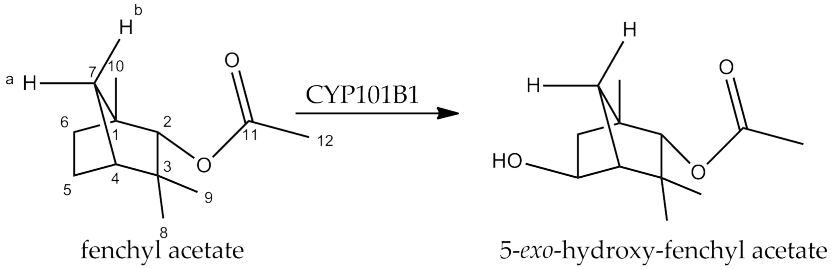

Figure 5.4: The single product produced from the whole-cell turnover of fenchyl acetate

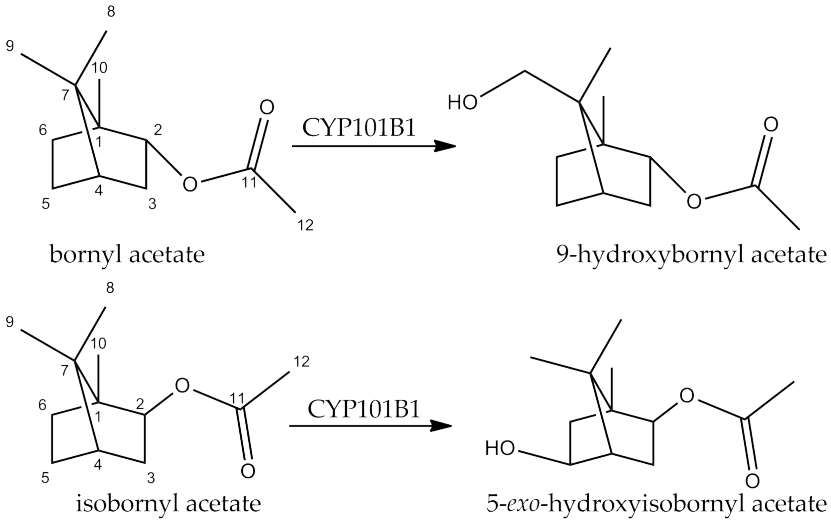

Figure 5.5: Isobornyl acetate and bornyl acetate products from the *in vitro* turnovers with CYP101B1

Isobornyl acetate and bornyl acetate are related to camphor and are the acetates of isoborneol (*exo*) and borneol (*endo*) (Figure 5.1). Isobornyl acetate and bornyl acetate induced spin state shifts of $\geq 95\,\%$ (Figure 5.6d and Figure 5.6f, respectively) with CYP101B1, compared to 60 % for isborneol and borneol (Figure 5.6c and Figure 5.6e, respectively). The dissociation constant of (1*R*)-(+)-camphor was $330 \pm 10\,\mu$M (Table 4.1), whereas isobornyl acetate and bornyl acetate had much tighter binding to CYP101B1, with dissociation constants of $14.2 \pm 0.2\,\mu$M and $0.71 \pm 0.04\mu$M, respectively. The NADH consumption rate ($2000 \pm 73\,\text{min}^{-1}$), product formation rate (1250 ± 45 min^{-1}) and coupling (61 %) for isobornyl acetate were all higher than those of (1*R*)-(+)-camphor (Table 4.1). CYP101B1 produced 5-*exo*-hydroxyisobornyl acetate regio- and stereoselectively from isobornyl acetate (Figure 5.5). This product was assigned due to the coupling between *endo* H5 at 3.80 ppm and H4 at 1.78 ppm and no coupling between *endo* H5 and H9 in the NOESY (Appendix F.18). This oxidation is more selective than (1*R*)-(+)-camphor, which formed four main oxidation products.

Table 5.1: Terpenoid acetate substrate binding, steady state kinetic data and coupling with CYP101B1. Steady state turnover activities were measured using a ArR:Arx:CYP101B1 concentration ratio of 1:10:1 (0.5 μM CYP enzyme, 50 mM Tris, pH 7.4). Coupling is the percentage efficiency of NADH utilization for the formation of products. Rates are reported as mean $\pm$ S.D.($n \geq 3$) and given in nmol(nmol-CYP)$^{-1}$min^{-1}.

CYP101B1/ substrate	%HS heme	K_d (μM)	NADH consumption rate (min^{-1})	Product formation rate (min^{-1})	Coupling %
(+)-fenchone	50	540 ± 20	1110 ± 78	198 ± 23	18
fenchyl acetate	80	7.3 ± 0.8	1220 ± 5	1110 ± 26	90
(1*R*)-(+)-camphor	55	330 ± 10	1040 ± 9	153 ± 24	15
isobornyl acetate	≥ 95	14.2 ± 0.2	2000 ± 73	1250 ± 45	61
bornyl acetate	≥ 95	0.71 ± 0.04	3080 ± 68	596 ± 48	19
(1*R*)-(−)-nopol	50	60 ± 2	553 ± 87	165 ± 32	30
myrtenyl acetate	≥ 95	5.04 ± 0.8	1700 ± 14	1520 ± 30	90
5-norborene-2-yl acetate	65	510 ± 15	139 ± 5	75 ± 18	54
α-terpinyl acetate	70	-	246 ± 28	-	-
neryl acetate	80	-	1070 ± 70	-	-
geranyl acetate	55	-	281 ± 5	-	-
linalyl acetate	35	-	109 ± 3	-	-

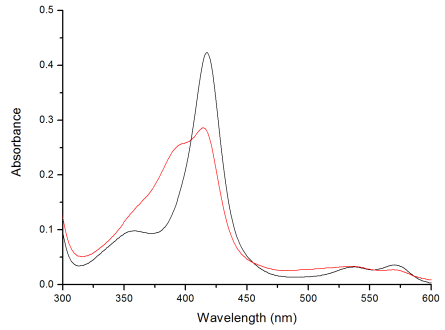

(a) (+)-fenchone

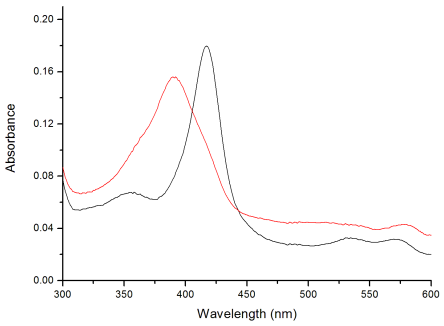

(b) fenchyl acetate

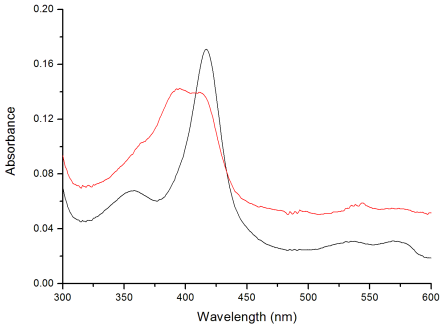

(c) isoborneol

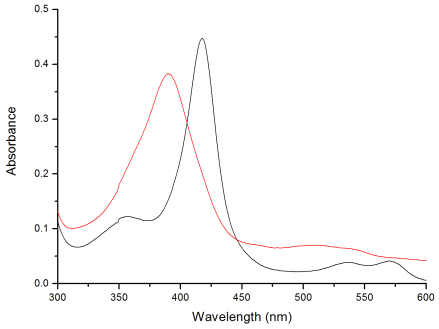

(d) isobornyl acetate

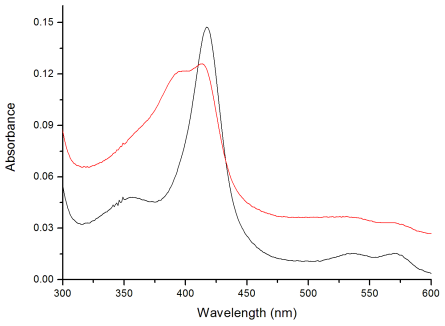

(e) borneol

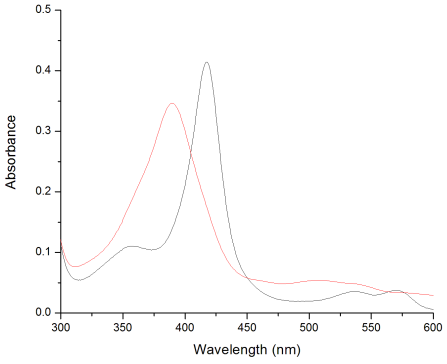

(f) bornyl acetate

Figure 5.6: Spin state shifts for selected terpenoid acetate and parent terpenoid substrates

The activity of CYP101B1 and bornyl acetate gave an NADH consumption rate of $3080 \pm 68\,\mathrm{min}^{-1}$, a product formation rate of $596 \pm 48\,\mathrm{min}^{-1}$ and a coupling of 19 %, all of which were higher than the activities of CYP101B1 with (1*R*)-(+)-camphor (Table 4.1). However, the product formation rate and coupling were lower than isobornyl and fenchyl acetate. One product was generated and identified as 9-hydroxybornyl acetate (Figure 5.5). This was one of the four sites where oxidation occurred for (1*R*)-(+)-camphor. The product was assigned from the two H9 signals and the loss of the methyl group signal, as well as the NOE correlation between H9 and H5 and between H2 and H8(Appendix F.17).

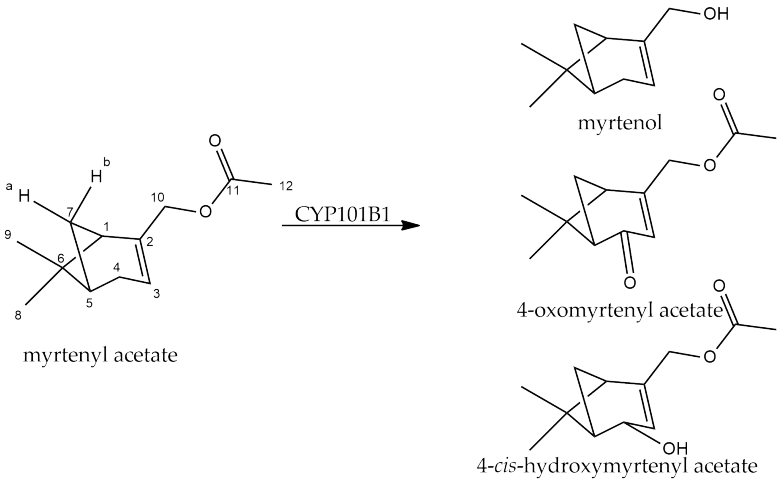

Figure 5.7: Myrtenyl acetate products from the *in vivo* turnover.

Myrtenyl acetate is the acetate of myrtenol, a hydroxylated version of α-pinene. The location of the acetyl group puts the ketone in the same relative position to the ring system as in the norisoprenoids. The [3.1.1] bicyclic ring structure differs from the fenchyl and bornyl acetate [2.2.1] bicyclyic ring structures (Figure 5.1). Myrtenyl acetate binding to CYP101B1 gave a spin state shift of ≥ 95 % and tight binding ($5.04 \pm 0.8\,\mu$M). The NADH consumption rate ($1700 \pm 14\,\mathrm{min}^{-1}$), product formation rate ($1520 \pm 30\,\mathrm{min}^{-1}$) and coupling (90 %) were all high, indicating highly efficient catalysis with CYP101B1. Myrtenyl acetate oxidation gave one product in the *in vitro* turnover, which was identified as 4-*cis*-hydroxymyrtenyl acetate (Figure 5.8). The coupling, shown in the COSY, between H4 and H5, and between H4 and H3 along with W coupling between H4 and H7a and an m/z of 210.2 AMU indicated the product was 4-*cis*-hydroxymyrtenyl acetate. The *in vivo* gave the 4-*cis*-hydroxymyrtenyl acetate product and the further oxidation product 4-oxomyrtenyl acetate, along with the hydrolysis product myrtenol

(Figure 5.7 and 5.8). Hydrolysis was only observed in the whole cell oxidation turnover. Myrtenol was easily identified by NMR due to the 2H signal at 3.99 ppm and the disappearance of the acetyl methyl group as well as the GC-MS m/z of 152.2 AMU. 4-Oxomyrtenyl acetate was then identified due to the ketone peak at 202.9 ppm, the absence of the alcohol H peak and the slightly decreased m/z of 208.2 AMU (Appendix F.20).

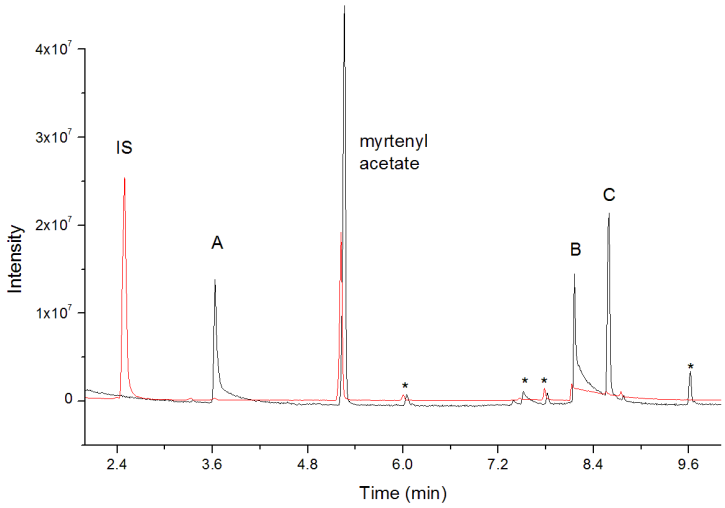

Figure 5.8: GC-MS analysis of CYP101B1 turnovers of myrtenyl acetate. *in vivo* (black), *in vitro* (red), myrtenol (A) 4-*cis*-hydroxymyrtenyl acetate (B), 4-oxomyrtenyl acetate (C), internal standard (IS) and impurities (*).

5.3 Discussion

All the monoterpenoid acetates, except bornyl acetate, had higher product formation rates and coupling than the terpenoid substrates in Chapter 4). This is most likely due to the substrate fitting better in the active site of CYP101B1, resulting in the NADH being used more efficiently. This better active site fit led to oxidation occurring at a single site on the monoterpenoid acetates. Comparing the site of oxidation for bornyl acetate and isobornyl acetate, oxidation shifted from C9 to C5, indicating that oxidation generally occurs 5 carbons away from the carbonyl and on the opposite side to the acetate group (Figure 5.9). Fenchyl acetate and bornyl acetate have the acetate group in the same orientation relative to the ring structure. The

only difference is the two methyl groups, which are shifted from C3 to C7. When just hydrogens are present on C7, they are too far away for oxidation to occur. However, the presence of a methyl group results in these C−H bonds being close enough for oxidation to occur. This resulted in the alcohol group being formed at C5 for fenchyl acetate and C9 for bornyl acetate. With these small structural changes, vital information was obtained about how CYP101B1 binds these acetate substrates and the dependence of the acetate group on the oxidation site.

Myrtenyl acetate was the only substrate for which hydrolysis of the acetate occurred to form myrtenol. The position of the acetate group further from the cyclohexane ring may result in easier access for hydrolysis. Oxidation of myrtenyl acetate occurs on the allylic carbon next to the alkene. This carbon is more reactive than alkyl group, which is probably why further oxidation occurred with this monoterpenoid acetate but not the others. The substrate also has a longer side chain, which is the same length as the ionone compounds and, as a result, is probably a better fit for the active site. This leads to better binding and, therefore, further oxidation.

α-Terpinyl acetate did not produce enough products for identification. The site where oxidation is most likely to occur would be where the alkene and methyl group are located on the cyclohexene ring. This is a non-ideal fit for the active site and results in no product being produced. Purification of the linear acetates did not result in significant yield for identification. This problem was also observed for pseudoionone and these substrates need further investigation into suitable purification methods.

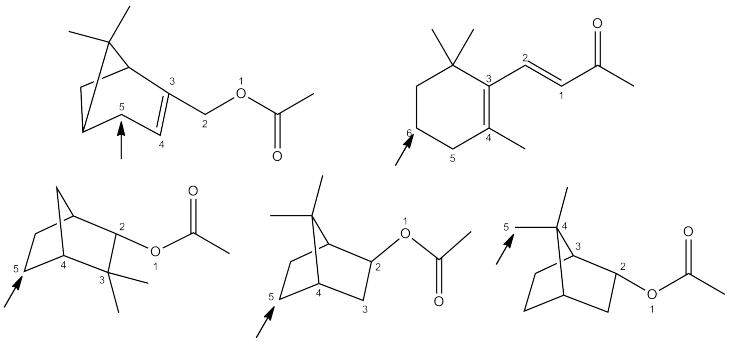

Figure 5.9: Showing the site of oxidation for the monoterpenoid acetates and β-ionone which is 6 or 7 carbons away from the ketone group.

Overall, from the few monoterpenoid acetate substrates tested it can be seen that there was a general increase in the activity and selectivity of CYP101B1 as a biocatalyst when compared to the monoterpenoids. This reinforces what was observed in Chapter 3; that is, a ketone on the side chain is important for selectivity and activity. Hence, it can be concluded that oxidation often occurs on the carbon 5 bonds, away from the carbonyl (Figure 5.9). There is a relationship between the orientation of the acetate group and the product formed. This was most obvious when comparing the sites of oxidation for fenchyl acetate, bornyl acetate and isobornyl acetate. Further investigation into other acetate- and ester- related compounds could allow selection of where oxidation occurs based on the location of the carbonyl. This could result in high activities and regio- and stereoselective C−H bond oxidation reactions.

Chapter 6

The Oxidation of Two-ring Aromatics by CYP101B1

6.1 Introduction

The reactions in Chapter 3 with indole, phenylcyclohexane and *p*-cymene indicated that CYP101B1 could bind aromatic structures. Further investigation of aromatic compounds was necessary to determine the affinity of CYP101B1 for a wider range of aromatic substrates. Substrates were chosen with a similar structures to phenylcyclohexane, as two-ring aromatics appeared to be favoured by CYP101B1.

6.2 Results

Initially, biphenyl and naphthalene were examined, but they did not induce a large spin state shift with CYP101B1 and only a small amount of product was observed. The NADH consumption rate for naphthalene was reasonably fast and increased as the reaction continued (Figure 6.1). This suggested the compound being formed might be turned over more efficiently by CYP101B1 than the initial substrate. Phenylphenols and naphthols were therefore tested as potential substrates for CYP101B1. Naphthols resulted in higher spin state shifts and very high NADH consumption rates, but after analysing the *in vitro* turnovers, no significant levels of product were observed. Further experiments were conducted with *in vitro* turnovers in the absence of CYP101B1 and a large NADH consumption rate was still observed.

The phenylphenols also had higher spin state shifts compared to biphenyl. The rates were lower than the naphthols and biphenyl, but again little or no product was observed (Table 6.1). β-Tetralone gave a reasonably high spin state shift of 40%. This substrate was tested initially before a normal *in vitro* turnover and a very high rate, 4540 min^{-1}, was observed. This led to the conclusion that naphthols, phenylphenols and tetralones can accept electrons from the electron partners faster than the P450. This causes increased NADH consumption rate and channels the reducing equivalents away from product formation. These results indicate CYP101B1 was not reacting with the aromatic substrates. The increased rates with naphthalene could be due to the generation of a small amount of naphthol, which then competes with CYP101B1 for the electrons from the reducing equivalents.

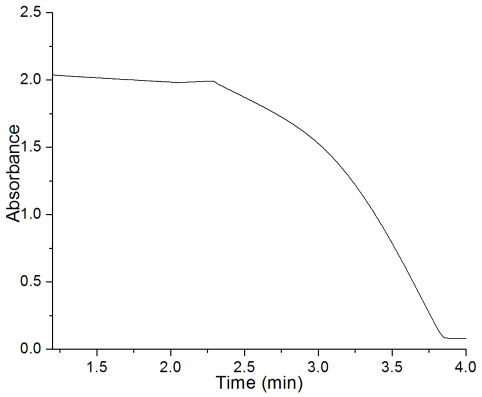

Figure 6.1: The NADH consumption of CYP101B1 turnover of naphthalene monitored at 340 nm by UV-Vis spectrometry.

Table 6.1: Phenylphenol and naphthol steady state kinetic data with CYP101B1. Steady state turnover activities were measured using a ArR:Arx:CYP101B1 concentration ratio of 1:10:1 (0.5 μM CYP enzyme, 50 mM Tris, pH 7.4). Rates are reported as mean $\pm$ S.D.($n \geq 3$) and given in nmol(nmol-CYP)$^{-1}$min^{-1}.

CYP101B1/ substrate	%HS heme	NADH consumption rate (min^{-1})	NADH rate No P450 (min^{-1})
naphthalene	20	90 $\pm$ 75	-
1-naphthol	65	2090 $\pm$ 90	1600
2-naphthol	40	560 $\pm$ 60	-
biphenyl	25	200 $\pm$ 10	-
2-phenylphenol	35	90 $\pm$ 1	74
3-phenylphenol	40	80 $\pm$ 8	-
4-phenylphenol	40	110 $\pm$ 10	-
β-tetralone	40	-	4540

The difficulty of recording the activity of CYP101B1 with naphthalene, biphenyl and their hydroxy analogues led to the choice of substrates with similar structures but containing more reactive benzylic sp^3 C−H bonds (Figure 6.2).

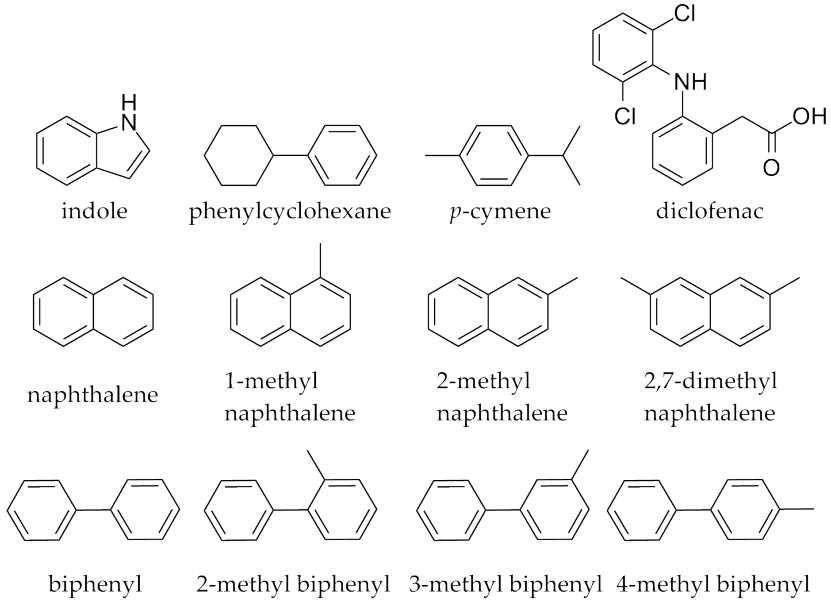

Figure 6.2: Aromatic Substrates tested with CYP101B1

1-Methyl naphthalene bound reasonably tightly to CYP101B1, with a spin state shift of 55 % (Figure 6.4a) and a dissociation constant of 62 ± 5 μM (Table 6.2). This spin state shift was higher than naphthalene (20 %) and 2-naphthol (40 %) and nearly as high as 1-naphthol (65 %). The dissociation constant was much higher than the norisoprenoids but tighter than most of the monoterpenoid compounds (Chapter 4). The NADH consumption rate (240 ± 17 min^{-1}), product formation rate (38 ± 10 min^{-1}) and coupling (16 %) were moderate compared to phenylcyclohexane, norisoprenoids and monoterpenoid acetates. A single product, observed by HPLC, co-eluted with 1-naphthyl methanol in accordance with the preference for aliphatic C−H bond oxidation (Figure 6.3, Appendix E.5).

2-Methyl naphthalene induced a lower spin state shift (40 %) than 1-methyl naphthalene. The activity of CYP101B1 with 2-methyl naphthalene gave an NADH consumption rate of 212 ± 24 min^{-1}, a product formation rate of 57 ± 18 min^{-1} and coupling of 26 % which were similar to 1-methyl naphthalene (Table 6.2). It produced 2-naphthyl methanol as the oxidised product *in vitro* which was identified by HPLC co-elution (Figure 6.3, Appendix E.6).

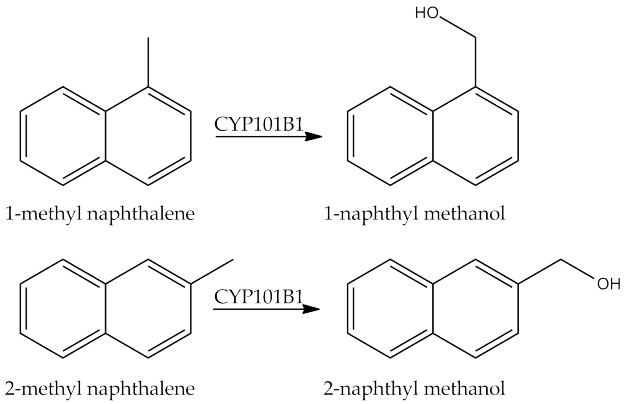

Figure 6.3: 1-methyl naphthalene and 2-methyl naphthalene products from the *in vitro* turnovers

Table 6.2: Aromatic substrate binding, steady state kinetic data and coupling with CYP101B1. Steady state turnover activities were measured using a ArR:Arx:CYP101B1 concentration ratio of 1:10:1 (0.5 μM CYP enzyme, 50 mM Tris pH 7.4). Coupling is the percentage efficiency of NADH utilization for the formation of Products. Rate are reported as mean $\pm$ S.D.($n \geq 3$) and given in nmol(nmol-CYP)$^{-1}$min^{-1}.

CYP101B1/ substrate	%HS heme	NADH consumption rate (min^{-1})	Product formation rate (min^{-1})	Coupling %
1-methyl naphthalene	55	240 $\pm$ 17	38 $\pm$ 10	16
2-methyl naphthalene	40	212 $\pm$ 24	57 $\pm$ 18	26
2,7-dimethyl naphthalene	30	448 $\pm$ 44	79 $\pm$ 10	18
1-ethyl naphthalene	20	482 $\pm$ 7	18 $\pm$ 3	4
2-ethyl naphthalene	20	284 $\pm$ 5	20 $\pm$ 1	7
2-methyl biphenyl	20	257 $\pm$ 9	35 $\pm$ 8	14
3-methyl biphenyl	20	127 $\pm$ 10	30 $\pm$ 2	23
4-methyl biphenyl	20	176 $\pm$ 10	39 $\pm$ 7	22
diclofenac	5	-	-	-

2,7-Dimethyl naphthalene had a lower spin state shift (30%, Figure 6.4b) than 1-methyl naphthalene and 2-methyl naphthalene. The activity of CYP101B1 with 2,7-dimethyl naphthalene was higher as measured by NADH consumption rate (448 $\pm$ 44 min^{-1}). The product formation rate (79 $\pm$ 10 min^{-1}) and the coupling (18 %) were moderate (Table 6.2). The *in vitro* turnover produced a single oxidation product. However, the likely benzylic alcohol prod-

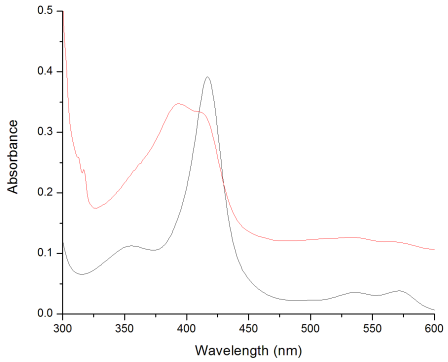

(a) 1-methyl naphthalene

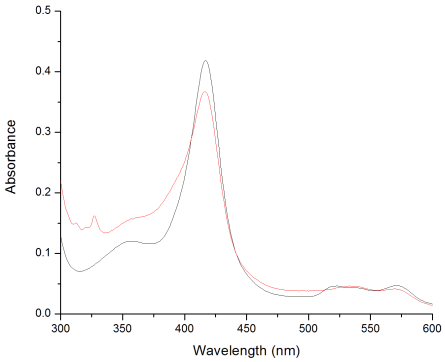

(b) 2,7-dimethyl naphthalene

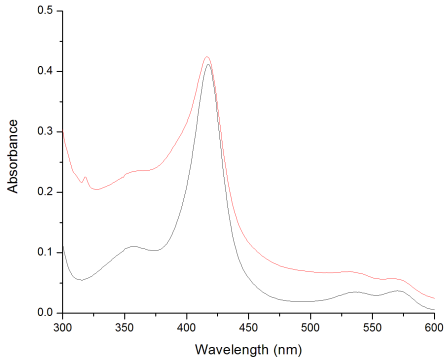

(c) 2-ethyl naphthalene

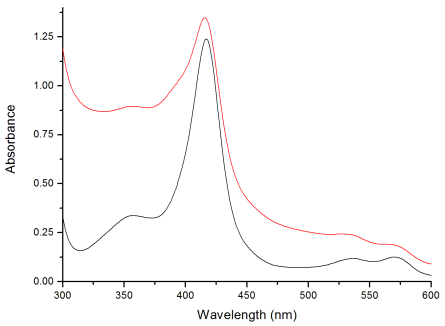

(d) 4-methyl biphenyl

Figure 6.4: Spin state shifts for selected aromatic compounds

uct of 2,7-dimethyl naphthalene was not available for co-elution so an *in vivo* turnover was conducted. The *in vivo* turnover converted all the substrate into a single oxidation product, but this did not co-elute with the *in vitro* turnover product. The *in vivo* turnover product was identified as a carboxylic acid instead of the alcohol by NMR, predominantly due to the lack of OH peak in ^{1}H NMR and a carboxylic acid shift of 168.38 ppm in the ^{13}C NMR (Figure 6.5, Appendix F.22). The limiting reagent in the *in vitro* turnover is NADH, so further oxidation rarely occurs as the substrate is present in excess (Figure 6.6). After reducing the carboxylic acid with lithium aluminium hydride, the alcohol product co-eluted with the product of the *in vitro* turnover, confirming that the product was 2-(7-mehtylnaphthyl)methanol (Figure 6.5).

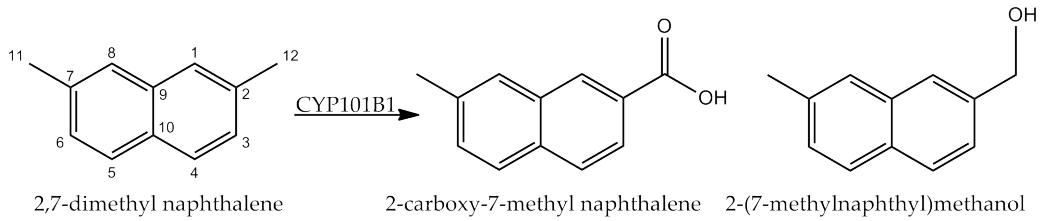

Figure 6.5: 2,7-Dimethyl naphthalene products from the *in vitro* and *in vivo* turnovers

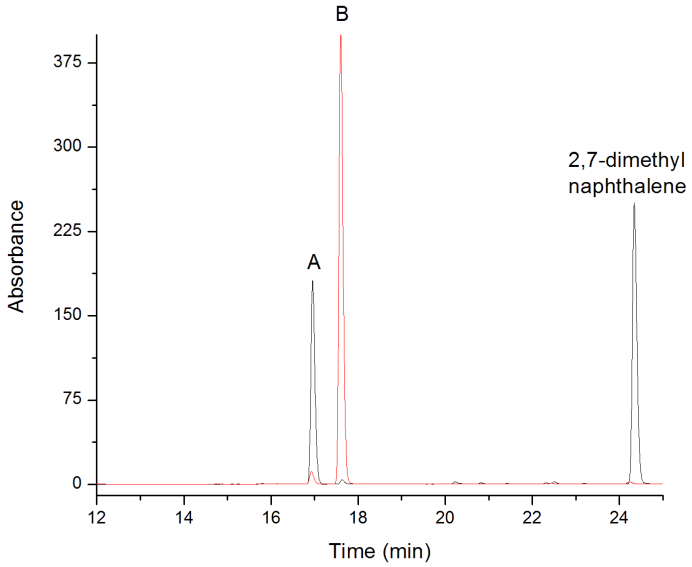

Figure 6.6: HPLC analysis of CYP101B1 turnovers with 2,7-dimethyl naphthalene. *in vitro* (black) and *in vivo* (red), 2-(7-mehtylnaphthyl)methanol (A) and 2-carboxy-7-methylnaphthalene (B).

Both ethyl naphthalenes had spin state shifts of 20% (Figure 6.4c). This was lower than the equivalent methyl naphthalene, indicating that the larger ethyl groups were not as well tolerated in the active site of CYP101B1. 1-Ethyl naphthalene had a larger NADH consumption rate ($482 \pm 7\,\mathrm{min}^{-1}$) compared to 2-ethyl naphthalene ($284 \pm 5\,\mathrm{min}^{-1}$), which agrees with the methyl naphthalenes data as the 1- substituted methyl naphthalene was also faster at consuming NADH. The product formation rate with 1-ethyl naphthalene ($18 \pm 3\,\mathrm{min}^{-1}$) was lower than 2-ethyl naphthalene ($20 \pm 1\,\mathrm{min}^{-1}$) (Table 6.2). The product formation rate and coupling for the ethyl naphthalenes were half the values of the methyl naphthalenes. This was consistent with the lower

spin state shift, indicating more water may be held in the active site, which is known to cause uncoupling reactions to form hydrogen peroxide.[7–9] However, the ethyl naphthalenes would be expected to be more reactive as the radical produced from the benzylic methylene is more stable than that produced from the benzylic methyl. This indicates the ethyl naphthalenes are a poor fit for the active site of CYP101B1. The oxidation occurred on the more reactive methylene carbon, with 1-ethyl naphthalene being converted to 1-naphthyl-1-ethanol and 2-ethyl naphthalene being converted to 2-naphthyl-1-ethanol (Figure 6.7). These were both identified by HPLC co-elution experiments with product standards (Appendix E.7 and E.8).

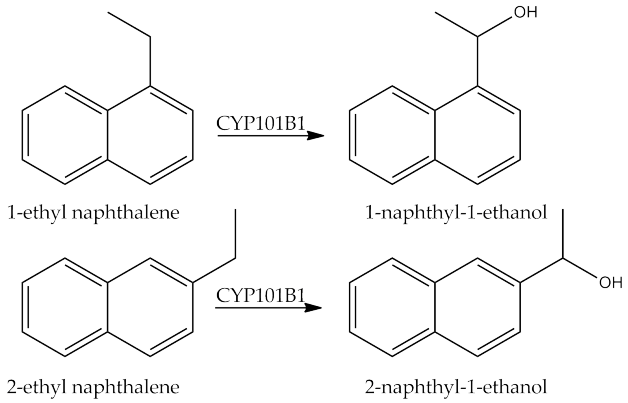

Figure 6.7: 1-ethyl naphthalene and 2-ethyl naphthalene products from the *in vitro* turnovers

Methyl biphenyls with the methyl group at the 2, 3 and 4 positions were investigated. These compounds produced low spin state shifts of only 20% with CYP101B1 (Figure 6.4d), which were lower than biphenyl and the equivalent phenylphenols. 2-Methyl biphenyl had the fastest NADH consumption rate ($257 \pm 9\,\mathrm{min}^{-1}$) but the product formation rate was moderate ($35 \pm 8\,\mathrm{min}^{-1}$) due to the coupling of only 14 %. 3-Methyl biphenyl had the slowest NADH consumption rate ($127 \pm 10\,\mathrm{min}^{-1}$) but its product formation rate ($30 \pm 2\,\mathrm{min}^{-1}$) was comparable to that of 2-methyl biphenyl due to a higher coupling (23 %) (Table 6.2). Turnovers of both substrates generated the appropriate methanol biphenyl products as the sole product (Figure 6.8). 2-Methanol biphenyl was identfied by HPLC co-elution experiments with a product standard (Appendix E.9). The product for 3-methyl biphenyl was identified by NMR after an *in vivo* turnover was conducted. The 2H signal at 4.77 ppm and the 9H signals in the aromatic region allowed easy characterisation (Appendix F.23). In contrast to 2,7-dimethyl naphthalene, the *in vivo* reaction did not further oxidise the 3-methanol biphenyl to the carboxylic acid despite only a small amount of substrate remaining in the turnover.

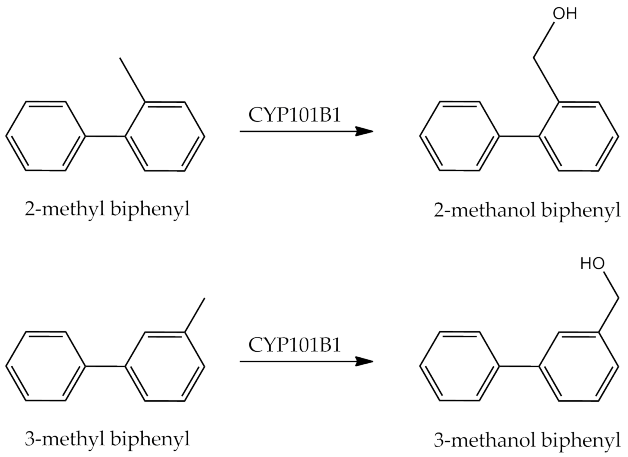

Figure 6.8: Products from the turnovers of 2-methyl biphenyl and 3-methyl biphenyl

4-Methyl biphenyl had an NADH consumption rate of $176 \pm 10\,\mathrm{min}^{-1}$ and the highest product formation rate of the methyl biphenyls ($39 \pm 7\,\mathrm{min}^{-1}$). The coupling (22%) was similar to 3-methyl biphenyl and higher than the 2-methyl biphenyl (Table 6.2). The *in vitro* enzyme turnover of 4-methyl biphenyl gave two major products. (1,1̂-Biphenyl)-4-methanol (30%) was identified via HPLC co-elution; however, the major product (70%) remained unknown. It was initially thought further oxidation of the (1,1̂-biphenyl)-4-methanol product may occur, producing the carboxylic acid as was seen with 2,7-dimethyl naphthalene. An *in vitro* turnover was conducted with the (1,1̂-biphenyl)-4-methanol in an attempt to prove this. However, this was not the case as the product from the 4-methyl biphenyl turnover did not co-elute with any peaks in the (1,1̂-biphenyl)-4-methanol turnover (Figure 6.10). Therefore, a whole-cell turnover was conducted with 4-methyl biphenyl in an attempt to isolate this unknown product. After isolation by column chromatography, it was identified as 4-methyl-4̂-hydroxybiphenyl (A) by NMR due to the presence of the characteristic methyl and the four doublets in the aromatic region (Figure 6.11, Appendix F.24). The major product formed via the NIH shift mechanism with an epoxide intermediate and was the only example of this activity observed with CYP101B1. None of the 4-methyl-3̂-hydroxybiphenyl potential product was observed in the turnover as it was the less favoured intermediate due to the resonance structures being less stable (Figure 6.9).

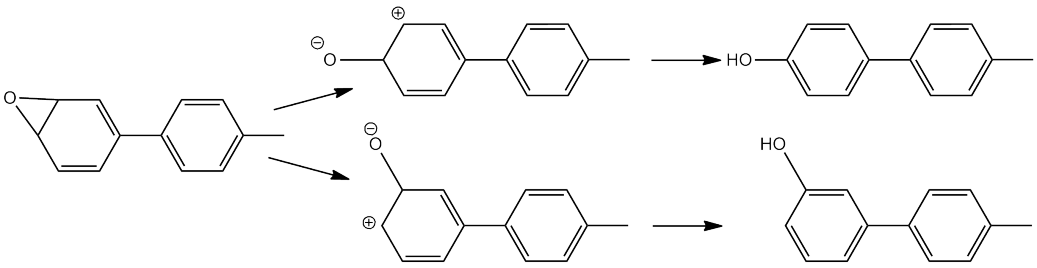

Figure 6.9: Reaction scheme for the oxidation of 4-methyl biphenyl via a NIH shift rearrangement.

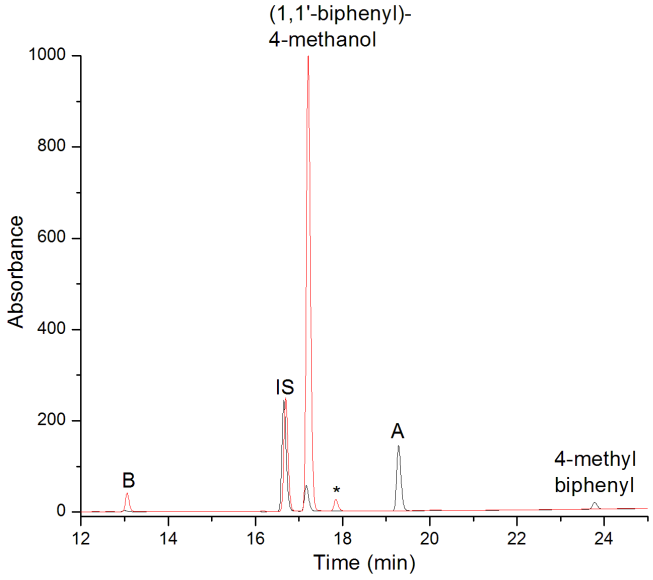

Figure 6.10: HPLC analysis of *in vitro* CYP101B1 turnovers for 4-methyl biphenyl (black) and (1,1'-biphenyl)-4-methanol (red), 4-methyl-4'-hydroxybiphenyl (A), 4-methanol-4'-hydroxybiphenyl (B), internal standard (IS) and impurities (*)

The further oxidation product of the (1,1'-biphenyl)-4-methanol oxidation was (4-hydroxy-1,1'-biphenyl)-4-methanol (B), which was purified from an *in vivo* turnover and analysed by NMR (Figure 6.11, Appendix F.25). This indicates that further oxidation on the other side of the ring is preferred over formation of the carboxylic acid. This was the only methyl biphenyl for which this activity was observed. The methyl group at the 4 position must give this molecule a shape which allows it to bind in a favourable orientation

in the substrate binding pocket of CYP101B1. Oxidation on the aromatic ring, which is achieved by an NIH shift mechanism, was not observed with the majority of the aromatic substrates tested with CYP101B1.

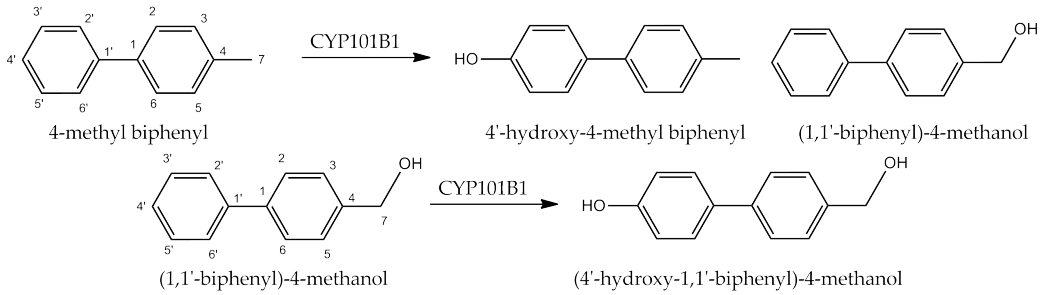

Figure 6.11: 4-Methyl biphenyl and (1,1'-biphenyl)-4-methanol products from the *in vitro* turnovers.

Finally, diclofenac was chosen as it has a similar structure to biphenyl. It is a nonsteroidal anti-inflammatory drug molecule which allowed testing into whether CYP101B1 had potential to react with larger compounds. Diclofenac induced a low spin state shift of 5% with CYP101B1 (Table 6.2). It absorbed strongly at 340 nm, preventing accurate *in vitro* NADH consumption analysis. However, a whole-cell turnover showed that CYP101B1 could turnover diclofenac to a single product. This was identified by literature NMR as 4-hydroxydiclofenac (Figure 6.12).[42,43]

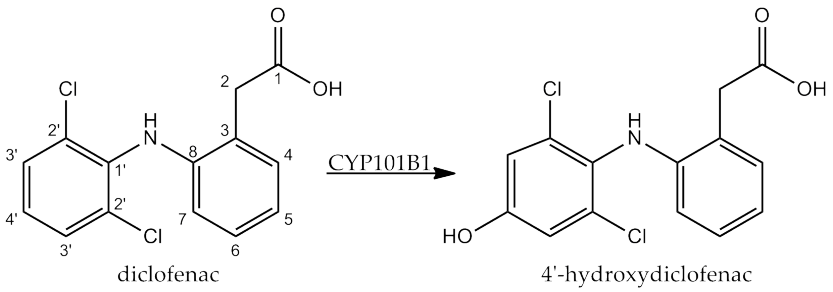

Figure 6.12: Product from the turnover over of diclofenac

6.3 Discussion

Naphthalene oxidation produces two products, 1-naphthol and 2-naphthol, via an NIH shift rearrangement. P450 oxidation on aromatic rings occurs

by the NIH shift rearrangement mechanism, which involves an epoxide intermediate (Figure 6.13).[44,45] There are two possible places for the epoxide to form: the 1,2-oxide or the 2,3-oxide. However, the 2,3-oxide is unstable so usually does not form.[46] Not enough product was obtained to determine which naphthols formed with naphthalene and CYP101B1. This was probably due to any naphthol product which formed accepting electrons from the ferredoxin and competing with product formation. However, in all likelihood 1-naphthol was the major product as it has more stable resonance structures for the intermediate compound (Figure 6.13). The turnover of biphenyl with CYP101B1 suffered from the same problem in that not enough product was made to allow characterisation.

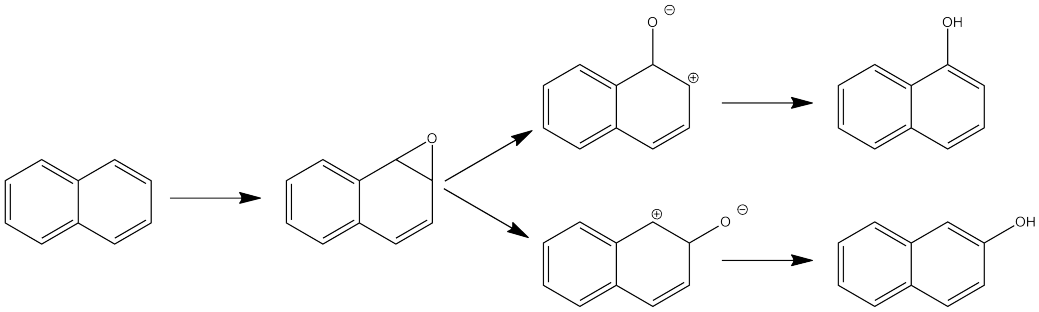

Figure 6.13: Reaction scheme for the oxidation of naphthalene via a NIH shift rearrangement.

Naphthalene has been reacted with CYP101A1 ($P450_{cam}$) with limited success; the NADH consumption rate was $23.9\,min^{-1}$ and coupling was 3% with the wild type enzyme.[46] The rate was increased by mutating the enzyme to give it a more hydrophobic active site. The Y96F mutant was more favourable for naphthalene oxidation, resulting in an NADH consumption rate of $181\,min^{-1}$ and coupling of 55%.[46] CYP101A1 and its other mutations all formed 1-naphthol (97%) as the major product and 2-naphthol (3%) in very small amounts.[46] This is due to the intermediate resulting in 1-naphthol formation being more stable from the more stable resonance structures (Figure 6.13). Naphthalene has been converted into naphthol by mutated forms of CYP102A1 ($P450_{Bm3}$). The A74G/F87V/L188Q mutant generates 1-naphthol (96%) and 2-naphthol as the minor product (4%). The NADH consumption rates were higher than those of the other P450s, with rates as high as $1420\,min^{-1}$ for one of the mutants; however, the coupling was lower at only 11 %.[47] 1-Naphthol was also formed from a turnover using a different mutant from CYP102A1 (A330P) which had higher rates ($1306\,min^{-1}$ for the NADH rate and $666\,min^{-1}$ for the product formation rate) which resulted in

higher coupling (51 %).[48] All the mutated P450s had higher rates of reaction and product formation than CYP101B1 due to the non-ideal fit in the enzyme active site with naphthalene.

Two methyl naphthalenes and some dimethyl naphthalenes, although not 2,7-dimethyl naphthalene, have also been investigated with mutant forms of CYP102A1 ($P450_{Bm3}$). 1-Methyl naphthalene produced almost equal amounts of 1-naphthyl methanol and 1-methanol-4-hydroxy naphthalene. Similarly, with 2-methyl naphthalene, 2-methyl-5-hydroxy naphthalene and 1-hydroxy-2-methyl naphthalene were observed in equal amounts.[49] None of the dimethyl naphthalenes tested formed a carboxlyic acid, although further oxidation was observed on the other methyl group resulting in dihydroxymethyl naphthalenes.[49] This is presumably due to structural differences between CYP101B1 and CYP102A1 defining the orientation of the naphthalenes analogs relative to the heme iron in the enzyme active site. Potentially, 2,7-dimehtyl naphthalene had a higher product formation rate compared to the other compounds due to the symmetric nature of the methyl groups leading to easier molecular recognition.

As diclofenac is a drug compound, its reaction with mammalian P450s has been extensively studied. CYP2C8 generated 5-hydroxydiclofenac, and CYP-2C9 oxidation resulted in 3-hydroxydiclofenac and 4-hydroxydiclofenac.[50] Bacterial enzymes have also been used with diclofenac and mutants of CYP-102A5, CYP505X and CYP102A5 all produced 4'-hydroxydiclofenac.[51]

With the exception of 4-methyl biphenyl, oxidation only occurred at the benzylic C−H bond. This is expected based on the chemical reactivity of the C−H bonds of these substrates. Aromatic oxidation occurs by a different mechanism with the P450.[7–9] The alkyl side chain must be held closer to the heme iron than any of the aromatic C−H bonds. 2,7-dimethyl naphthalene underwent further oxidation in the *in vivo* turnover to the carboxylic acid counterpart. This occurred when most of the substrate was consumed in the *in vivo* turnover; as a result, the alcohol product reacted further. Further oxidation was not observed with the methyl naphthalenes or 2,7-dimethyl naphthalene *in vitro*.

Overall, for the substituted aromatics the most reactive sp^3 carbon was oxidised by CYP101B1. However, in the case of 4-methyl biphenyl and (1,1'-biphenyl)-4-methanol it is the more favourable binding orientation which results in oxidation on the aromatic ring. This interaction needs to be further investigated by testing other substrates, such as 4-ethyl biphenyl, to determine whether they also form this product. Alternatively, this could be done by obtaining a crystal structure of CYP101B1 with 4-methyl biphenyl or

(1,1'-biphenyl)-4-methanol in the active site. Clearly, the enzyme has some affinity for binding and moderate activity with aromatic substrates. This could be improved by mutating CYP101B1. Further investigations into drug molecules could generate drug metabolites using CYP101B1.

Chapter 7

Conclusion and Future Directions

The results with the norisoprenoid substrates indicate that moving or changing the ketone group on the butenone side chain has the most effect on the binding and activity of CYP101B1. In all cases where the ketone was modified, there was a decrease in the binding and activity of the substrate. The linear analogue of the cyclic norisoprenoids, pseudoionone, showed a decrease in binding affinity and activity. CYP101B1 did not show any activity when the cyclohexene ring of the norisoprenoids was changed to an aromatic ring. Overall, the norisoprenoids were good substrates for CYP101B1 and the ketone group on the butenone side chain is key for the substrates' binding and reactivity. Further investigations into which amino acids interact with the ketone oxygen would be useful. This could be obtained from a crystal structure of CYP101B1 with β-ionone bound or could be inferred from sequence alignments of CYP101B1 with other structurally characterised members of the CYP101 family.

The oxidation of the monoterpenoid substrates, similar to camphor, was not as successful as the norisoprenoids; it resulted in less selective product formation, with a large amount of NADH lost due to uncoupling reactions. Most of these structures contained a ketone or an alcohol group in the structure; however, these results show that for better selectivity and reactivity the oxygen group needs to be on a side chain rather than directly on the ring. Therefore, the butenone side chain on the norisoprenoids is important in determining binding, activity and selectivity. With this in mind, further substrates were chosen which were similar to the monoterpenoids but with an acetate protecting group in place of the ketone or alcohol groups. This led

to an increase in selectivity, as only one product was formed. Coupling was also increased resulting in a higher rate of product formation. The monoterpenoid acetates and related substrates are potential targets for further study with CYP101B1. For example, the products of the linear acetates still need to be characterised in detail. Further investigation into other acetate and ester protected substrates would clarify how these acetate substrates bind to CYP101B1. For instance, testing smaller ester containing compounds that are not terpenoid acetates would further aid our understanding of the binding preferences of CYP101B1. This could potentially result in selective C−H bond oxidation processes for a wider range of substrates. In some instances, the observation of stereoselective hydroxylation is important, so more detailed analysis into the ability of CYP101B1 to catalyse stereoselective C−H bond oxidation could be undertaken.

Phenylcyclohexane, indole and *p*-cymene were examined to determine whether CYP101B1 can react with aromatic compounds. Larger two-ring compounds were the preferred substrates of CYP101B1. This led to further studies of naphthalene and biphenyl. However, these compounds did not react well and, after the oxygen was inserted, the newly formed alcohol product competed with the P450 for the electrons from the ferredoxin of the electron transfer chain, resulting in low levels of product formation. Modification of the naphthalene and biphenyl by adding a methyl group increased the affinity and activity for CYP101B1, allowing products to be isolated in sufficient yield for identification. For the substituted naphthalenes and biphenyls, the oxygen was inserted onto the benzylic C−H bonds. 2,7-Dimethyl naphthalene was oxidised all the way to the carboxylic acid. 4-Methyl biphenyl was unusual in that it was oxidised on the aromatic ring, as well as on the methyl group. Further investigation into why this occurred would be useful to explain which enzyme-substrate interactions cause these differences in product selectivity. This could be discovered from a crystal structure or by testing other similar substrates. The protein could be modified to improve both product formation rates and coupling for aromatic substrates, by making the protein active site more hydrophobic. Random mutagenesis or selective mutagenesis methods based on sequence alignments or a crystal structure could be attempted. Further investigations into the stereoselectivity of the oxidation of ethyl naphthalenes would also be informative. This could be achieved by chiral column chromatography and would indicate how the substrate is bound in the active site of CYP101B1 relative to the heme iron.

Diclofenac oxidation by CYP101B1 generated a single product. Other similar drug compounds could react selectively with CYP101B1 and further studies into other drug compounds could assist in generating libraries of potential drug metabolites.

Overall, CYP101B1 shows great potential as a biocatalyst as it has been shown to bind, and react with, a wide range of substrates with high activity and selectivity. Norisoprenoids and cyclic monoterpenoid acetates give good binding and activity, but there are also favourable interactions with some aromatic compounds. Ultimately, this P450 needs further investigation to fully discover its potential as a biocatalyst.

Bibliography

[1] Bell, S. G.; Dale, A.; Rees, N. H.; Wong, L.-L. *Applied Microbiology and Biotechnology* **2010**, *86*, 163–175.

[2] Gillam, E.; Aguinaldo, A.; Notley, L.; Kim, D.; Mundkowski, R.; Volkov, A.; Arnold, F.; Soucek, P.; DeVoss, J.; Guengerich, F. *Biochemical and Biophysical Research Communications* **1999**, *265*, 469–472.

[3] Bell, S.; Harford-Cross, C.; Wong, L. *Protein Engineering* **2001**, *14*, 797–802.

[4] Guengerich, F. *Nature Reviews Drug Discovery* **2002**, *1*, 359–366.

[5] Nelson, D.; Koymans, L.; Kamataki, T.; Stegeman, J.; Feyereisen, R.; Waxman, D.; Waterman, M.; Gotoh, O.; Coon, M.; Estabrook, R.; Gunsalus, I.; Nebert, D. *Pharmacogenetics* **1996**, *6*, 1–42.

[6] Yang, W.; Bell, S. G.; Wang, H.; Zhou, W.; Hoskins, N.; Dale, A.; Bartlam, M.; Wong, L.-L.; Rao, Z. *Journal of Biological Chemistry* **2010**, *285*, 27372–27384.

[7] Guengerich, F. *Chemical Research in Toxicology* **2001**, *14*, 611–650.

[8] Meunier, B.; de Visser, S. P.; Shaik, S. *Chemical Reviews* **2004**, *104*, 3947–3980.

[9] Wong, L.-L.; Bell, S. G. *Encyclopedia of Inorganic Chemistry*; John Wiley & Sons, Ltd, 2006; pp 1–30.

[10] Hollmann, F.; Arends, I. W. C. E.; Buehler, K.; Schallmey, A.; Buehler, B. *Green Chemistry* **2011**, *13*, 226–265.

[11] Urlacher, V. B.; Eiben, S. *Trends in Biotechnology* **2006**, *24*, 324–330.

[12] O'Reilly, E.; Koehler, V.; Flitsch, S. L.; Turner, N. J. *Chemical Communications* **2011**, *47*, 2490–2501.

[13] Julsing, M. K.; Cornelissen, S.; Buehler, B.; Schmid, A. *Current Opinion in Chemical Biology* **2008**, *12*, 177–186.

[14] Zhou, R.; Huang, C.; Zhang, A.; Bell, S. G.; Zhou, W.; Wong, L.-L. *Acta Crystallogaphica Section F-structural Biology and Crystallization Communications* **2011**, *67*, 964–967.

[15] Bell, S. G.; Wong, L.-L. *Biochemical and Biophysical Research Communications* **2007**, *360*, 666–672.

[16] Bell, S. G.; Yang, W.; Yorke, J. A.; Zhou, W.; Wang, H.; Harmer, J.; Copley, R.; Zhang, A.; Zhou, R.; Bartlam, M.; Rao, Z.; Wong, L.-L. *Acta Crystallographica Section D-Biological Crystallography* **2012**, *68*, 277–291.

[17] Bell, S. G.; Yang, W.; Dale, A.; Zhou, W.; Wong, L.-L. *Applied Microbiology and Biotechnology* **2012**,

[18] Yang, W.; Bell, S. G.; Wang, H.; Zhou, W.; Bartlam, M.; Wong, L.-L.; Rao, Z. *Biochemical Journal* **2011**, *433*, 85–93.

[19] Ma, M.; Bell, S. G.; Yang, W.; Hao, Y.; Rees, N. H.; Bartlam, M.; Zhou, W.; Wong, L.-L.; Rao, Z. *ChemBioChem* **2011**, *12*, 88–99.

[20] Michaelis, L.; Menten, M. *Bisochemische Zeitschrift* **1913**, *49*, 333–369.

[21] Briggs, G.; Haldane, J. *Biochemical Journal* **1925**, *19*, 338–339.

[22] Jeffrey W. Williams and John F. Morrison, *Methods in Enzymology* **1979**, *63*, 437 – 467.

[23] Hall, E. A.; Bell, S. G. *RSC Advances* **2015**, *5*, 5762–5773.

[24] Venkataraman, H.; de Beer, S. B. A.; Geerke, D. P.; Vermeulen, N. P. E.; Commandeur, J. N. M. *Advanced Synthesis & Catalysis* **2012**, *354*, 2172–2184.

[25] Celik, A.; Flitsch, S. L.; Turner, N. J. *Organic & Biomolecular Chemistry* **2005**, *3*, 2930–2934.

[26] Zhang, A.; Zhang, T.; Hall, E. A.; Hutchinson, S.; Cryle, M. J.; Wong, L.-L.; Zhou, W.; Bell, S. G. *Molecular BioSystems* **2015**, –.

[27] Ly, T. T. B.; Khatri, Y.; Zapp, J.; Hutter, M. C.; Bernhardt, R. *Applied Microbiology and Biotechnology* **2012**, *95*, 123–133.

[28] Girhard, M.; Klaus, T.; Khatri, Y.; Bernhardt, R.; Urlacher, V. B. *Applied Microbiology and Biotechnology* **2010**, *87*, 595–607.

[29] Khatri, Y.; Girhard, M.; Romankiewicz, A.; Ringle, M.; Hannemann, F.; Urlacher, V.; Hutter, M.; Bernhardt, R. *Applied Microbiology and Biotechnology* **2010**, *88*, 485–495.

[30] England, P. A.; Rouch, D. A.; Westlake, A. C. G.; Bell, S. G.; Nickerson, D. P.; Webberley, M.; Flitsch, S. L.; Wong, L.-L. *Chemical Communications* **1996**, 357–358.

[31] Jones, N. E.; England, P. A.; Rouch, D. A.; Wong, L.-L. *Chemical Communications* **1996**, 2413–2414.

[32] Bell, S. G.; Rouch, D. A.; Wong, L.-L. *Journal of Molecular Catalysis B: Enzymatic* **1997**, *3*, 293 – 302.

[33] Nakahashi, H.; Miyazawa, M. *Journal of Oleo Science* **2011**, *60*, 545–548.

[34] Slessor, K. E.; Hawkes, D. B.; Farlow, A.; Pearson, A. G.; Stok, J. E.; De Voss, J. J. *Journal of Molecular Catalysis B: Enzymatic* **2012**, *79*, 15–20.

[35] ur Rahman, A.; Farooq, A.; Choudhary, M. *Journal of Natural Products* **1997**, *60*, 1038–1040.

[36] Zhang, K.; El Damaty, S.; Fasan, R. *Journal of the American Chemical Society* **2011**, *133*, 3242–3245.

[37] White, R. E.; McCarthy, M.-B.; Egeberg, K. D.; Sligar, S. G. *Archives of Biochemistry and Biophysics* **1984**, *228*, 493 – 502.

[38] Stevenson, J.; Jones, J.; Wong, L. *Israel Journal of Chemistry* **2000**, *40*, 55–62.

[39] Slessor, K. E.; Farlow, A. J.; Cavaignac, S. M.; Stok, J. E.; De Voss, J. J. *Archives of Biochemistry and Biophysics* **2011**, *507*, 154–162.

[40] Farlow, A. J.; Bernhardt, P. V.; De Voss, J. J. *Tetrahedron-Asymmetry* **2013**, *24*, 324–333.

[41] Furuya, T.; Kanno, T.; Yamamoto, H.; Kimoto, N.; Matsuyama, A.; Kino, K. *Journal of Molecular Catalysis B: Enzymatic* **2013**, *94*, 111–118.

[42] Marco-Urrea, E.; Perez-Trujillo, M.; Cruz-Morato, C.; Caminal, G.; Vicent, T. *Journal of Hazardous Materials* **2010**, *176*, 836–842.

[43] Kim, S.-H.; Kwon, J.-H.; Yoon, S.-H. *Bulletin of the Korean Chemical Society* **2010**, *31*, 3007–3009, used NMR.

[44] Guroff, G.; Daly, J.; Jerina, D.; Renson, J.; Witkop, B.; Udenfrie.S, *Science* **1967**, *157*, 1524–&.

[45] Jerina, D.; Daly, J. *Science* **1974**, *185*, 573–582.

[46] England, P. A.; Harford-Cross, C. F.; Stevenson, J.-A.; Rouch, D. A.; Wong, L.-L. *FEBS Letters* **1998**, *424*, 271 – 274.

[47] Li, Q.; Ogawa, J.; Schmid, R.; Shimizu, S. *Applied and Enviromental Microbiology* **2001**, *67*, 5735–5739.

[48] Whitehouse, C. J. C.; Bell, S. G.; Tufton, H. G.; Kenny, R. J. P.; Ogilvie, L. C. I.; Wong, L.-L. *Chemical Communications* **2008**, 966–968.

[49] Misawa, N.; Nodate, M.; Otomatsu, T.; Shimizu, K.; Kaido, C.; Kikuta, M.; Ideno, A.; Ikenaga, H.; Ogawa, J.; Shimizu, S.; Shindo, K. *Applied Microbiology and Biotechnology* **2011**, *90*, 147–157.

[50] Bort, R.; Mac, K.; Boobis, A.; Gmez-Lechn, M.-J.; Pfeifer, A.; Castell, J. *Biochemical Pharmacology* **1999**, *58*, 787 – 796.

[51] Weis, R.; Winkler, M.; Schittmayer, M.; Kambourakis, S.; Vink, M.; Rozzell, J. D.; Glieder, A. *Advanced Synthesis & Catalysis* **2009**, *351*, 2140–2146.

List of Figures

List of Tables

Appendix A

Retention Times of Substrates and Products

Table A.1: The GC-MS m/z and retention times and/or HPLC retention times of substrates and isolated products.

Product	m/z AMU	GC-MS RT (min)	HPLC RT (min)
β-ionone	192.2	7.5	23.7
3-hydroxy-β-ionone	208.2	10.2	14.7
4-hydroxy-β-ionone	208.2	9.9	13.5
α-ionone	192.2	6.7	23.5
trans-3-hydroxy-α-ionone	208.2	9.6	13.5
3-oxo-α-ionone	206.2	9.8	14.5
cis-3-hydroxy-α-ionone	208.2	9.4	14.2
β-damascone	192.2	6.6	23.2
3-hydroxy-β-damascone	208.2	9.3	14.6
4-hydroxy-β-damascone	208.2	9.0	13.5
α-methyl ionone	206.2	7.5	-
trans-3-hydroxy-α-methyl ionone	222.2	10.0	-
3-oxo-α-methyl ionone	220.2	10.5	-
cis-3-hydroxy-α-methyl ionone	222.2	10.3	-
α-ionol	194.2	6.0	-
trans-3-hydroxy-α-ionol	210.2	8.7	-
3-oxo-α-ionol	208.2	9.7	-
cis-3-hydroxy-α-ionol	210.2	9.0	-
β-ionol	194.2	6.6	-
3-hydroxy-β-ionol	210.2	9.3	-

4-hydroxy-β-ionol	210.2	9.4	-
phenylcyclohexane	160.1	5.3	-
trans-4-phenylcyclohexanol	176.1	8.5	-
p-cymene	134.1	4.3	24.9
p, α, α-trimethylbenzyl alcohol	150.1	7.2	15.6
4-isopropybenzyl alcohol	150.1	8.9	16.7
(1*R*)-(+)-camphor	152.1	6.5	-
6-*exo*-hydroxy-(1*R*)-(+)-camphor	168.1	9.7	-
5-*exo*-hydroxy-(1*R*)-(+)-camphor	168.1	10.1	-
5-*endo*-hydroxy-(1*R*)-(+)-camphor	168.1	10.5	-
9-hydroxy-(1*R*)-(+)-camphor	168.1	10.8	-
(1*S*)-(−)-camphor	152.1	6.5	-
6-*exo*-hydroxy-(1*S*)-(−)-camphor	168.1	9.7	-
5-*exo*-hydroxy-(1*S*)-(−)-camphor	168.1	10.1	-
5-*endo*-hydroxy-(1*S*)-(−)-camphor	168.1	10.5	-
9-hydroxy-(1*S*)-(−)-camphor	168.1	10.8	-
1,8-cineole	152.1	4.5	-
3-oxo-1,8-cineole	166.1	7.1	-
3-*endo*-hydroxy-1,8-cineole	168.1	8.1	-
3-*endo*-hydroxy-5-oxo-1,8-cineole	182.1	10.3	-
3,5-*endo*-dihydroxy-1,8-cineole	184.1	11.5	-
1,4-cineole	152.1	4.2	-
6-*endo*-hydroxy-1,4-cineole	168.1	7.1	-
(+)-fenchone	152.1	5.5	-
5-*exo*-hydroxy-(+)-fenchone	168.1	9.0	-
(1*R*)-(−)-nopol	166.1	5.6	-
1-hydroxy-(1*R*)-(−)-nopol	182.1	11.2	-
4-hydroxy-(1*R*)-(−)-nopol	182.1	11.0	-
4-oxo-(1*R*)-(−)-nopol	180.1	13.2	-
cis-jasmone	164.1	5.6	-
4-hydroxy-*cis*-jasmone	180.1	12.8	-
11-hydroxy-*cis*-jasmone	180.1	13.9	-
1-adamantanol	152.1	8.3	-
6-hydroxy-1-adamantanol	168.1	12.9	-
5-hydroxy-1-adamantanol	168.1	10.9	-
2-adamantanol	152.1	9.3	-
6-hydroxy-2-adamantanol	168.1	12.0	-
2-adamantanone	150.1	9.3	-
6-hydroxy-2-adamantanone	166.1	12.8	-
5-hydroxy-2-adamantanone	166.1	11.5	-
fenchyl acetate	196.2	3.8	-

5-*exo*-hydroxy-fenchyl acetate	212.2	6.7	-
bornyl acetate	196.2	4.7	-
9-hydroxybornyl acetate	212.2	8.4	-
isobornyl acetate	196.2	4.7	-
5-*exo*-hydroxyisobornyl acetate	212.2	7.9	-
5-norbornen-2-yl acetate	152.1	5.5	-
5-epoxynorborane-2-yl acetate	168.1	8.9	-
myrtenyl acetate	194.2	5.2	-
myrtenol	152.2	3.7	-
4-*cis*-hydroxymyrtenyl acetate	210.2	8.6	-
4-oxomyrtenyl acetate	208.2	8.2	-
(+)-sclareolide	250.3	17.7	-
(*S*)-3-(+)-hydroxysclareolide	266.3	21.4	-
1-methyl naphthalene	-	-	22.4
1-naphthyl methanol	-	-	15.1
2-methyl naphthalene	-	-	22.4
2-naphthyl methanol	-	-	15.3
2,7-dimethyl naphthalene	-	-	24.4
2-(7-mehtylnaphthyl)methanol	-	-	17.0
2-carboxy-7-methylnaphthalene	-	-	17.6
1-ethyl naphthalene	-	-	23.7
1-naphthyl-1-ethanol	-	-	16.5
2-ethyl naphthalene	-	-	24.1
2-naphthyl-1-ethanol	-	-	16.5
2-methyl biphenyl	-	-	23.7
2-methanol biphenyl	-	-	17.4
3-methyl biphenyl	-	-	23.7
3-methanol biphenyl	-	-	17.2
4-methyl biphenyl	-	-	23.7
(1,1̂-biphenyl)-4-methanol	-	-	17.1
4̂-hydroxy-4-methylbiphenyl	-	-	19.2
(4̂-hydroxy-1,1̂-biphenyl)-4-methanol	-	-	13.0
diclofenac	-	-	20.0
4̂-hydroxydiclofenac	-	-	16.7

Appendix B

Spin State Shifts

Table B.1: Spin state shifts for other substrates with CYP101B1

CYP101B1/ substrate	%HS heme
carvone	30
α-(+)-pinene	20
α-(−)-pinene	30
α-(−)-pinene	10
α-bisabolol	25
cis-nerolidol	25
guaiazulene	20
indane	30
indene	25
resveratrol	15
sclareol	0
α-santonin	5
tolbutamide	10
nicotine	0
ibuprofen	0

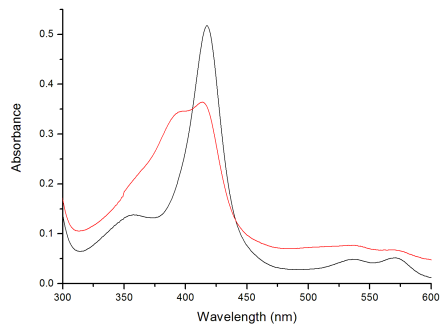

(a) 1,4-cineole

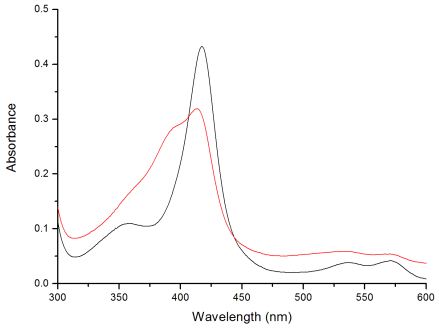

(b) (1R)-(−)-nopol

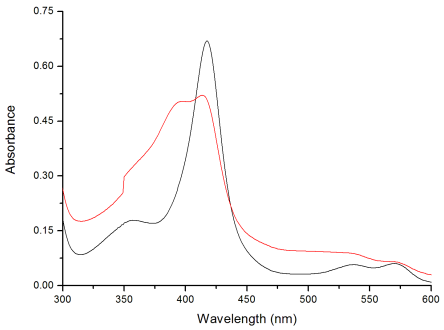

(c) 2-adamantanol

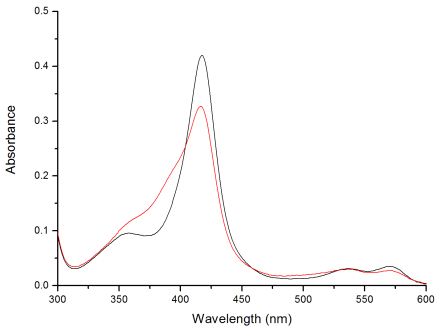

(d) 2-adamantanone

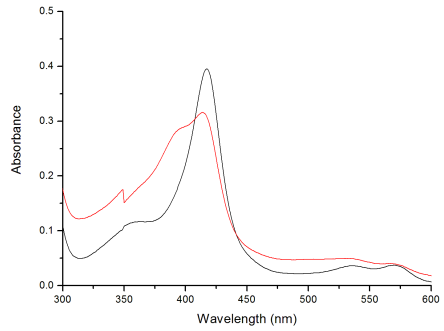

(e) (+)-sclareolide

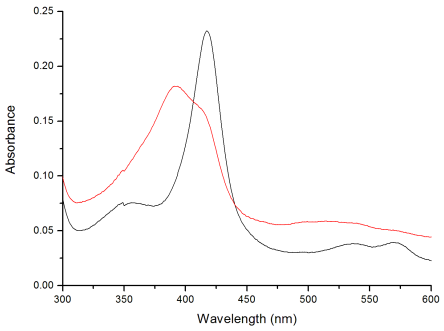

(f) 5-norbornen-2-yl acetate

Figure B.1: Spin state shifts for selected substrates

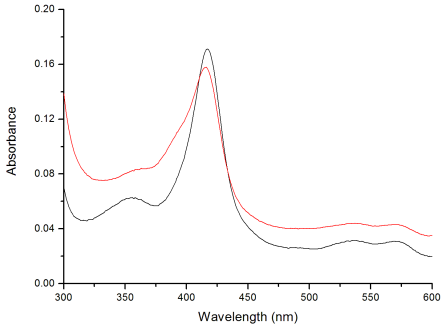

(g) nerol

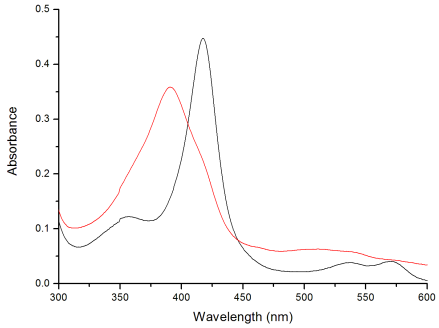

(h) neryl acetate

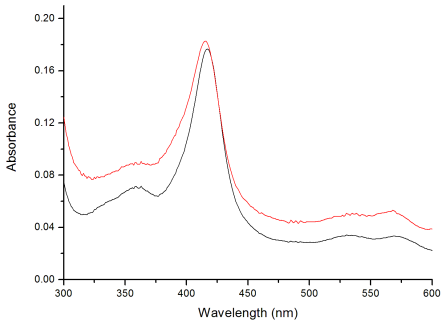

(i) geraniol

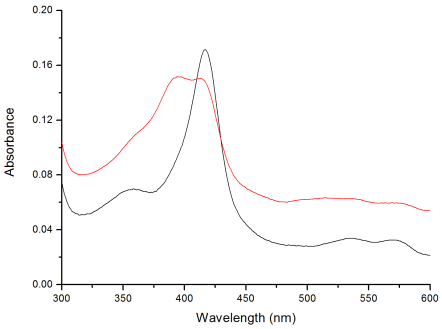

(j) geranyl acetate

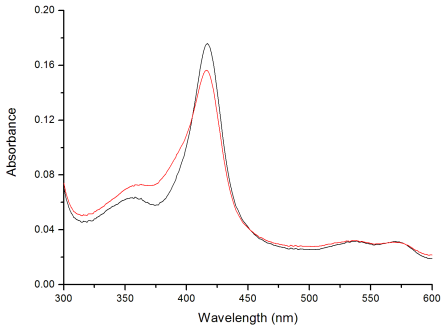

(k) linalool

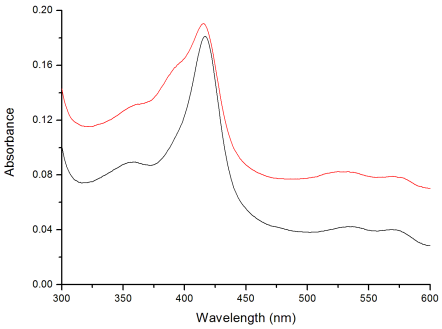

(l) linalyl acetate

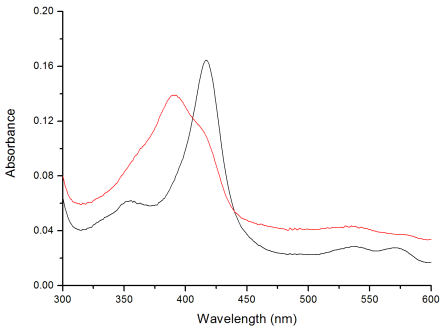

(m) terpinyl acetate

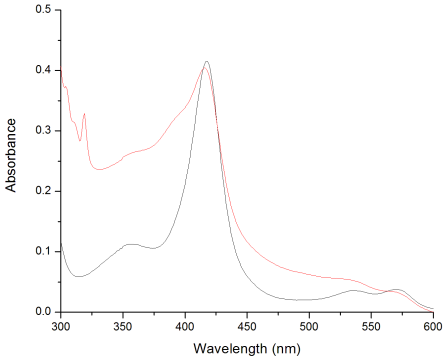

(n) 2-methyl naphthalene

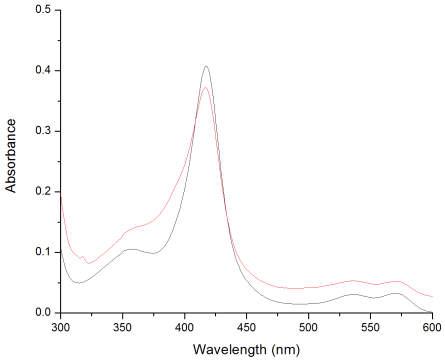

(o) 1-ethyl naphthalene

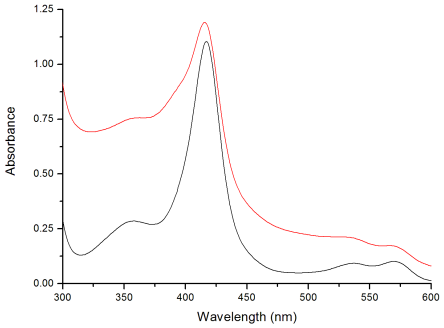

(p) 2-methyl biphenyl

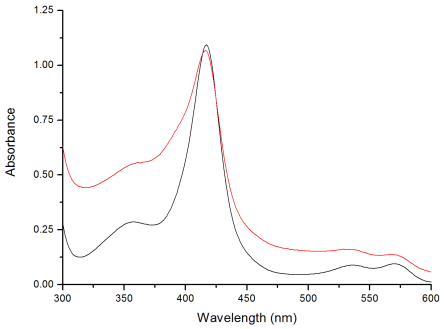

(q) 3-methyl biphenyl

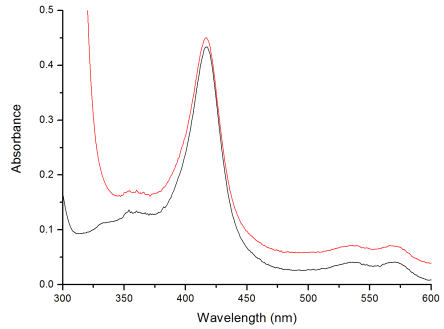

(r) diclofenac

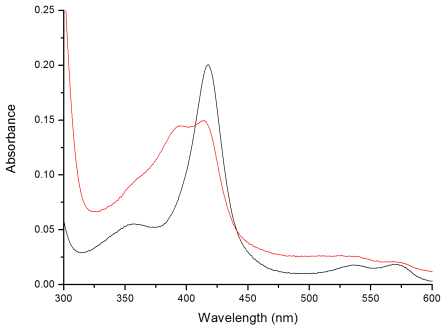

(s) 1*S*-(−)-camphor

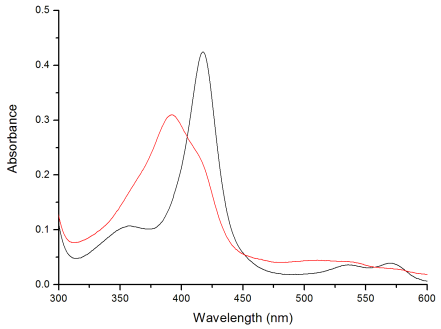

(t) 1,8-cineole

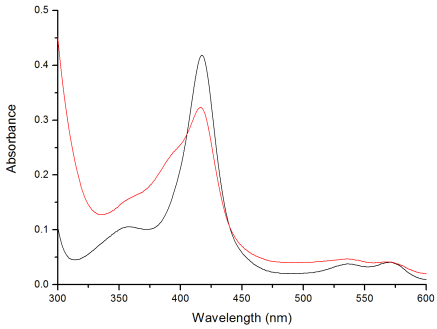

(u) *cis*-jasmone

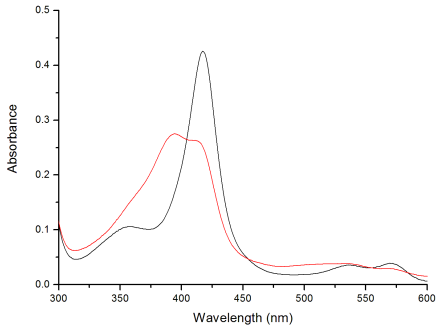

(v) 1-adamantanol

Appendix C

Dissociation Constant Analysis

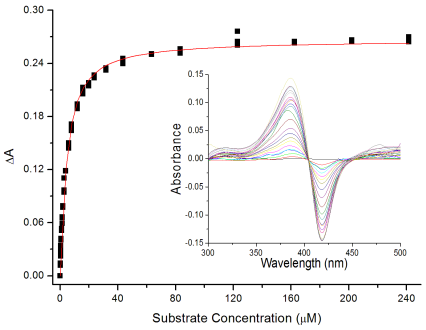

(a) myrtenyl acetate

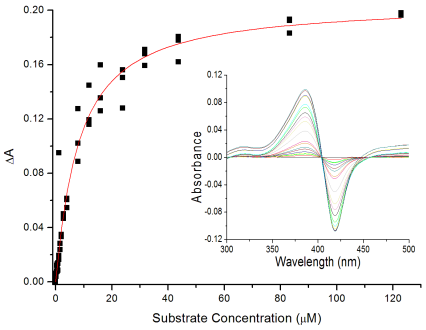

(b) fenchyl acetate

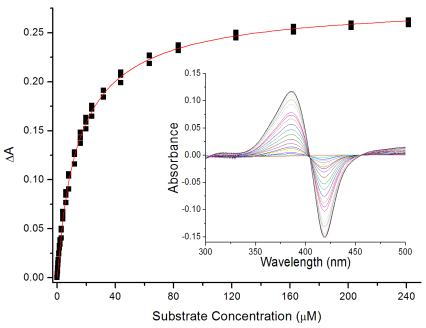

(c) isobornyl acetate

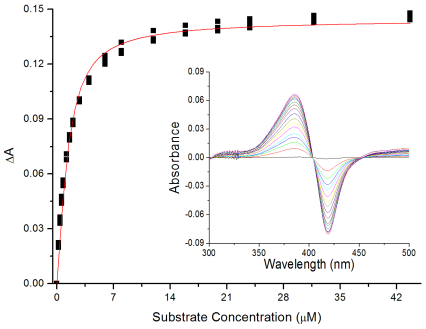

(d) bornyl acetate

Figure C.1: Dissociation constants for selected substrates

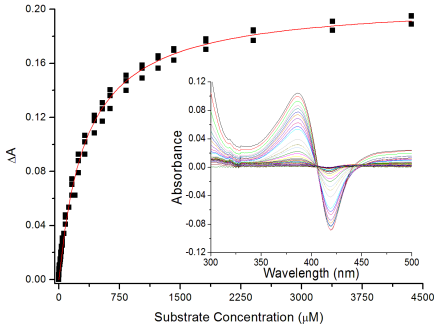

(e) (1R)-(+)-camphor

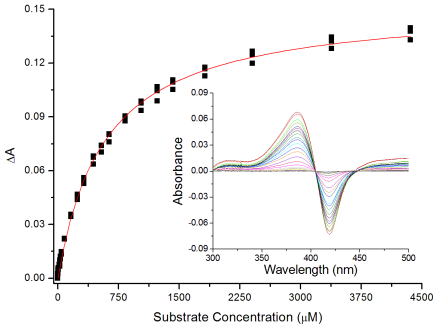

(f) 1,8-cineole

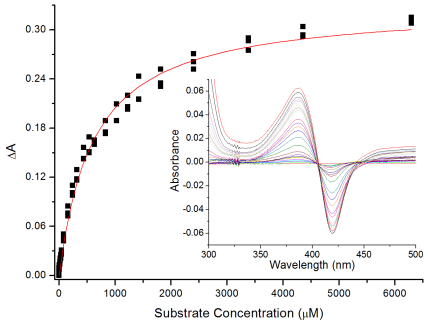

(g) 1,4-cineole

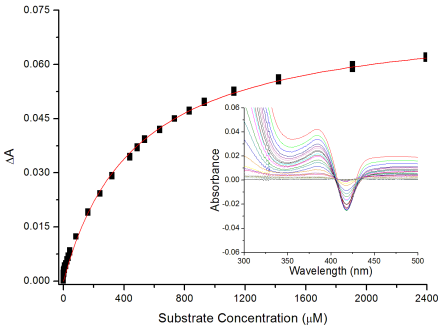

(h) *cis*-jasmone

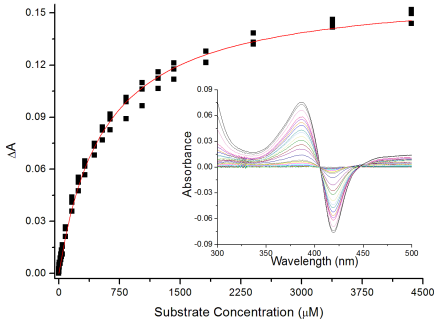

(i) 2-adamantanone

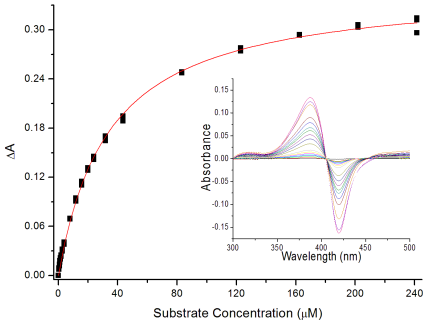

(j) (+)-sclareolide

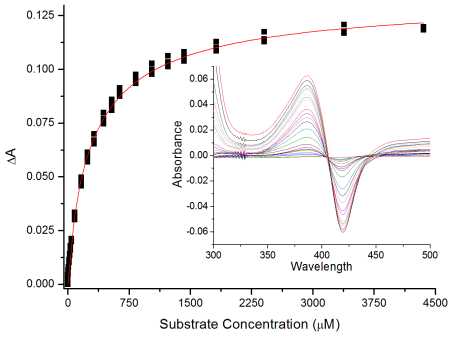

(k) 1S-(−)-camphor

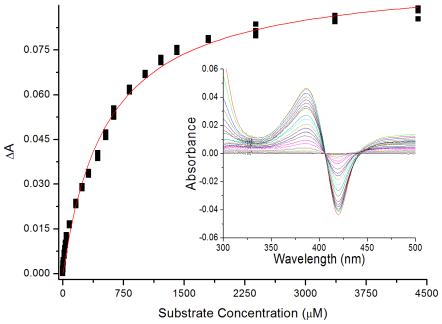

(l) (+)-fenchone

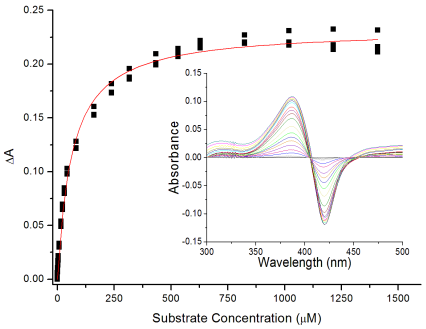

(m) (1R)-(−)-nopol

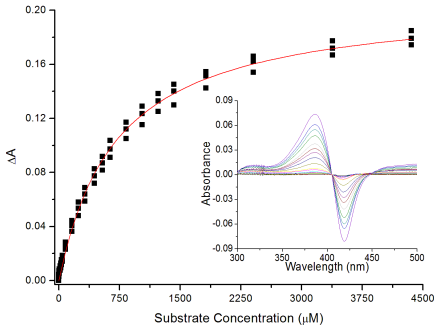

(n) 1-adamantanol

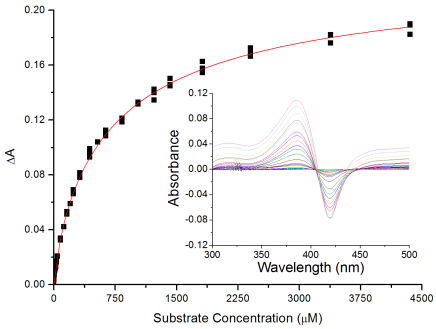

(o) 5-norbornen-2-yl acetate

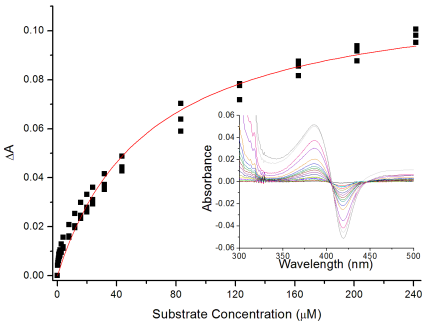

(p) 1-methyl naphthalene

Appendix D

In vitro NADH Consumption Rates

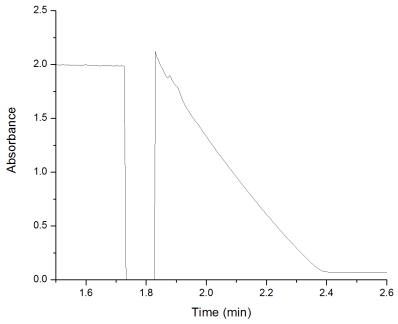

(a) myrtenyl acetate

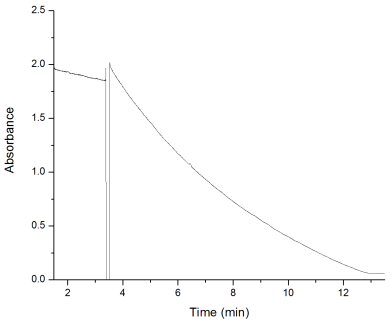

(b) linalyl acetate

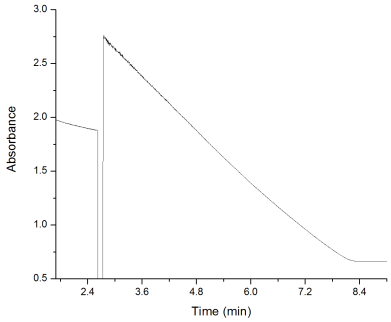

(c) 3-methyl biphenyl

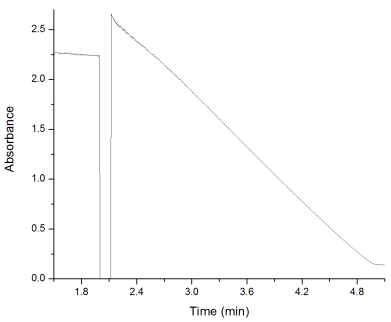

(d) 1-methyl naphthalene

Figure D.1: NADH consumption rates for selected substrates

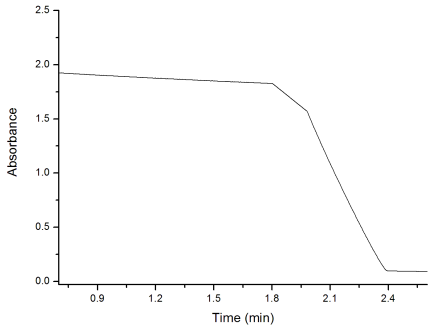

(e) α-ionone

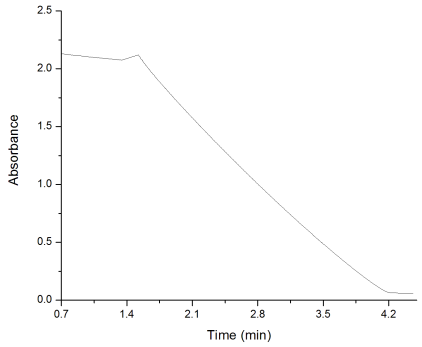

(f) *p*-cymene

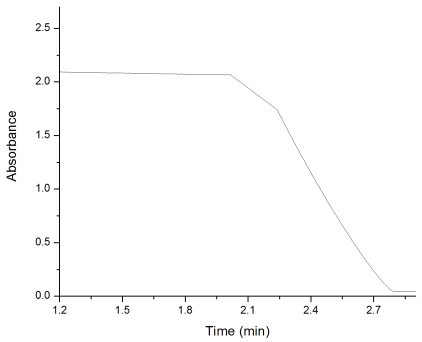

(g) (1*S*)-(−)-camphor

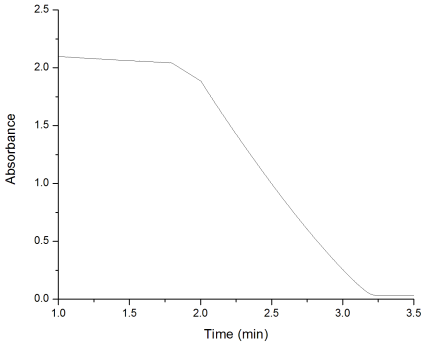

(h) (1*R*)-(−)-nopol

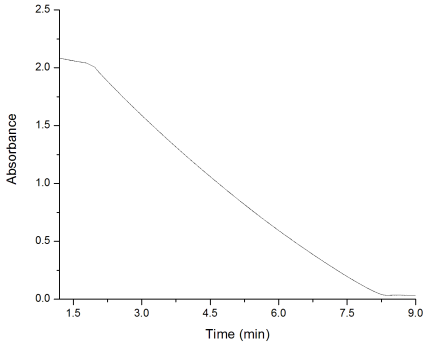

(i) *cis*-jasmone

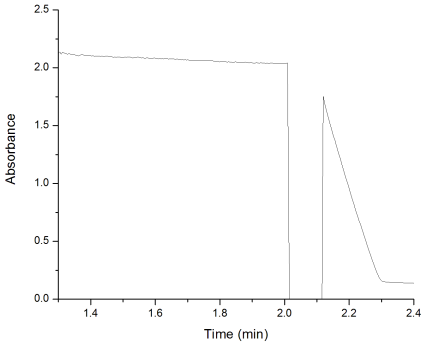

(j) bornyl acetate

Appendix E

GC-MS and HPLC Analysis of Turnovers

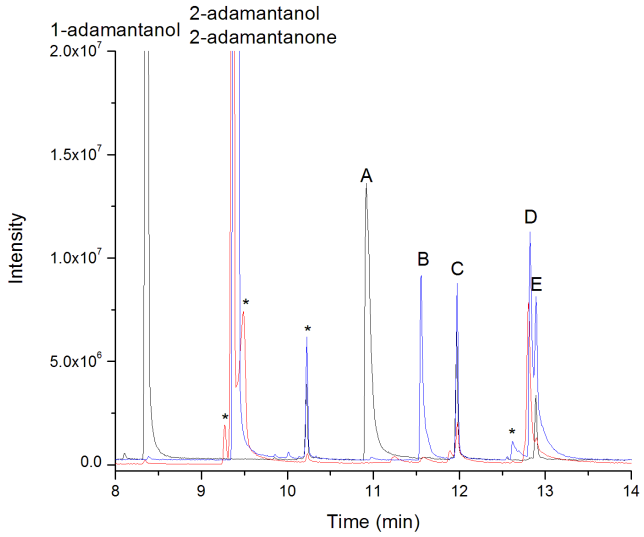

Figure E.1: GC-MS analysis of *in vitro* CYP101B1 turnovers of 1-adamantanol, 2-adamantanol and 2-adamantanone co-eluted. 1-Adamantanol (black), 2-adamantanol (red), 2-adamantanone (blue), 5-hydroxy-1-adamantanol (A), 5-hydroxy-2-adamantanone (B), 6-hydroxy-2-adamantanol (C), 6-hydroxy-2-adamantanone (D), 6-hydroxy-1-adamantanol (E) and impurities (*).

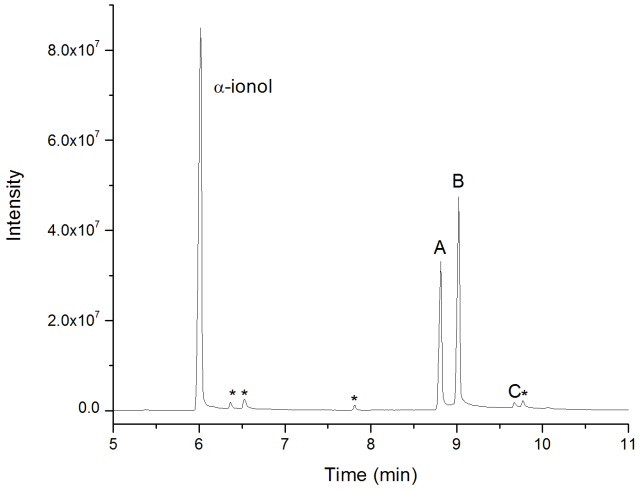

Figure E.2: GC-MS analysis of *in vivo* CYP101B1 turnover of α-ionol, *trans*-3-hydroxy-α-ionol (A), *cis*-3-hydroxy-α-ionol (B), 3-oxo-α-ionol (C) and impurities (*).

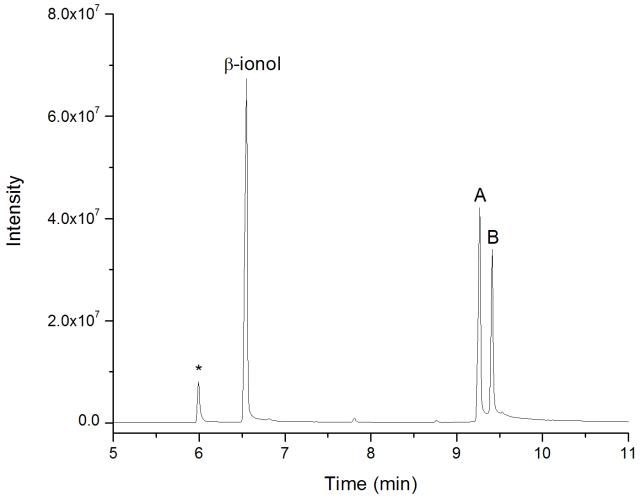

Figure E.3: GC-MS analysis of *in vivo* CYP101B1 turnover of β-ionol, 3-hydroxy-β-ionol (A), 4-hydroxy-β-ionol (B) and impurities (*).

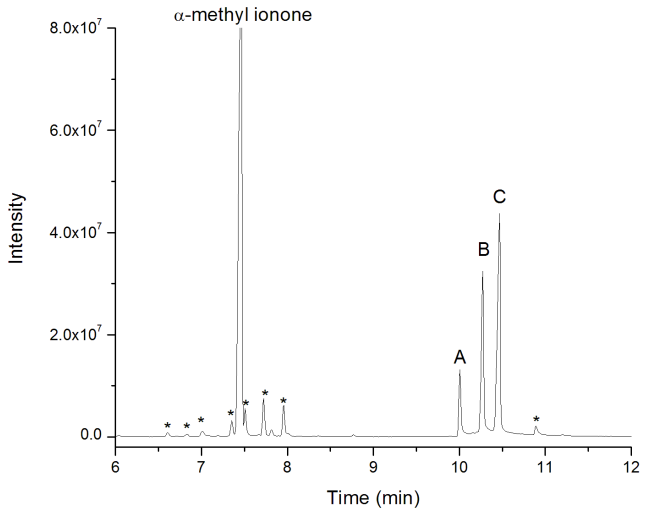

Figure E.4: GC-MS analysis of *in vivo* CYP101B1 turnover of α-methyl ionone, *trans*-3-hydroxy-α-methyl ionone (A), *cis*-3-hydroxy-α-methyl ionone (B), 3-oxo-α-methyl ionone (C) and impurities (*).

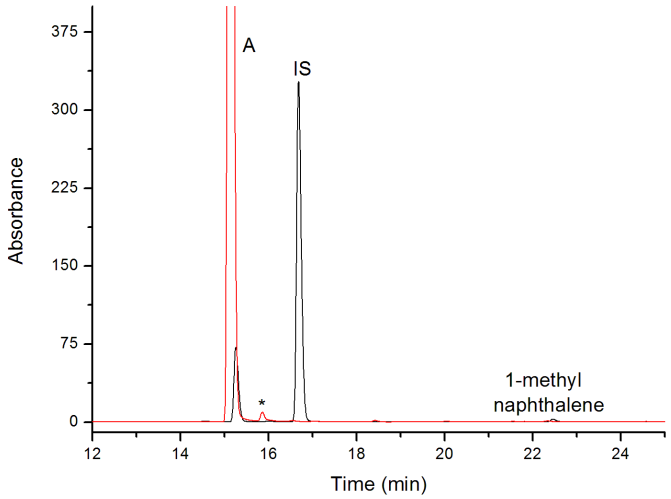

Figure E.5: HPLC analysis of *in vitro* CYP101B1 turnover of 1-methyl naphthalene co-eluted with 1-naphthyl methanol. Black is the *in virto* turnover and red is the co-eluted 1-naphthyl methanol. 1-naphthyl methanol (A), internal standard (IS) and impurities (*).

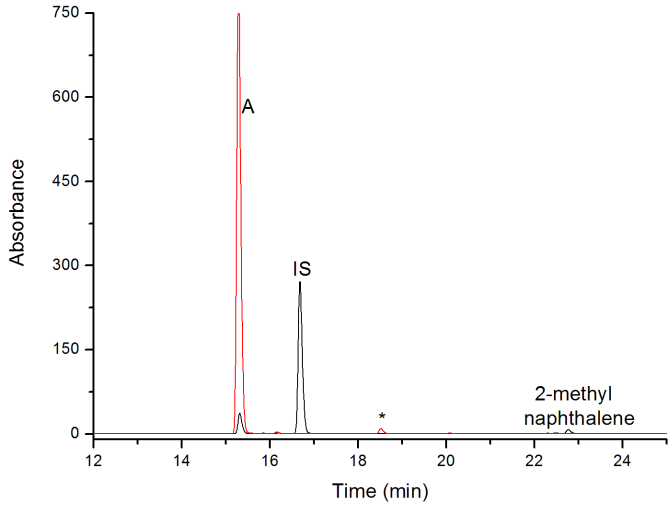

Figure E.6: HPLC analysis of *in vitro* CYP101B1 turnover of 2-methyl naphthalene co-eluted with 2-naphthyl methanol. Black is the *in vitro* turnover and red is the co-eluted 2-naphthyl methanol. 2-naphthyl methanol (A), internal standard (IS) and impurities (*).

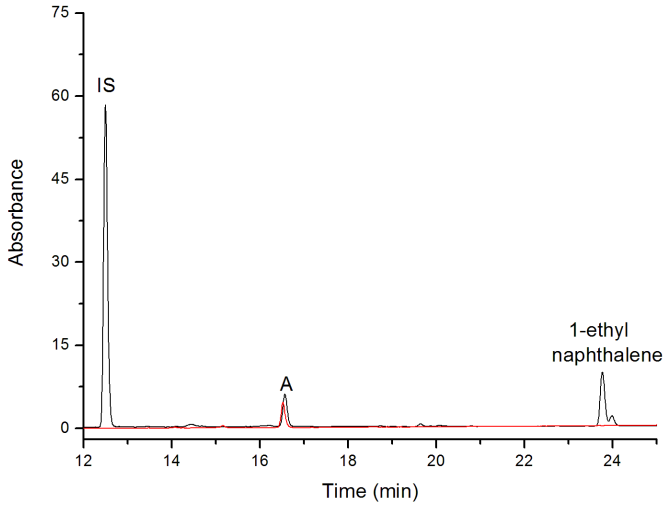

Figure E.7: HPLC analysis of *in vitro* CYP101B1 turnover of 1-ethyl naphthalene co-eluted with 1-naphthyl-1-ethanol. Black is the *in vitro* turnover and red is the co-eluted 1-naphthyl-1-ethanol. 1-naphthyl-1-ethanol (A), internal standard (IS) and impurities (*).

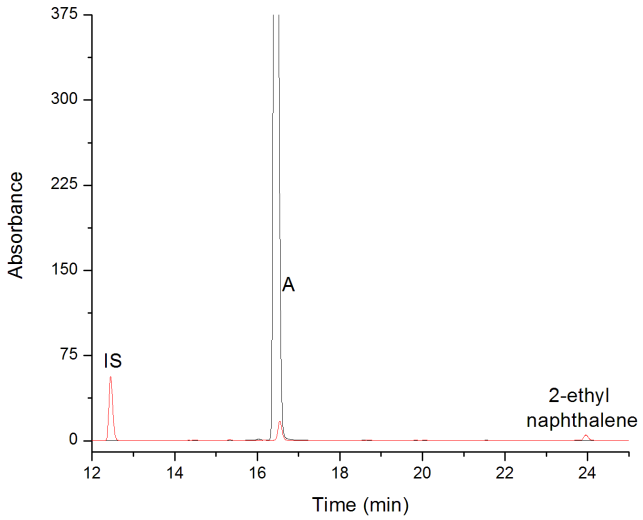

Figure E.8: HPLC analysis of *in vitro* CYP101B1 turnover of 2-ethyl naphthalene co-eluted with 2-naphthyl-1-ethanol. Black is the *in vitro* turnover and red is the co-eluted 2-naphthyl-1-ethanol. 2-naphthyl-1-ethanol (A), internal standard (IS) and impurities (*).

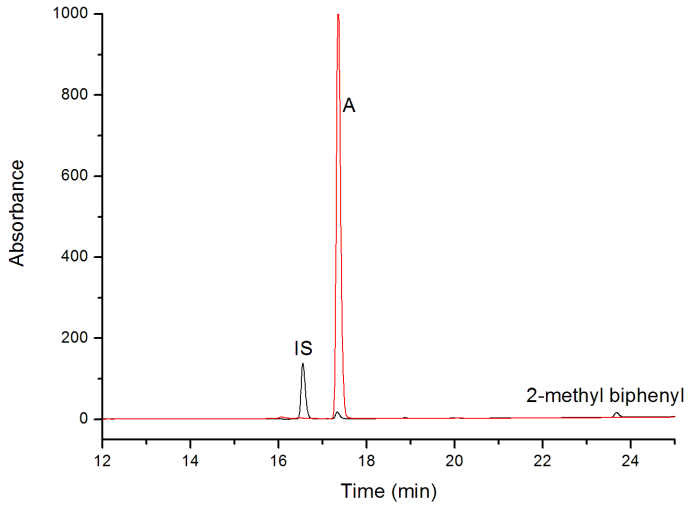

Figure E.9: HPLC analysis of *in vitro* CYP101B1 turnover of 2-methyl biphenyl co-eluted with 2-methanol biphenyl. Black is the *in virto* turnover and red is the co-eluted 2-methanol biphenyl. 2-methanol biphenyl (A), internal standard (IS) and impurities (*).

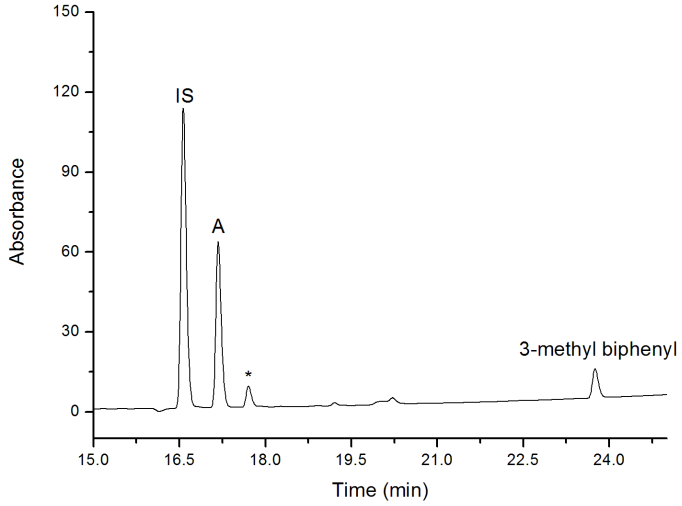

Figure E.10: HPLC analysis of *in vitro* CYP101B1 turnover of 3-methyl biphenyl. Black is the *in virto* turnover, 3-methanol biphenyl (A), internal standard (IS) and impurities (*).

Appendix F

NMR Data of Products

F.1 β-Ionone

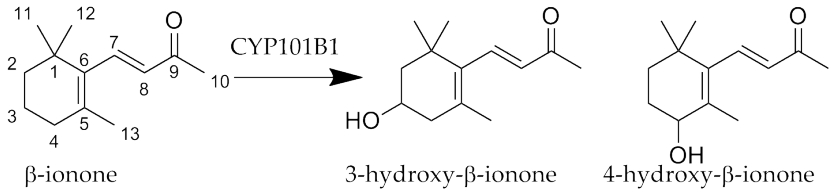

Figure F.1: β-Ionone products

Data for 3-hydroxy-β-ionone:
^{1}H NMR (600 MHz, $CDCl_3$) δ 7.21 (d, J = 16.4 Hz, 1H, H8), 6.11 (d, J = 16.4 Hz, 1H, H7), 3.99 (s, 1H, H3), 2.43 (d, J = 17.5 Hz, 1H, H4), 2.29 (s, 3H, H10), 2.09 (dd, J = 17.3, 9.7 Hz, 1H, H4), 1.83 - 1.78 (m, 1H, H2), 1.77 (s, 3H, H13), 1.49 (t, J = 12.0 Hz, 1H, H2), 1.11 (s, 3H, H11), 1.10 (s, 3H, H12); ^{13}C NMR (151 MHz, $CDCl_3$) δ 198.68 (C9), 142.47 (C8), 135.52 (C6), 132.50 (C5), 132.19 (C7), 64.27 (C3), 48.31 (C2), 42.70 (C4), 36.82 (C1), 30.03 (C11), 28.51 (C12), 27.22 (C10), 21.54 (C13).

Data for 4-hydroxy-β-ionone:
^{1}H NMR (600 MHz, $CDCl_3$) δ 7.19 (d, J = 16.4 Hz, 1H, H8), 6.12 (d, J = 16.4 Hz, 1H, H7), 4.02 (t, J = 4.9 Hz, 1H, H4), 2.31 (s, 3H, H10), 1.93 (ddd, J = 14.0, 7.4, 3.2 Hz, 1H, H3), 1.85 (s, 3H, H13), 1.73 (ddd, J = 13.0, 7.6, 3.9 Hz, 1H, H3), 1.69- 1.63 (m, 1H, H2), 1.46 (ddd, J = 11.3, 7.3, 2.7 Hz, 1H, H2), 1.07 (s, 3H, H11), 1.04 (s, 3H, H12); ^{13}C NMR (151 MHz, $CDCl_3$) δ 198.38 (C9), 142.63 (C8), 139.44 (C6), 133.88 (C5), 133.11 (C7), 69.94 (C4), 34.65 (C2), 28.85 (C11), 28.31 (C3), 27.49 (C12), 27.38 (C10), 18.48 (C13).

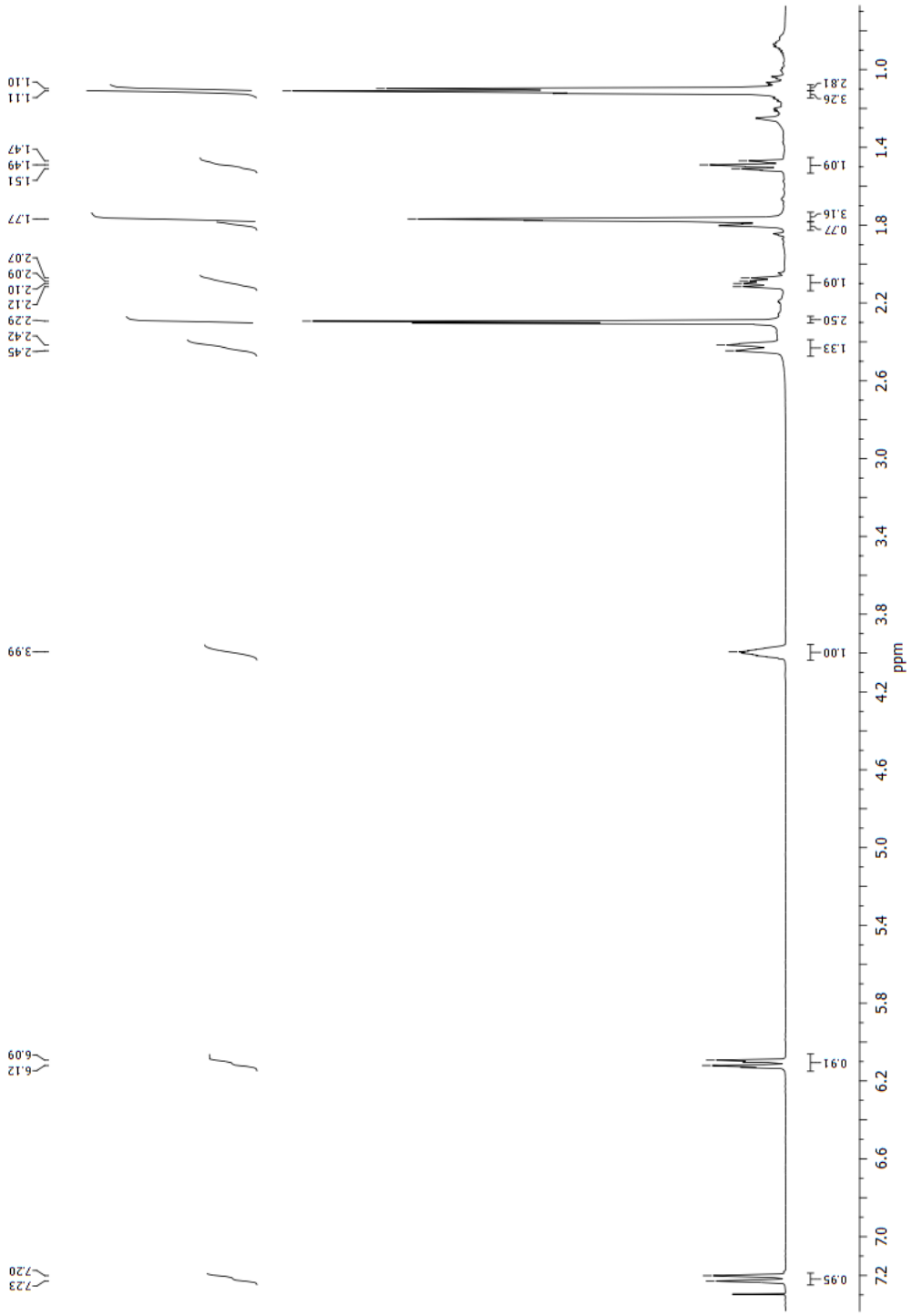

Figure F.2: ^{1}H NMR of 3-hydroxy-β-ionone

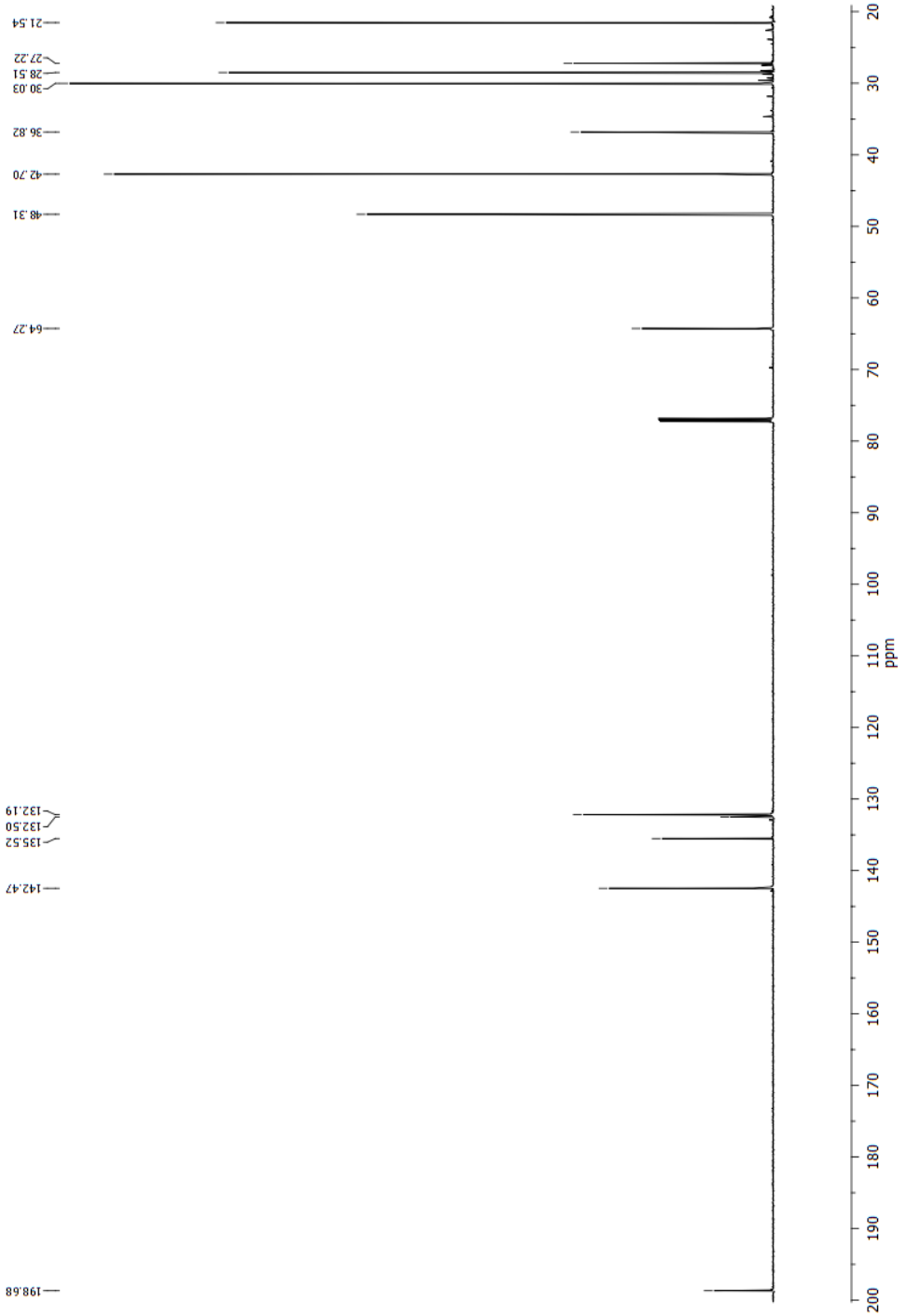

Figure F.3: ^{13}C NMR of 3-hydroxy-β-ionone

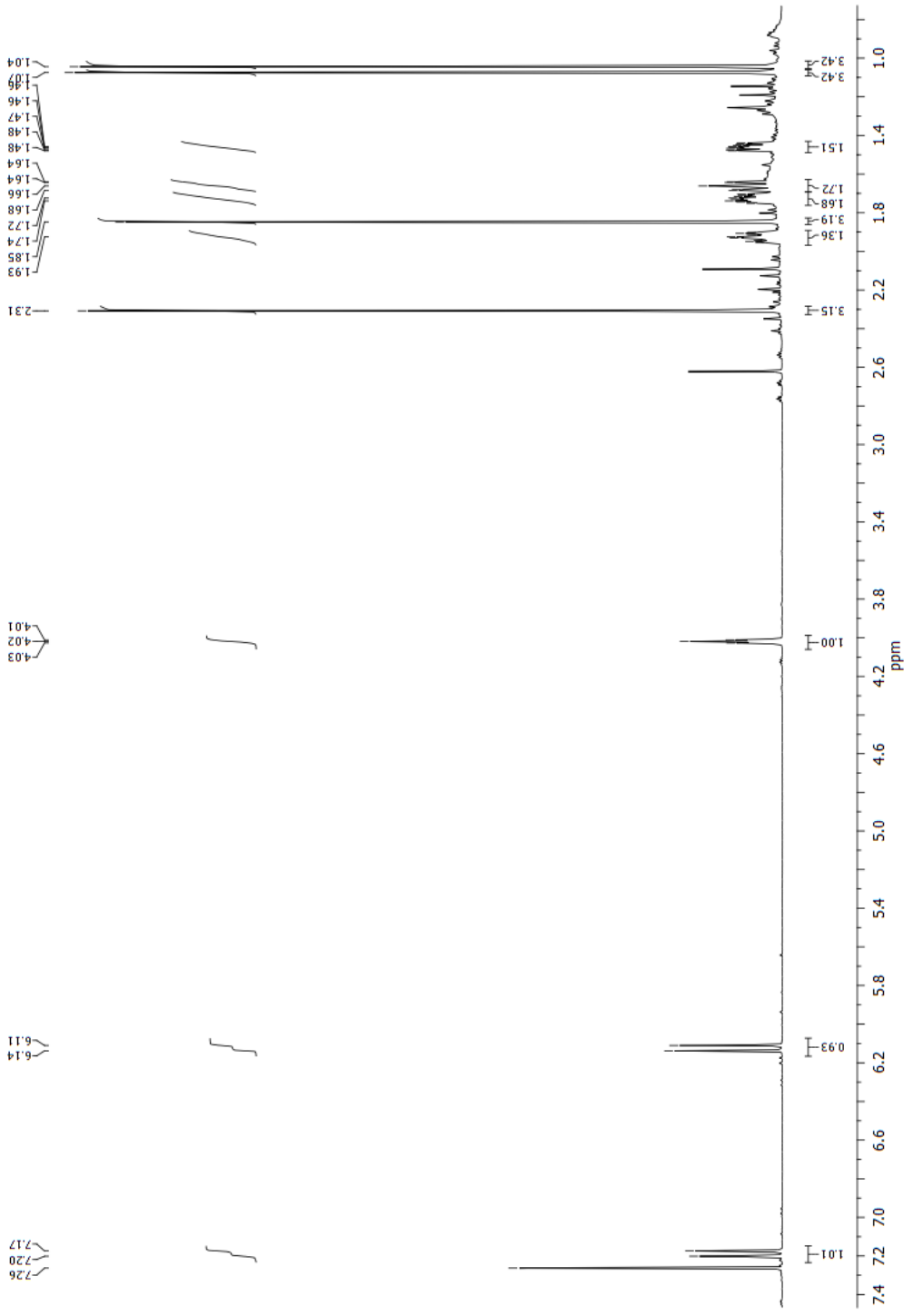

Figure F.4: ^{1}H NMR of 4-hydroxy-β-ionone

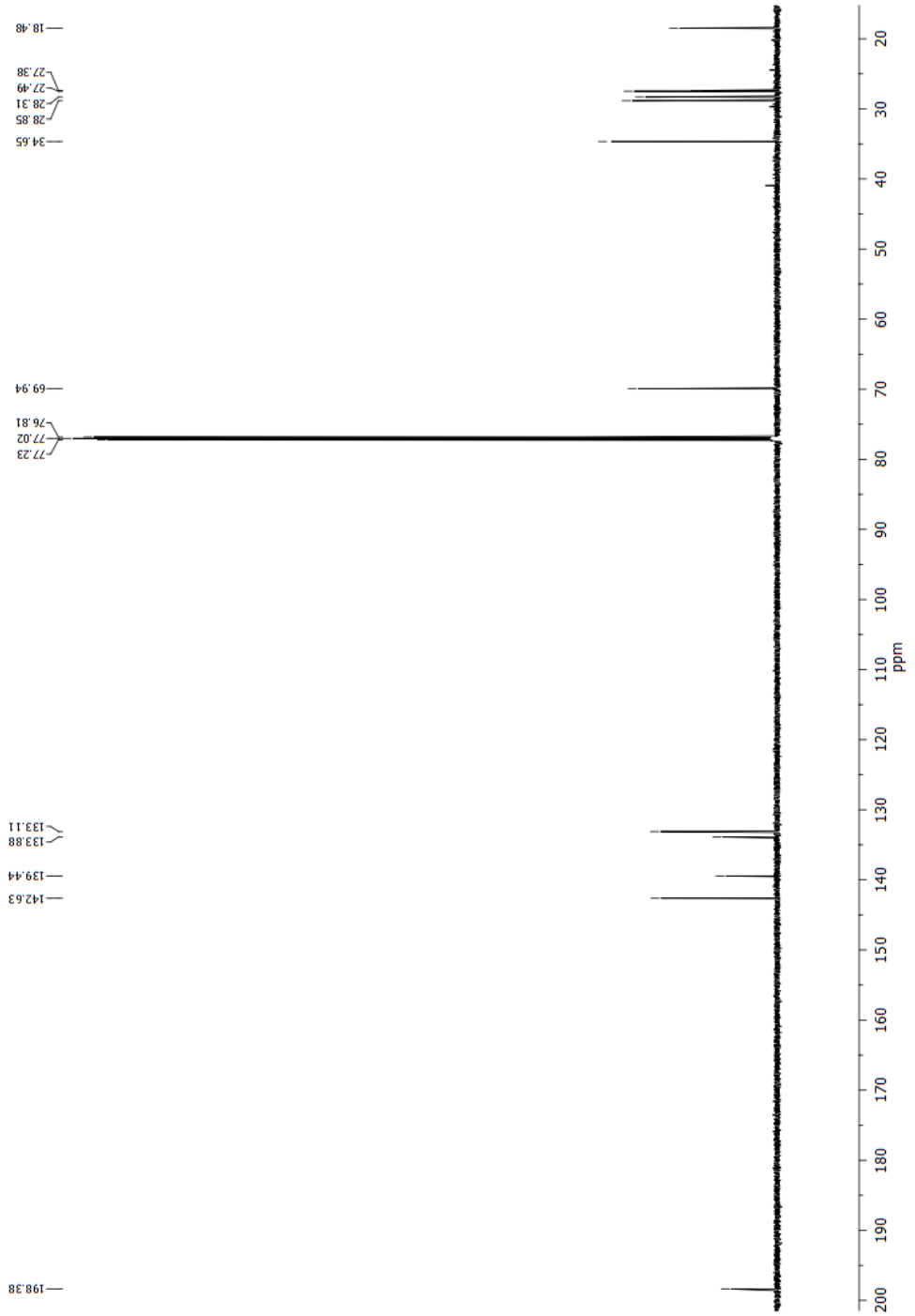

Figure F.5: ^{13}C NMR of 4-hydroxy-β-ionone

F.2 α-Ionone

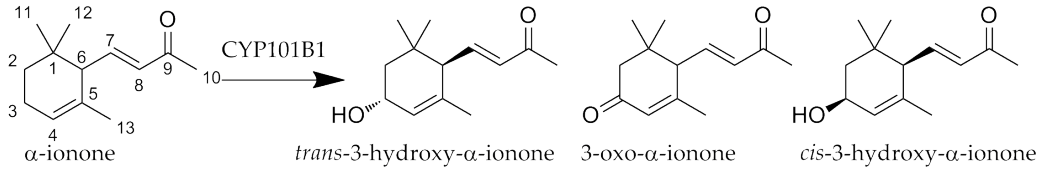

Figure F.6: α-Ionone products

Data for *trans*-3-hydroxy-α-ionone:
^{1}H NMR (500 MHz, $CDCl_3$) δ 6.54 (dd, J = 15.8, 10.1 Hz, 1H, H7), 6.10 (d, J = 15.8 Hz, 1H, H8), 5.65 - 5.61 (m, 1H, H4), 4.27 (s, 1H, H3), 2.50 (d, J = 10.1 Hz, 1H, H6), 2.26 (s, 3H, H10), 1.84 (dd, J = 13.5, 5.9 Hz, 1H, axial H2), 1.62 (d, J = 0.6 Hz, 3H, H3), 1.41 (dd, J = 13.6, 6.2 Hz, 1H, equatorial H2), 1.03 (s, 3H, H11), 0.89 (s, 3H, H12); ^{13}C NMR (126 MHz, $CDCl_3$) δ 198.03 (C9), 147.09 (C7), 135.43 (C5), 133.61 (C8), 125.83 (C4), 65.47 (C3), 54.30 (C6), 43.83 (C2), 33.86 (C1), 29.31 (C11), 27.20 (C10), 24.70 (C12), 22.66 (C13).

Data for 3-oxo-α-ionone:
^{1}H NMR (600 MHz, $CDCl_3$) δ 6.69 (dd, J = 15.8, 9.5 Hz, 1H, H7), 6.20 (d, J = 15.8 Hz, 1H, H8), 5.98 (s, 1H, H4), 2.73 (d, J = 9.6 Hz, 1H, H6), 2.37 (d, J = 16.9 Hz, 1H, axial H2), 2.29 (s, 3H, H10), 2.15 (d, J = 17.0 Hz, 1H, equatorial H2), 1.91 (s, 3H, H13), 1.09 (s, 3H, H11), 1.02 (s, 3H, H12); ^{13}C NMR (151 MHz, $CDCl_3$) δ 198.20 (C3), 197.49 (C9), 159.12 (C5), 143.57 (C7), 133.74 (C8), 126.88 (C4), 55.40 (C6), 47.33 (C2), 36.67 (C1), 27.89 (C10), 27.55 (C11), 27.31 (C12), 23.48 (C13).

Data for *cis*-3-hydroxy-α-ionone:
^{1}H NMR (600 MHz, $CDCl_3$) δ 6.64 (dd, J = 15.8, 9.6 Hz, 1H, H7), 6.08 (d, J = 15.8 Hz, 1H, H8), 5.59 (s, 1H, H4), 4.25 (t, J = 7.6 Hz, 1H, H3), 2.29 - 2.25 (m, 4H, H6 and H10), 1.69 (dd, J = 12.9, 6.5 Hz, 1H, axial H2), 1.63 (s, 3H, H13), 1.40 (dd, J = 12.8, 9.9 Hz, 1H, equatorial H2), 0.98 (s, 3H, H11), 0.89 (s, 3H, H12); ^{13}C NMR (151 MHz, $CDCl_3$) δ 198.46 (C9), 147.83 (C7), 135.30 (C5), 132.68 (C8), 126.47 (C4), 66.37 (C3), 54.32 (C6), 40.65 (C2), 34.97 (C1), 29.10 (C11), 27.61 (C10), 26.41 (C12), 22.41 (C13).

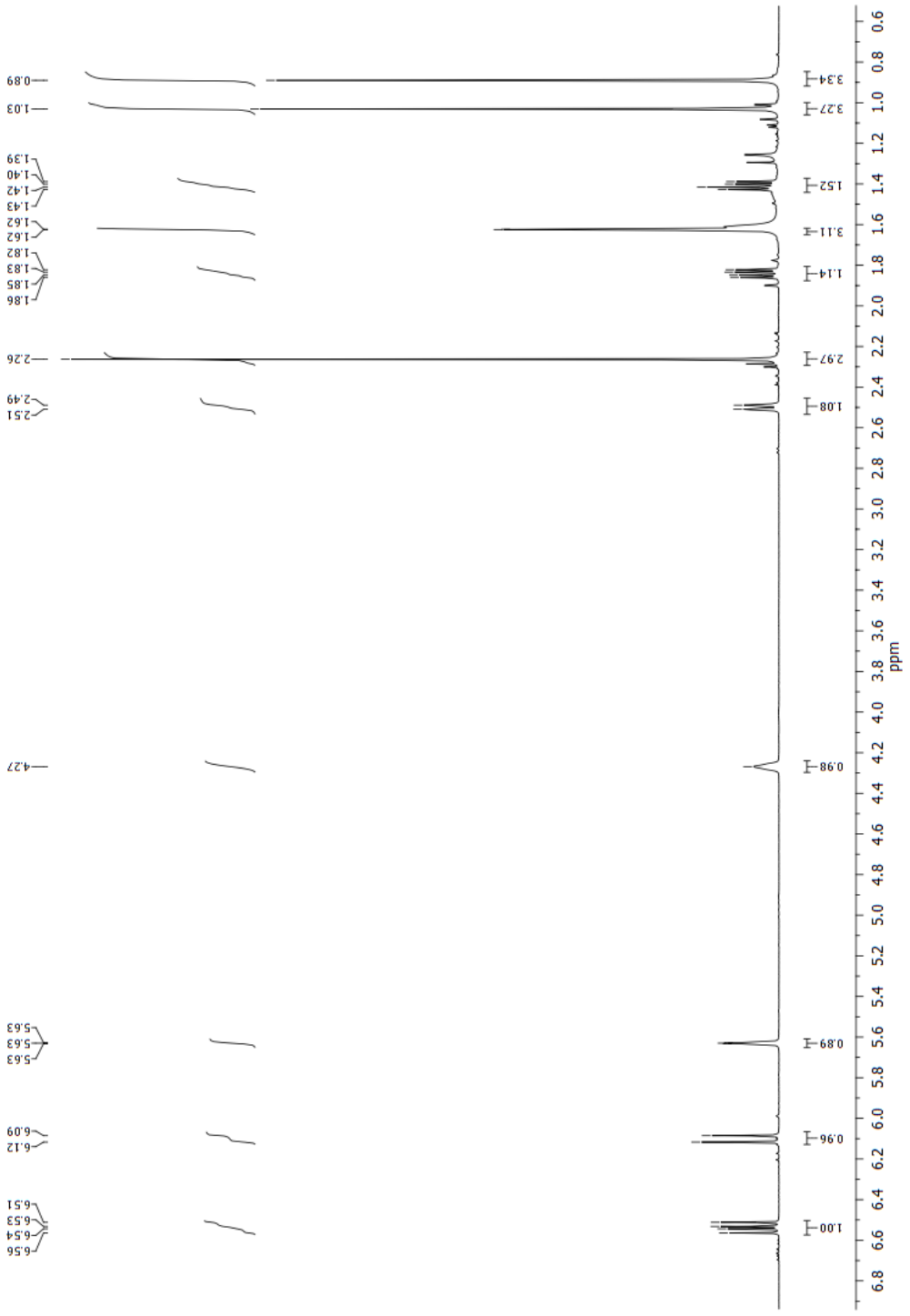

Figure F.7: ^{1}H NMR of *trans*-3-hydroxy-α-ionone

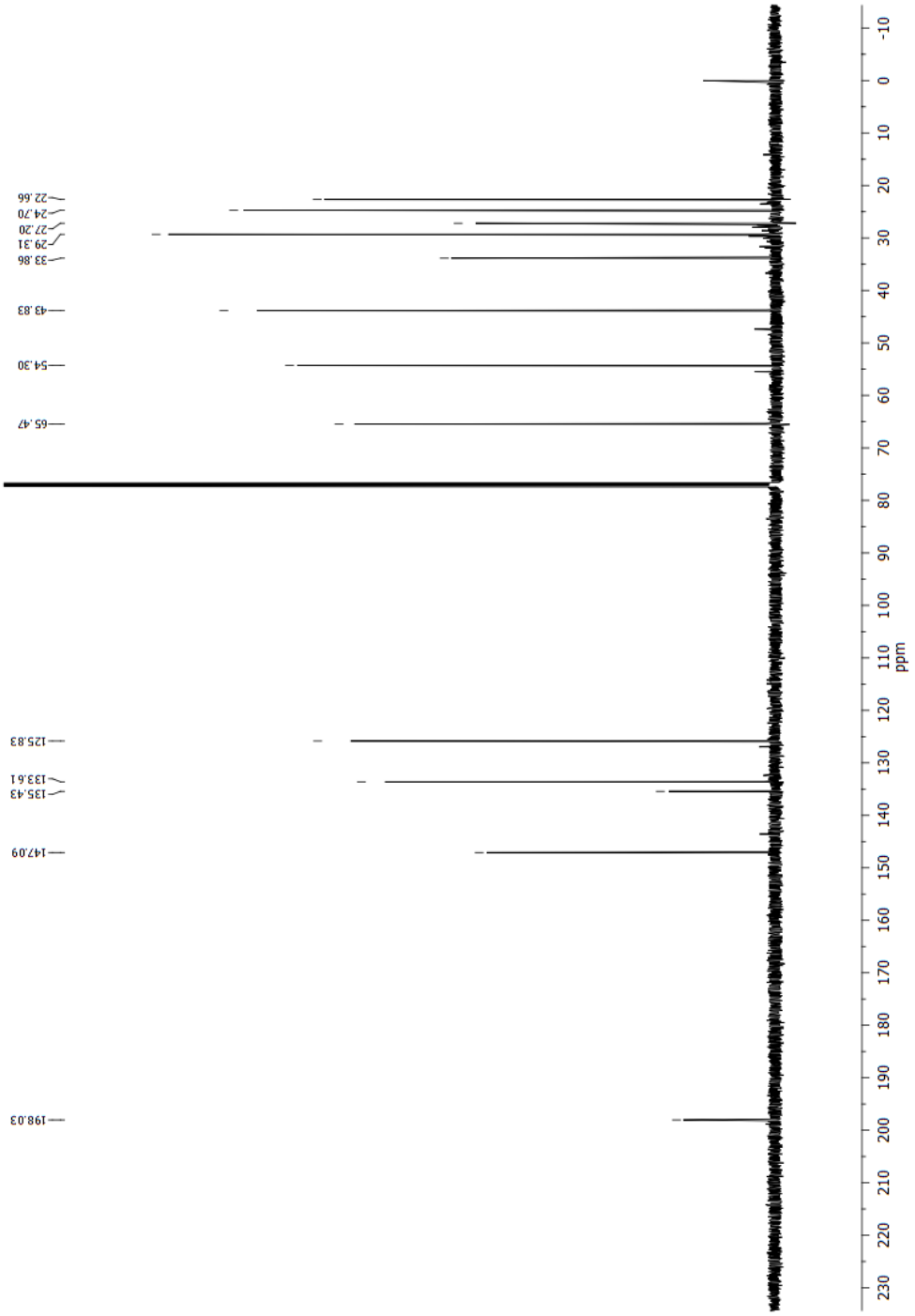

Figure F.8: ^{13}C NMR of *trans*-3-hydroxy-α-ionone

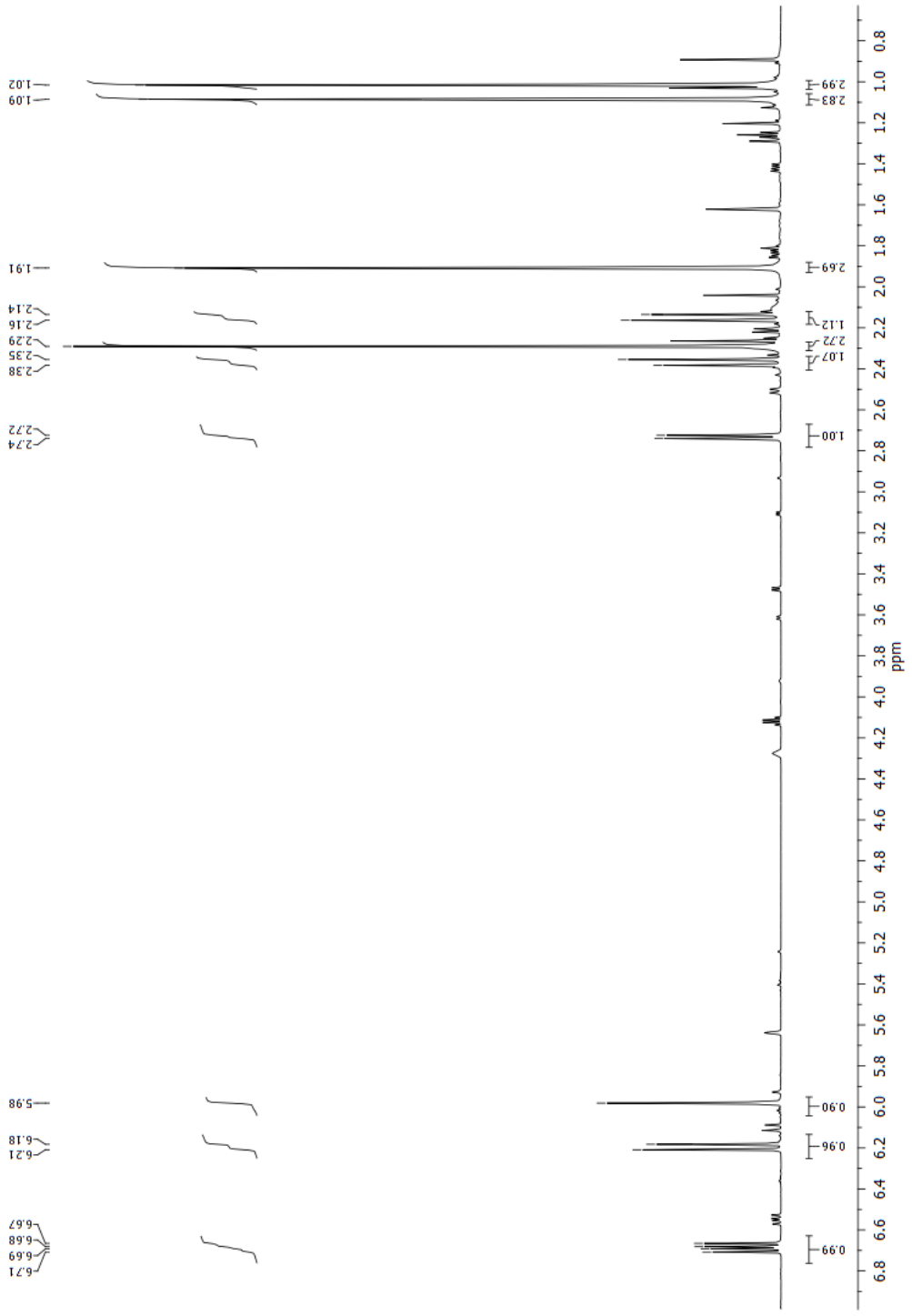

Figure F.9: ^{1}H NMR of 3-oxo-α-ionone

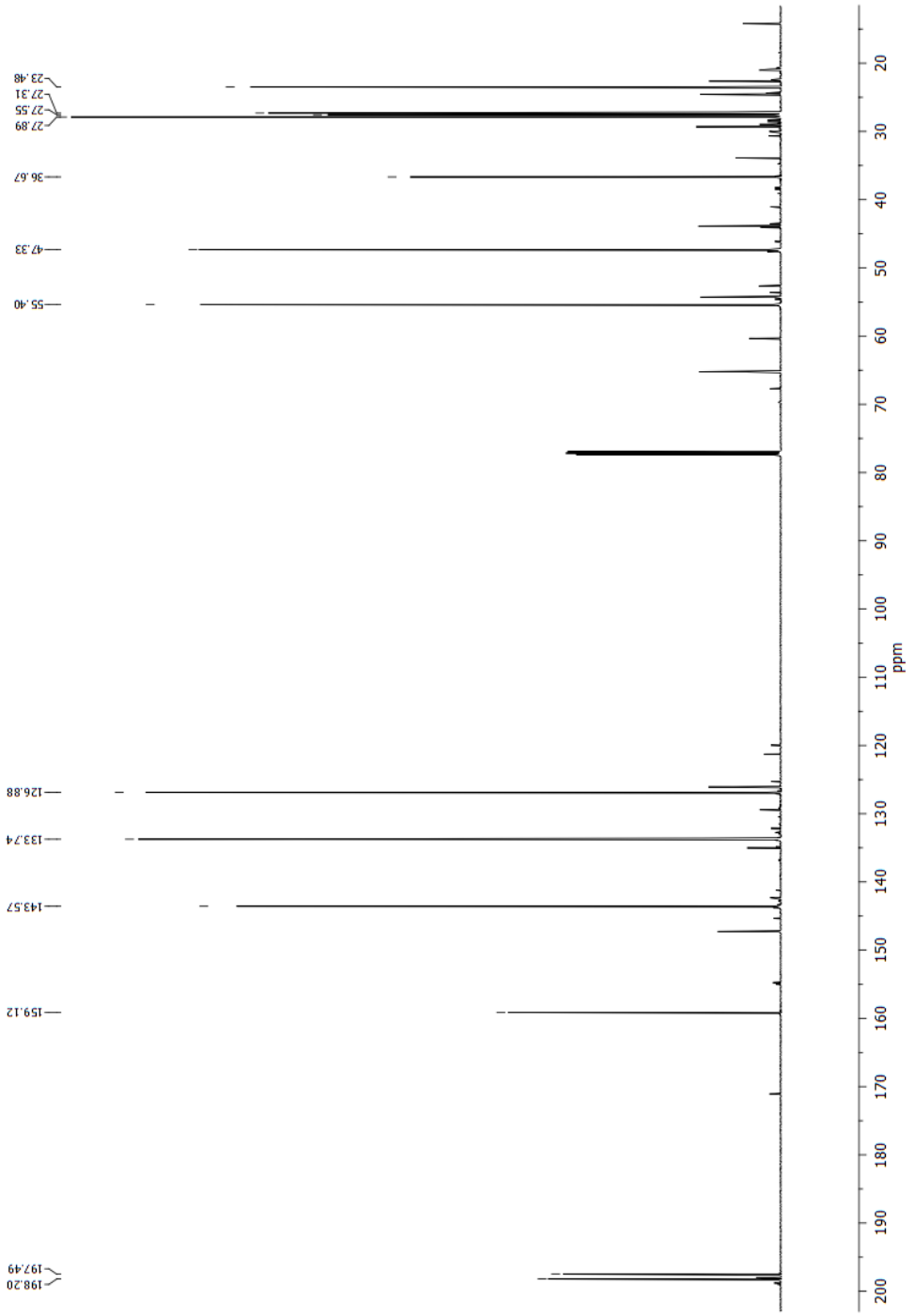

Figure F.10: ^{13}C NMR of 3-oxo-α-ionone

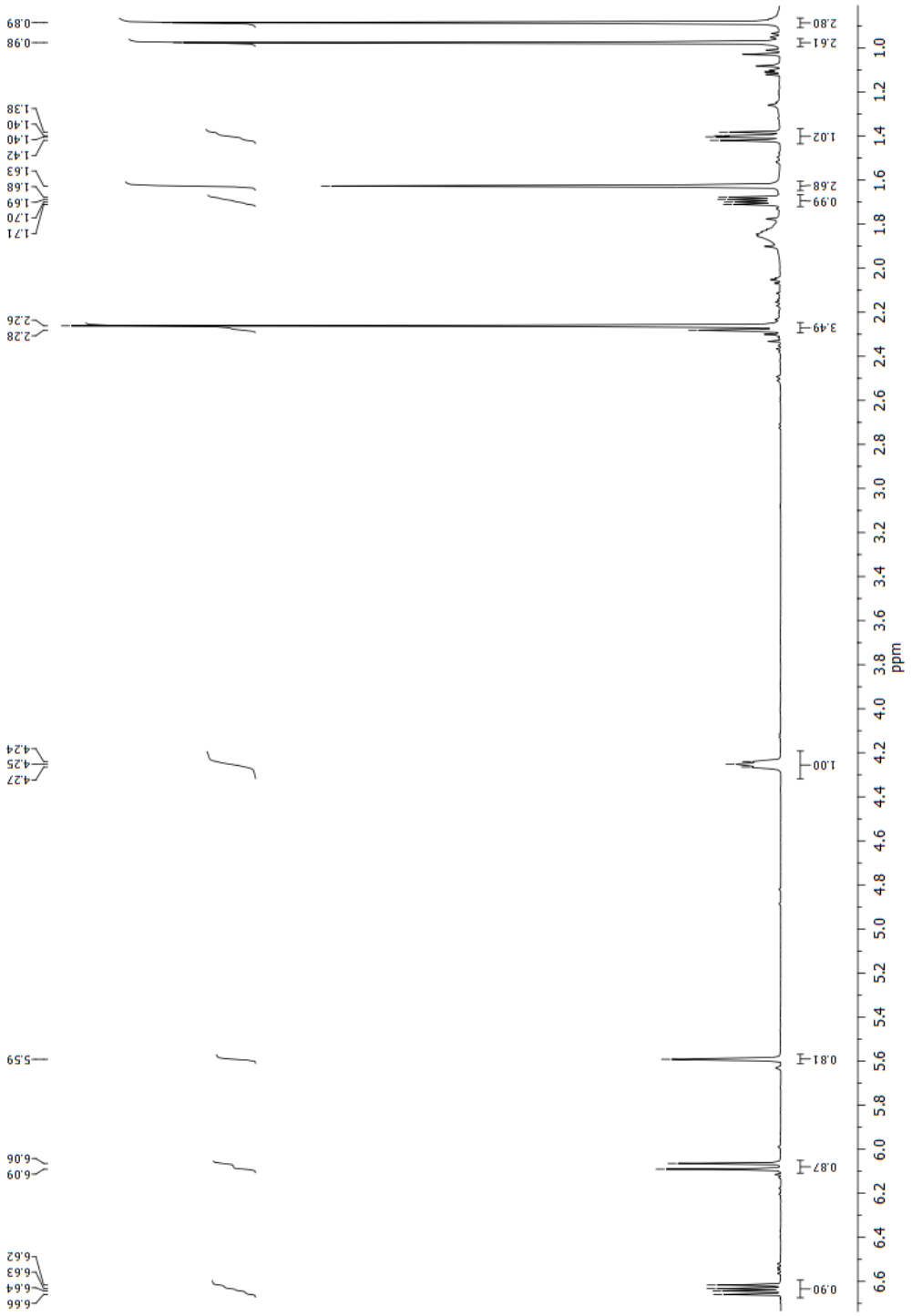

Figure F.11: ^{1}H NMR of *cis*-3-hydroxy-α-ionone

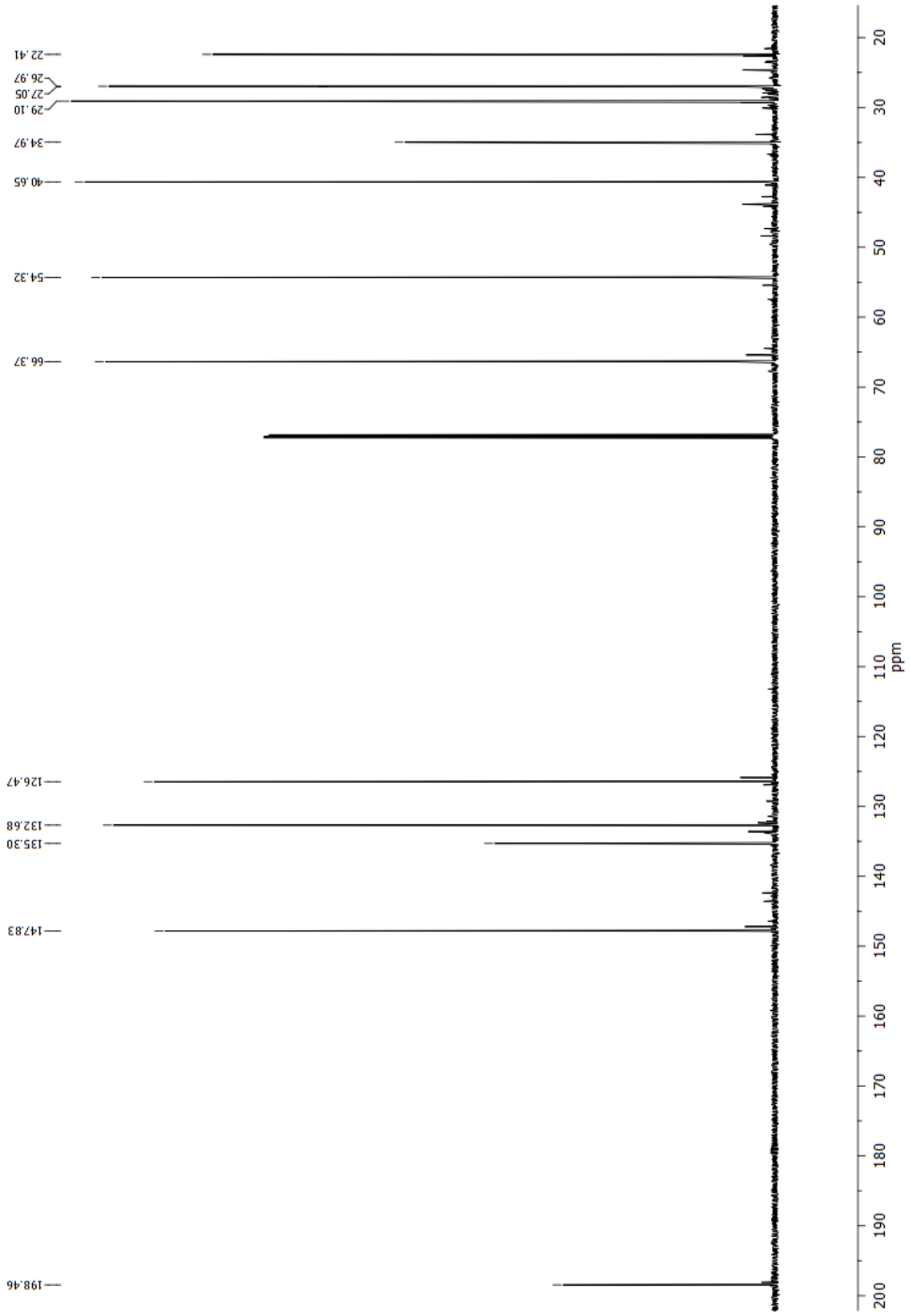

Figure F.12: ^{13}C NMR of *cis*-3-hydroxy-α-ionone

F.3 β-Damascone

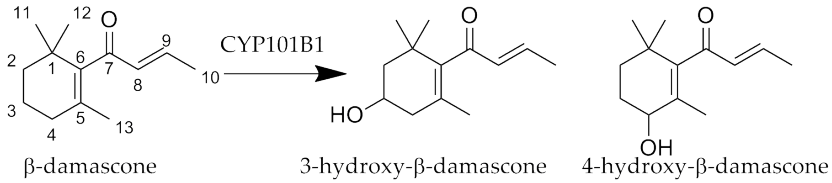

Figure F.13: β-Damascone products

Data for 3-hydroxy-β-damascone:
^{1}H NMR (600 MHz, $CDCl_3$) δ 6.74 (dq, J = 13.8, 6.9 Hz, 1H, H9), 6.16 (dd, J = 15.7, 1.3 Hz, 1H, H8), 4.11 - 4.04 (m, 1H, H3), 2.36 (dd, J = 16.8, 5.8 Hz, 1H, H4), 2.04 (dd, J = 17.1, 9.3 Hz, 1H, H4), 1.93 (dd, J = 6.9, 1.4 Hz, 3H, H10), 1.79 - 1.73 (m, 1H, H2), 1.54 (s, 3H, H13), 1.51 (t, J = 12.0 Hz, 1H, H2), 1.15 (s, 3H, H11), 0.99 (s, 3H, H12); ^{13}C NMR (151 MHz, $CDCl_3$) δ 201.85 (C7), 146.41 (C9), 139.87 (C6), 134.40 (C8), 128.23 (C5), 64.65 (C3), 47.78 (C2), 40.87 (C4), 36.31 (C1), 29.70 (C12), 29.08 (C11), 21.04 (C13), 18.41 (C10).

Data for 4-hydroxy-β-damascone:
^{1}H NMR (600 MHz, $CDCl_3$) δ 6.77 (dq, J = 15.6, 6.9 Hz, 1H, H9), 6.15 (dd, J = 15.7, 1.5 Hz, 1H, H8), 4.00 (t, J = 5.0 Hz, 1H, H4), 2.03 - 1.96 (m, 1H, H3), 1.93 (dd, J = 6.9, 1.5 Hz, 3H, H10), 1.80 - 1.74 (m, 1H, H3), 1.69 - 1.65 (m, 1H, H2), 1.65 (s, 3H, H13), 1.45 (ddd, J = 13.4, 7.7, 3.1 Hz, 1H, H2), 1.04 (s, 6H, H11 and H12); ^{13}C NMR (151 MHz, $CDCl_3$) δ 200.89 (C7), 146.46 (C9), 143.59 (C6), 133.92 (C8), 130.98 (C5), 69.01 (C4) 34.64 (C2), 33.98 (C1), 28.82 (C11), 28.64 (C3), 27.64 (C12), 18.46 (C10), 17.96 (C13).

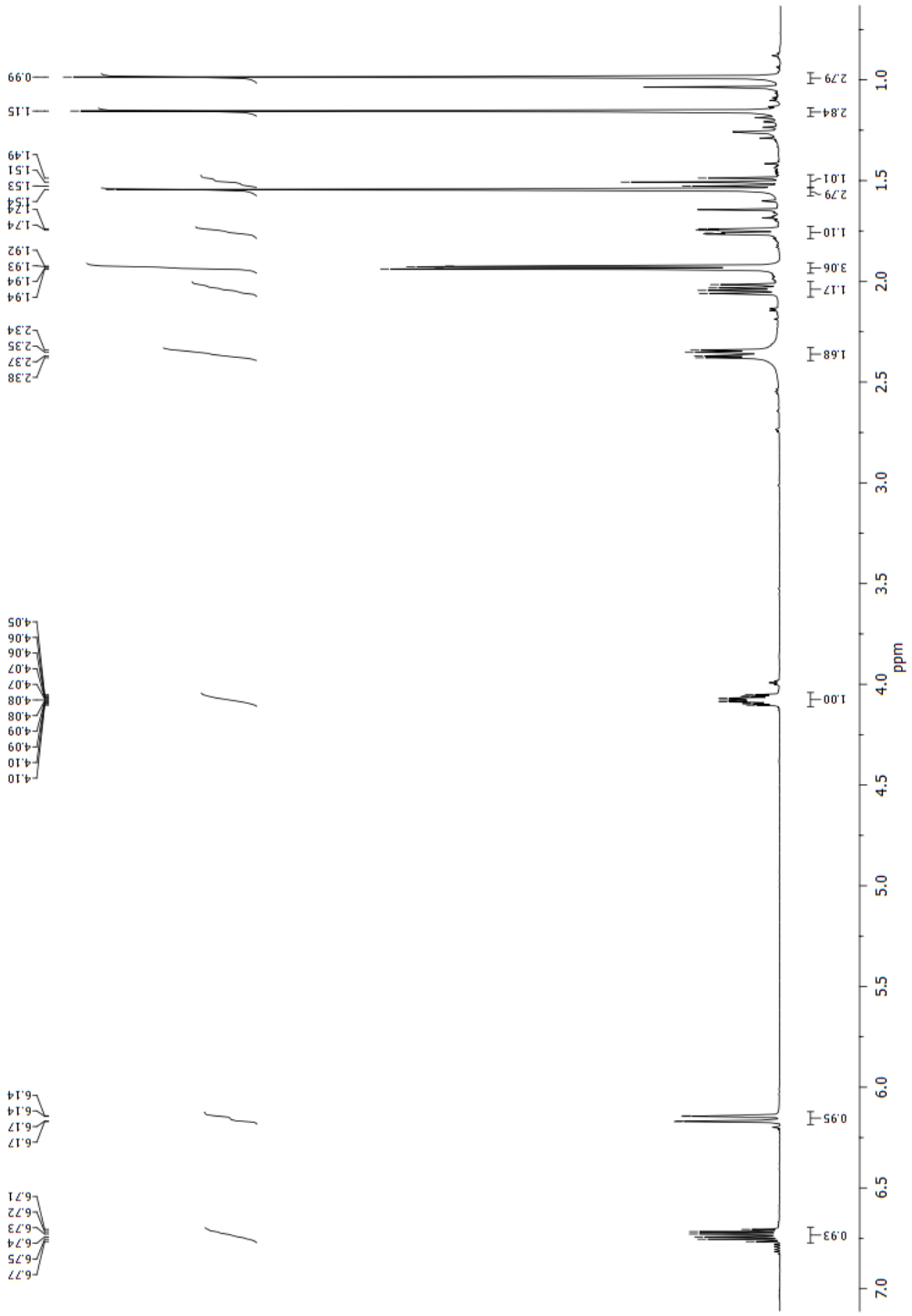

Figure F.14: ^{1}H NMR of 3-hydroxy-β-damascone

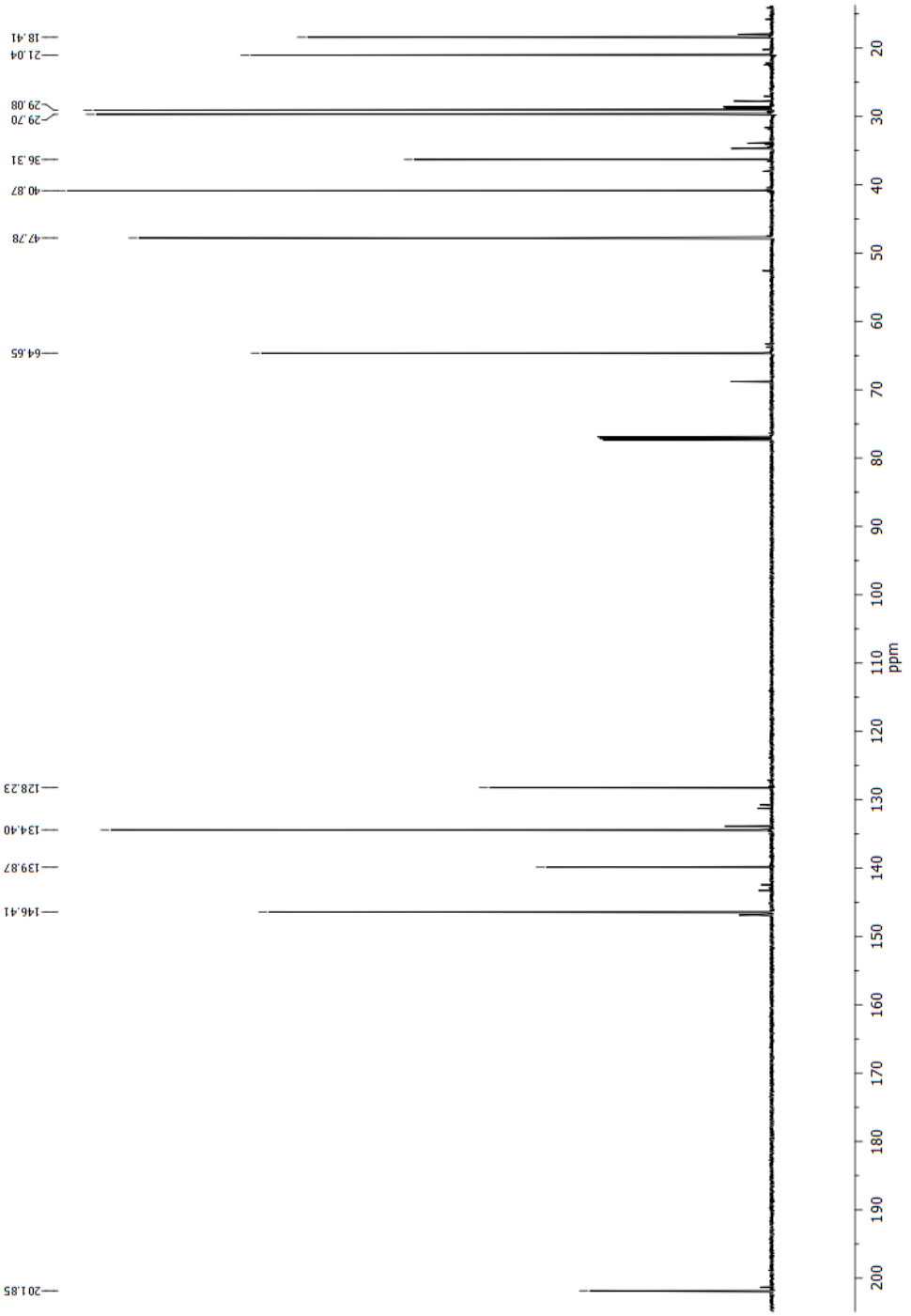

Figure F.15: ^{13}C NMR of 3-hydroxy-β-damascone

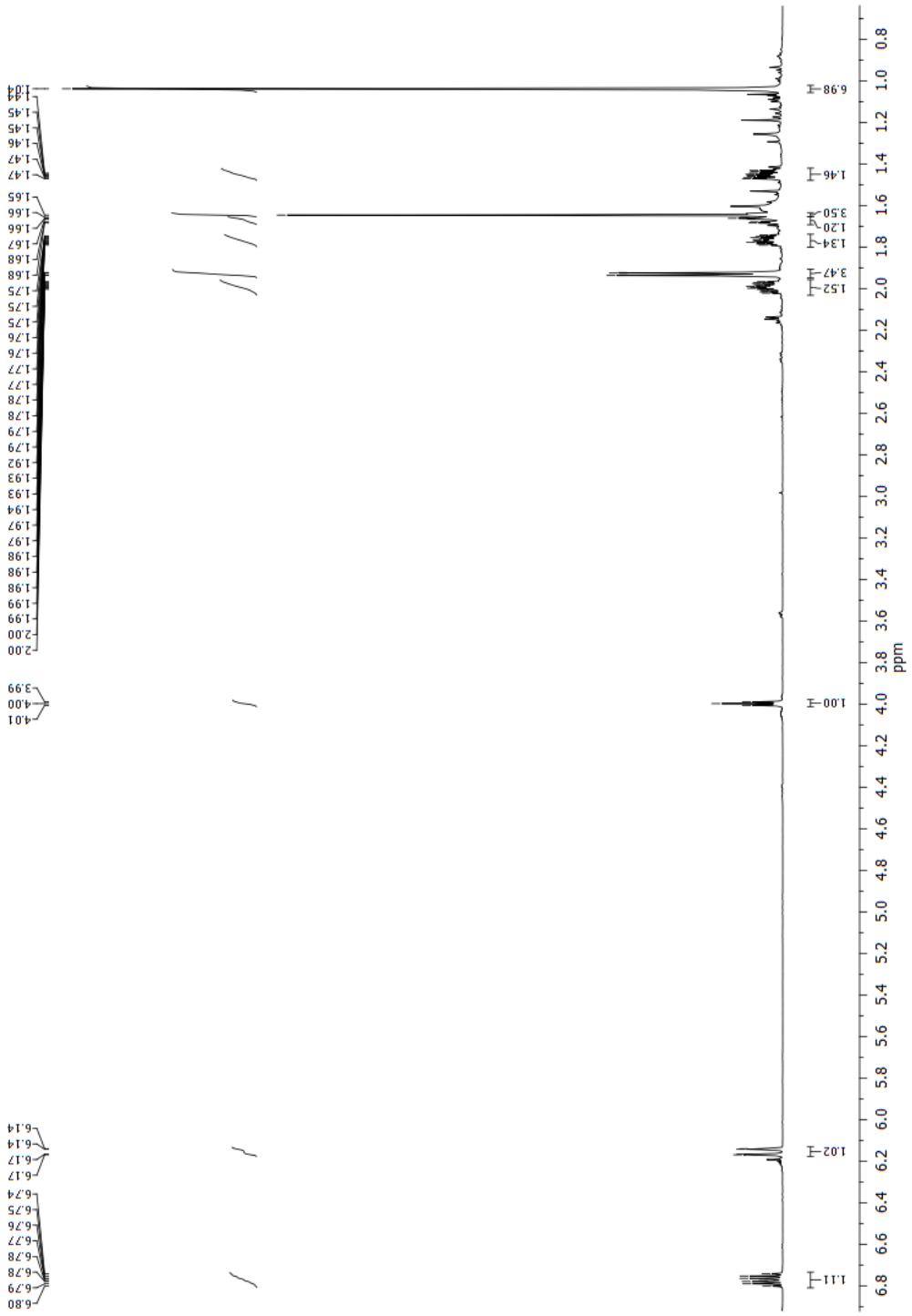

Figure F.16: ^{1}H NMR of 4-hydroxy-β-damascone

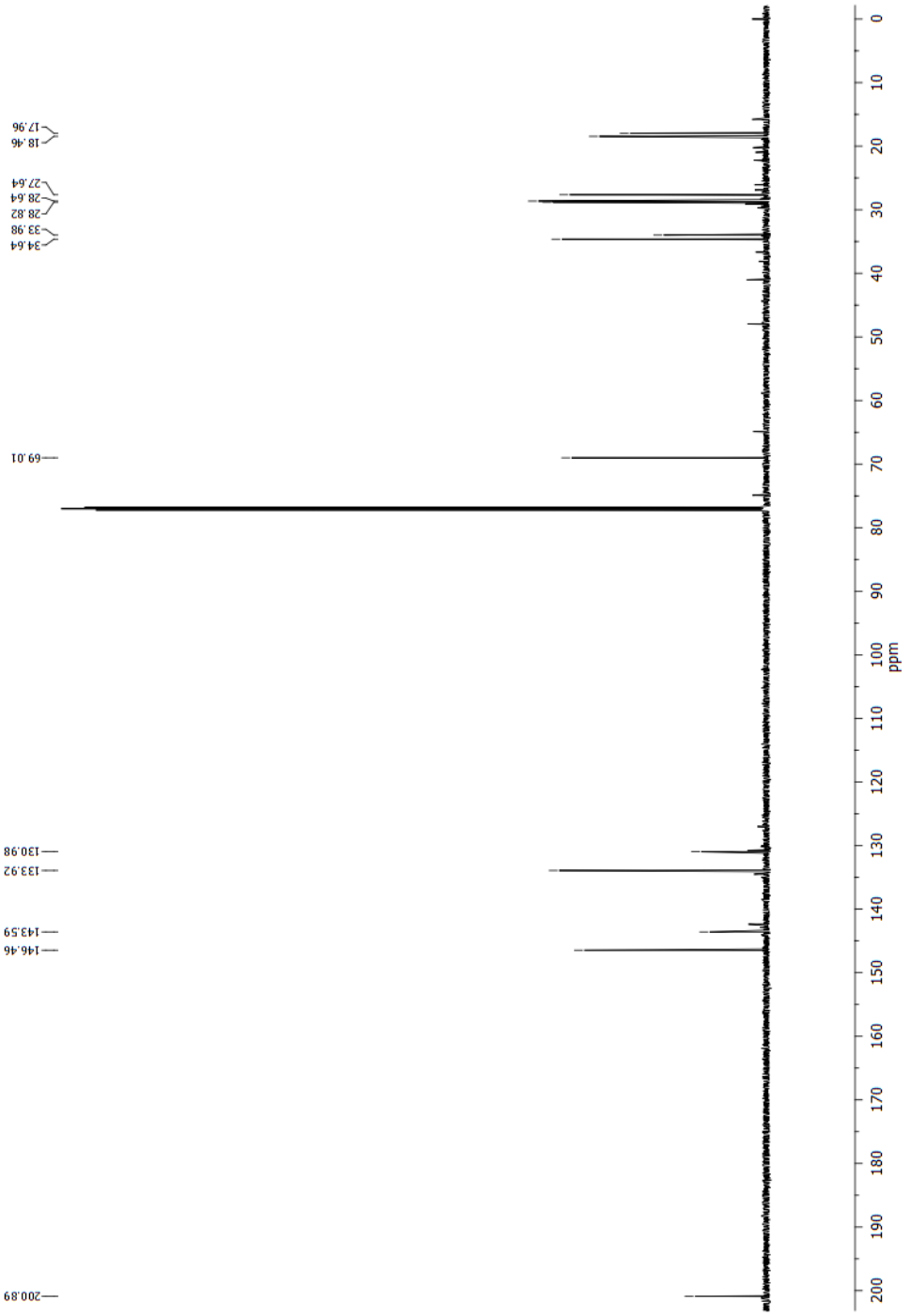

Figure F.17: ^{13}C NMR of 4-hydroxy-β-damascone

F.4 α-Methyl ionone

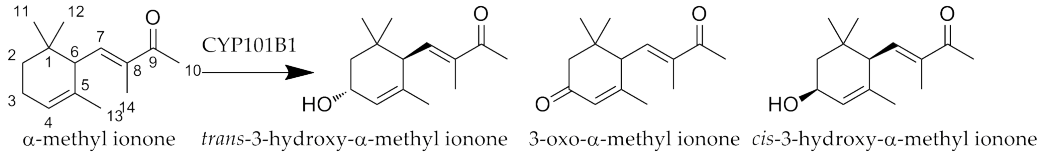

Figure F.18: α-methyl ionone products

Data for 3-oxo-α-methyl ionone:
^{1}H NMR (500 MHz, $CDCl_3$) δ 6.42 (dd, J = 10.9, 1.0 Hz, 1H H7), 5.96 (s, 1H, H4), 3.08 (d, J = 10.9 Hz, 1H, H6), 2.43 (d, J = 16.9 Hz, 1H, H2), 2.34 (s, 3H, H10), 2.20 (d, J = 16.9 Hz, 1H, H2), 1.93 (d, J = 1.0 Hz, 3H, H13), 1.87 (d, J = 0.4 Hz, 3H, H14), 1.10 (s, 3H, H11), 0.97 (s, 3H, H12); ^{13}C NMR (126 MHz, $CDCl_3$) δ 199.22 (C9), 198.36 (C3), 160.41 (C8), 140.66 (C5), 139.22 (C7), 126.35 (C4), 51.77 (C6), 47.80 (C2), 36.85 (C1), 28.05 (C11), 26.57 (C12), 25.82 (C14), 23.50 (C13), 12.13 (C10).

Data for *trans*-3-hydroxy-α-methyl ionone:
^{1}H NMR (500 MHz, $CDCl_3$) δ 6.41 (dd, J = 11.0, 1.3 Hz, 1H, H7), 5.54 (d, J = 0.9 Hz, 1H, H4), 4.29 (t, J = 6.8 Hz, 1H, H3), 2.63 (d, J = 10.9 Hz, 1H, H6), 2.32 (s, 3H, H10), 1.87 (d, J = 1.3 Hz, 3H, H13), 1.71 (dd, J = 12.9, 6.5 Hz, 1H, H2), 1.61 - 1.59 (m, 3H, H14), 1.48 (dd, J = 12.7, 9.5 Hz, 1H, H2), 1.00 (s, 3H, H11), 0.85 (s, 3H, H12).

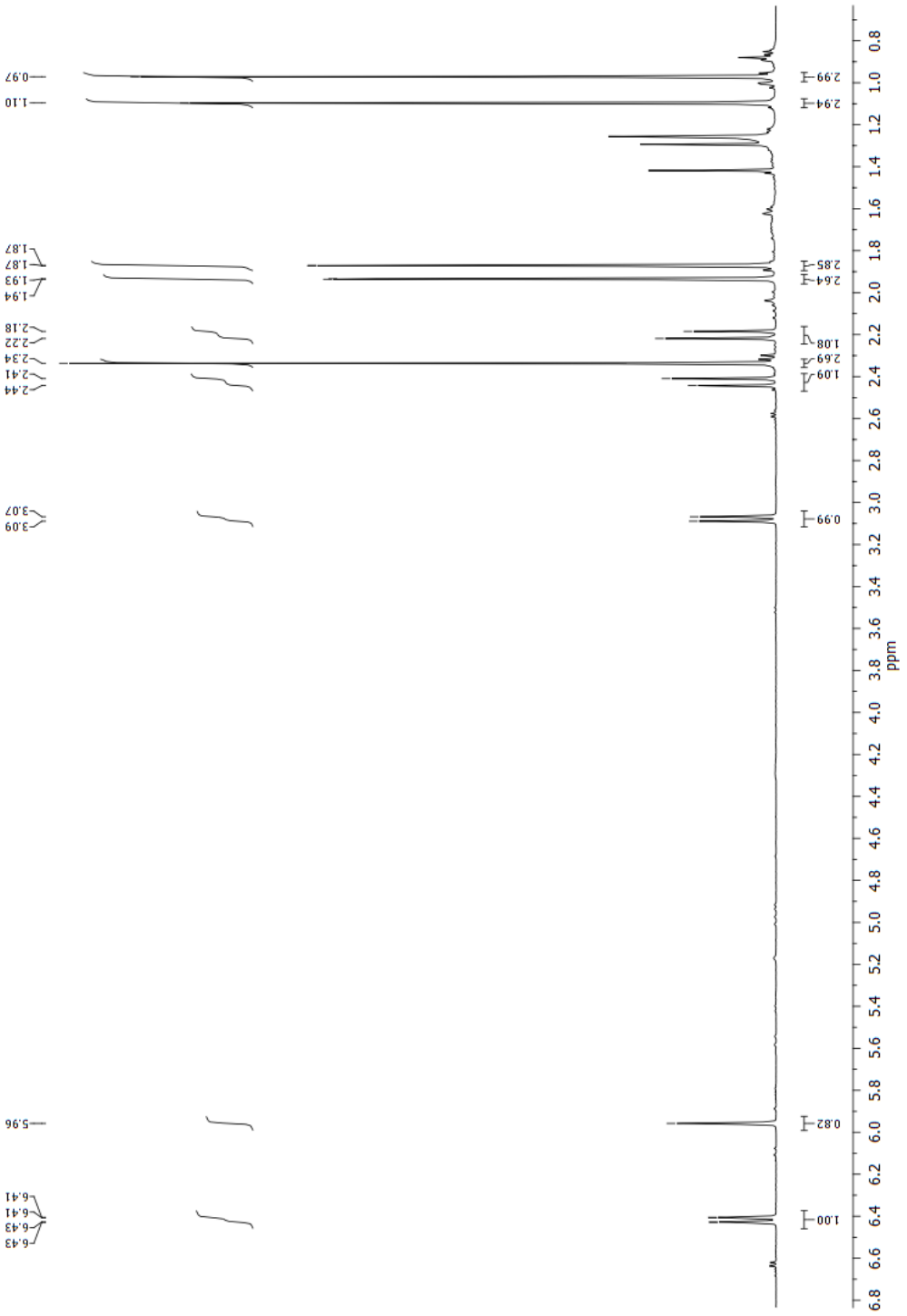

Figure F.19: ^{1}H NMR of 3-oxo-α-methyl ionone

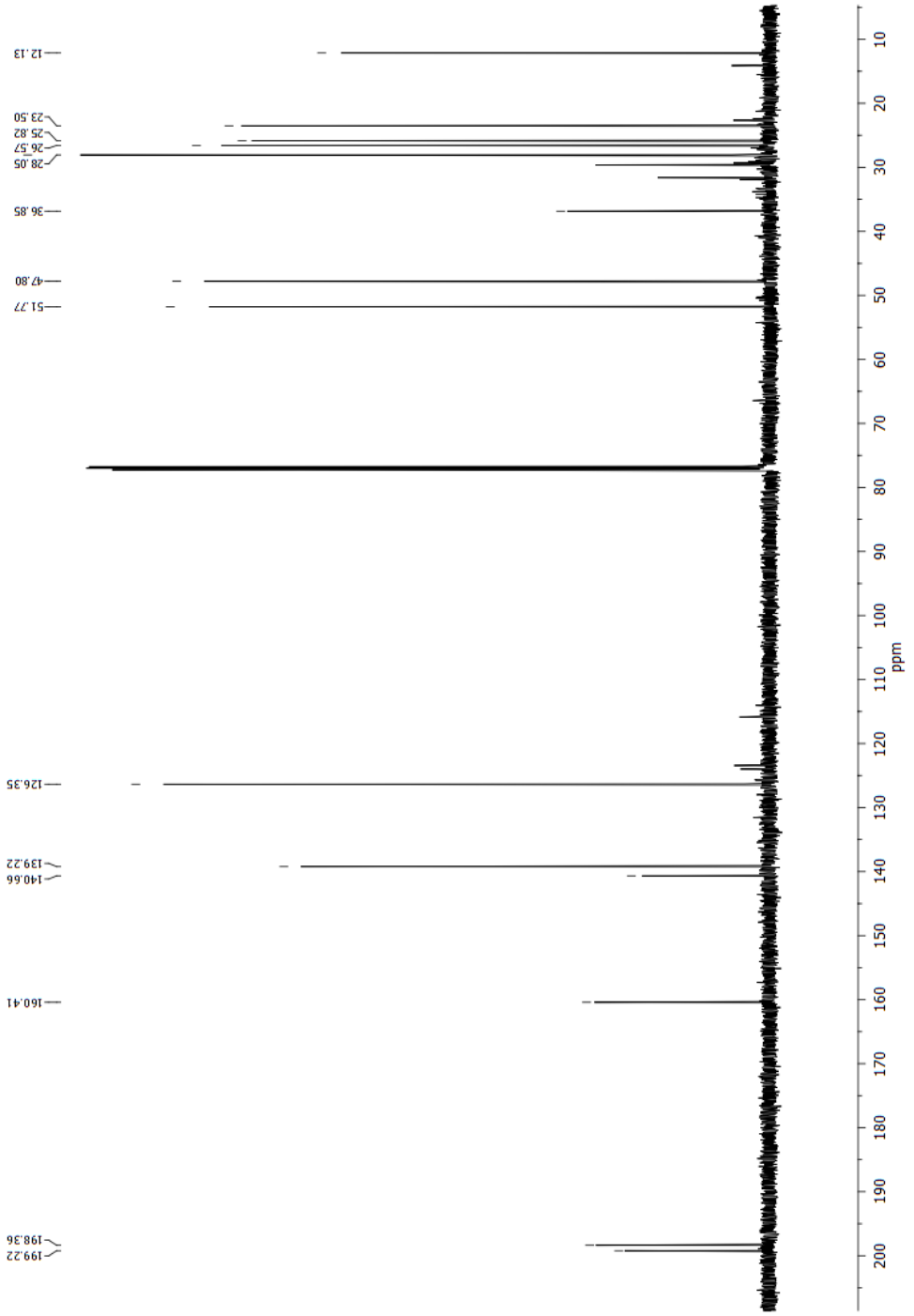

Figure F.20: ^{13}C NMR of 3-oxo-α-methyl ionone

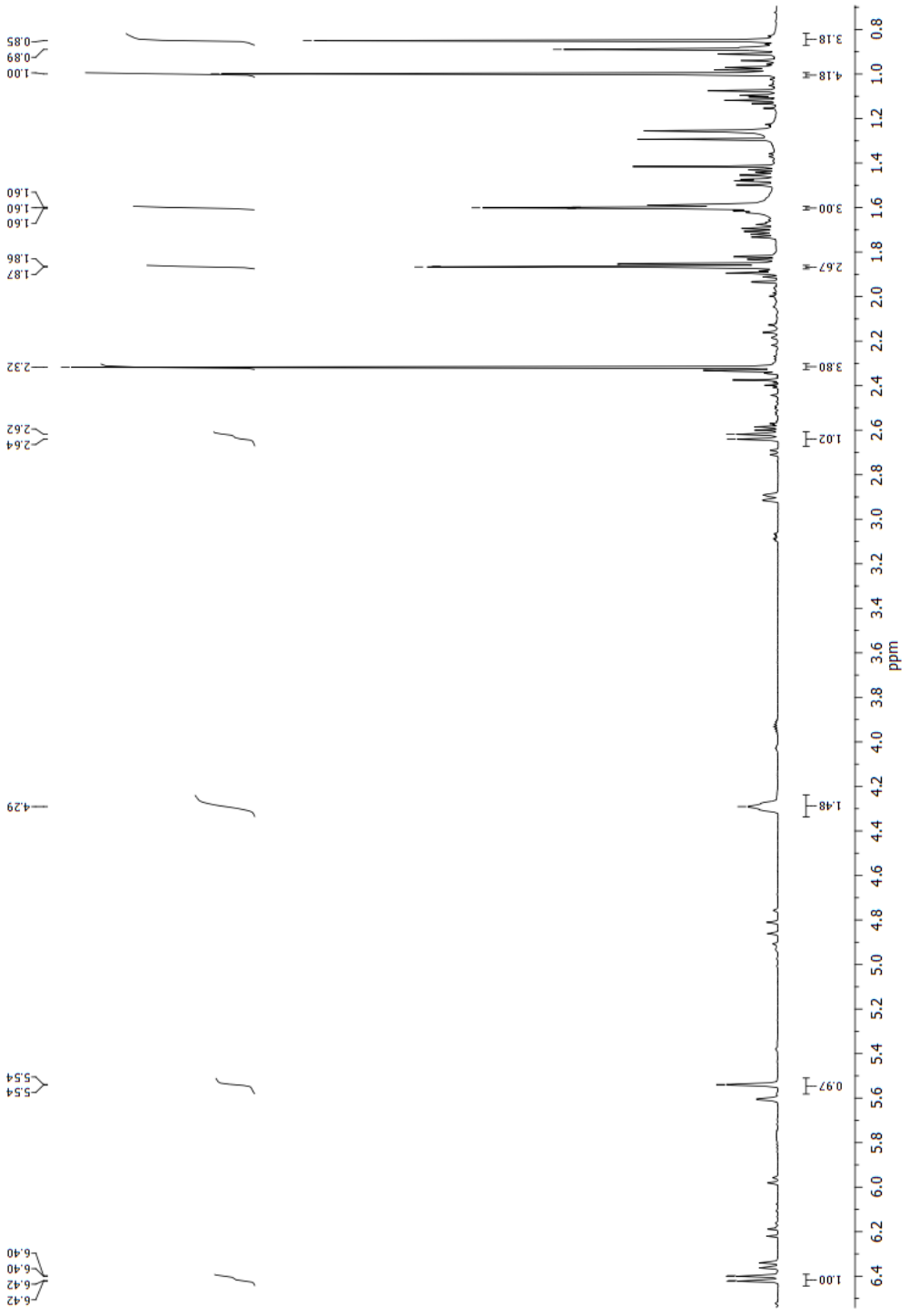

Figure F.21: ^{1}H NMR of *trans*-3-hydroxy-α-methyl ionone

F.5 α-Ionol

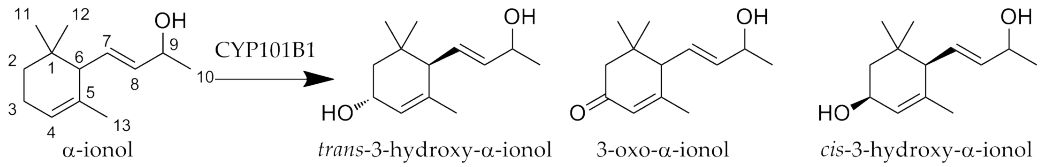

Figure F.22: α-Ionol products

Data for *trans*-3-hydroxy-α-ionol:
^{1}H NMR (500 MHz, $CDCl_3$) δ 5.90 (s, 1H, H4), 5.69 (d, J = 6.0 Hz, 1H, H8), 5.57 (t, J = 6.3 Hz, 1H, H7), 4.36 (dd, J = 12.5, 6.3 Hz, 1H, H9), 4.21 (d, J = 8.2 Hz, 1H, H3), 2.53 (d, J = 9.1 Hz, 1H, H6), 1.89 (s, 3H, H13), 1.66 - 1.60 (m, 1H, H2), 1.35 (dd, J = 13.1, 9.1 Hz, 1H, H2), 1.26 (d, J = 4.1 Hz, 3H, H10), 1.04 (s, 3H, H12), 0.98 (s, 3H, H11); ^{13}C NMR (126 MHz, $CDCl_3$) δ 138.44 (C4), 130.26 (C5), 126.56 (C8), 125.84 (C7), 68.32 (C9), 55.38 (C3), 53.93 (C6), 47.41 (C2), 29.02 (C1), 27.87 (C10), 27.14 (C11), 23.63 (C12), 23.48 (C13).

Data for 3-oxo-α-ionol:
^{1}H NMR (500 MHz, $CDCl_3$) δ 5.90 (s, 1H, H4), 5.68 (dd, J = 15.3, 6.0 Hz, 1H, H8), 5.54 (dd, J = 15.3, 9.2 Hz, 1H, H7), 4.43 - 4.28 (m, 1H, H9), 2.52 (d, J = 9.2 Hz, 1H, H6), 2.34 (d, J = 16.7 Hz, 1H, H2), 2.09 (d, J = 16.7 Hz, 1H, H2), 1.91 (s, 3H, H13), 1.30 (d, J = 6.2 Hz, 3H, H10), 1.03 (s, 3H, H12), 0.96 (s, 3H, H11); ^{13}C NMR (126 MHz, $CDCl_3$) δ 199.21 (C3), 161.95 (C5), 138.59 (C7), 126.65 (C8), 125.81 (C4), 68.31 (C9), 55.47 (C6), 47.50 (C2), 36.16 (C1), 27.90 (C13), 27.15 (C10), 23.70 (C12), 23.55 (C11).

Data for *cis*-3-hydroxy-α-ionol:
^{1}H NMR (500 MHz, $CDCl_3$) δ 6.67 (dd, J = 15.7, 9.6 Hz, 1H, H7), 6.19 (d, J = 15.8 Hz, 1H, H8), 5.99 (s, 1H, H4), 4.32 (dd, J = 12.3, 6.2 Hz, 1H, H9), 4.22 (s, 1H, H3), 2.71 (d, J = 9.6 Hz, 1H, H6), 2.29 (s, 3H, H13), 1.68 - 1.59 (m, 1H, H2), 1.35 (dd, J = 15.5, 9.4 Hz, 1H, H2), 1.29 (d, J = 7.9 Hz, 3H, H10), 1.08 (s, 3H, H12), 1.01 (s, 3H, H11); ^{13}C NMR (126 MHz, $CDCl_3$) δ 143.54 (C4), 136.83 (C5), 133.71 (C8), 126.92 (C7), 66.70 (C9), 55.43 (C3), 53.95 (C6), 47.32 (C2), 31.90 (C1), 31.60 (C10), 27.90 (C12), 27.32 (C11), 23.48 (C13).

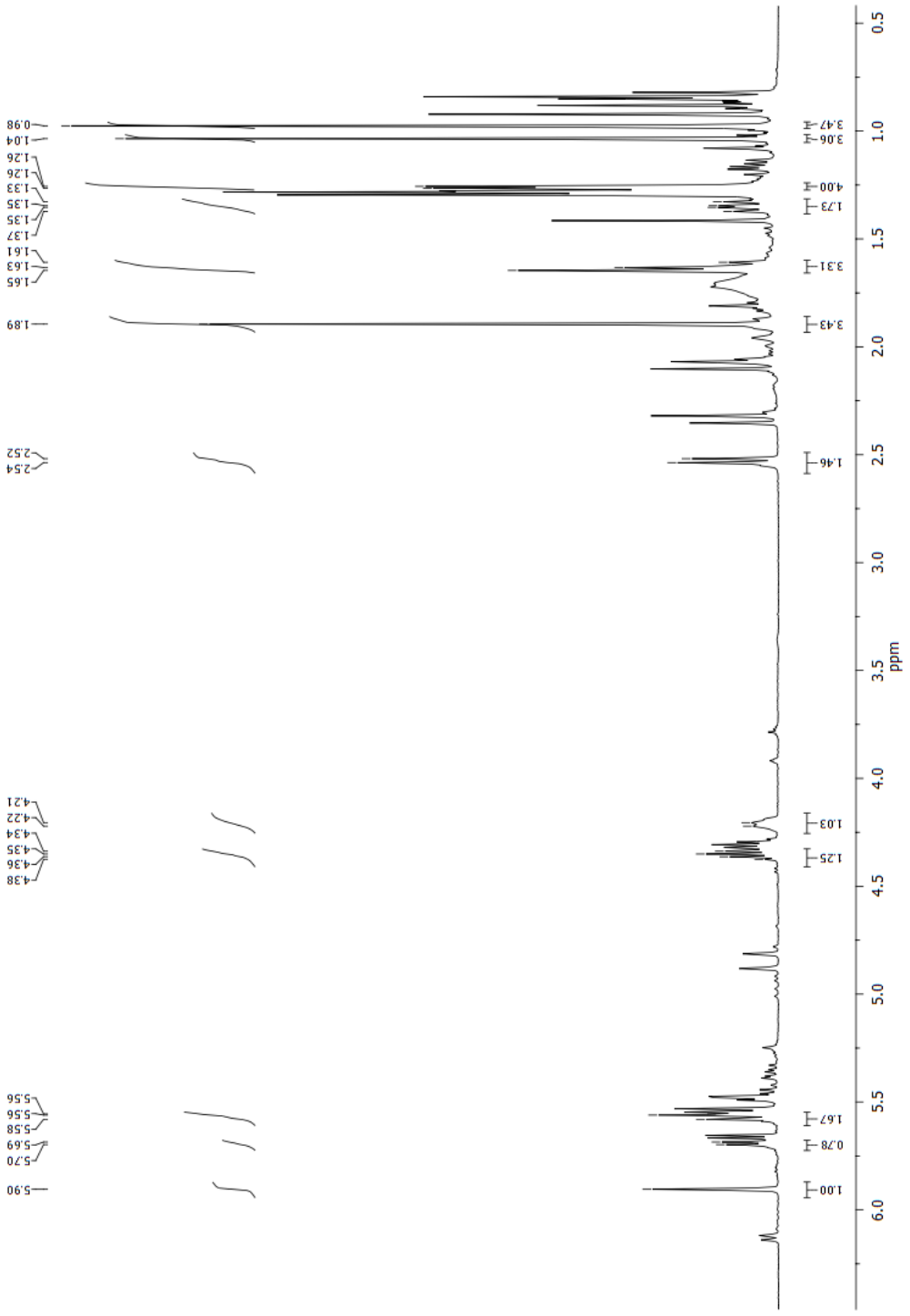

Figure F.23: ^{1}H NMR of *trans*-3-hydroxy-α-ionol

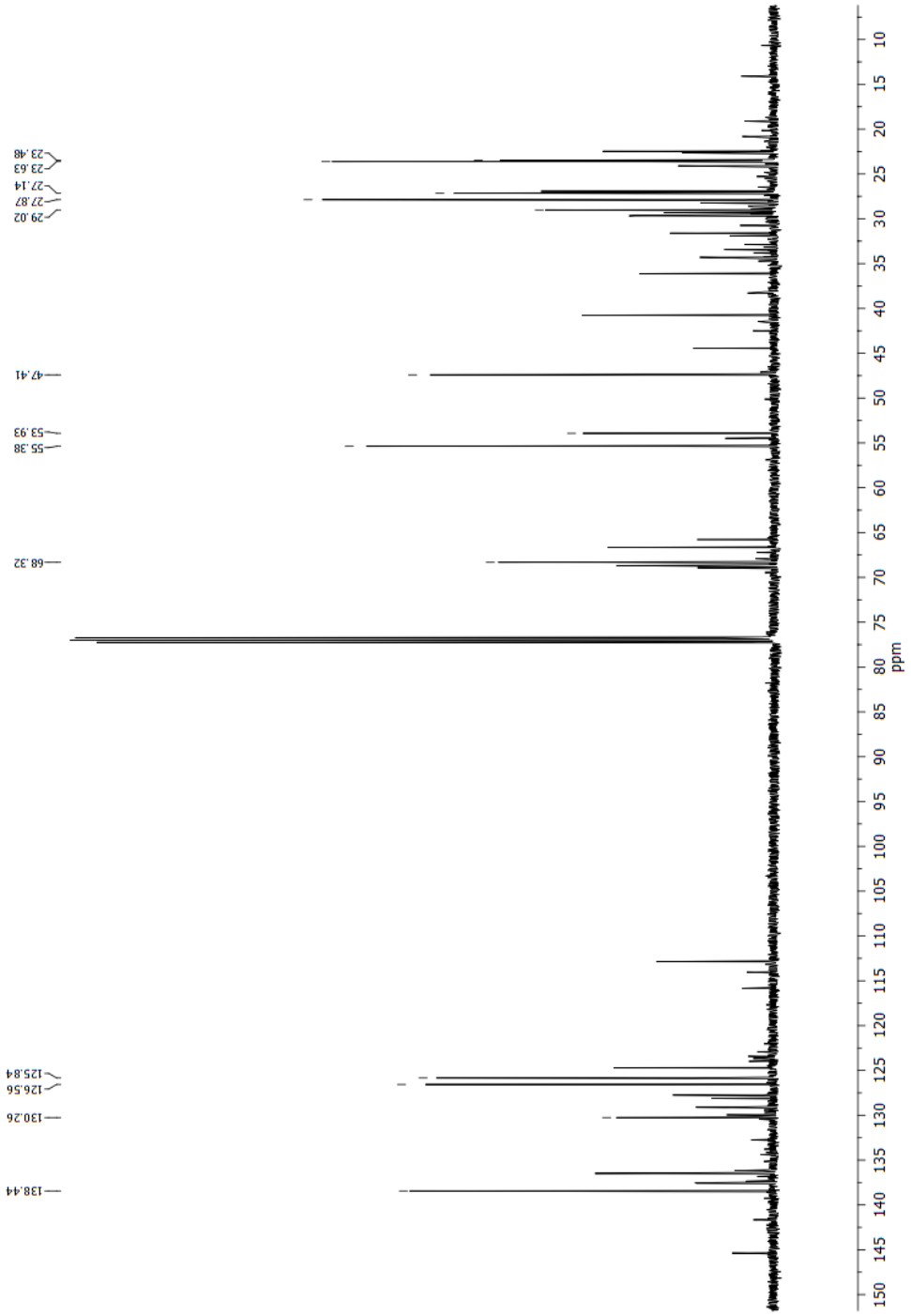

Figure F.24: ^{13}C NMR of *trans*-3-hydroxy-α-ionol

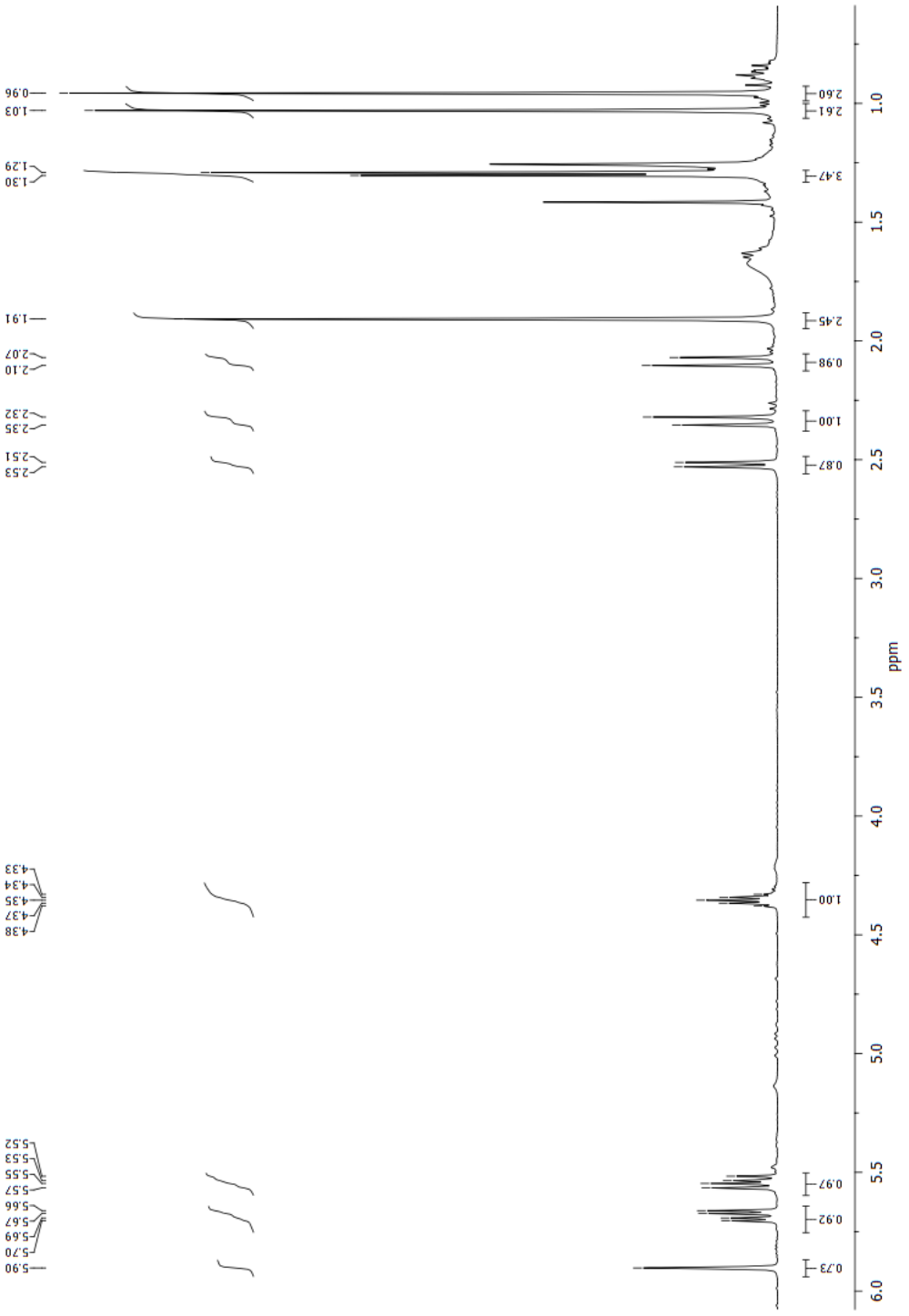

Figure F.25: ^{1}H NMR of 3-oxo-α-ionol

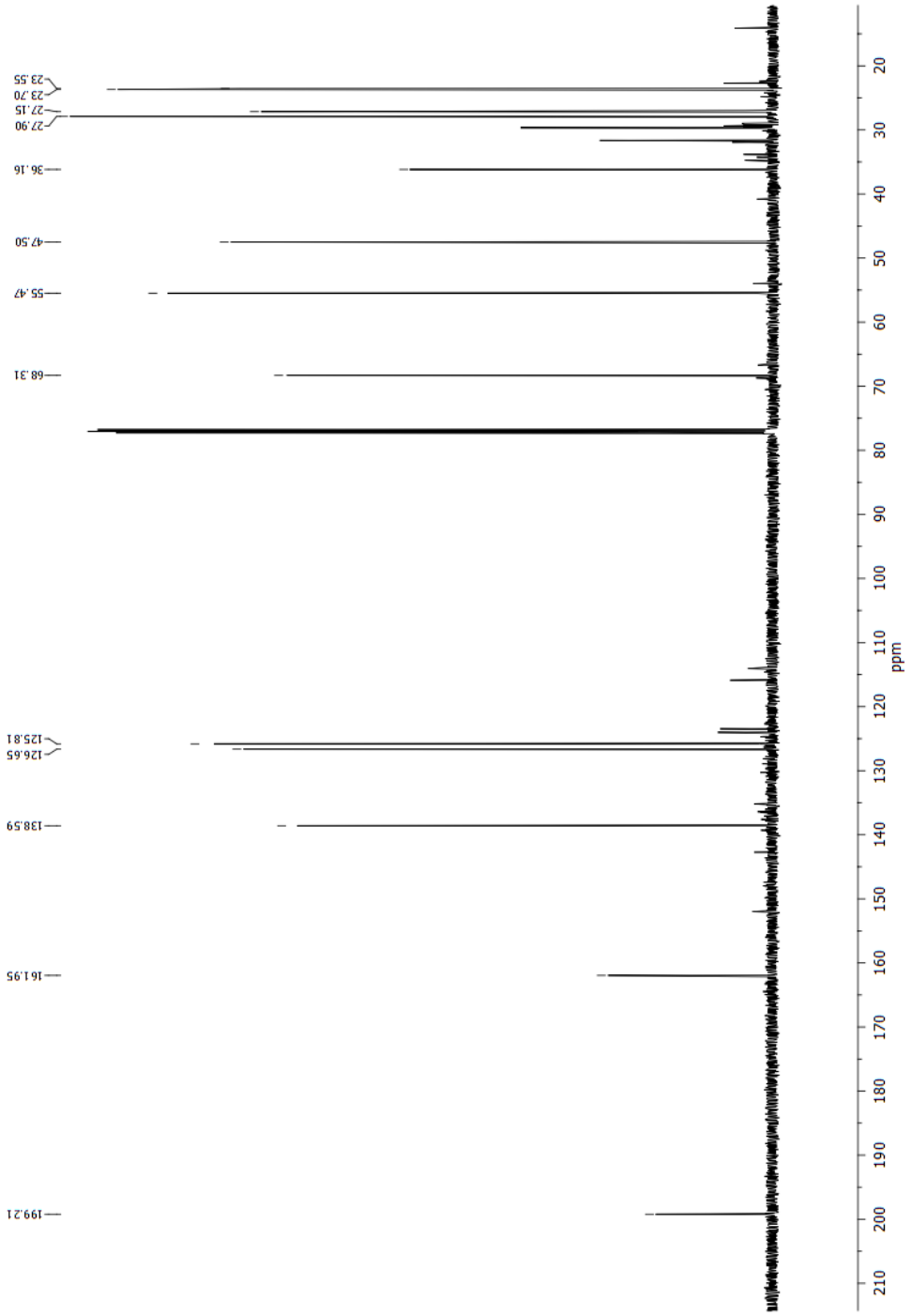

Figure F.26: ^{13}C NMR of 3-oxo-α-ionol

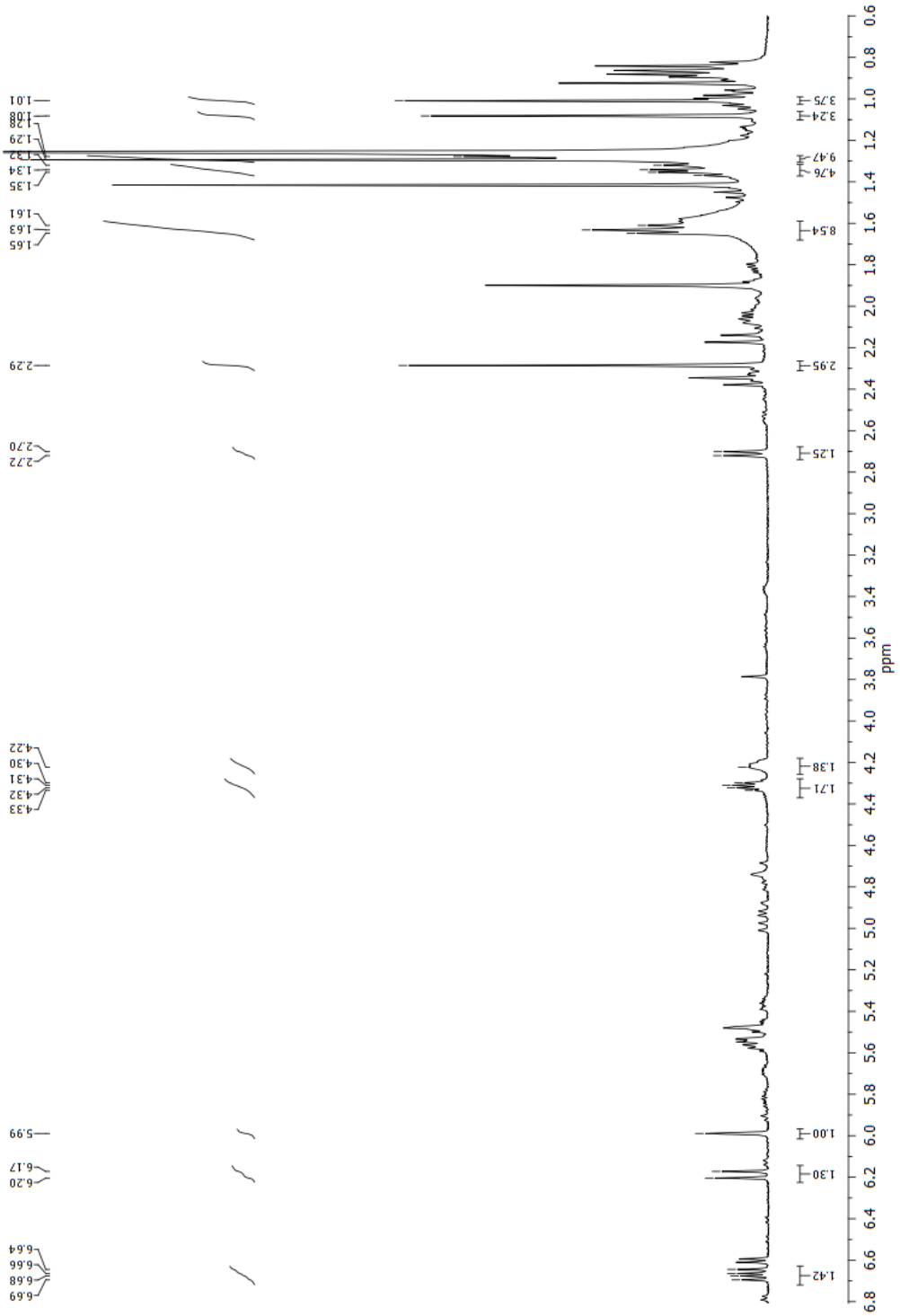

Figure F.27: ^{1}H NMR of *cis*-3-hydroxy-α-ionol

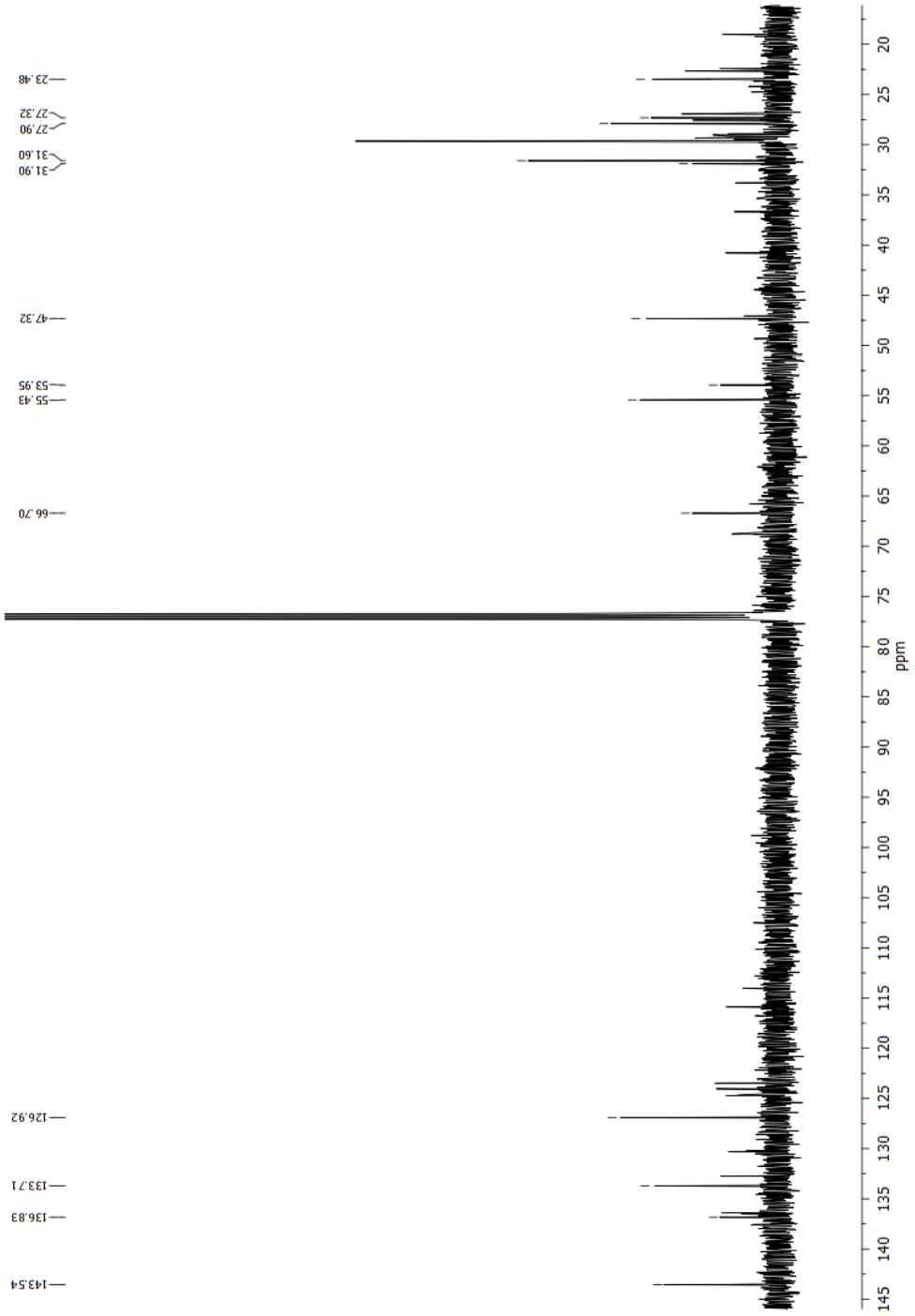

Figure F.28: ^{13}C NMR of *cis*-3-hydroxy-α-ionol

F.6 β-Ionol

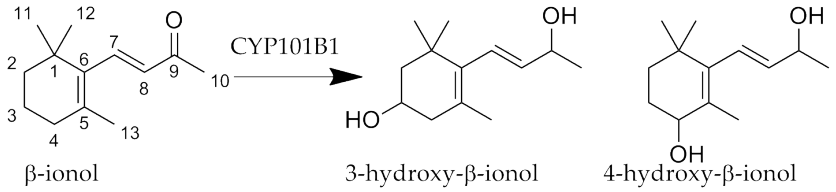

Figure F.29: β-Ionol products

Data for 3-hydroxy-β-ionol:
^{1}H NMR (500 MHz, $CDCl_3$) δ 6.01 (d, J = 15.9 Hz, 1H, H7), 5.50 (dd, J = 15.9, 6.5 Hz, 1H, H8), 4.37 (dt, J = 14.0, 6.8 Hz, 1H, H9), 4.03 - 3.94 (m, 1H, H3), 2.35 (dd, J = 15.4, 6.5 Hz, 1H, H4), 2.12 - 1.96 (m, 1H, H4), 1.76 (ddd, J = 12.1, 3.4, 2.1 Hz, 1H, H2), 1.72 - 1.67 (m, 3H, H13), 1.49 - 1.42 (m, 1H, H2), 1.32 (d, J = 6.4 Hz, 3H, H10), 1.05 (s, 3H, H11), 1.04 (s, 3H, H12); ^{13}C NMR (126 MHz, $CDCl_3$) δ 138.44 (C8), 136.50 (C6), 129.24 (C5), 126.63 (C7), 69.36 (C9), 65.08 (C3), 48.22 (C2), 42.18 (C4), 31.93 (C1), 31.62 (C10), 30.05 (C11), 28.41 (C12), 23.60 (C13).

Data for 4-hydroxy-β-ionol:
^{1}H NMR (500 MHz, $CDCl_3$) δ 6.04 (d, J = 16.0 Hz, 1H, H7), 5.54 (dd, J = 16.0, 6.4 Hz, 1H H8), 4.44 - 4.34 (m, 1H, H9), 3.98 (t, J = 4.7 Hz, 1H, H4), 1.94 - 1.85 (m, 1H, H3), 1.80 (s, 3H, H13), 1.68 - 1.59 (m, 2H, H2 and H3), 1.41 - 1.38 (m, 1H, H2), 1.32 (d, J = 6.4 Hz, 3H, H10), 1.01 (d, J = 2.5 Hz, 3H, H11), 0.98 (d, J = 1.8 Hz, 3H, H12); ^{13}C NMR (126 MHz, $CDCl_3$) δ 138.56 (C8), 129.46 (C6), 127.05 (C5), 126.58 (C7), 70.01 (C4), 69.18 (C9), 37.35 (C1), 34.33 (C2), 28.81 (C12), 26.82 (C11), 23.56 (C10), 18.26 (C13).

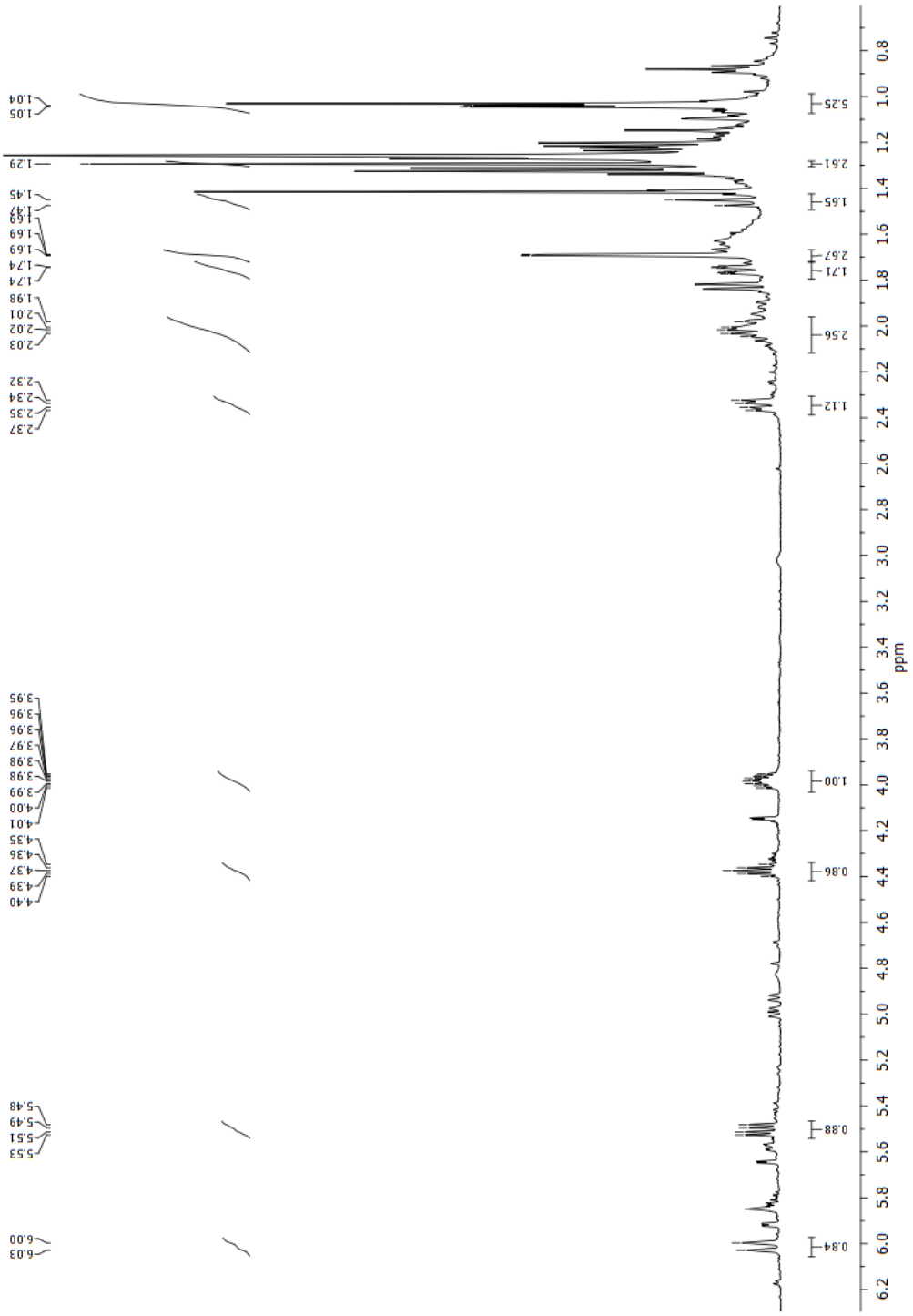

Figure F.30: ^{1}H NMR of 3-hydroxy-β-ionol

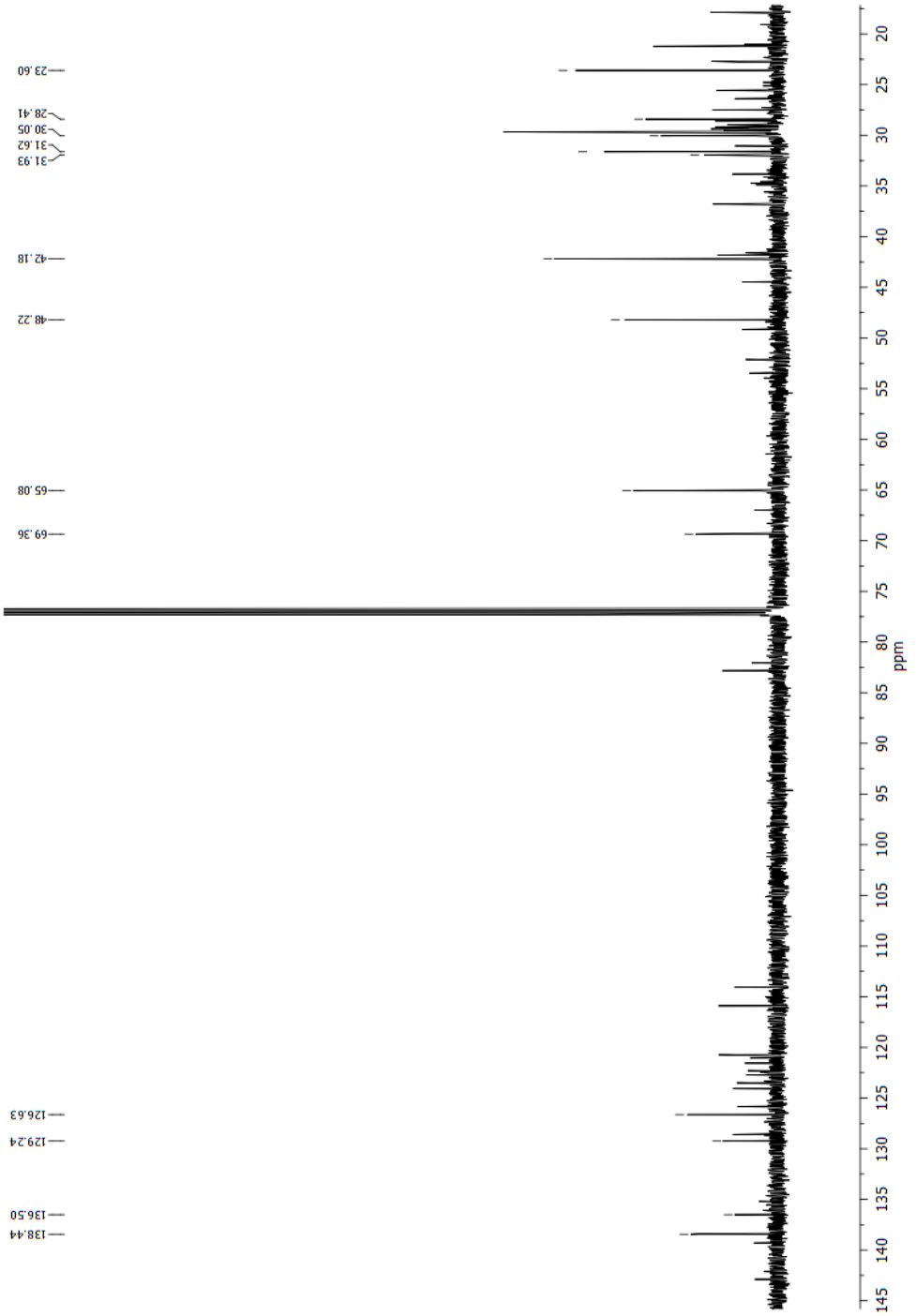

Figure F.31: ^{13}C NMR of 3-hydroxy-β-ionol

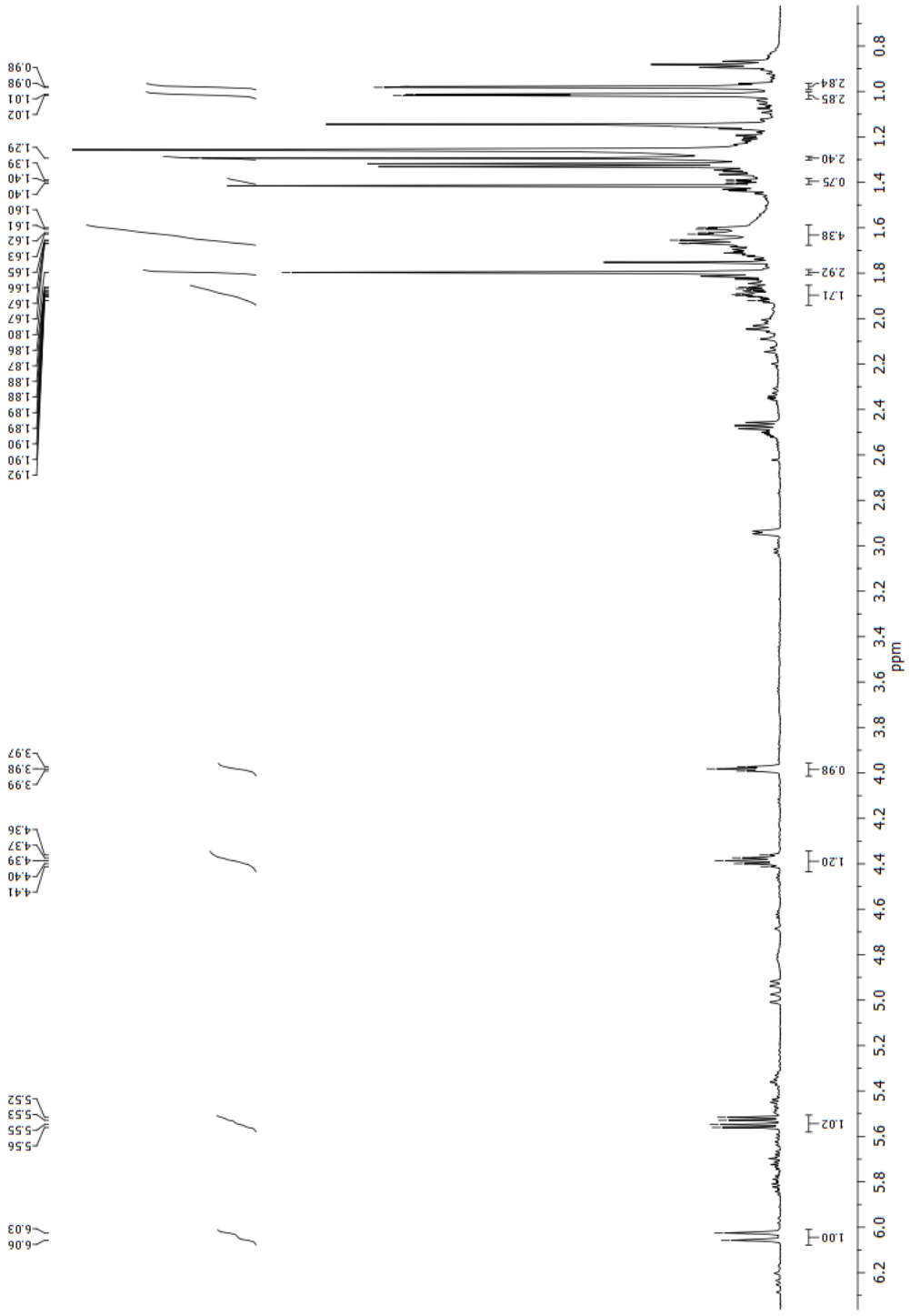

Figure F.32: ^{1}H NMR of 4-hydroxy-β-ionol

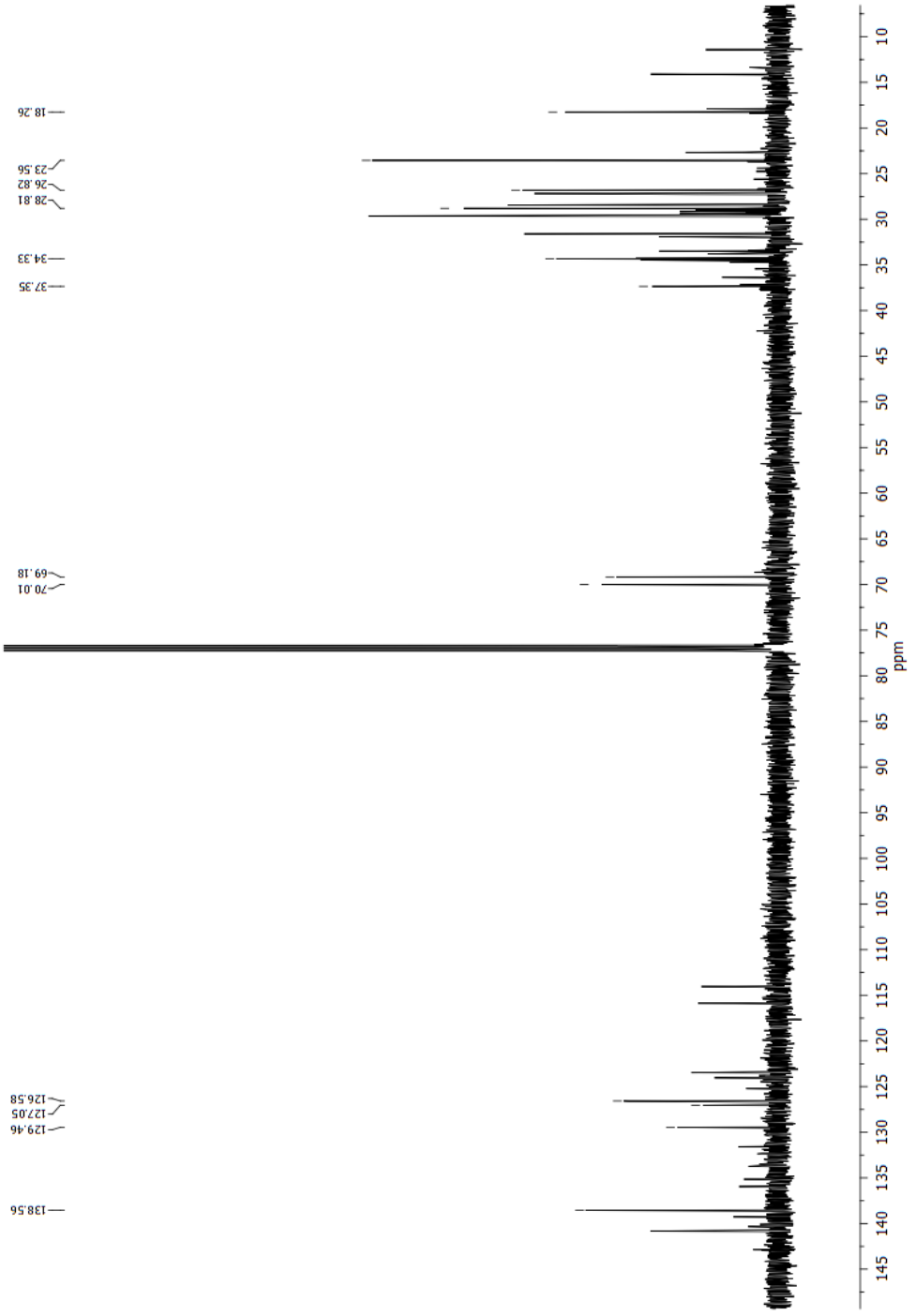

Figure F.33: ^{13}C NMR of 4-hydroxy-β-ionol

F.7 Phenylcyclohexane

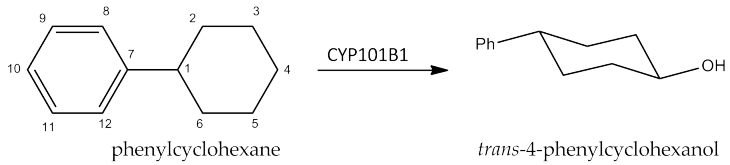

Figure F.34: Phenylcyclohexane product

Data for *trans*-4-phenylcyclohexanol:
^{1}H NMR (600 MHz, $CDCl_3$) δ 7.31 - 7.16 (m, 5H, C8 - H12), 3.70 (tt, J = 10.7, 4.3 Hz, 1H, axial H4), 2.50 (tt, J = 12.1, 3.4 Hz, 1H, axial H1), 2.13 - 2.07 (m, 2H, equatorial H2 and equatorial H6), 1.96 - 1.90 (m, 2H, equatorial H3 and equatorial H5), 1.50 - 1.58 (m, 2H, axial H2 and axial H6), 1.48 - 1.40 (m, 2H, axial H3 and axial H5).

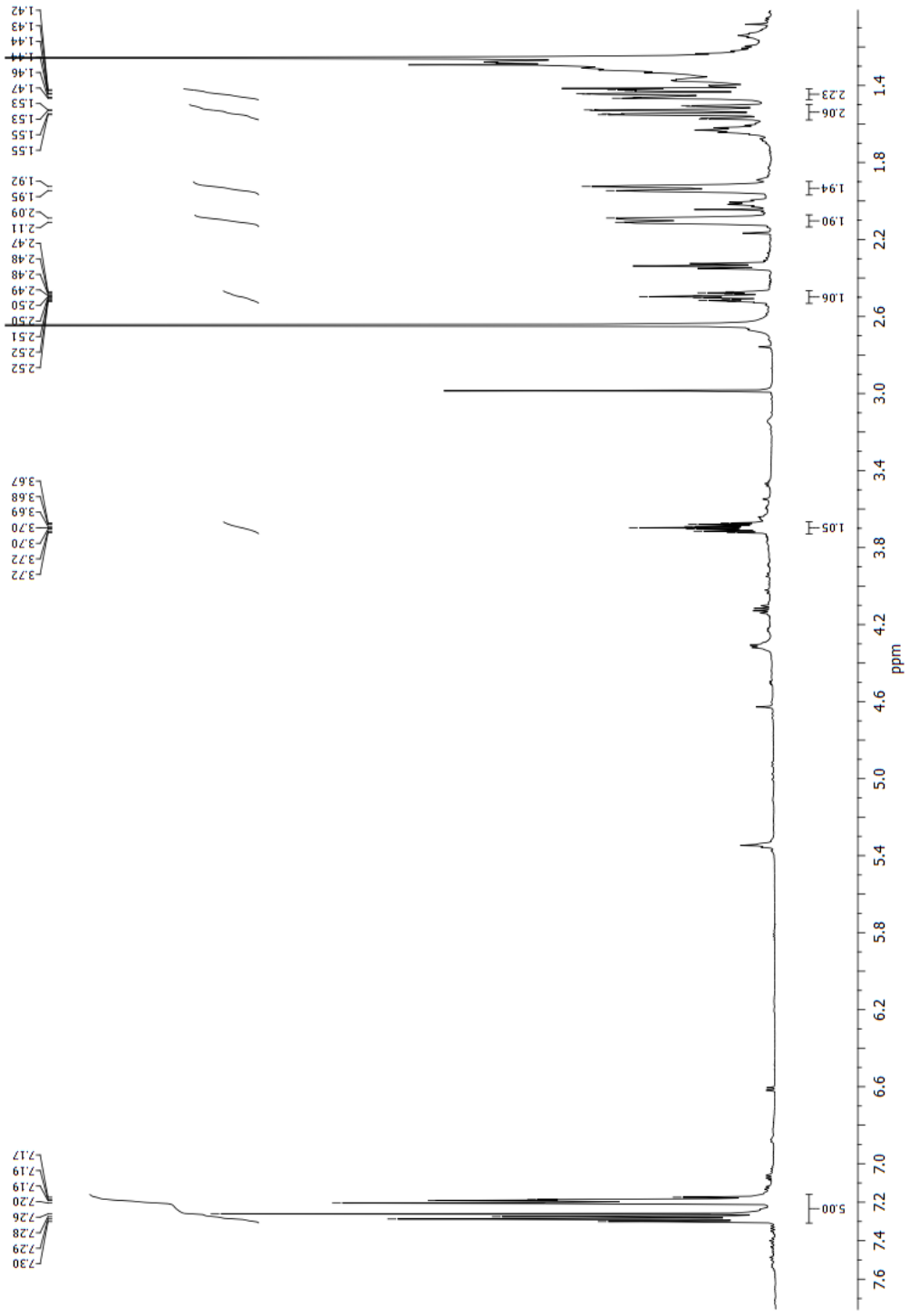

Figure F.35: ^{1}H NMR of *trans*-4-phenylcyclohexanol

F.8 Camphor

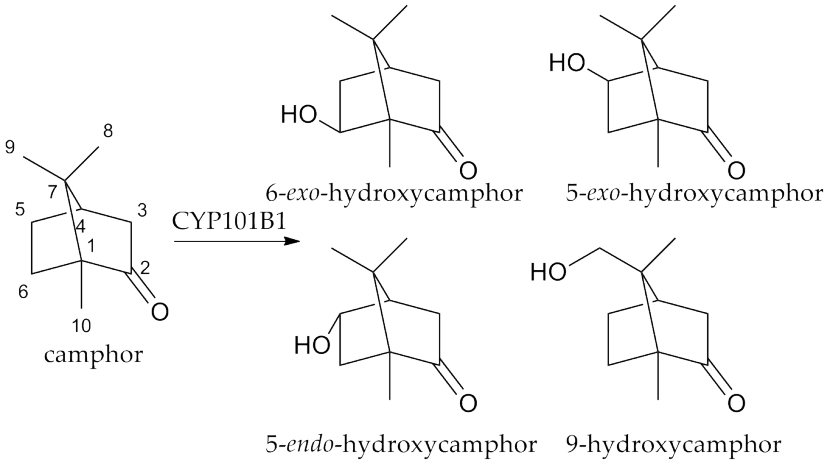

Figure F.36: Camphor products

Data for 9-hydroxy-(1R)-(+)-camphor:
^{1}H NMR (600 MHz, $CDCl_3$) δ 3.74 (d, J = 10.9 Hz, 1H, H9), 3.52 (d, J = 10.9 Hz, 1H, H9), 2.26 - 2.41 (m, 2H, H4 and *exo* H3), 1.98 (ddd, J = 16.2, 8.1, 4.1 Hz, 1H, *exo* H5), 1.90 (d, J = 17.8 Hz, 1H, *endo* H3), 1.77 - 1.70 (m, 1H, *exo* H6), 1.51 - 1.39 (m, 2H, *endo* H6 and *endo* H5), 0.97 (s, 6H, H8 and H10); ^{13}C NMR (151 MHz, $CDCl_3$) δ 218.26 (C2), 64.80 (C8), 57.38 (C1), 51.32 (C7), 42.95 (C3), 39.37 (C4), 29.77 (C5), 26.61 (C6), 14.93 (C9), 10.09 (C10).

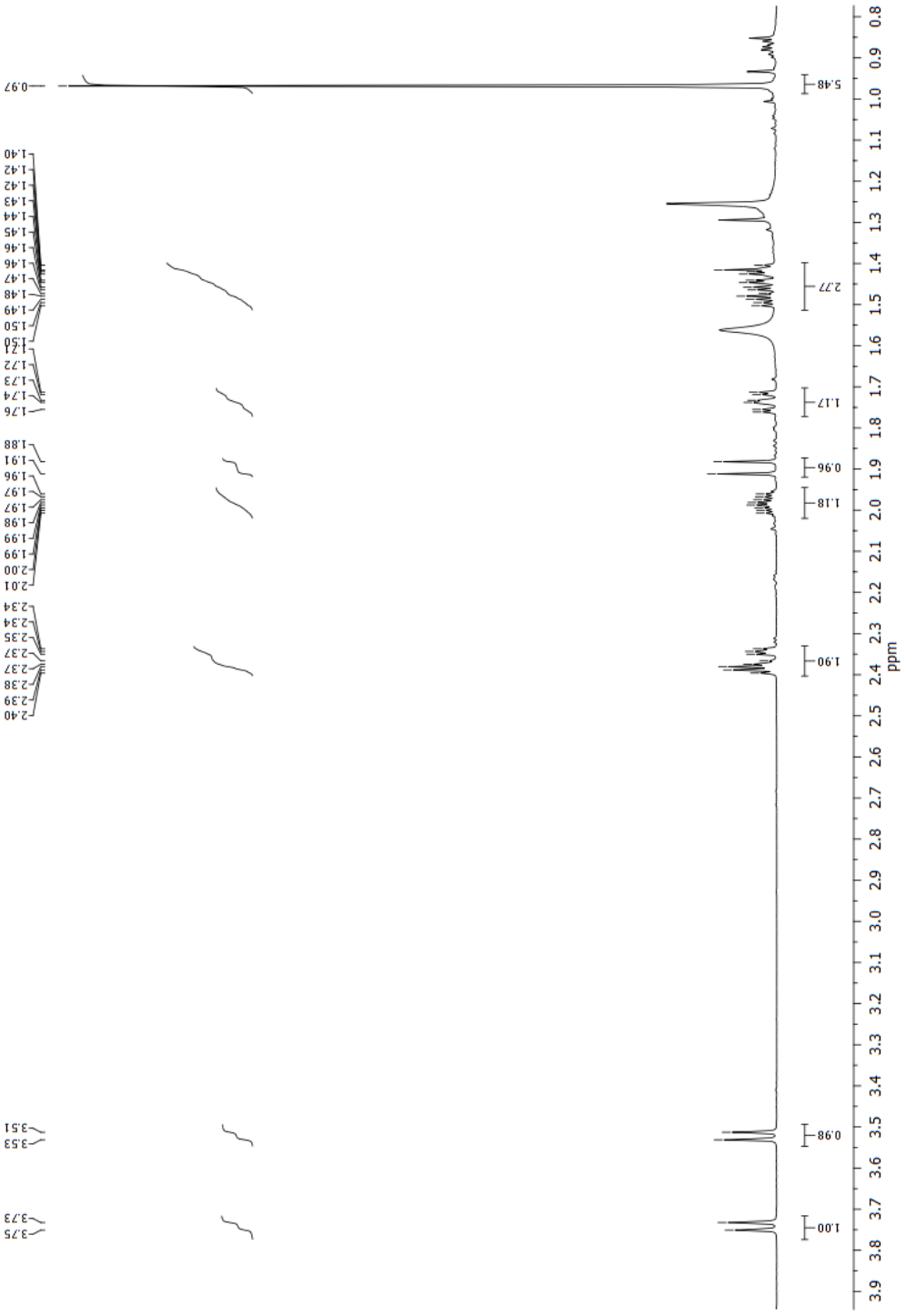

Figure F.37: ^{1}H NMR of 9-hydroxy-(1R)-(+)-camphor

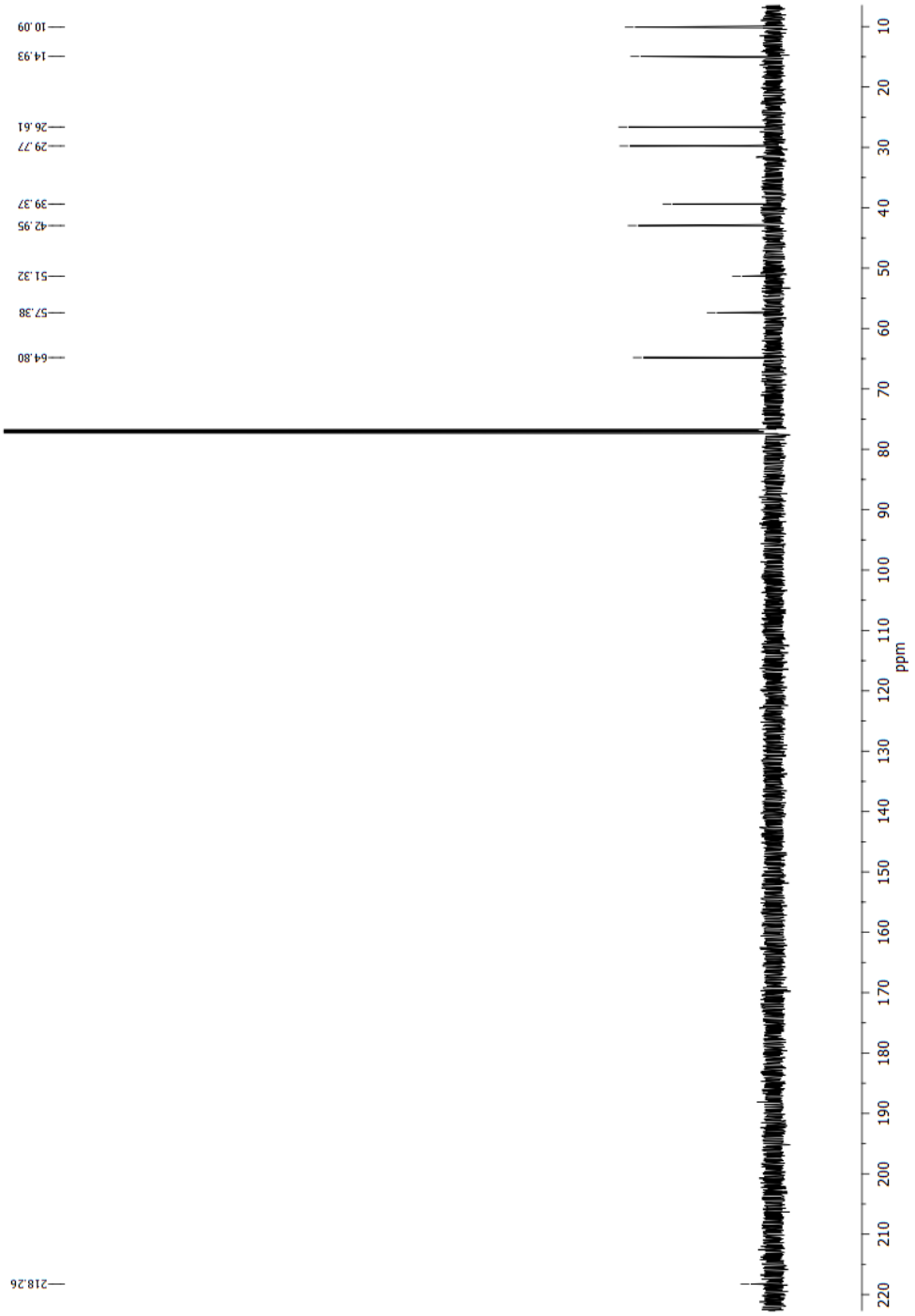

Figure F.38: ^{13}C NMR of 9-hydroxy-(1R)-(+)-camphor

F.9 1,8-Cineole

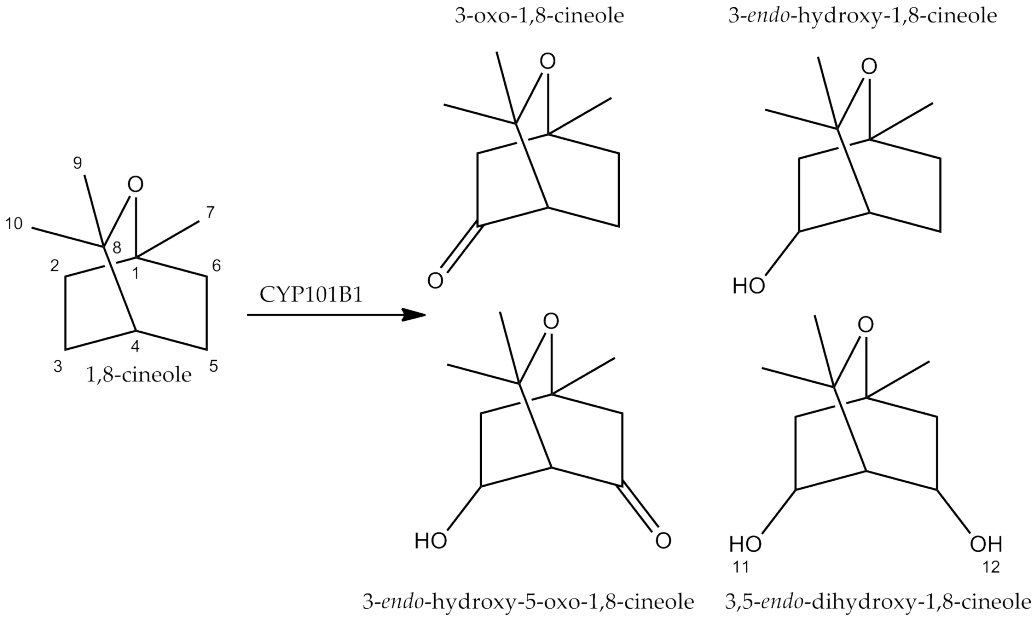

Figure F.39: 1,8-Cineole products

Data for 3-oxo-1,8-cineole:
^{1}H NMR (600 MHz, $CDCl_3$) δ 2.38 (dd, J = 18.8, 3.1 Hz, 1H, *exo* H2), 2.29 - 2.20 (m, 2H, *endo* H2 and *exo* H5), 2.17 (dd, J = 3.9, 2.0 Hz, 1H, H4), 1.91 - 1.83 (m, 1H, *exo* H6), 1.75 (dddd, J = 14.1, 11.7, 6.3, 2.0 Hz, 1H, *endo* H5), 1.66 - 1.59 (m, 1H, *endo* H6), 1.32 (s, 3H, H10), 1.24 (s, 3H, H9), 1.15 (s, 3H, H7); ^{13}C NMR (151 MHz, $CDCl_3$) δ 213.22 (C3), 73.60 (C8), 73.58 (C1), 51.89 (C4), 49.10 (C2), 30.64 (C10), 30.38 (C6), 26.94 (C7), 26.28 (C9), 18.30 (C5).

Data for 3-*endo*-hydroxy-1,8-cineole:
^{1}H NMR (600 MHz, $CDCl_3$) δ 4.46 (dt, J = 9.3, 3.9 Hz, 1H, *exo* H3), 2.12 (ddd, J = 14.1, 9.5, 3.3 Hz, 1H, *exo* H2), 2.07 - 2.03 (m, 1H, *exo* H5), 1.82 - 1.74 (m, 1H, *endo* H5), 1.68 - 1.59 (m, 1H, *exo* H6), 1.54 (dd, J = 6.1, 3.5 Hz, 1H, H4), 1.51 (ddd, J = 13.3, 12.0, 3.4 Hz, 1H, *endo* H6), 1.32 (dd, J = 14.2, 2.8 Hz, 1H, *endo* H2), 1.30 (s, 3H, H10), 1.22 (s, 3H, H9), 1.07 (s, 3H, H7); ^{13}C NMR (151 MHz, $CDCl_3$) δ 73.36 (C8), 71.00 (C1), 65.08 (C3), 42.84 (C2), 40.33 (C4), 31.07 (C6), 28.98 (C10), 28.34 (C9), 27.12 (C7), 13.91 (C5).

Data for 3-*endo*-hydroxy-5-oxo-1,8-cineole:
^{1}H NMR (600 MHz, $CDCl_3$) δ 4.61 - 4.55 (m, 1H, *exo* H3), 2.49 (d, J = 4.7

Hz, 1H, H4), 2.38 - 2.28 (m, 3H, *exo* H2, *exo* H6 and *endo* H6), 1.63 (d, J = 14.4 Hz, 1H, *endo* H2), 1.28 (s, 3H, H10), 1.27 (s, 1H, H9), 1.15 (s, 3H, H7); ^{13}C NMR (151 MHz, $CDCl_3$) δ 210.48 (C5), 72.58 (C8), 72.11 (C1), 63.46 (C3), 58.99 (C4), 47.72 (C6), 40.68 (C2), 29.56 (C7), 26.58 (C10), 24.73 (C9).

Data for 3,5-*endo*-dihydroxy-1,8-cineole:
^{1}H NMR (600 MHz, $CDCl_3$) δ 4.55 (dd, J = 9.4, 2.4 Hz, 2H, *exo* H3 and *exo* H5), 4.00 (Br s, 2H, OH11 and OH12), 2.27 (ddd, J = 12.9, 9.7, 2.7 Hz, 2H, *exo* H2 and *exo* H6), 1.98 (t, J = 3.4 Hz, 1H, H4), 1.59 (dd, J = 13.7, 2.2 Hz, 2H, *endo* H2 and *endo* H6), 1.23 (s, 6H, H10 and H9), 1.14 (s, 3H, H7); ^{13}C NMR (151 MHz, $CDCl_3$) δ 73.13 (C8), 71.21 (C1), 67.43 (C3 and C5), 43.84 (C2 and C6), 43.73 (C4), 28.66 (C10 and C9), 26.53 (C7).

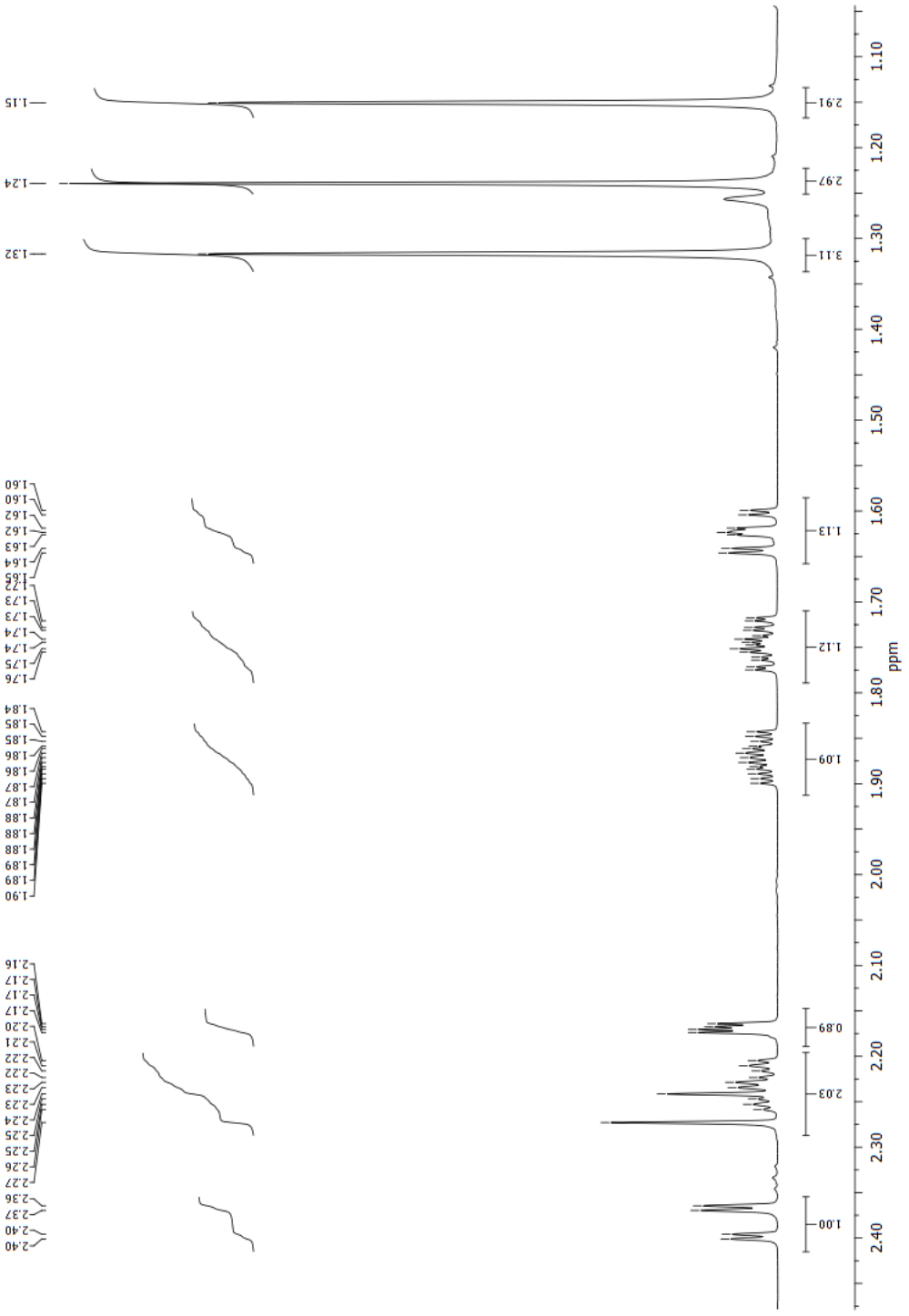

Figure F.40: ^{1}H NMR of 3-oxo-1,8-cineole

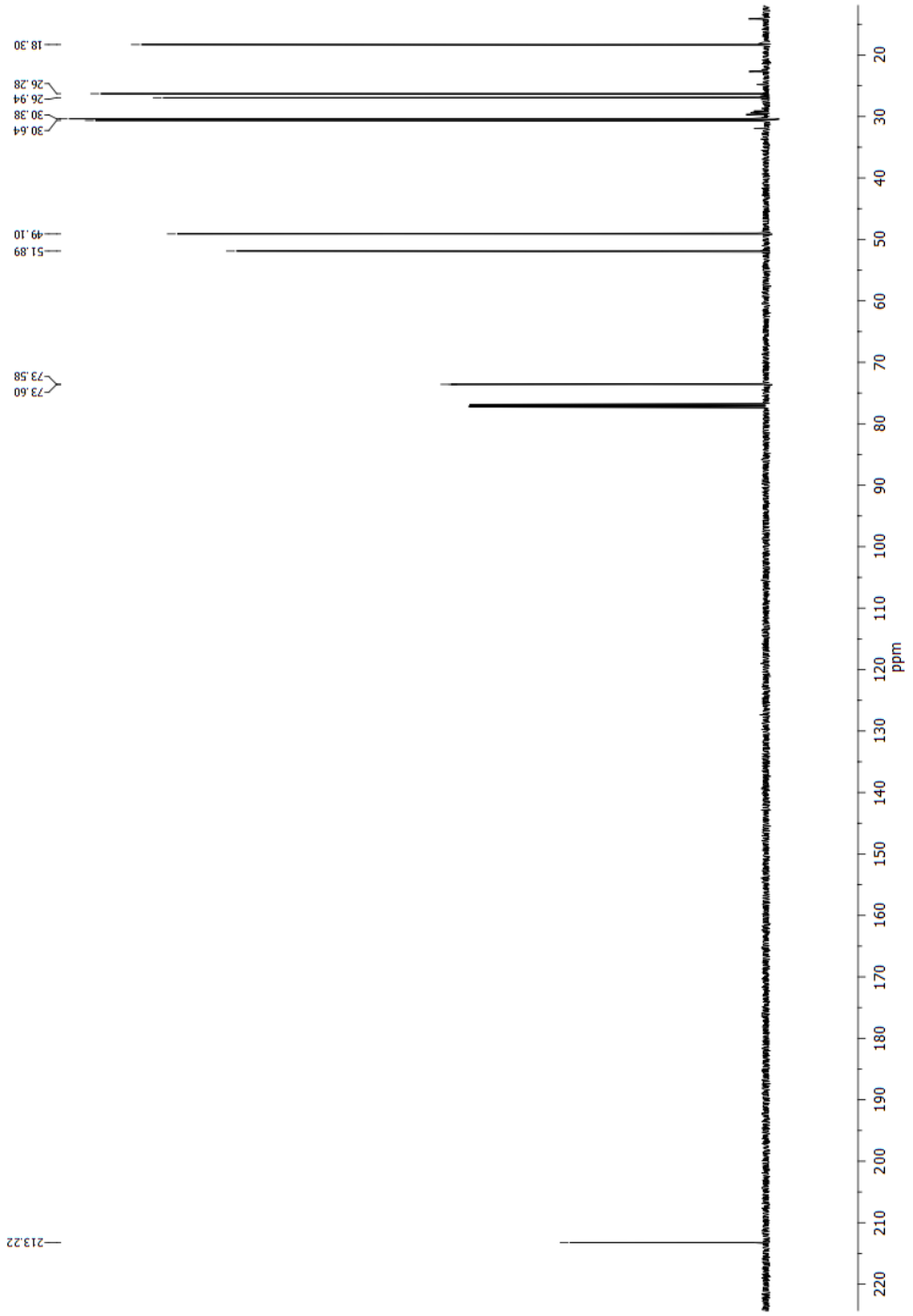

Figure F.41: ^{13}C NMR of 3-oxo-1,8-cineole

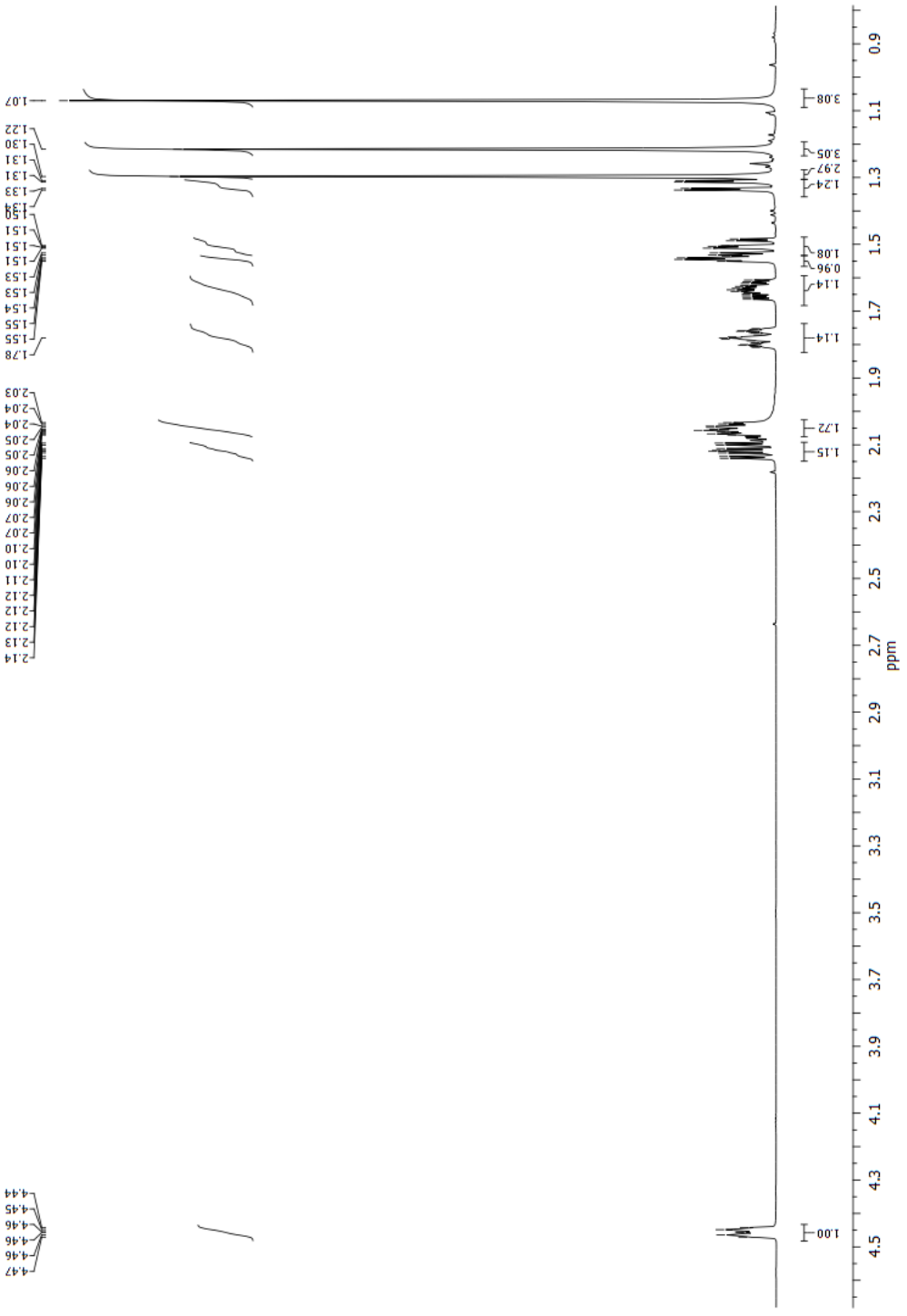

Figure F.42: ^{1}H NMR of 3-*endo*-hydroxy-1,8-cineole

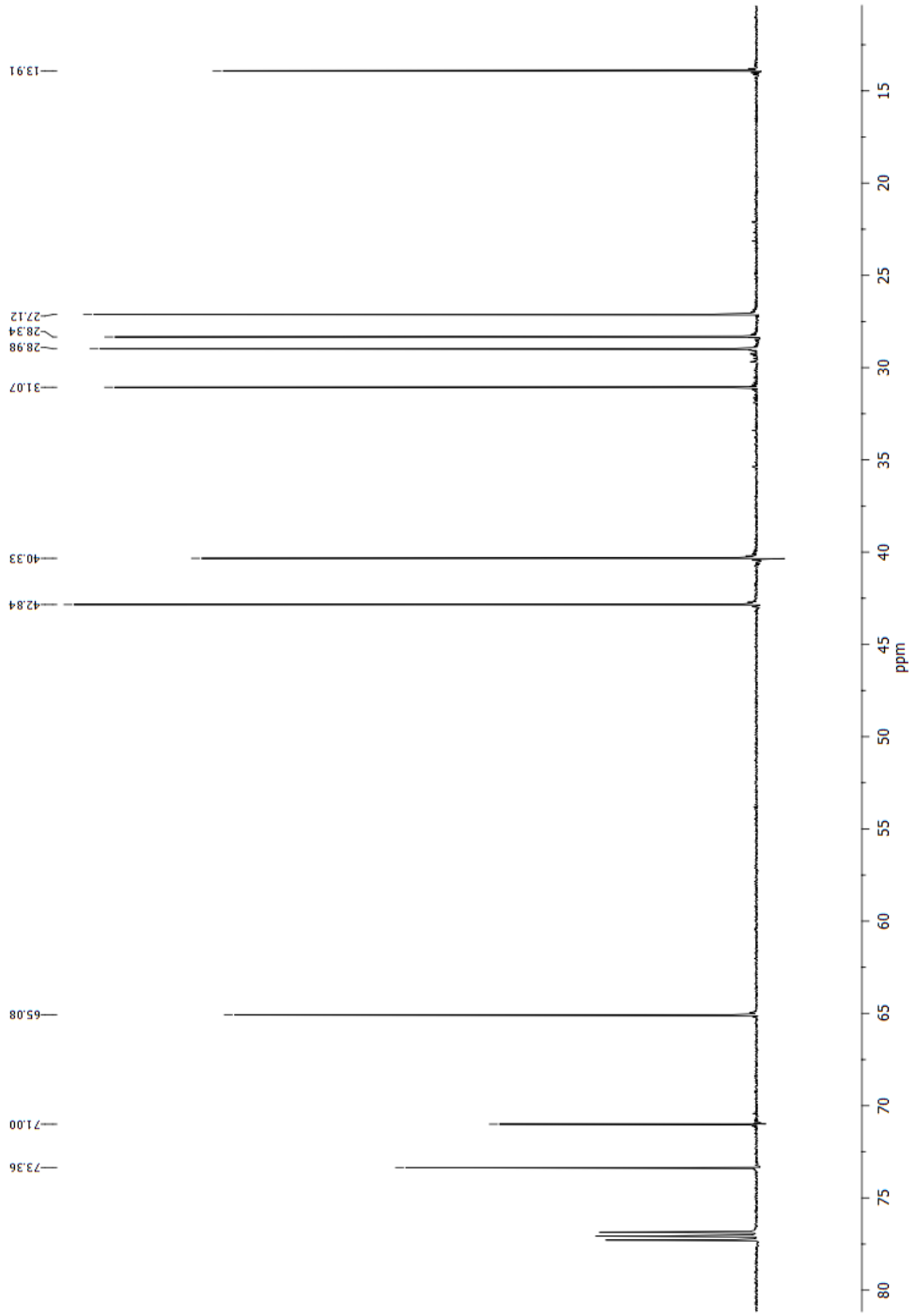

Figure F.43: ^{13}C NMR of 3-*endo*-hydroxy-1,8-cineole

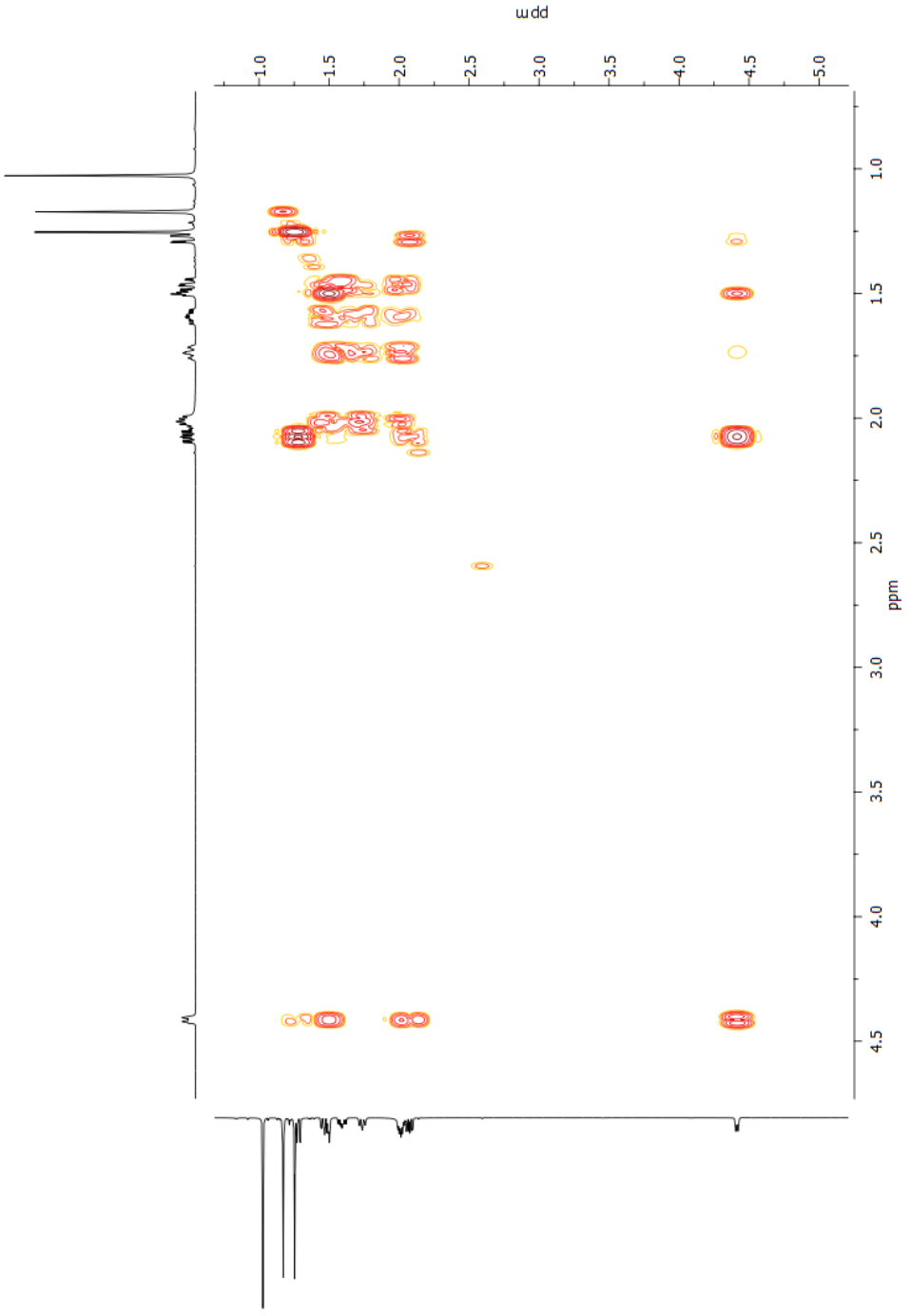

Figure F.44: COSY of 3-*endo*-hydroxy-1,8-cineole

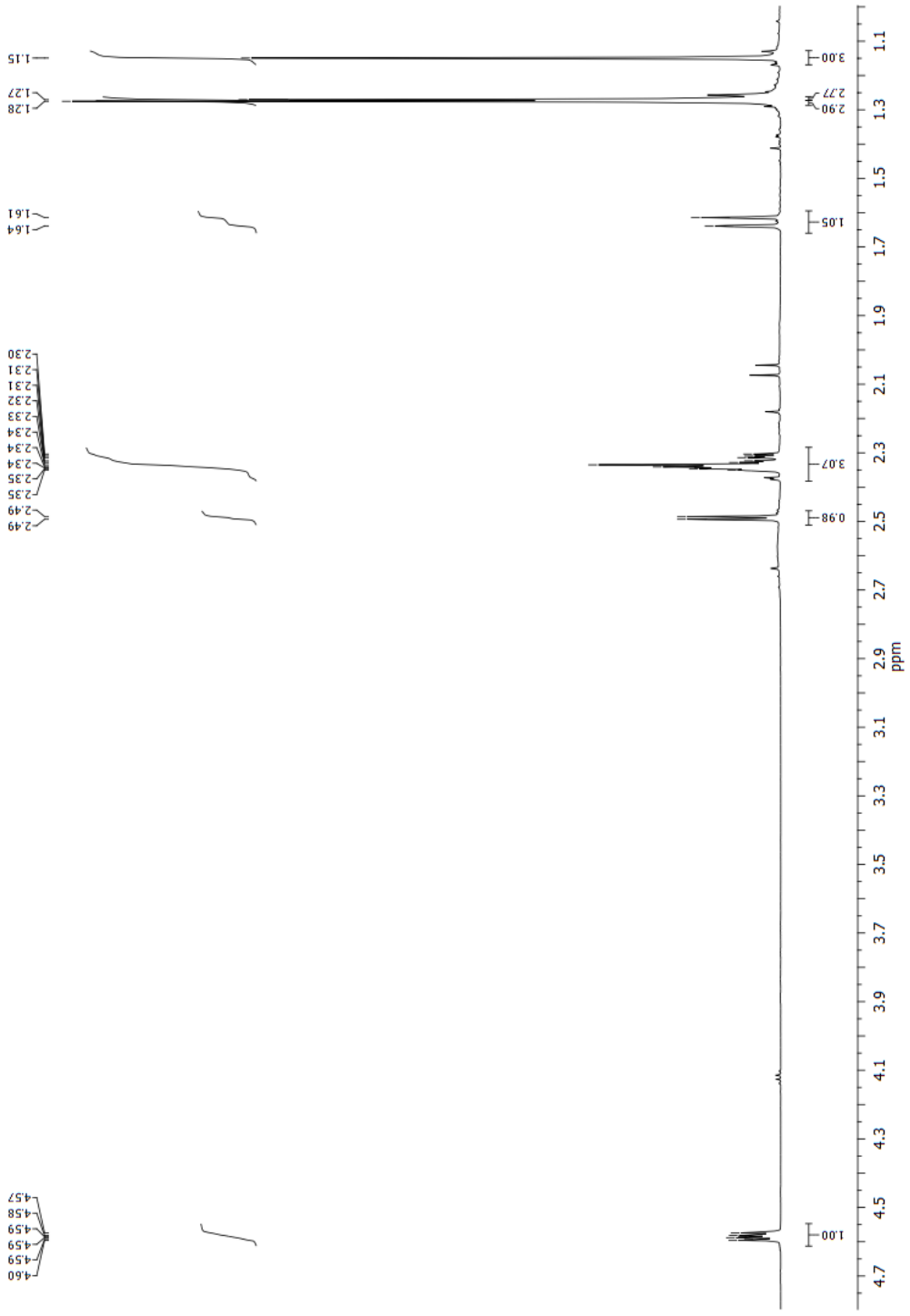

Figure F.45: ^{1}H NMR of 3-*endo*-hydroxy-5-oxo-1,8-cineole

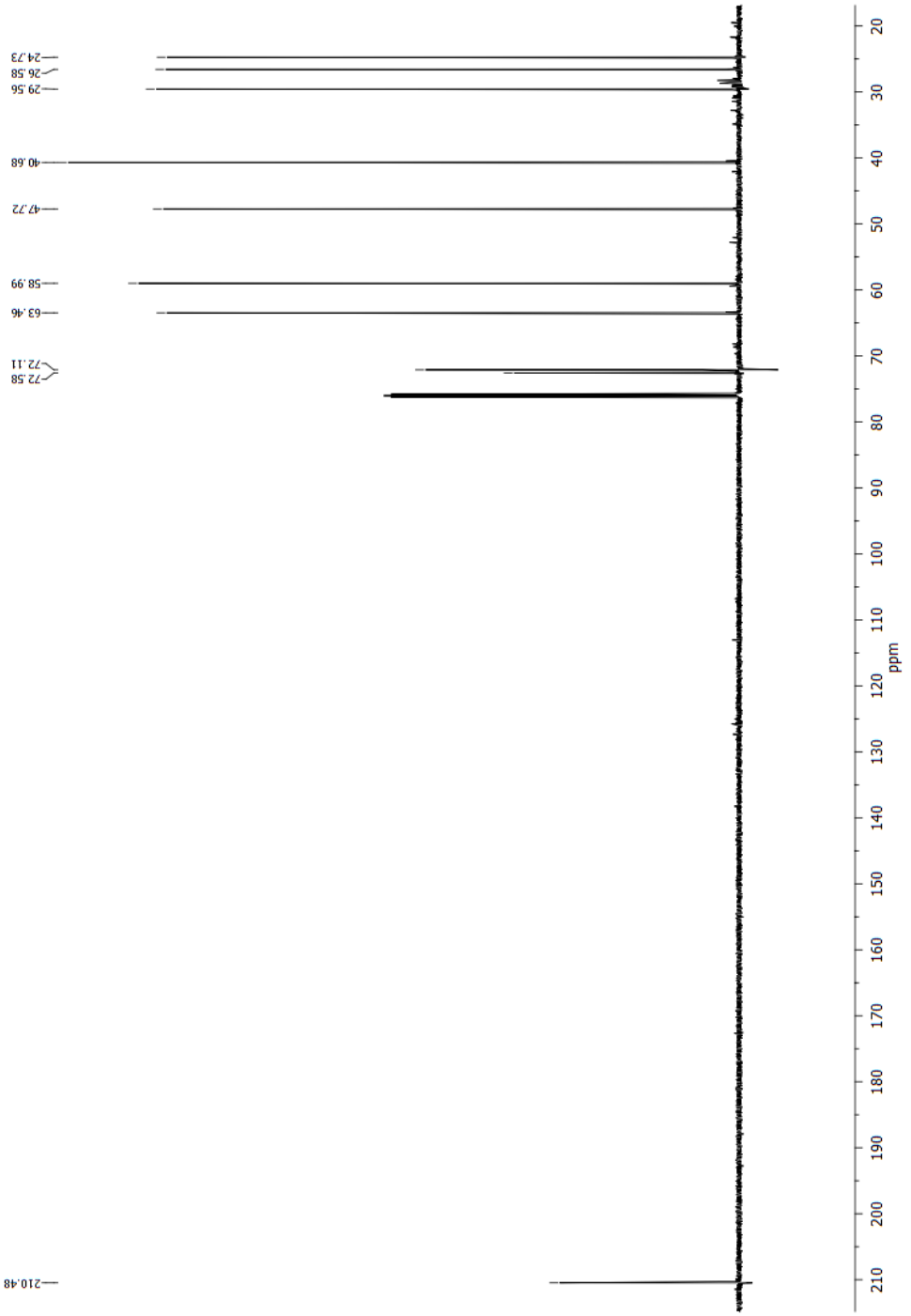

Figure F.46: ^{13}C NMR of 3-*endo*-hydroxy-5-oxo-1,8-cineole

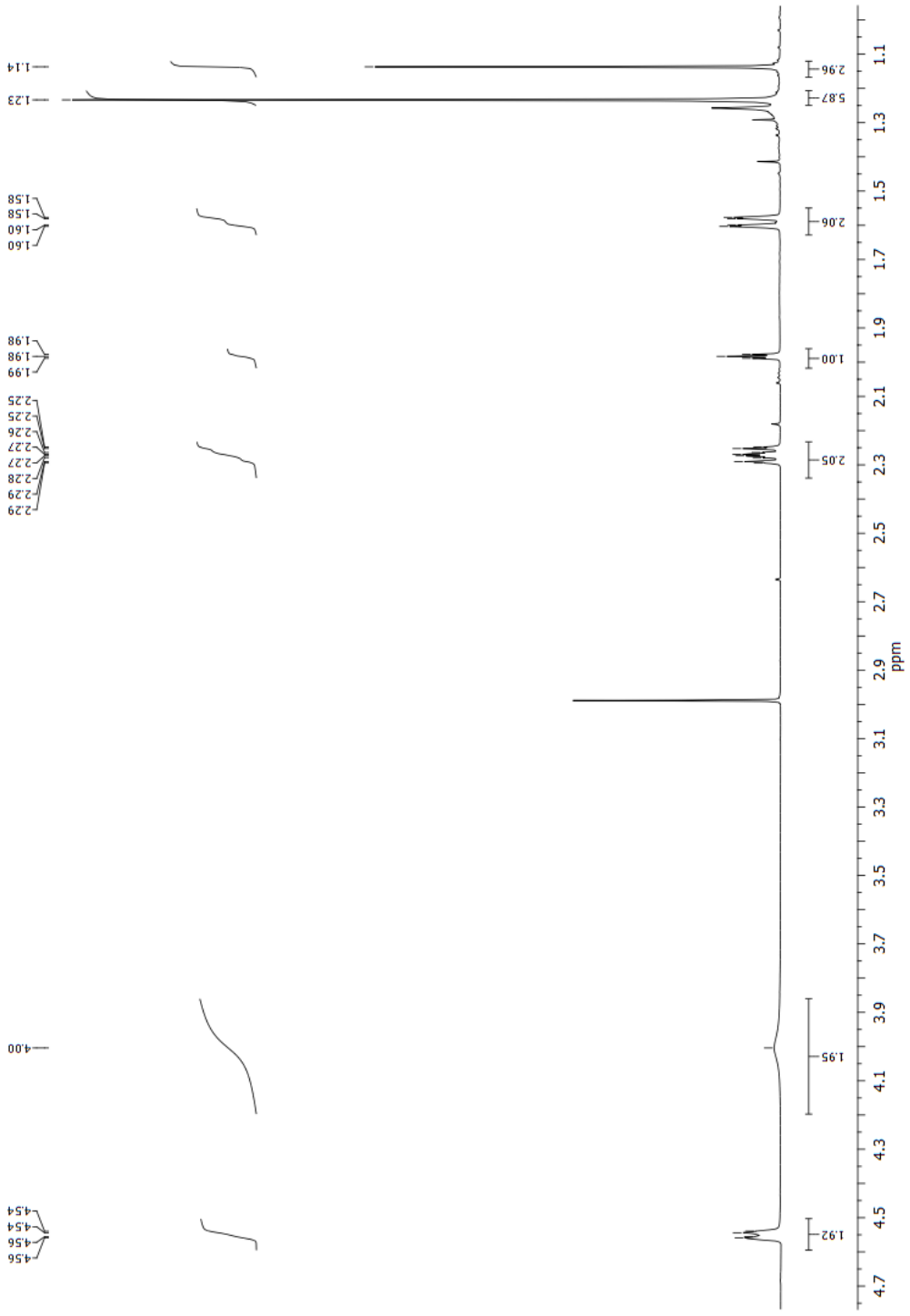

Figure F.47: ^{1}H NMR of 3,5-*endo*-dihydroxy-1,8-cineole

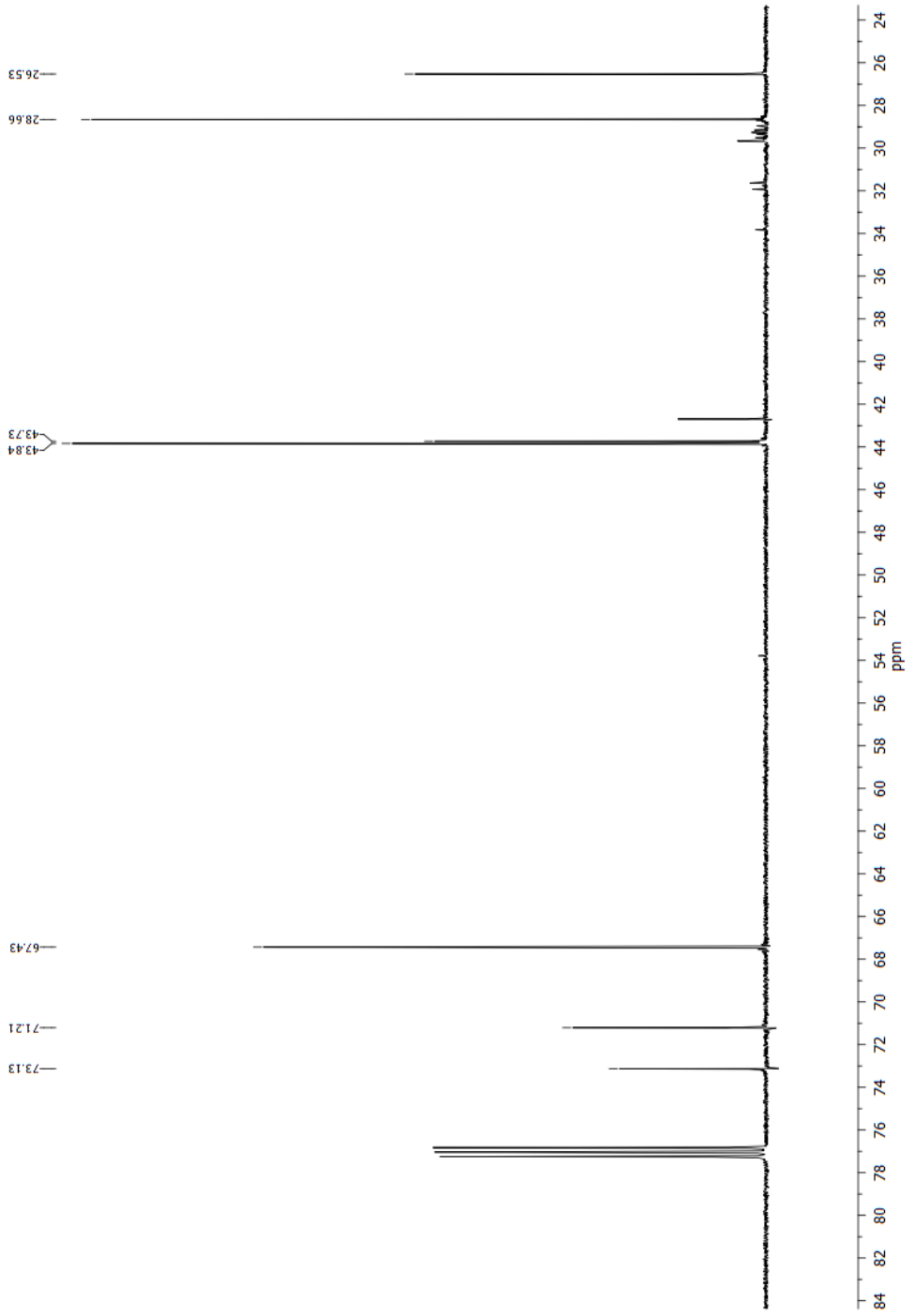

Figure F.48: ^{13}C NMR of 3,5-*endo*-dihydroxy-1,8-cineole

F.10 1,4-Cineole

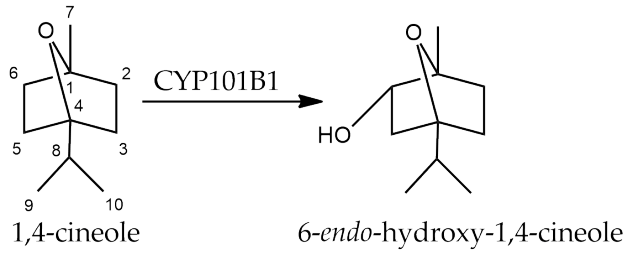

Figure F.49: 1,4-Cineole product

Data for 6-*endo*-hydroxy-1,4-cineole:
^{1}H NMR (500 MHz, $CDCl_3$) δ 3.93 (ddd, J = 10.2, 3.6, 1.5 Hz, 1H, *exo* H6), 2.30 (ddd, J = 12.4, 8.9, 5.5 Hz, 1H, *exo* H2), 2.12 - 2.03 (m, 1H, *exo* H5), 1.95 (sep, J = 6.7 Hz, 1H, H8), 1.71 - 1.60 (m, 2H, *exo* H3 and *endo* H3), 1.51 - 1.36 (m, 4H, *endo* H2 and H7), 1.32 - 1.27 (m, 1H, *endo* H5), 0.92 (d, J = 6.9 Hz, 6H, H9 and H10); ^{13}C NMR (126 MHz, $CDCl_3$) δ 90.03 (C4), 84.59 (C1), 77.64 (C6), 41.97 (C5), 33.33 (C2), 33.17 (C8), 29.27 (C3), 19.18 (C7), 17.96 (C9), 17.62 (C10).

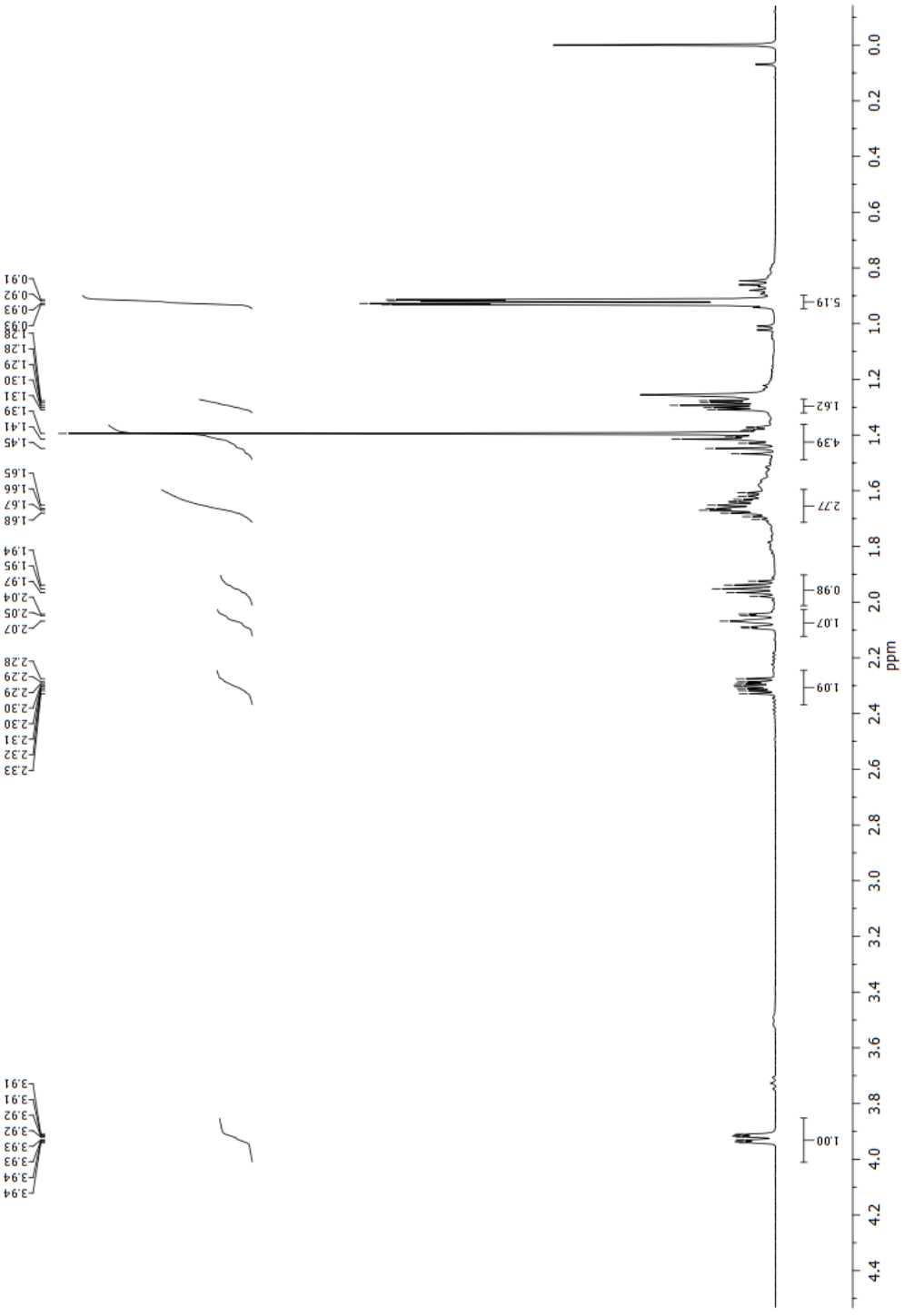

Figure F.50: ^{1}H NMR of 6-*endo*-hydroxy-1,4-cineole

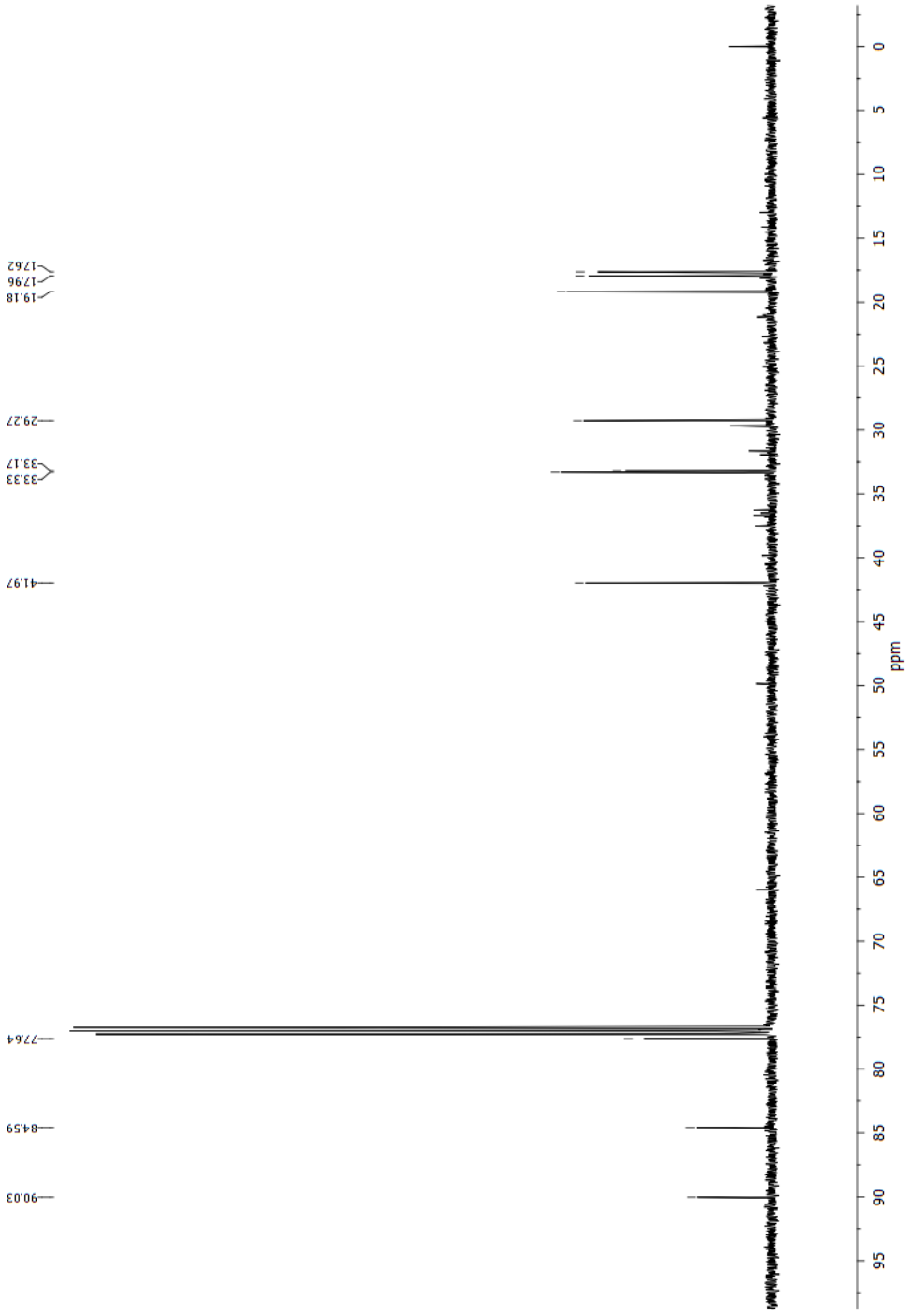

Figure F.51: ^{13}C NMR of 6-*endo*-hydroxy-1,4-cineole

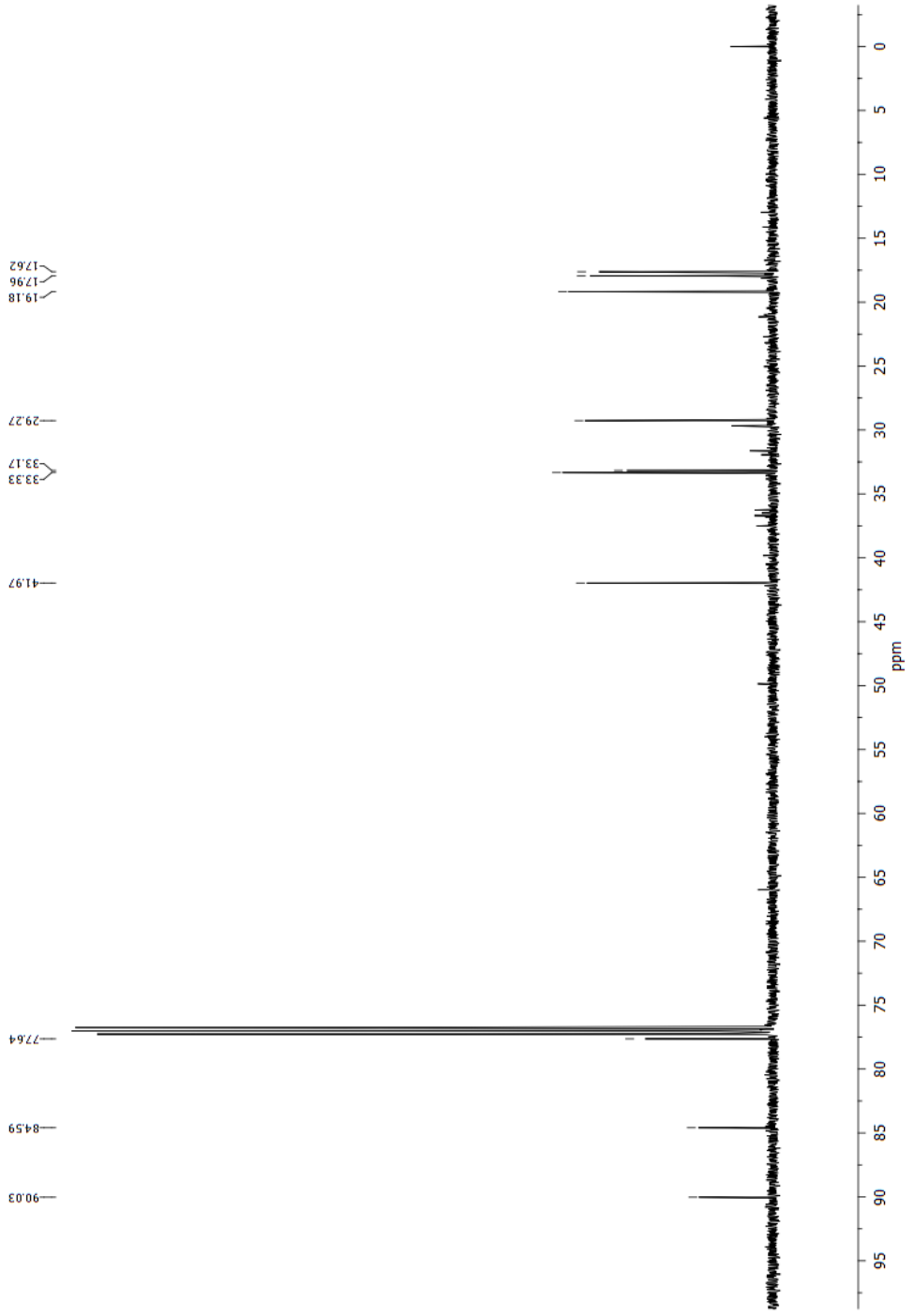

Figure F.52: COSY NMR of 6-*endo*-hydroxy-1,4-cineole

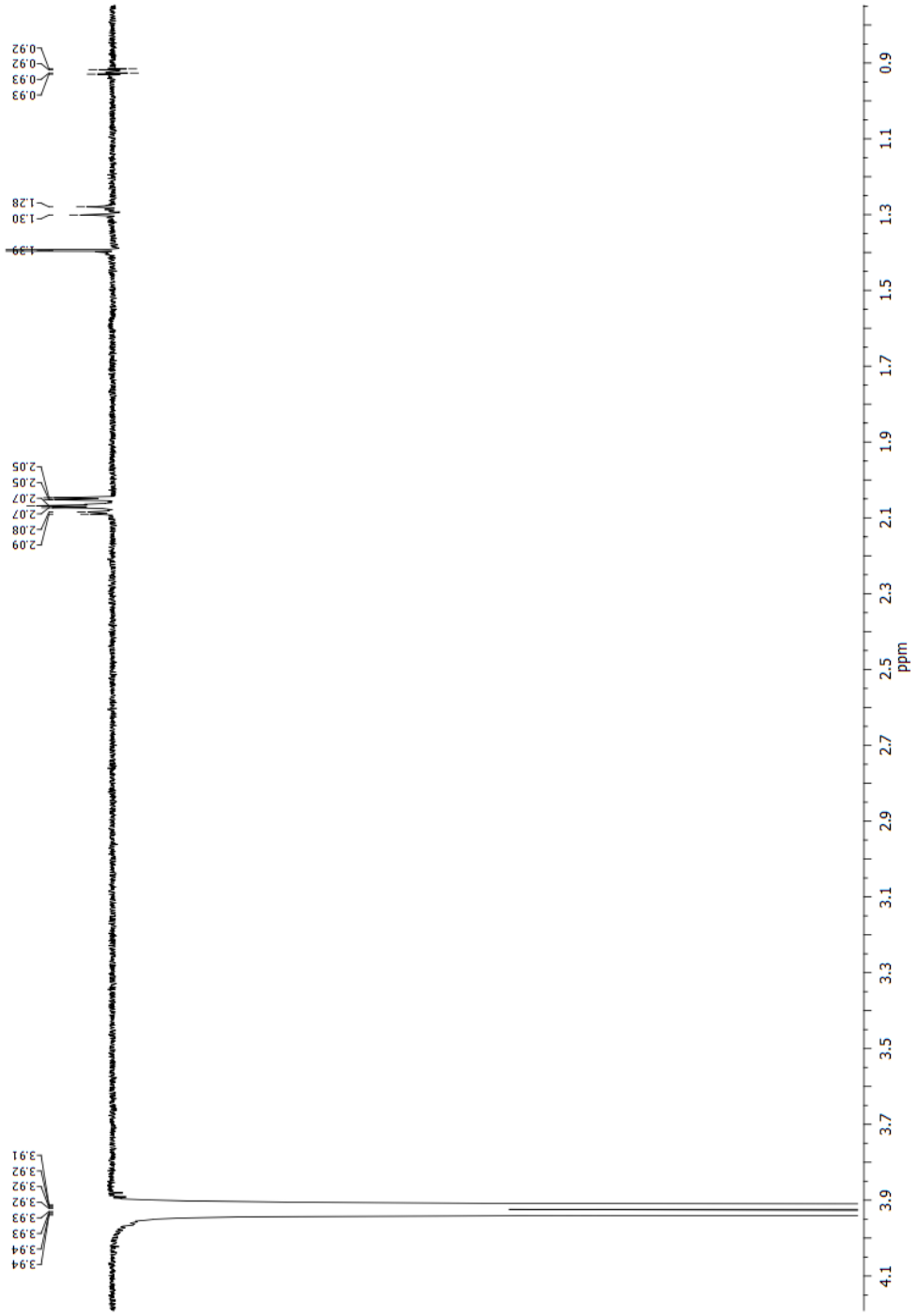

Figure F.53: DPFGSE NOESY for 6-*endo*-hydroxy-1,4-cineole for the exo H6 signal

F.11 (+)-Fenchone

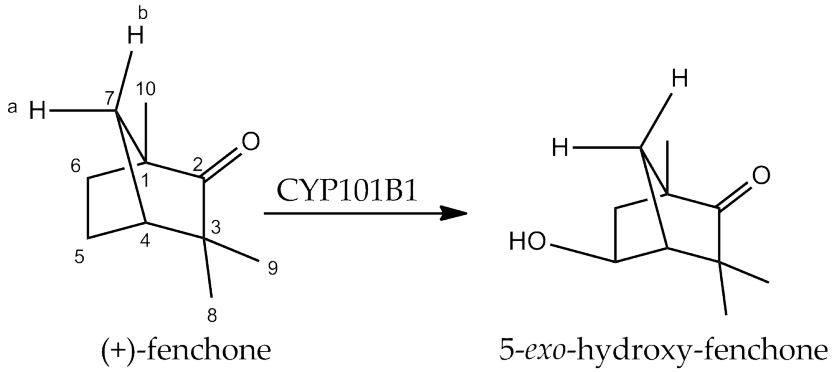

Figure F.54: (+)-fenchone product

Data for 5-*exo*-hydroxy-(+)-fenchone:
^{1}H NMR (600 MHz, $CDCl_3$) δ 4.37 (d, J = 6.5 Hz, 1H, *endo* H5), 2.14 (s, 1H, H4), 2.07 (dd, J = 10.9, 1.9 Hz, 1H, H7a), 1.89 (ddd, J = 14.1, 6.5, 2.3 Hz, 1H, *exo* H6), 1.74 (d, J = 11.1 Hz, 1H, H7b), 1.46 (dt, J = 14.1, 1.6 Hz, 1H, *endo* H6), 1.15 (s, 3H, H10), 1.06 (s, 3H, H9), 1.03 (s, 3H, H8); ^{13}C NMR (151 MHz, $CDCl_3$) δ 222.07 (C2), 70.67 (C5), 53.59 (C1), 53.22 (C4), 45.30 (C3), 43.20 (C6), 37.46 (C7), 23.68 (C9), 21.29 (C8), 14.21 (C10).

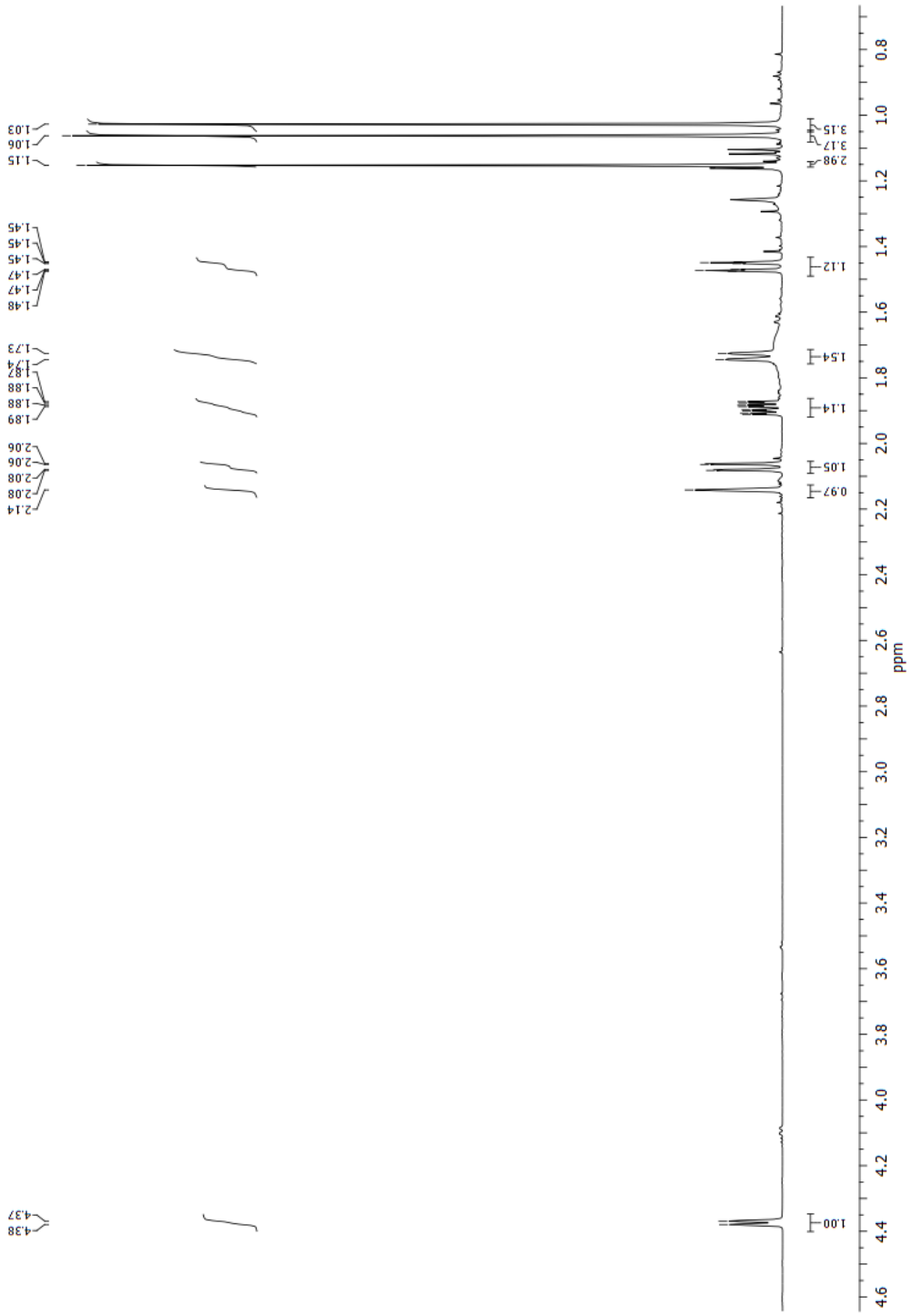

Figure F.55: ^{1}H NMR of 5-*exo*-hydroxy-(+)-fenchone

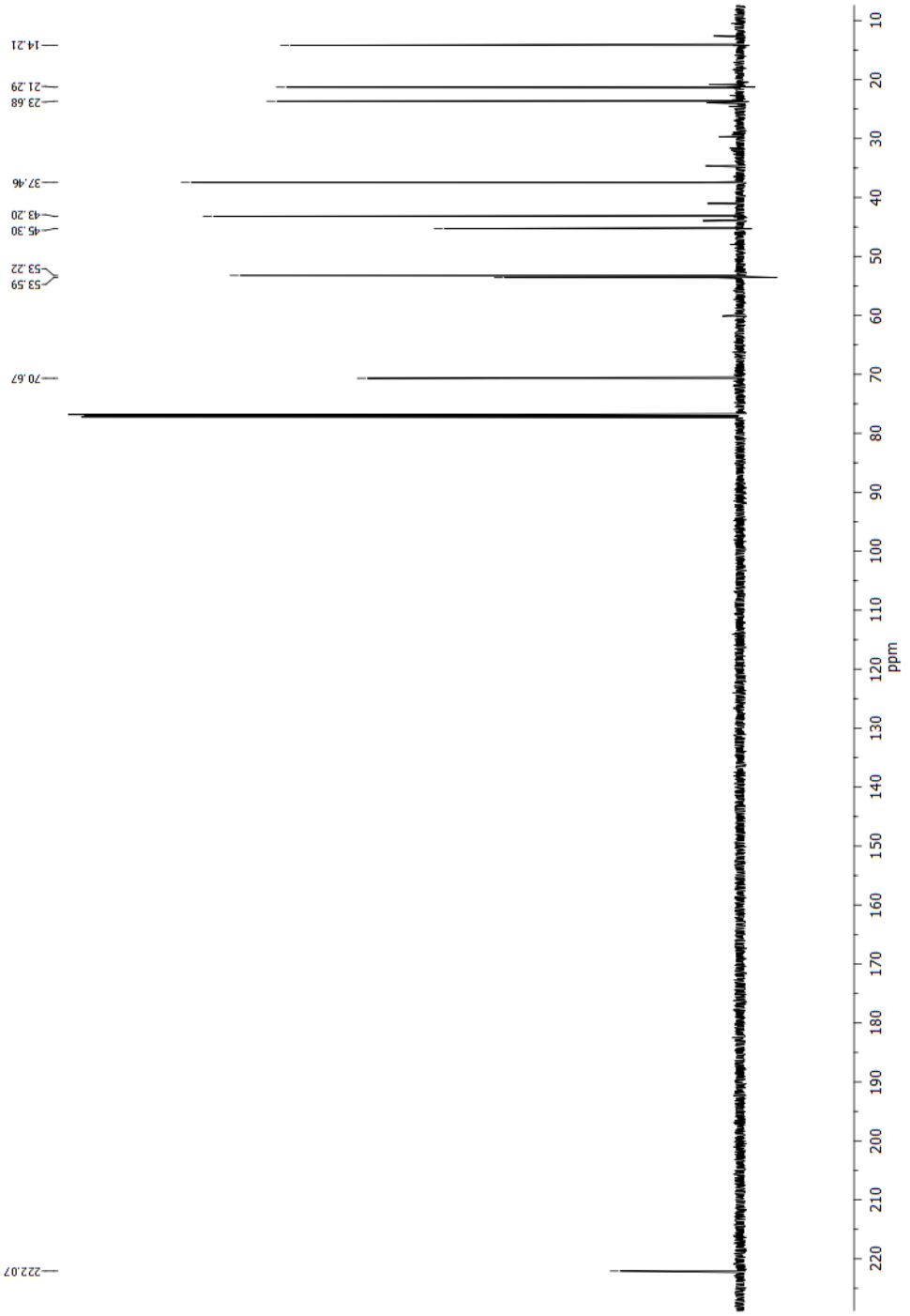

Figure F.56: ^{13}C NMR of 5-*exo*-hydroxy-(+)-fenchone

F.12 (1*R*)-(−)-Nopol

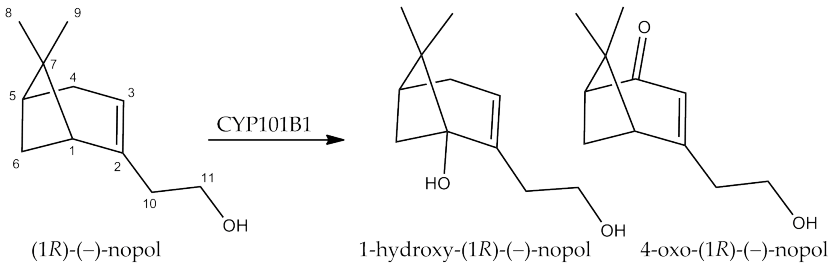

Figure F.57: (1*R*)-(−)-Nopol products

Data for 1-hydroxy-(1*R*)-(−)-nopol:
^{1}H NMR (600 MHz, $CDCl_3$) δ 5.46 (s, 1H, H3), 3.66 - 3.58 (m, 2H, H11), 2.38 - 2.16 (m, 5H, H4, *exo* H6 and H10), 1.98 (dd, J = 6.5, 2.0 Hz, 1H, H5), 1.56 (d, J = 8.4 Hz, 1H, *endo* H6), 1.23 (s, 3H, H8), 0.85 (s, 3H, H9); ^{13}C NMR (151 MHz, $CDCl_3$) δ 143.77 (C2), 121.53 (C3), 74.86 (C1), 60.14 (C11), 44.61 (C7), 41.02 (C6), 40.83 (C5), 39.41 (C10), 38.11 (C4), 20.85 (C8), 18.65 (C9).

Data for 4-oxo-(1*R*)-(−)-nopol:
^{1}H NMR (600 MHz, $CDCl_3$) δ 5.79 (s, 1H, H3), 3.86 - 3.78 (m, 2H, H11), 2.84 (dt, J = 9.3, 5.5 Hz, 1H, *exo* H6), 2.71 - 2.65 (m, 1H, H1), 2.55 (ddd, J = 10.2, 6.3, 0.9 Hz, 2H, H10), 2.52 (t, J = 5.9 Hz, 1H, H5), 2.10 (d, J = 9.2 Hz, 1H, *endo* H6), 1.51 (s, 3H, H8), 1.02 (s, 3H, H9); ^{13}C NMR (151 MHz, $CDCl_3$) δ 203.75 (C4), 169.81 (C2), 121.70 (C3), 59.73 (C11), 57.83 (C1), 48.65 (C5), 42.65 (C7), 41.13 (C6), 39.96 (C10), 26.57 (C8), 22.30 (C9).

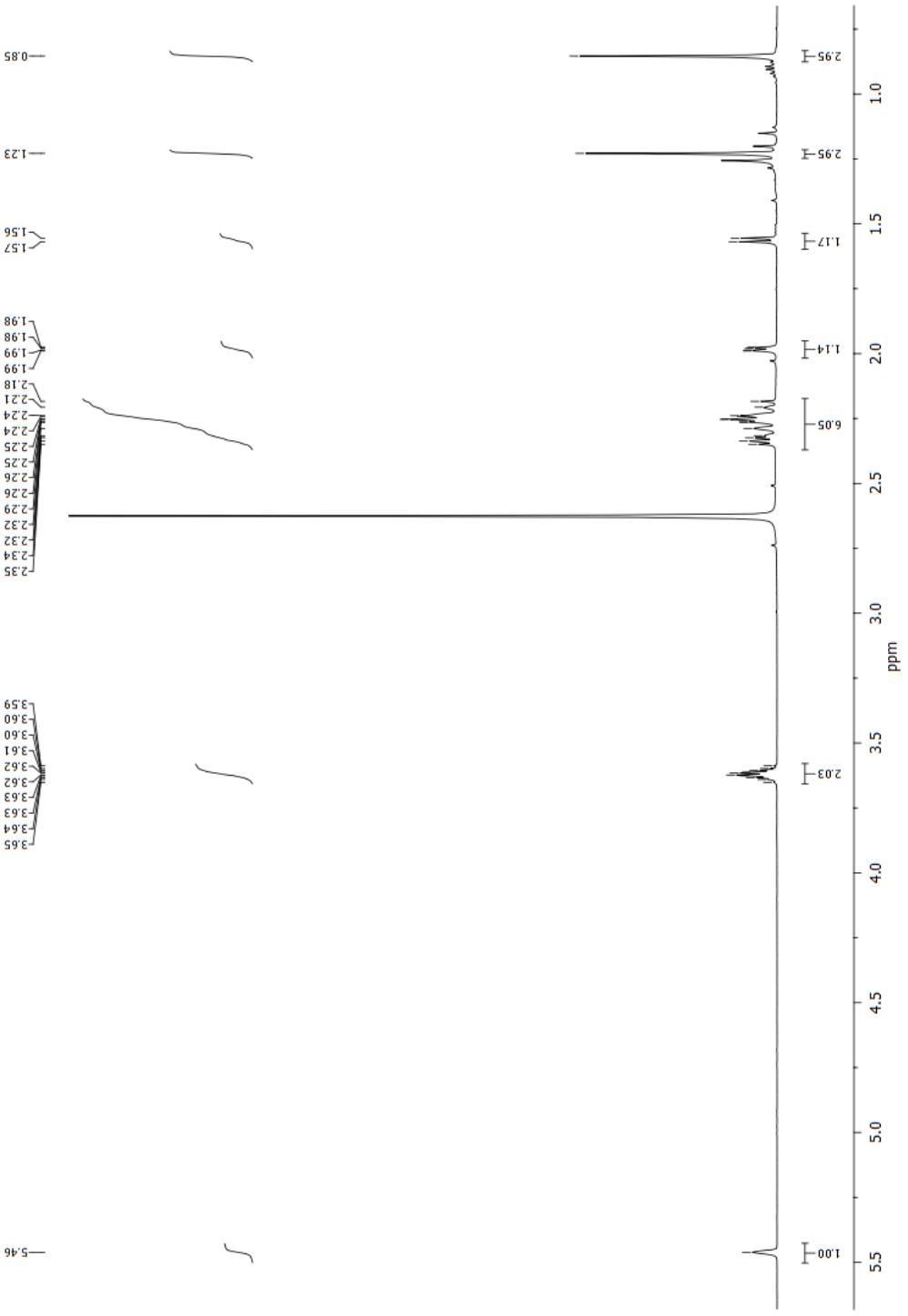

Figure F.58: ^{1}H NMR of 1-hydroxy-(1R)-(−)-nopol

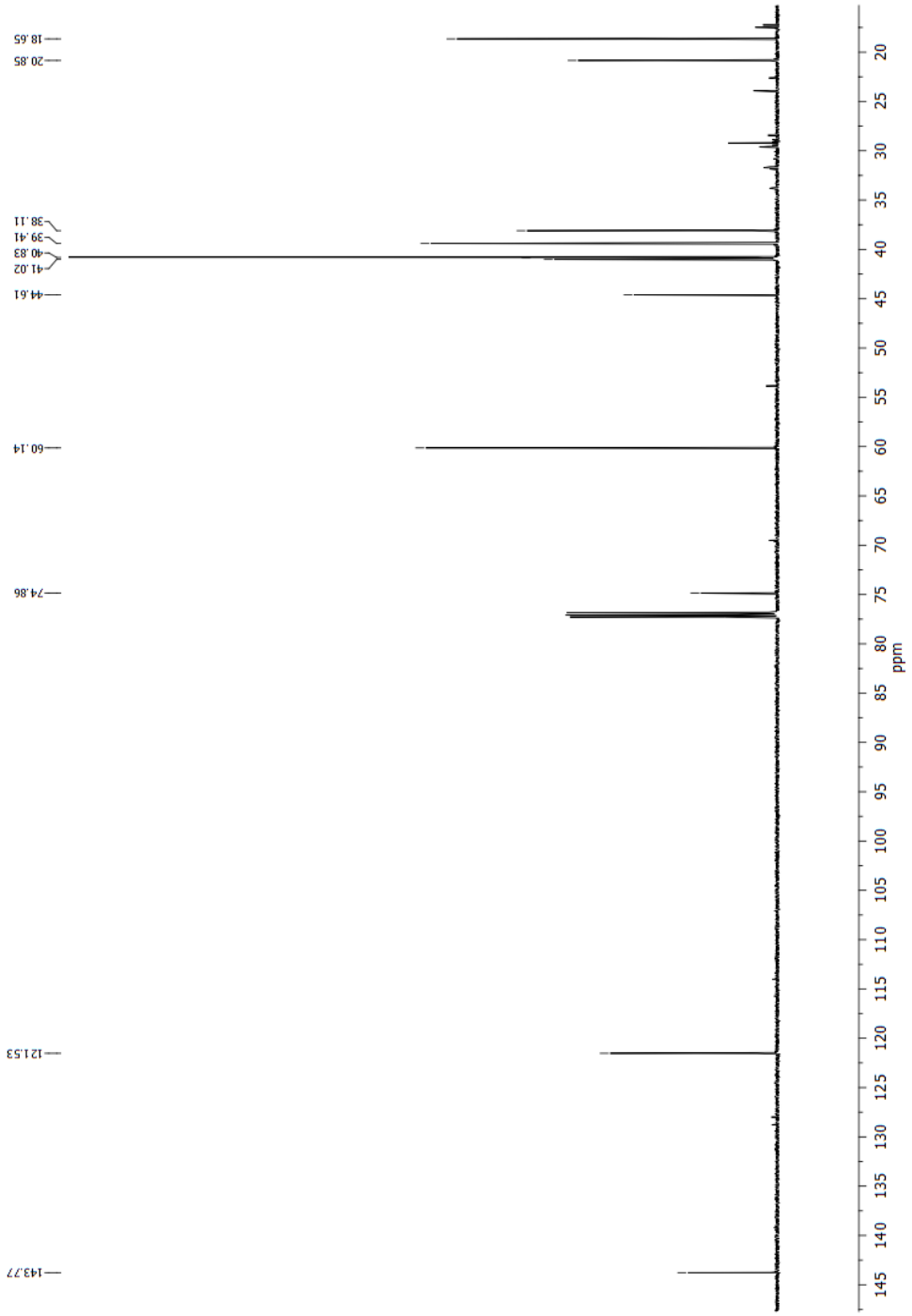

Figure F.59: ^{13}C NMR of 1-hydroxy-(1R)-(−)-nopol

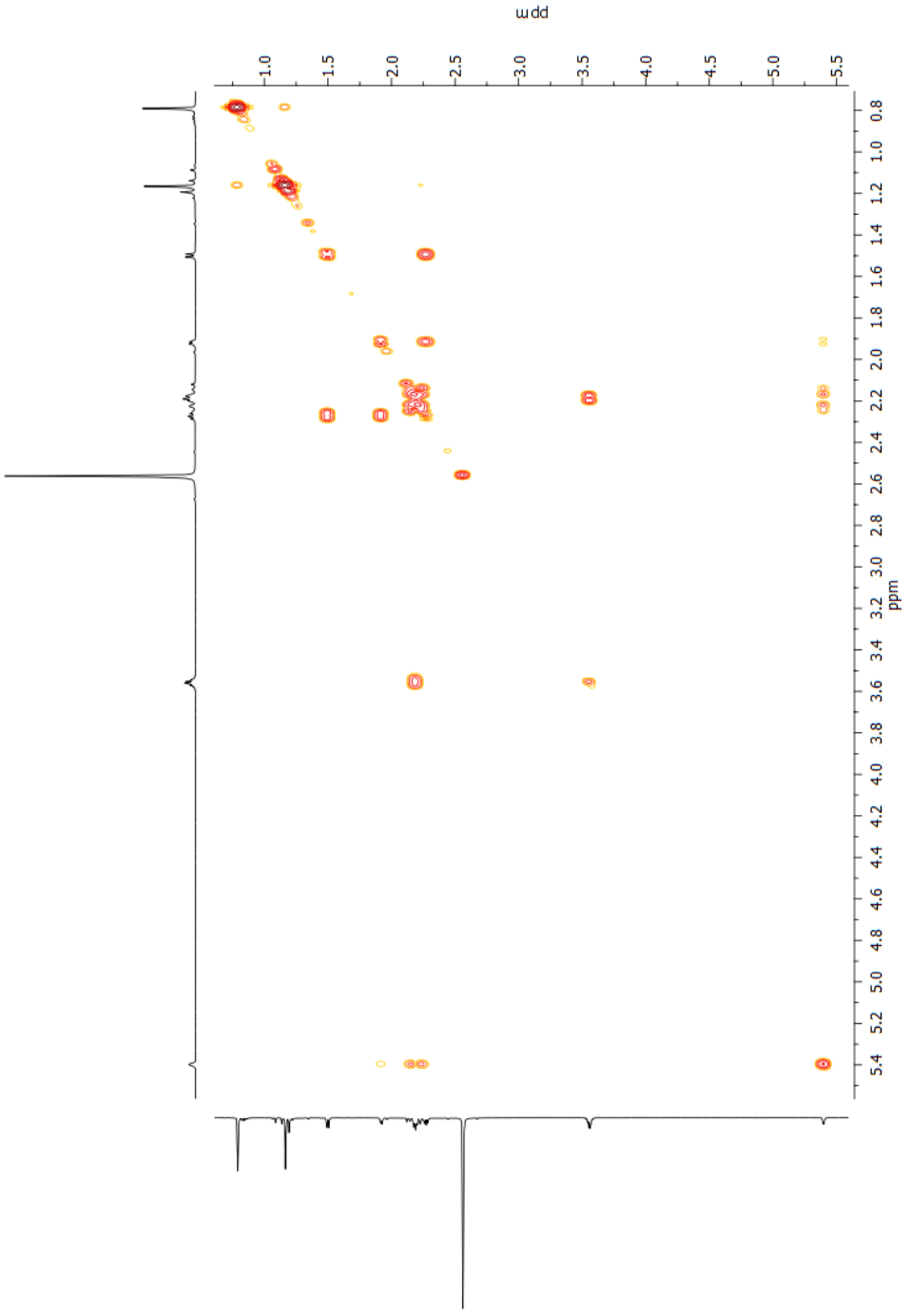

Figure F.60: COSY NMR of 1-hydroxy-(1R)-(−)-nopol

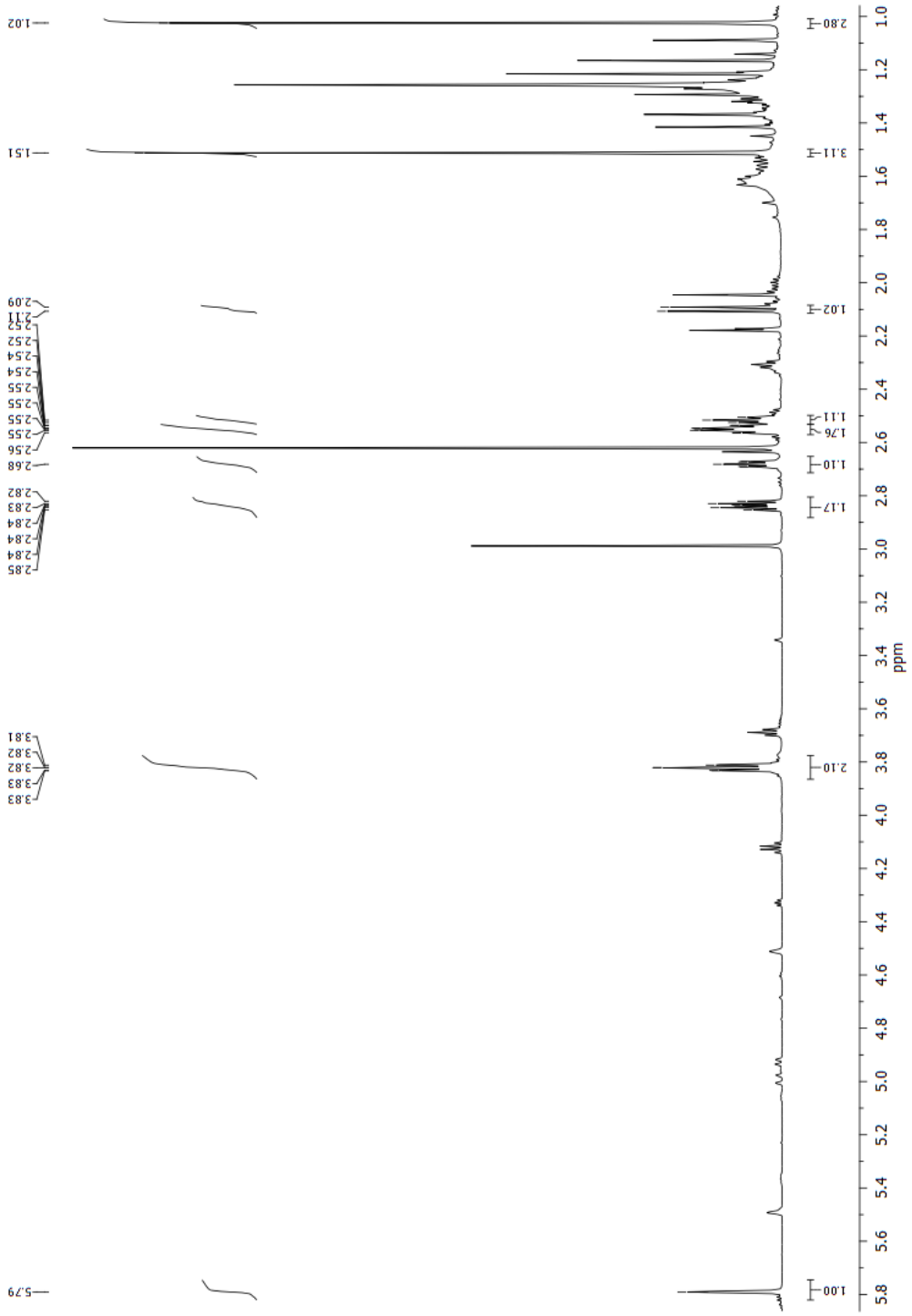

Figure F.61: ^{1}H NMR of 4-oxo-(1R)-(−)-nopol

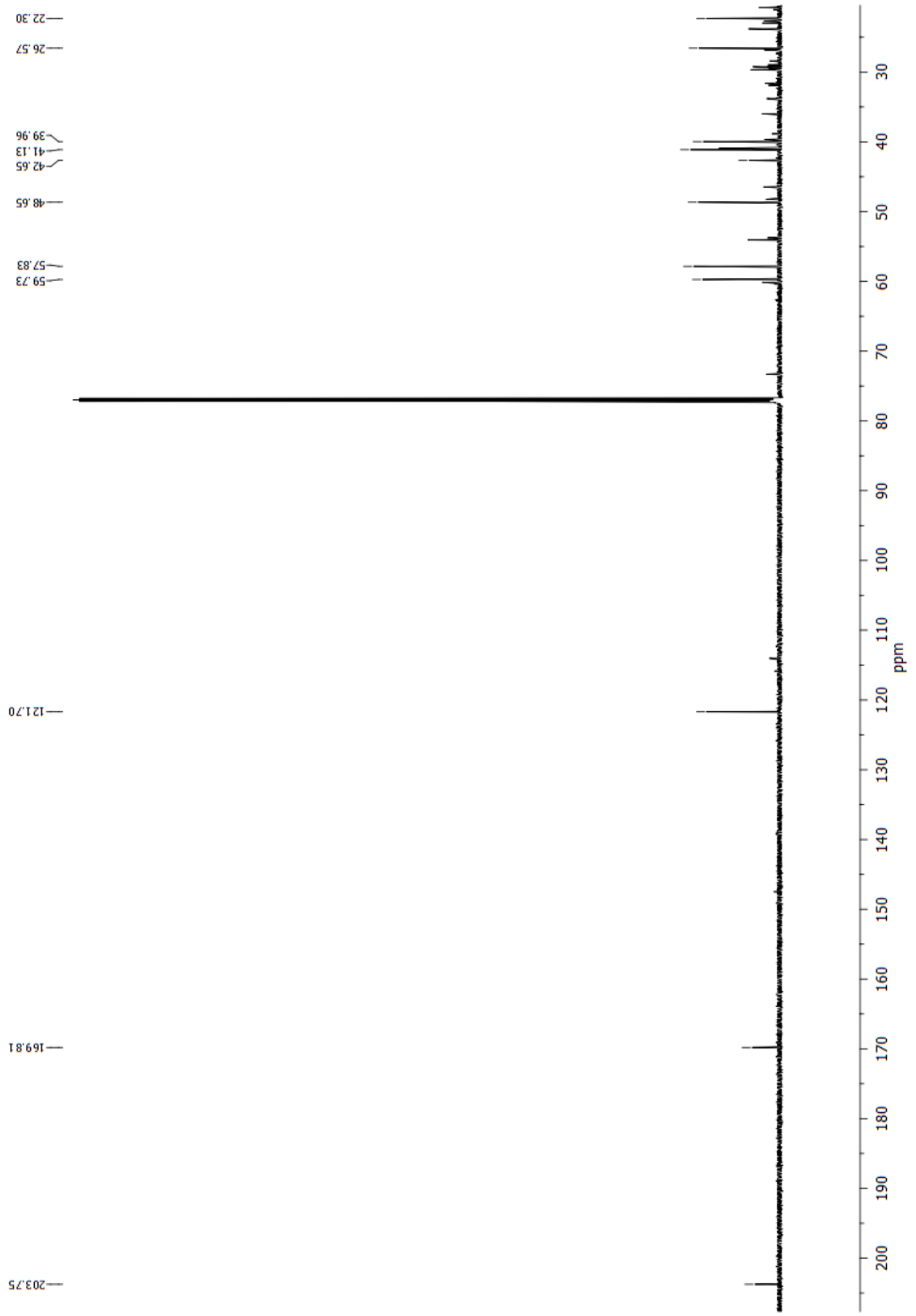

Figure F.62: ^{13}C NMR of 4-oxo-(1R)-(−)-nopol

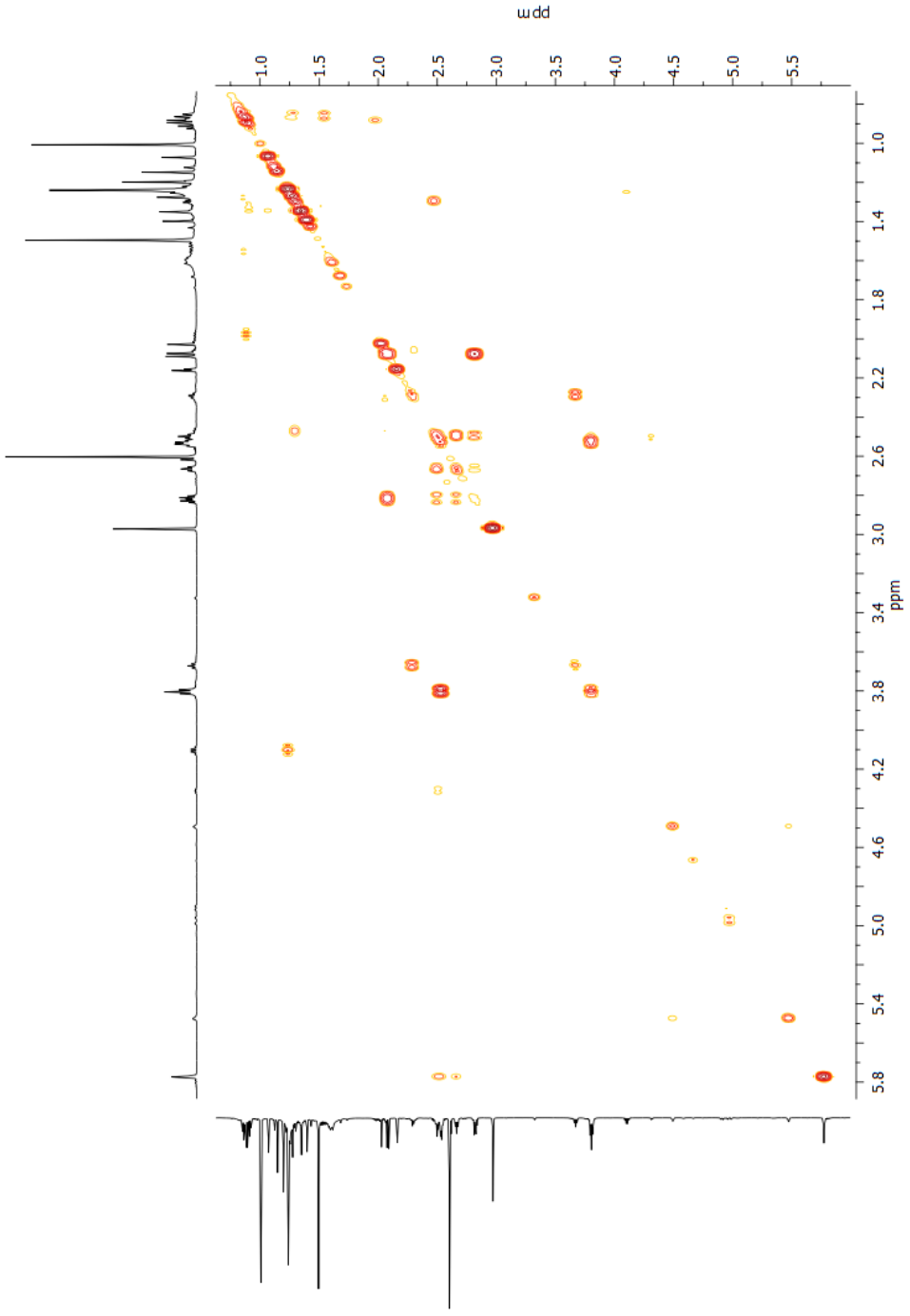

Figure F.63: COSY NMR of 4-oxo-(1R)-(−)-nopol

F.13 *cis*-Jasmone

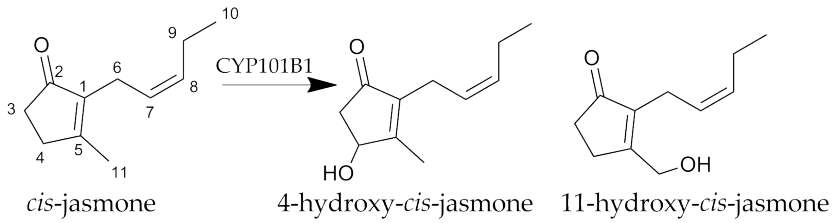

Figure F.64: *cis*-jasmone products

Data for 4-hydroxy-*cis*-jasmone:
^{1}H NMR (600 MHz, $CDCl_3$) δ 5.44 - 5.36 (m, 1H, H8), 5.26 - 5.18 (m, 1H, H7), 4.71 (d, J = 5.9 Hz, 1H, H4), 2.94 (d, J = 7.3 Hz, 2H, H6), 2.76 (dd, J = 18.4, 6.2 Hz, 1H, H3), 2.27 (dd, J = 18.4, 1.5 Hz, 1H, H3), 2.20 - 2.11 (m, 2H, H9), 2.10 (s, 3H, H11), 0.99 (t, J = 7.5 Hz, 3H, H10); ^{13}C NMR (151 MHz, $CDCl_3$) δ 205.18 (C2), 169.02 (C5), 140.83 (C1), 132.96 (C8), 124.16 (C7), 71.58 (C4), 44.29 (C3), 21.12 (C6), 20.58 (C9), 14.12 (C10), 13.72 (C11).

Data for 11-hydroxy-*cis*-jasmone:
^{1}H NMR (600 MHz, $CDCl_3$) δ 5.46 - 5.37 (m, 1H, H8), 5.28 - 5.17 (m, 1H, H7), 4.58 (s, 2H, H11), 2.98 (d, J = 7.2 Hz, 2H, H6), 2.69 - 2.61 (m, 2H, H4), 2.46 - 2.38 (m, 2H, H3), 2.19 - 2.12 (m, 2H, H9), 0.99 (t, J = 7.5 Hz, 3H, H10); ^{13}C NMR (151 MHz, $CDCl_3$) δ 209.10 (C2), 170.66 (C5), 139.12 (C1), 132.93 (C8), 125.00 (C7), 60.90 (C11), 33.93 (C3), 27.01 (C4), 21.14 (C6), 20.57 (C9), 14.09 (C10).

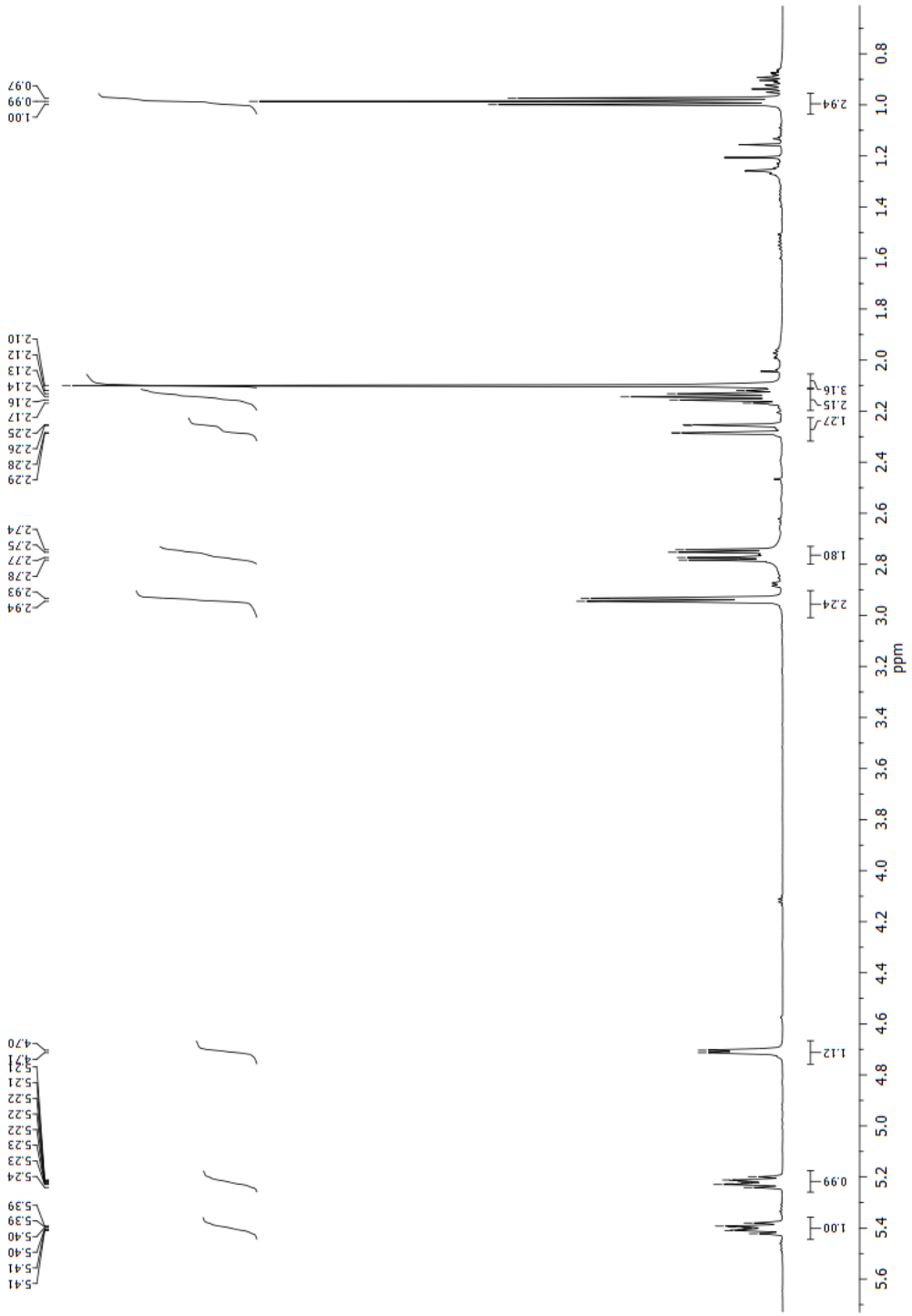

Figure F.65: ^{1}H NMR of 4-hydroxy-*cis*-jasmone

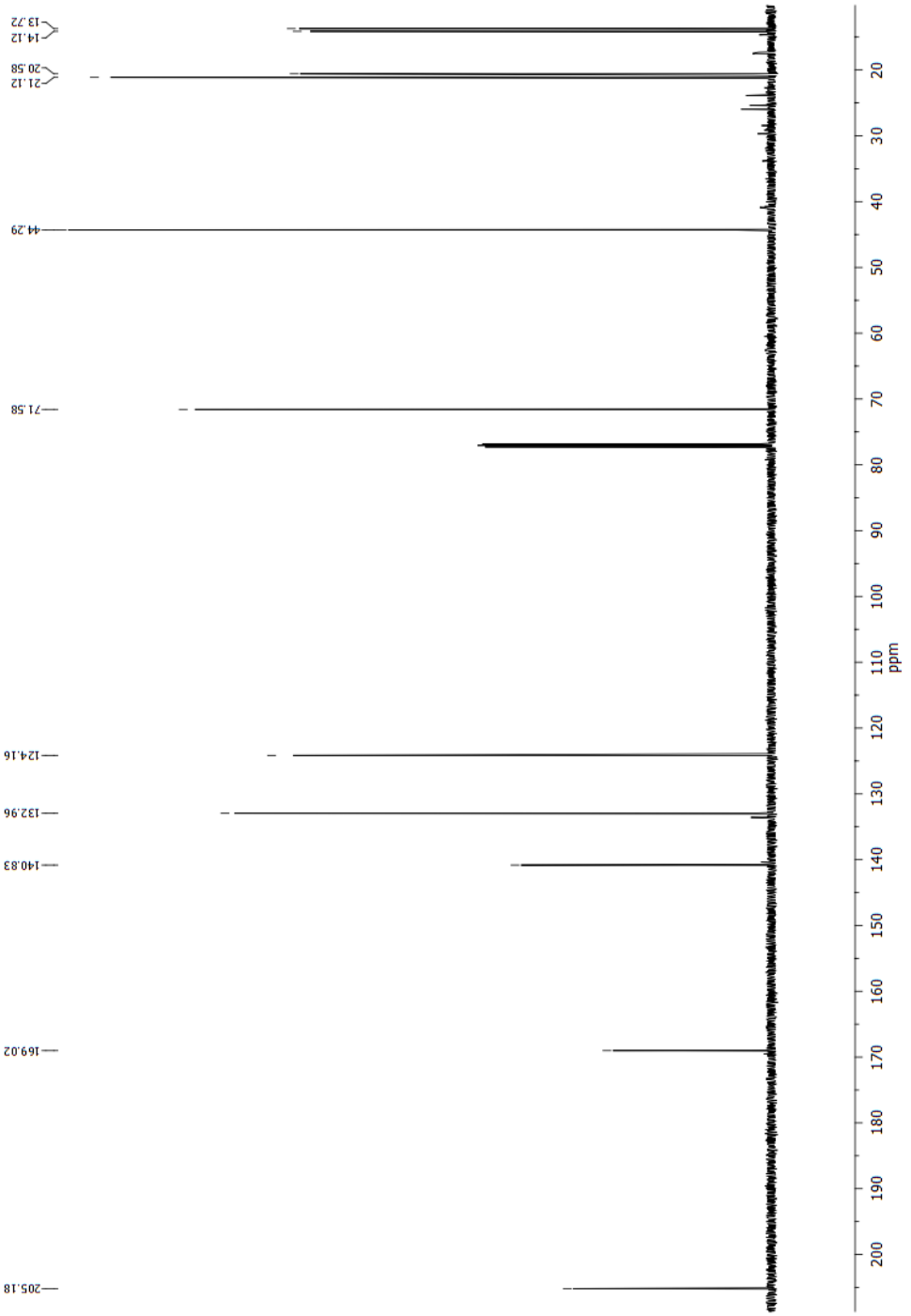

Figure F.66: ^{13}C NMR of 4-hydroxy-*cis*-jasmone

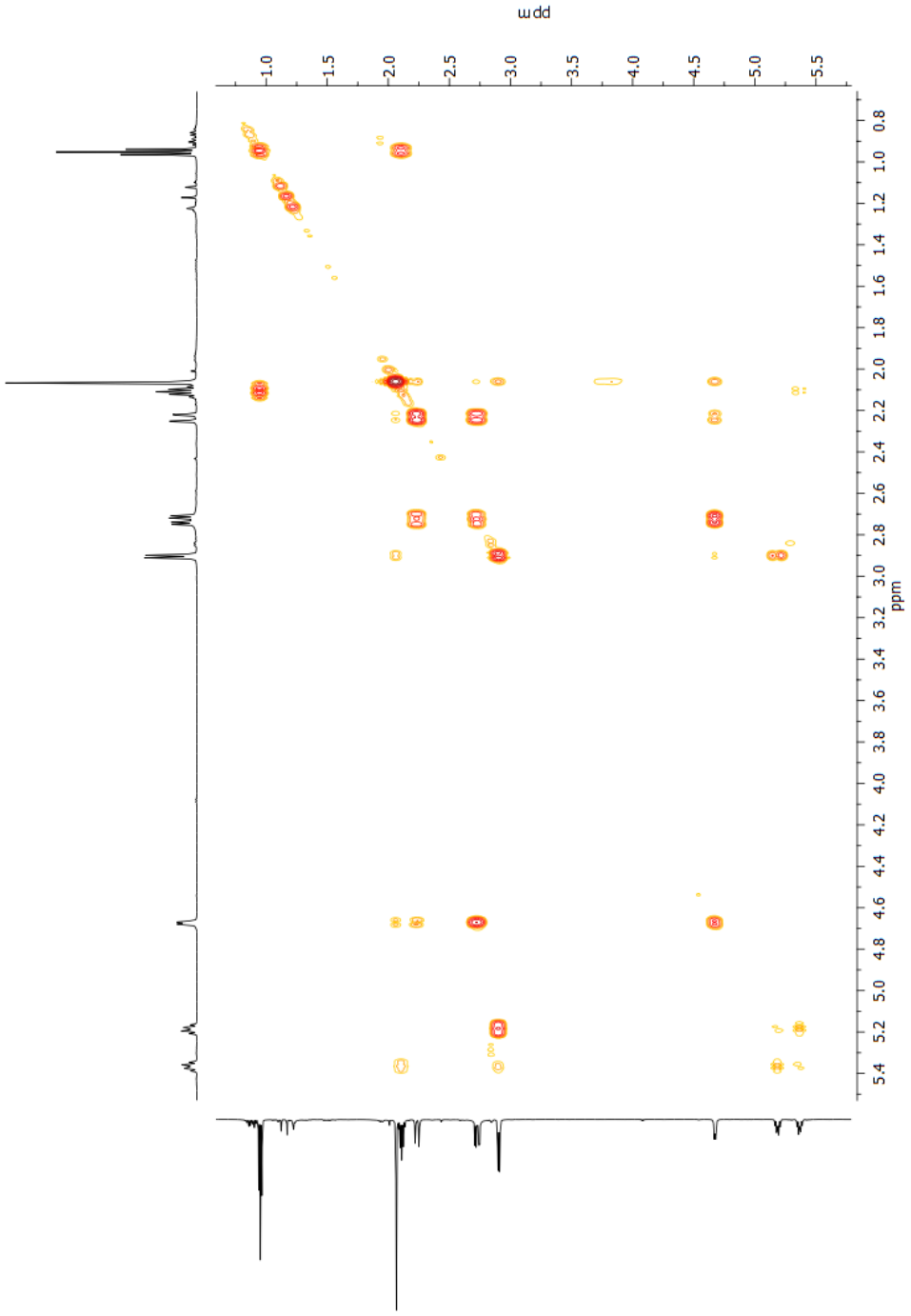

Figure F.67: COSY NMR of 4-hydroxy-*cis*-jasmone

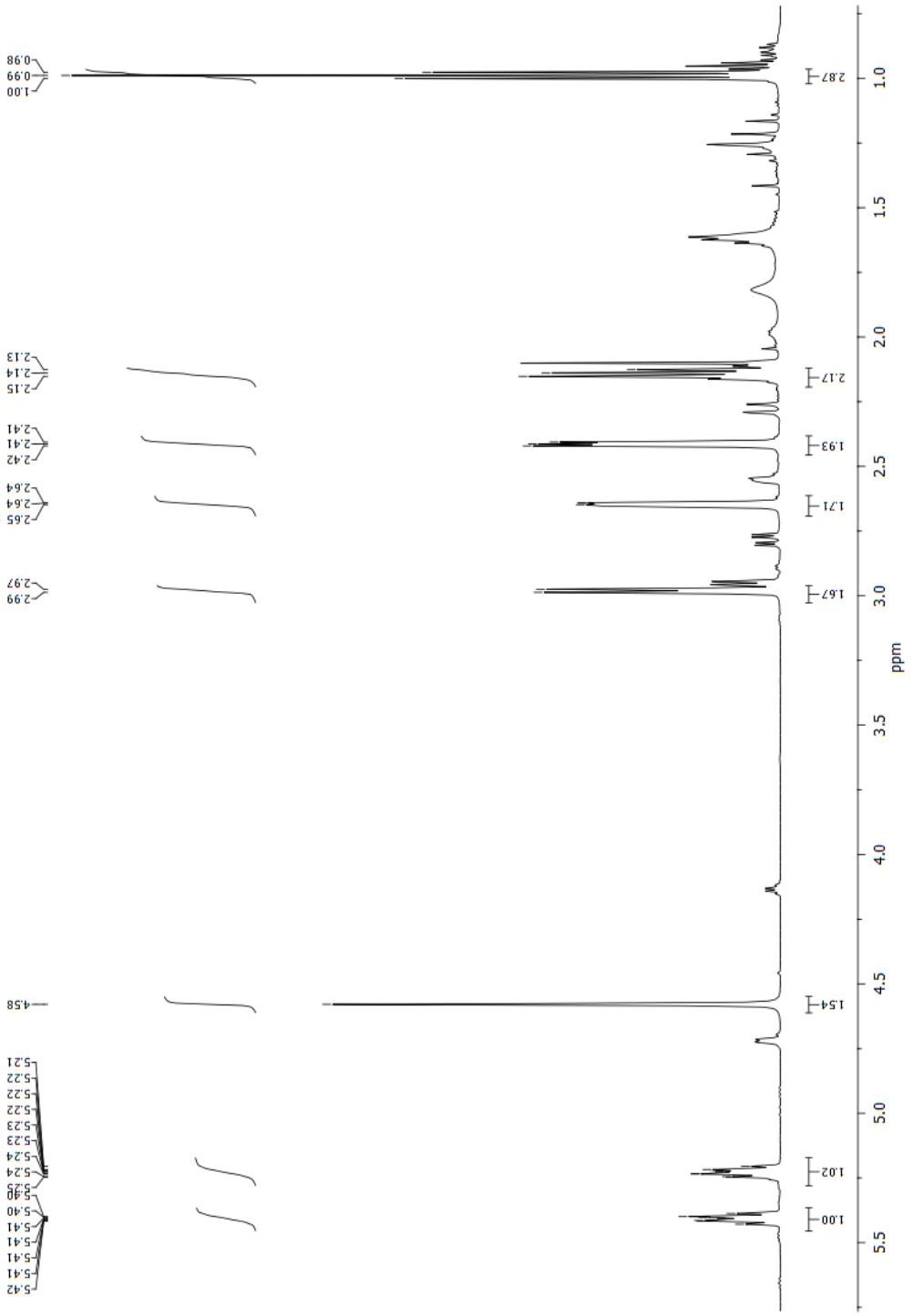

Figure F.68: ^{1}H NMR of 11-hydroxy-*cis*-jasmone

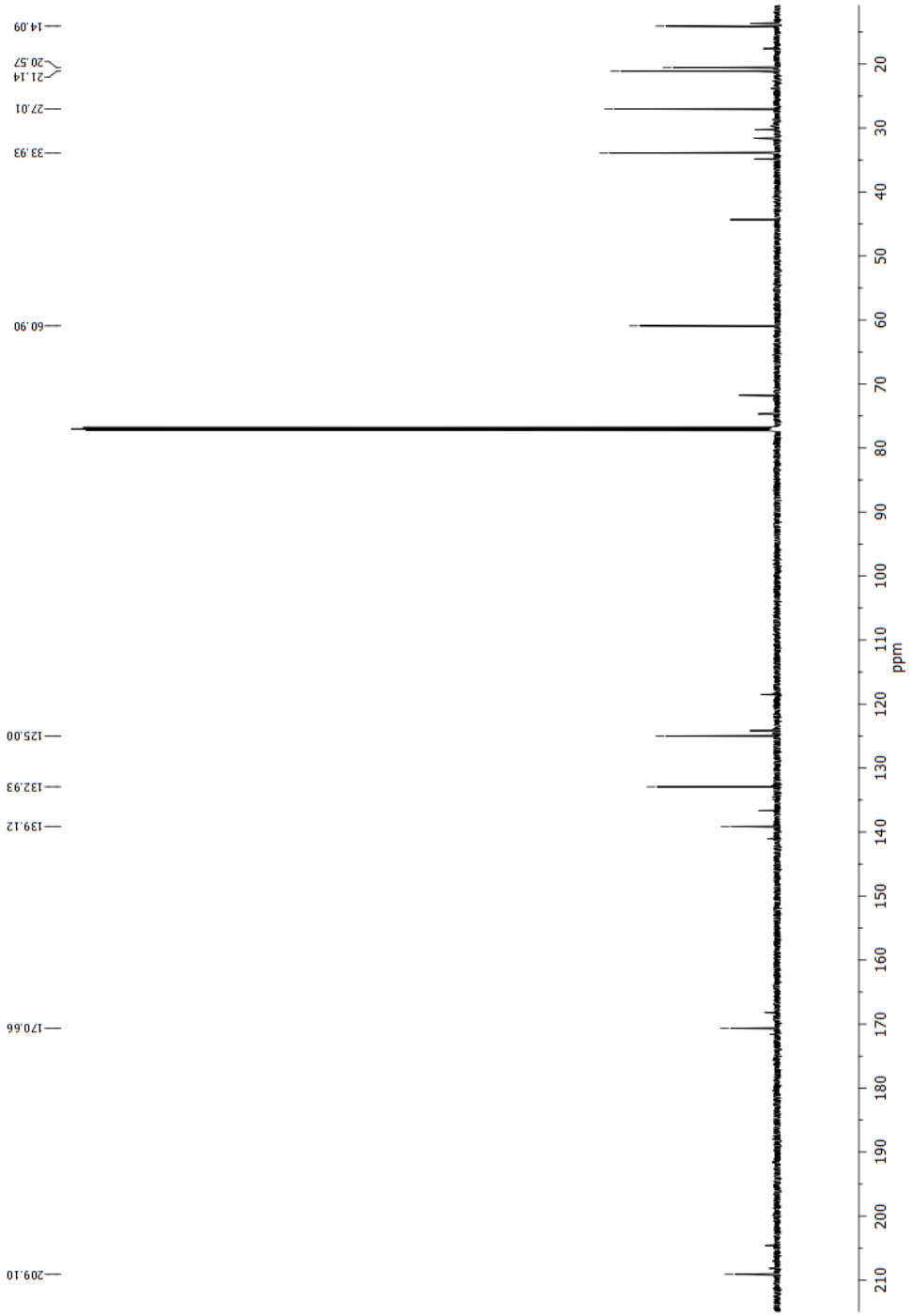

Figure F.69: ^{13}C NMR of 11-hydroxy-*cis*-jasmone

F.14 2-Adamantanol

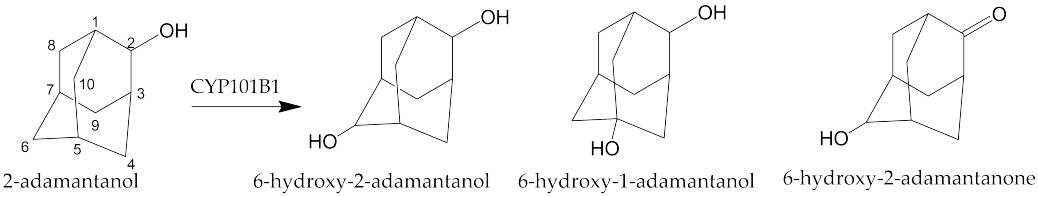

Figure F.70: 2-adamantanol products

Data for 5-hydroxy-2-adamantanol:
^{1}H NMR (500 MHz, d_6-acetone) δ 3.74 (s, 1H, H2), 2.25 (d, J = 12.6 Hz, 2H, H8 and H10), 2.00 - 1.81 (m, 6H, H4, H6 and H9), 1.77 - 1.67 (m, 3H, H1, H3 and H7), 1.44 - 1.32 (m, 2H, H8 and H10); ^{13}C NMR (126 MHz, d_6-acetone) δ 73.23 (C2), 71.48 (C5), 45.06 (C6), 34.90 (C4 and C9), 34.32 (C1 and C3), 33.71 (C7), 29.86 (C8 and C10).

F.15 2-Adamantanone

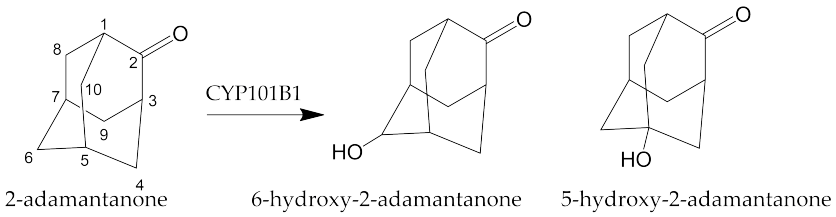

Figure F.71: 2-adamantanone products

Data for 6-hydroxy-2-adamantanone:
^{1}H NMR (600 MHz, $CDCl_3$) δ 4.08 (s, 1H, H6), 2.48 (d, J = 16.5 Hz, 4H, H5, H7, H8 and H9), 2.05 (dt, J = 19.9, 5.5 Hz, 6H, H1, H3, H4 and H10), 1.76 (d, J = 12.6 Hz, 2H, H8 and H9); ^{13}C NMR (151 MHz, $CDCl_3$) δ 217.31 (C2), 72.56 (C6), 46.18 (C7), 45.32 (C5), 37.56 (C4 and C10), 33.86 (C1 and C3), 32.64 (C8 and C9).

Data for 5-hydroxy-2-adamantanone:
^{1}H NMR (500 MHz, CDCl3) δ 2.62 (s, 2H, H6), 2.4 - 2.3 (m, 1H, H7), 2.13 - 1.94 (m, 10H, H1, H3, H4, H8, H9 and H10); ^{13}C NMR (126 MHz, CDCl3) δ 216.39 (C2), 67.30 (C5), 46.98 (C6), 45.04 (C4 and C9), 44.21 (C1 and C3), 38.15 (C8 and C10), 29.87(C7).

F.16 Fenchyl acetate

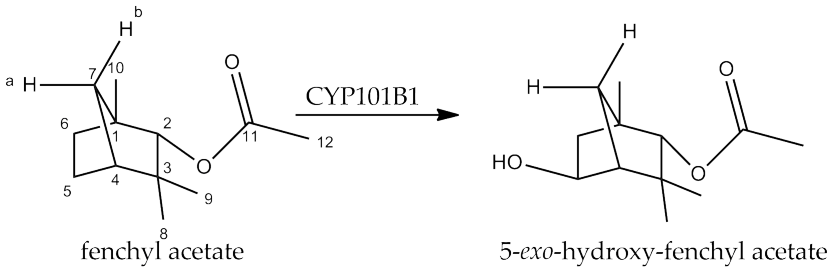

Figure F.72: Fenchyl acetate product

Data for 5-*exo*-hydroxy-fenchyl acetate:
^{1}H NMR (500 MHz, $CDCl_3$) δ 4.32 (s, 1H, *exo* H2), 4.18 (d, J = 6.6 Hz, 1H, *endo* H5), 2.24 (dd, J = 13.8, 6.6 Hz, 1H, *endo* H6), 2.06 (s, 3H, H12), 1.72 (s, 1H, H4), 1.61 (d, J = 10.7 Hz, 1H, H7a), 1.48 (d, J = 10.8 Hz, 1H, H7b), 1.14 (s, 3H, H9), 1.07 (s, 3H, H10), 0.99 (d, J = 13.8 Hz, 1H, *exo* H6), 0.75 (s, 3H, H8); ^{13}C NMR (126 MHz, $CDCl_3$) δ 171.41 (C11), 84.62 (C2), 71.25 (C5), 55.93 (C4), 47.56 (C3), 39.55 (C6), 39.04 (C1), 36.95 (C7), 29.68 (C9), 20.90 (C12), 19.27 (C8), 18.76 (C10).

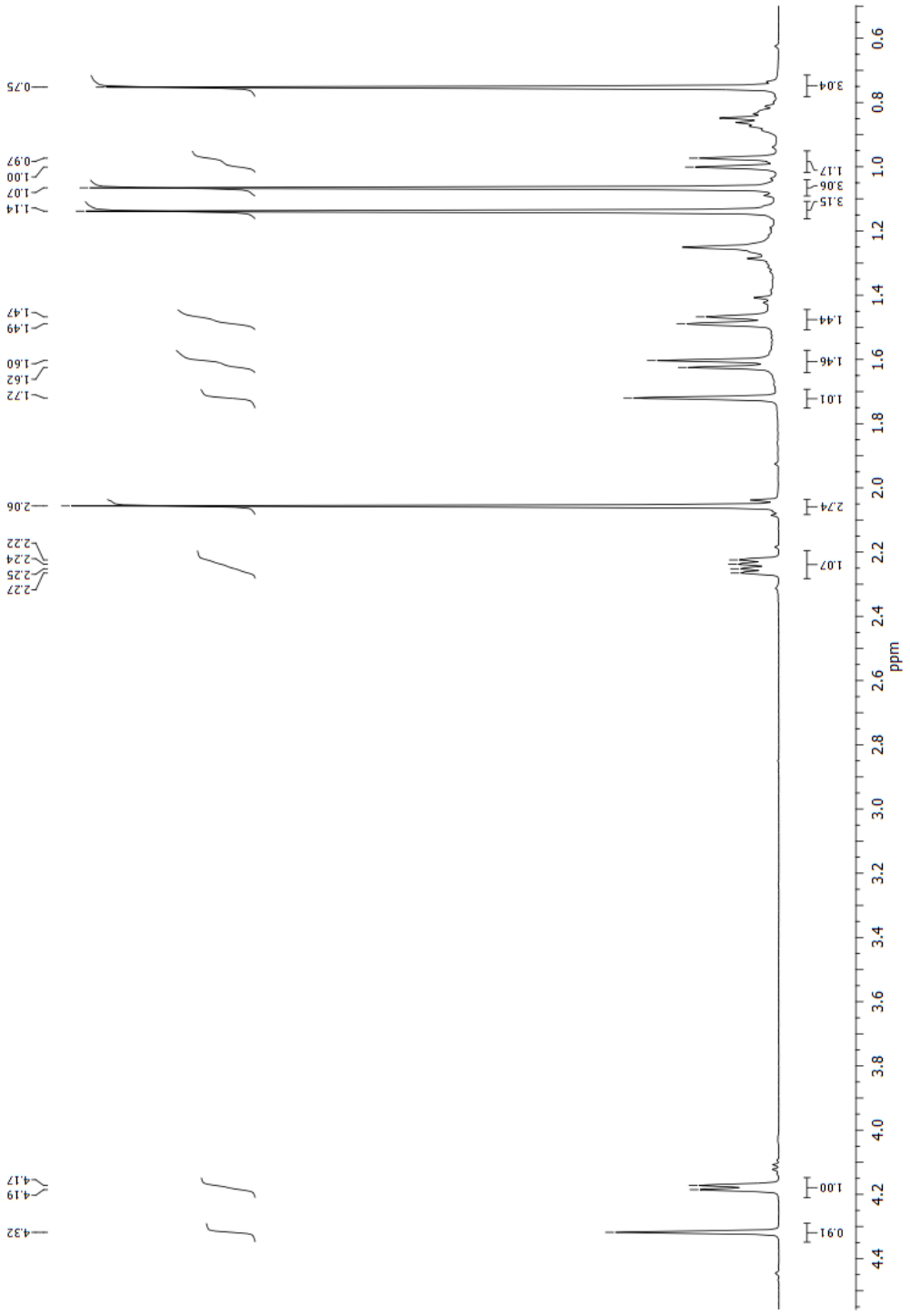

Figure F.73: ^{1}H NMR of 5-*exo*-hydroxy-fenchyl acetate

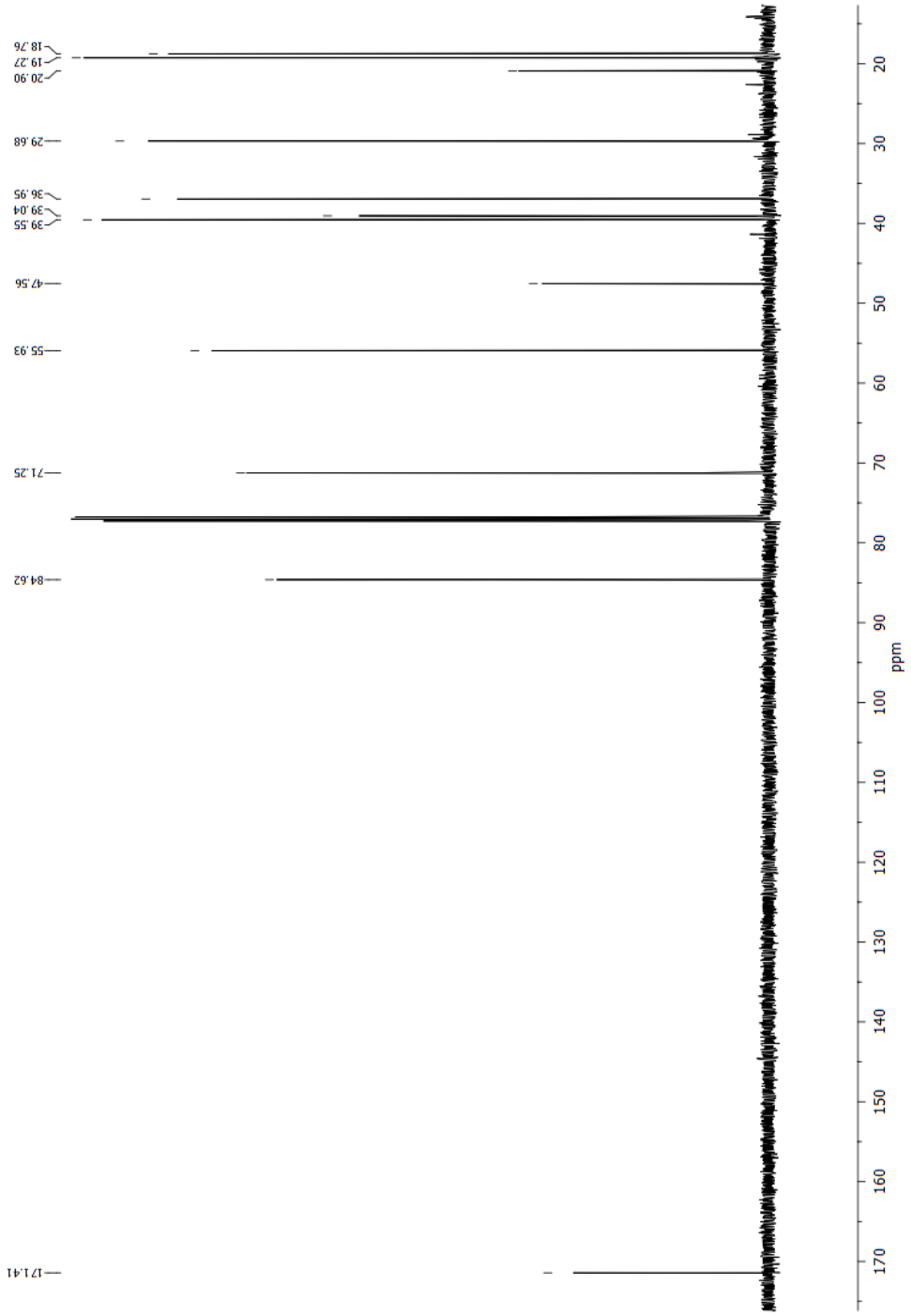

Figure F.74: ^{13}C NMR of 5-*exo*-hydroxy-fenchyl acetate

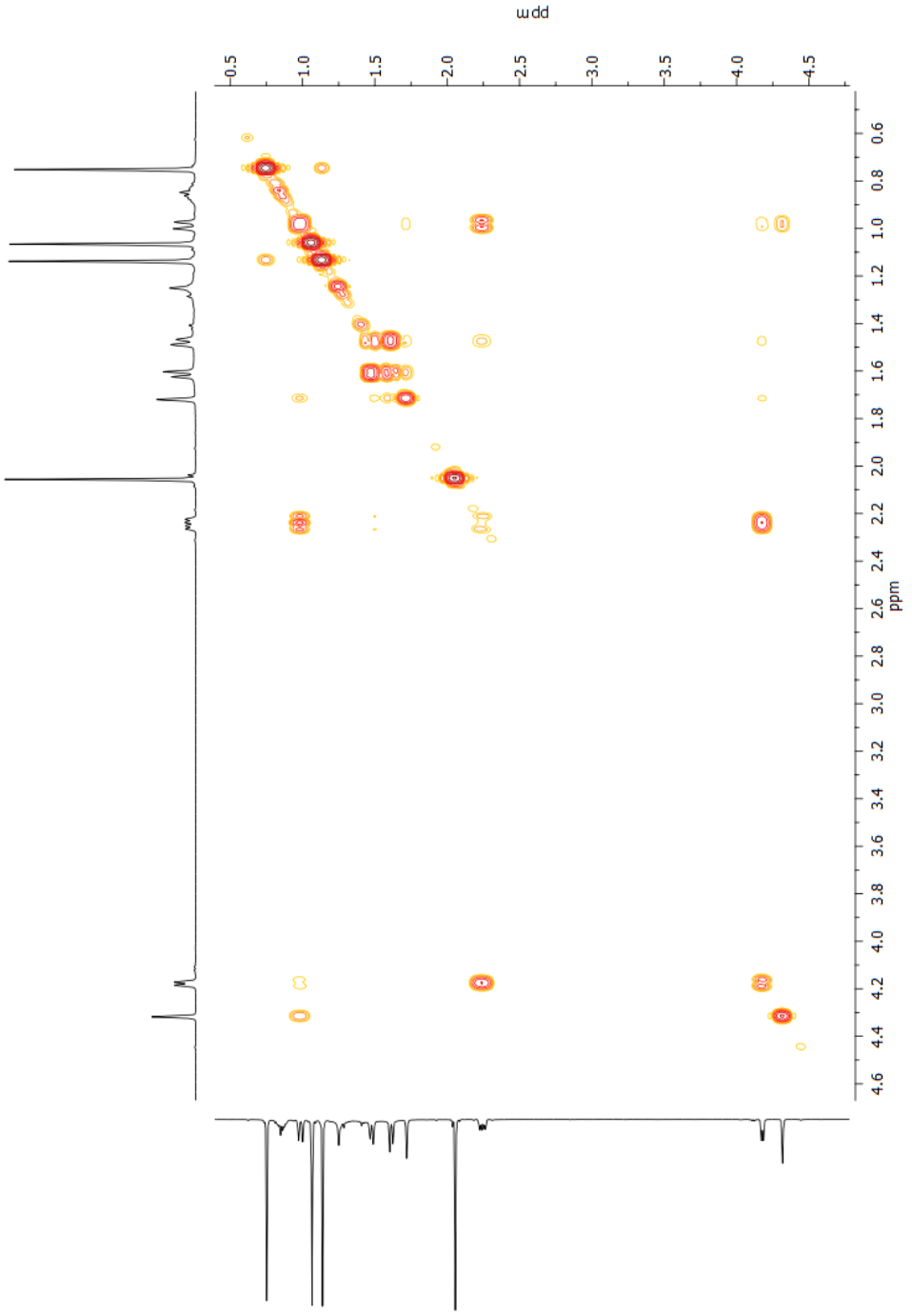

Figure F.75: COSY NMR of 5-*exo*-hydroxy-fenchyl acetate

F.17 Bornyl acetate

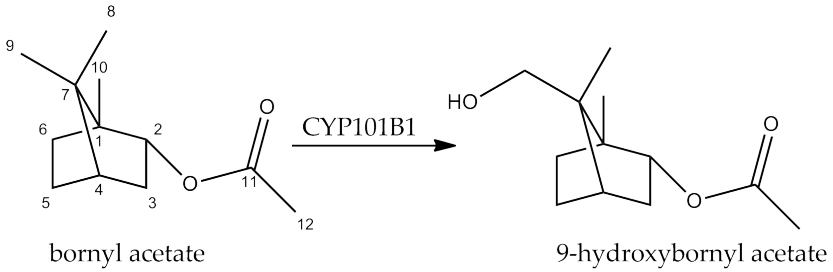

Figure F.76: Bornyl acetate product

Data for 9-hydroxybornyl acetate: ^{1}H NMR (500 MHz, $CDCl_3$) δ 4.92 - 4.86 (m, 1H, *exo* H2), 3.70 (d, J = 10.9 Hz, 1H, H9), 3.45 (d, J = 10.9 Hz, 1H, H9), 2.42 - 2.31 (m, 1H, *exo* H3), 2.10 - 2.00 (m, 4H, *exo* H6 and H12), 1.95 (t, J = 4.5 Hz, 1H, H4), 1.77 (ddd, J = 12.5, 8.5, 4.7 Hz, 1H, *exo* H5), 1.39 - 1.29 (m, 2H, *endo* H6 and *endo* H5), 1.06 - 0.98 (m, 4H, *endo* H3 and H8), 0.88 (s, 3H, H10); ^{13}C NMR (126 MHz, $CDCl_3$) δ 171.43 (C11), 79.50 (C2), 65.60 (C8), 52.45 (C1), 48.74 (C7), 41.26 (C4), 36.62 (C3), 27.62 (C5), 27.11 (C6), 21.27 (C12), 14.08 (C10), 13.58 (C8).

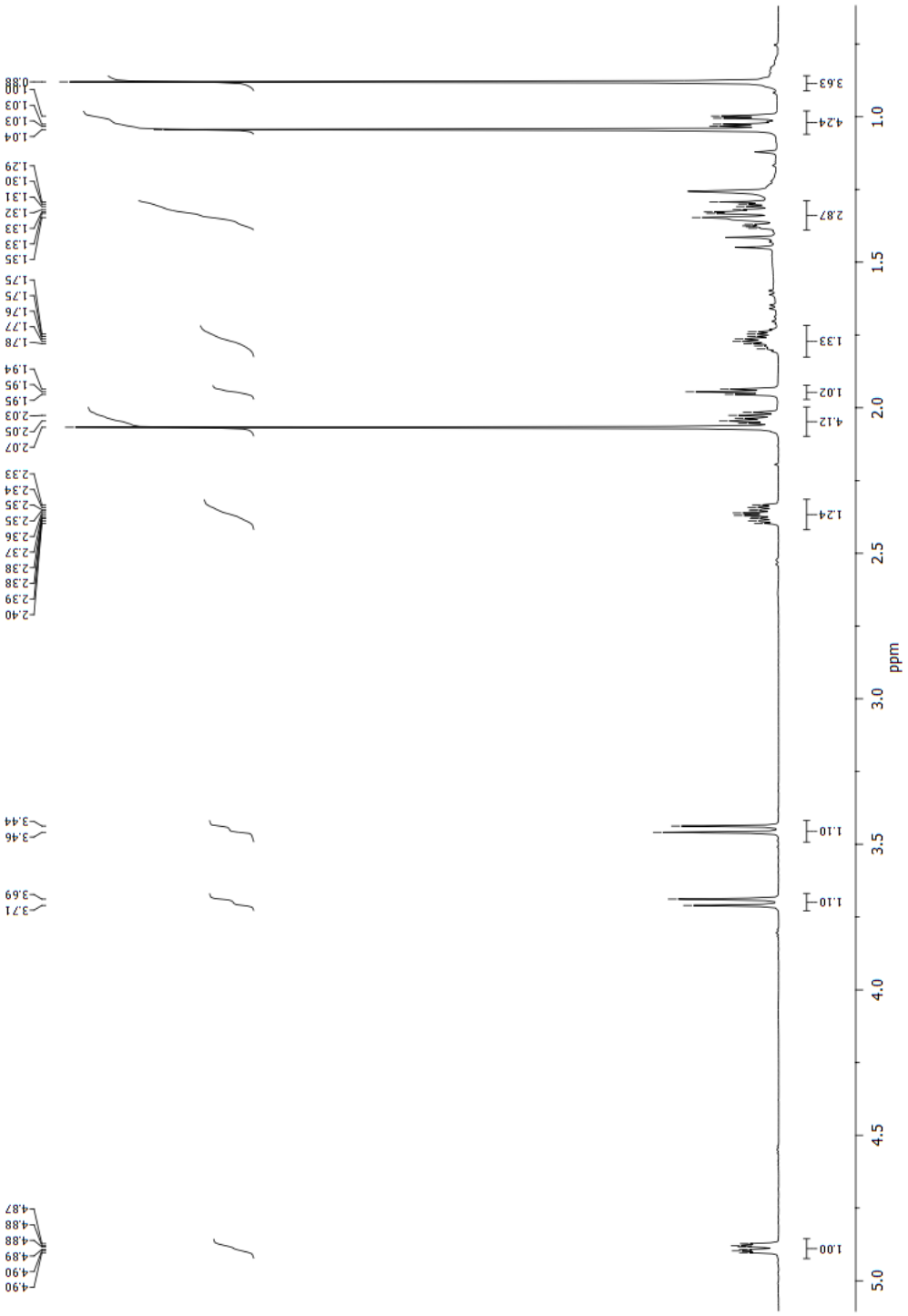

Figure F.77: ^{1}H NMR of 9-hydroxybornyl acetate

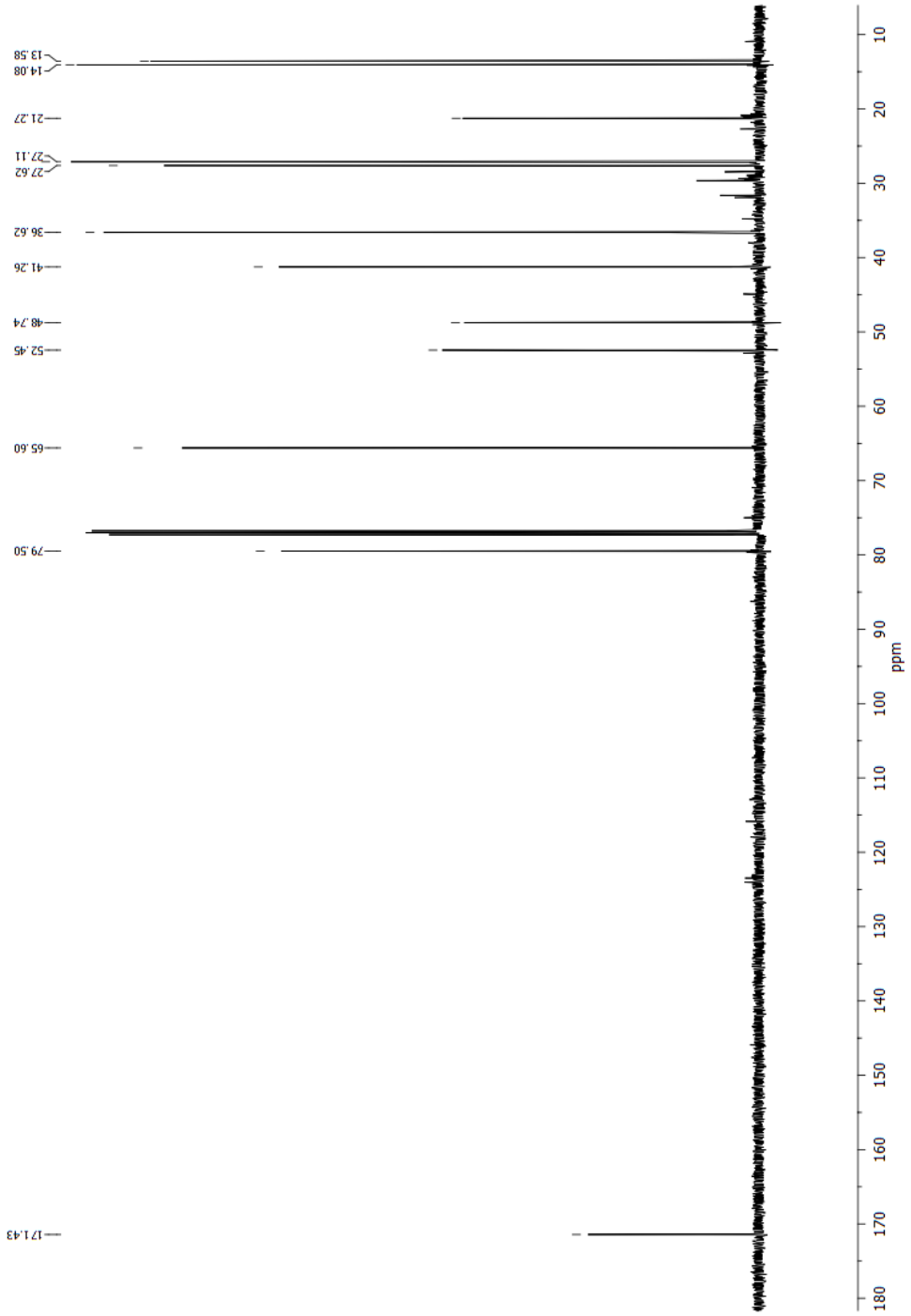

Figure F.78: ^{13}C NMR of 9-hydroxybornyl acetate

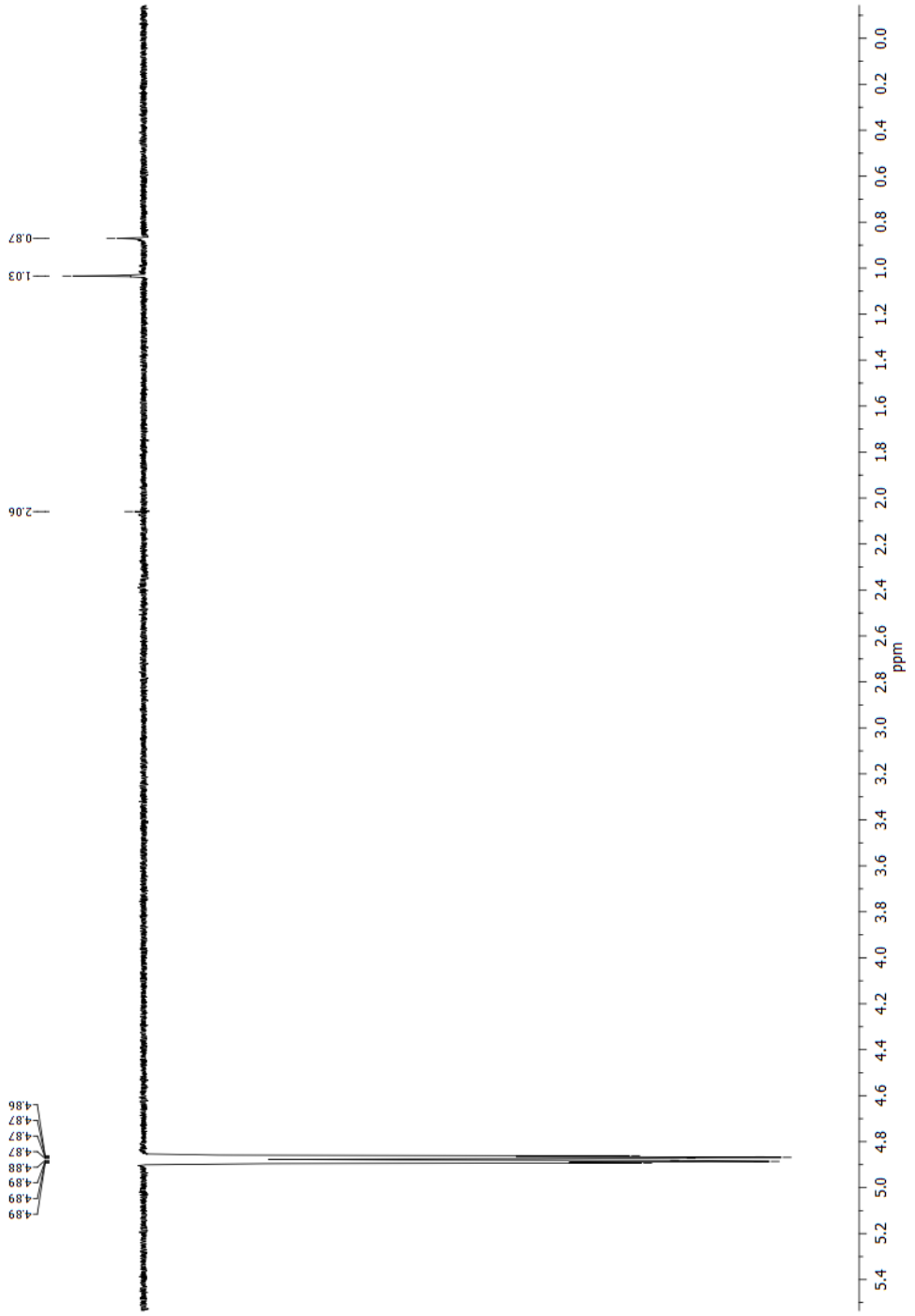

Figure F.79: DPFGSE NOESY of 9-hydroxybornyl acetate for the exo H2 signal

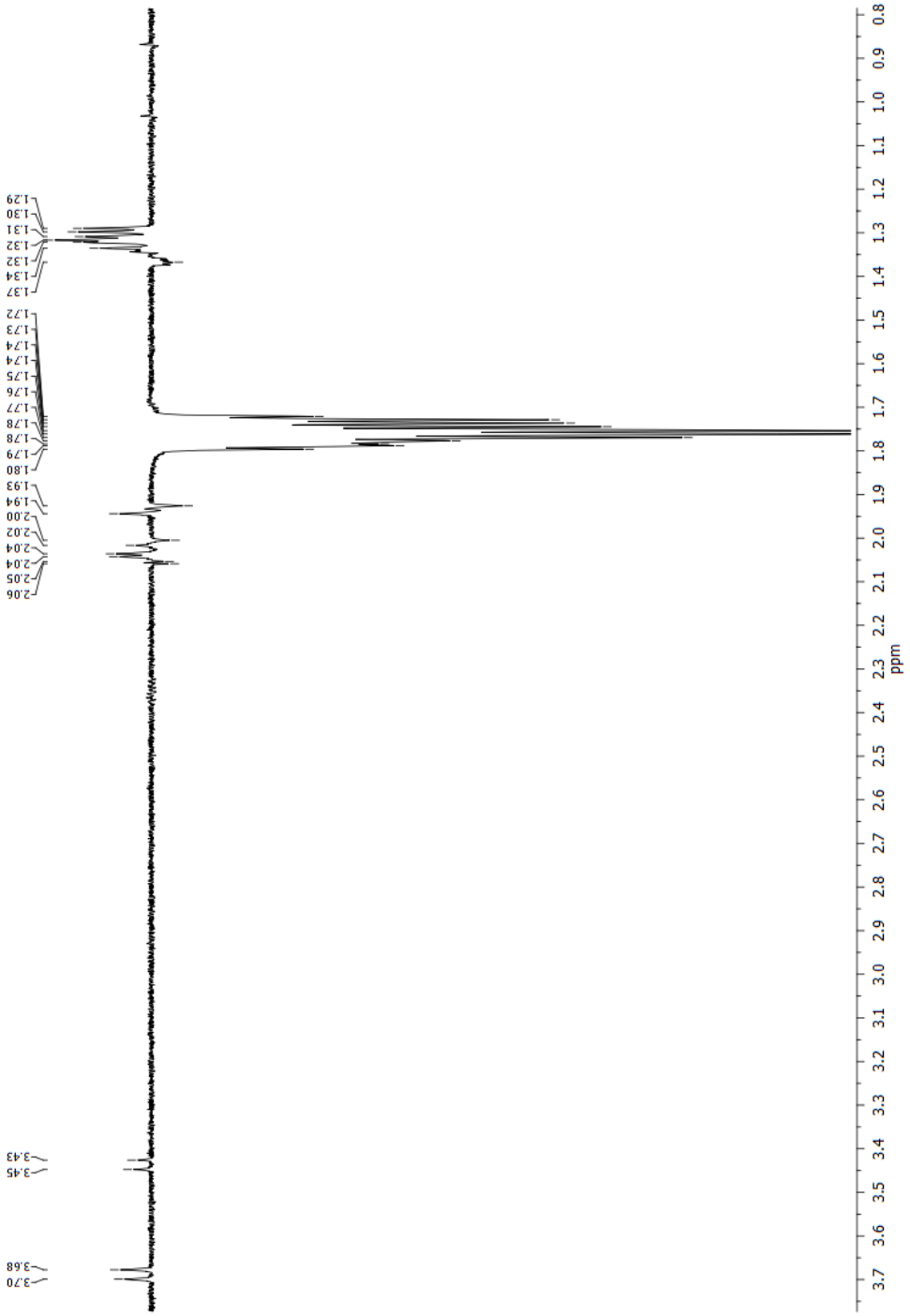

Figure F.80: DPFGSE NOESY of 9-hydroxybornyl acetate for the exo H5 signal

F.18 Isobornyl acetate

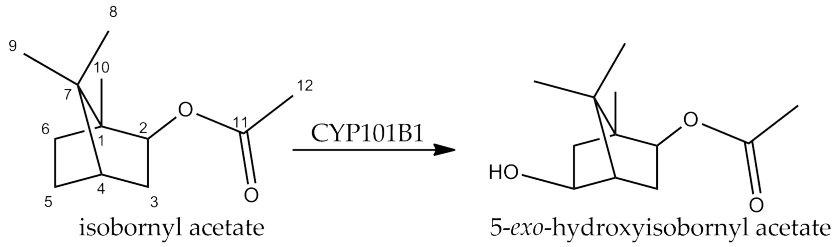

Figure F.81: Isobornyl acetate product

Data for 5-*exo*-hydroxyisobornyl acetate:
^{1}H NMR (500 MHz, $CDCl_3$) δ 4.55 (dd, J = 7.0, 4.8 Hz, 1H, *endo* H2), 3.80 (t, J = 5.7 Hz, 1H, *endo* H5), 2.03 (s, 3H, H12), 1.78 (d, J = 3.5 Hz, 1H, H4), 1.72 - 1.68 (m, 2H, H3), 1.65 (d, J = 5.5 Hz, 2H, H6), 1.12 (s, 3H, H9), 0.99 (s, 3H, H8), 0.88 (s, 3H, H10); ^{13}C NMR (126 MHz, $CDCl_3$) δ 170.77 (C11), 79.62 (C2), 74.96 (C5), 52.83 (C4), 49.93 (C1), 46.60 (C11), 44.88 (C6), 34.80 (C3), 21.25 (C12), 21.03 (C9), 20.89 (C8), 10.96 (C10).

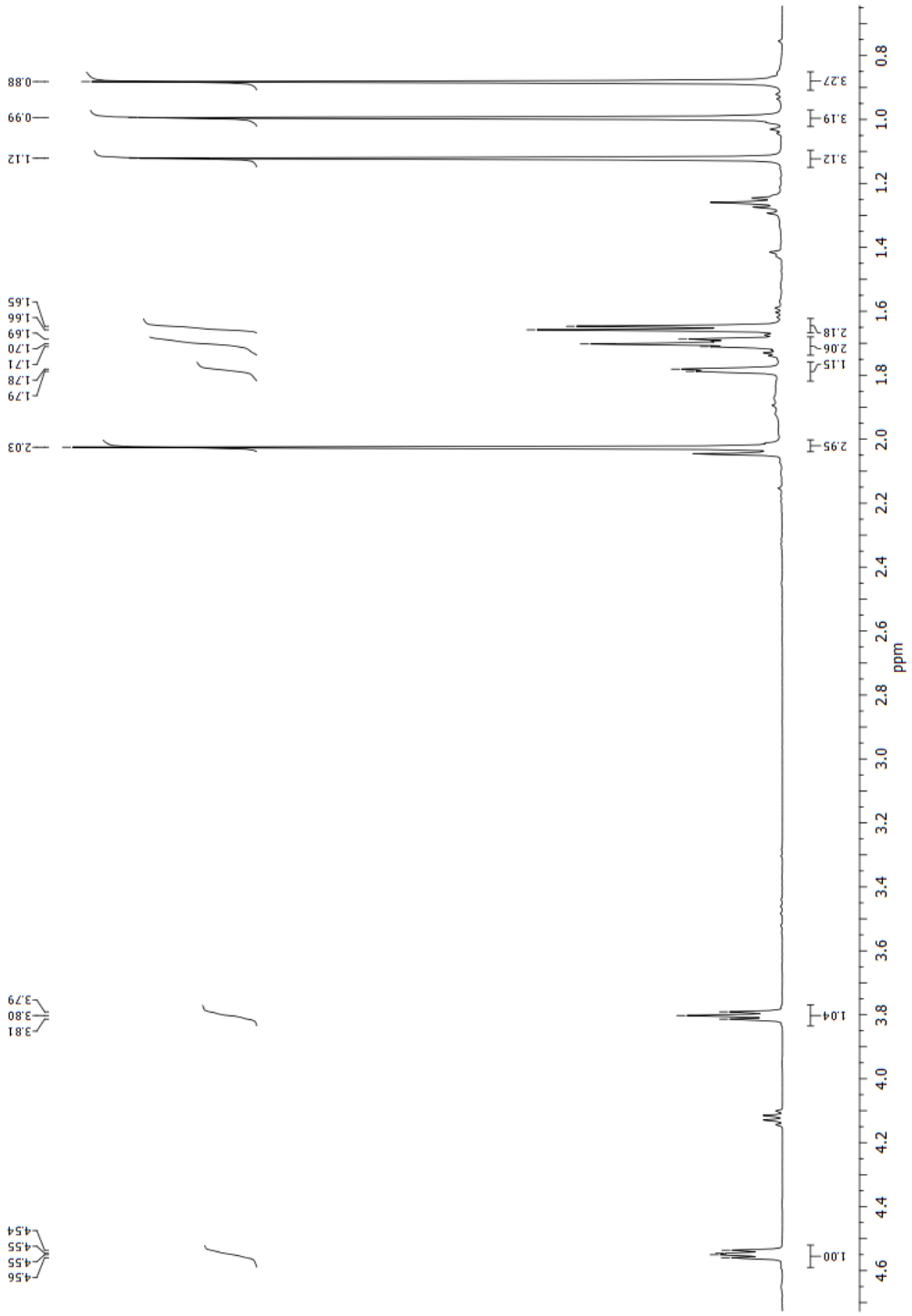

Figure F.82: ^{1}H NMR of 5-*exo*-hydroxyisobornyl acetate

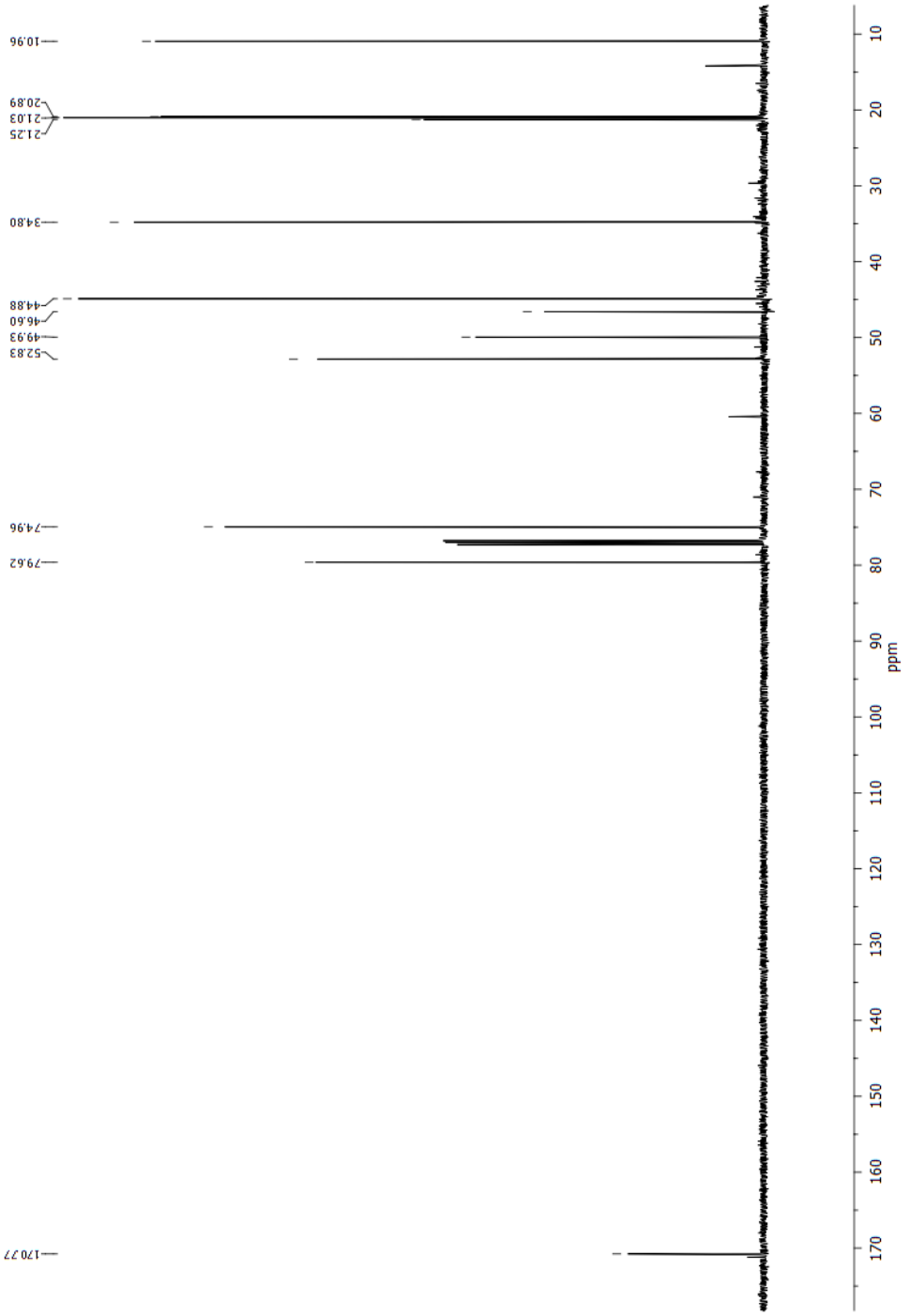

Figure F.83: ^{13}C NMR of 5-*exo*-hydroxyisobornyl acetate

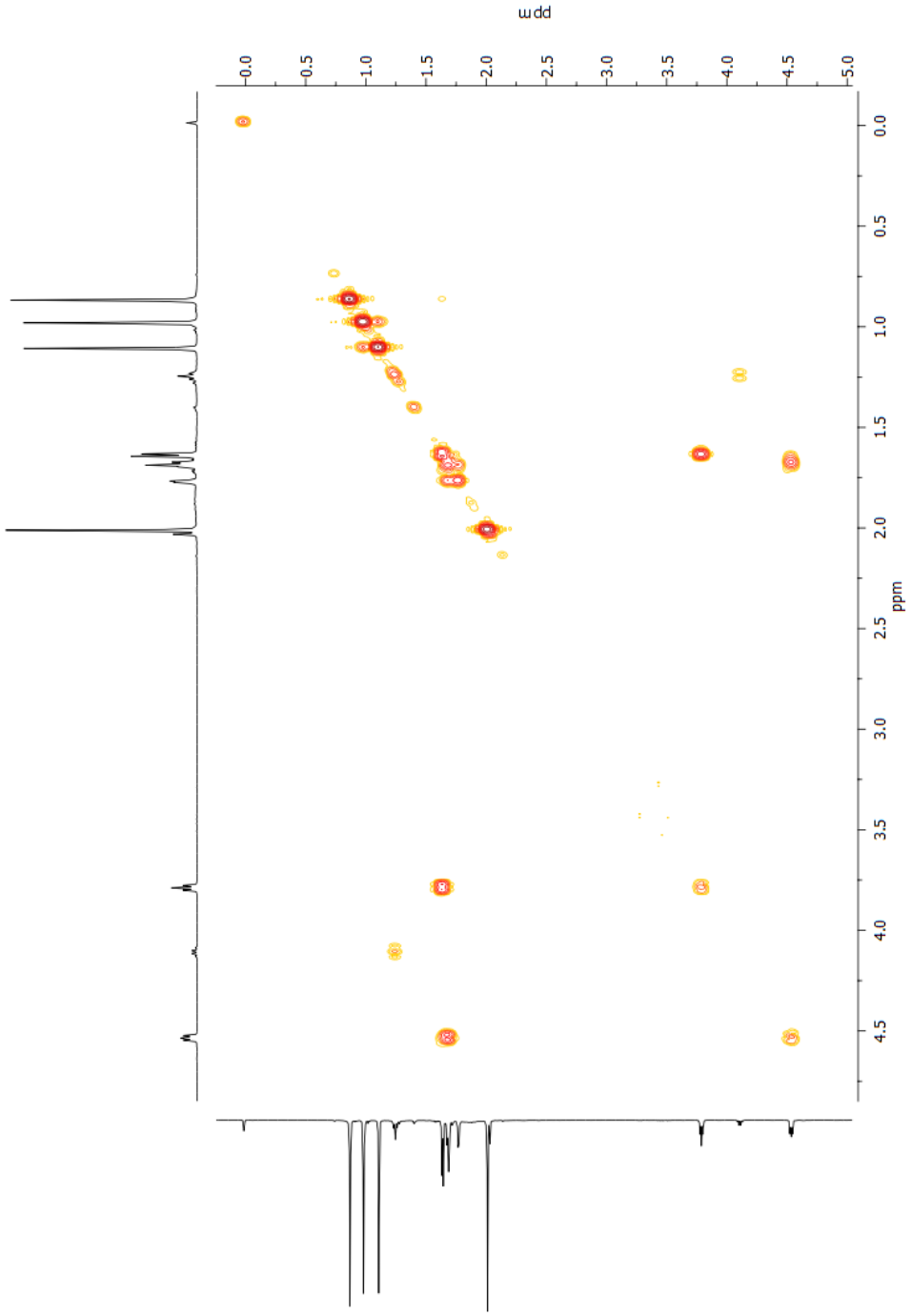

Figure F.84: COSY NMR of 5-*exo*-hydroxyisobornyl acetate

F.19 5-Norbornen-2-yl acetate

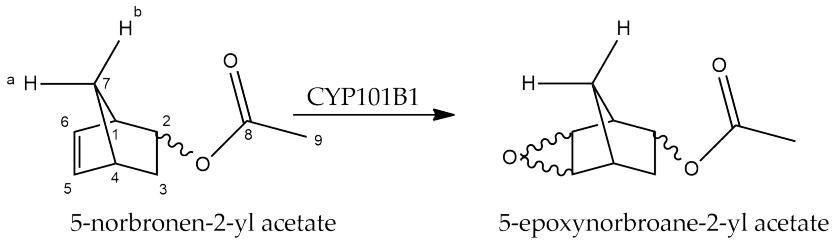

Figure F.85: 5-Norbornen-2-yl acetate product

Data for 5-epoxynorborane-2-yl acetate:
^{1}H NMR (500 MHz, $CDCl_3$) δ 5.06 (ddd, J = 8.9, 4.0, 3.2 Hz, 1H, H2), 3.35 (d, J = 3.4 Hz, 1H, H6), 3.25 (d, J = 3.4 Hz, 1H, H5), 2.77 (dd, J = 3.9, 1.6 Hz, 1H, H1), 2.51 (d, J = 2.1 Hz, 1H H4), 2.09 (ddd, J = 13.4, 9.0, 4.3 Hz, 1H, H3), 2.04 (s, 3H, H9), 1.38 - 1.33 (m, 1H, H7a or H7b), 1.09 (dt, J = 13.6, 3.5 Hz, 1H, H3), 0.85 - 0.79 (m, 1H, H7a or H7b); ^{13}C NMR (126 MHz, $CDCl_3$) δ 170.98 (C8), 76.41 (C2), 50.97 (C5), 48.28 (C6), 40.38 (C1), 36.80 (C4), 32.98 (C3), 24.70 (C7), 21.00 (C9).

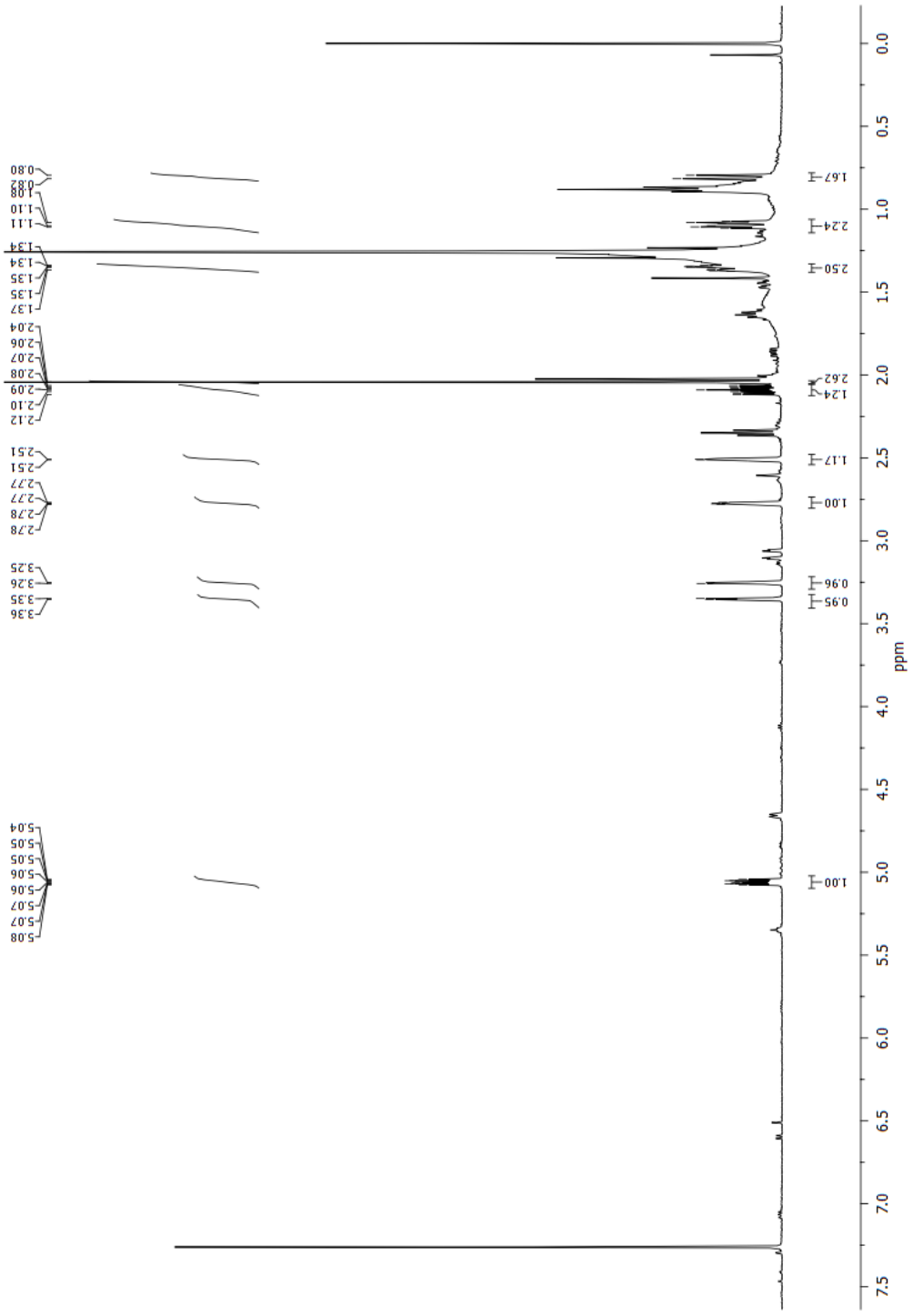

Figure F.86: ^{1}H NMR of 5-epoxynorborane-2-yl acetate

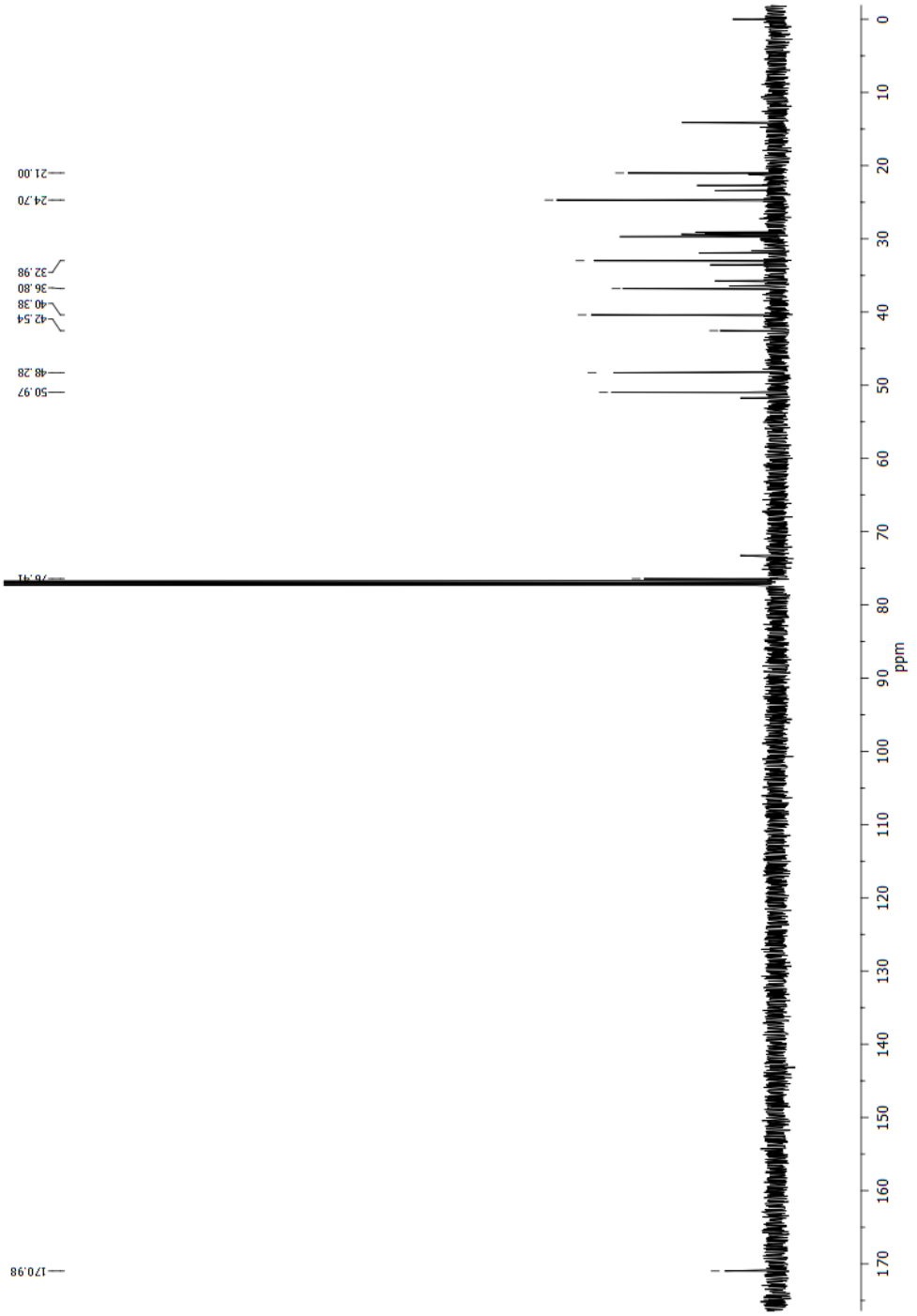

Figure F.87: ^{13}C NMR of 5-epoxynorborane-2-yl acetate

F.20 Myrtenyl acetate

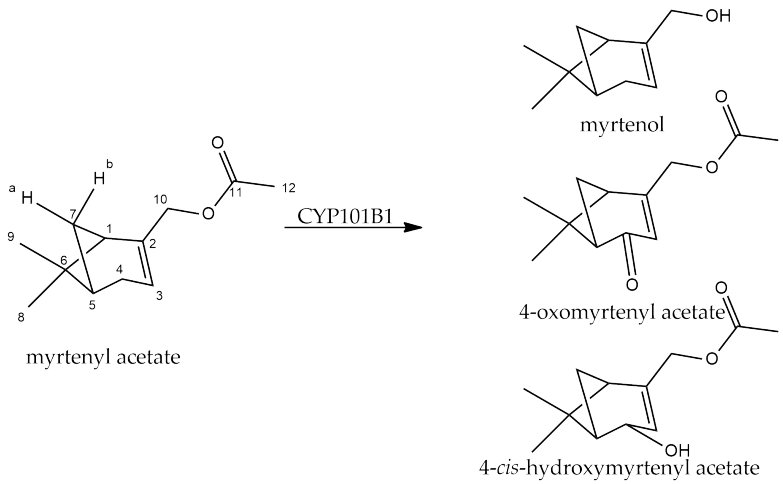

Figure F.88: Myrtenyl acetate products

Data for myrtenol:
^{1}H NMR (500 MHz, $CDCl_3$) δ 5.52 - 5.45 (m, 1H, H3), 3.99 (s, 2H, H10), 2.41 (dt, J = 8.6, 5.6 Hz, 1H, H7b), 2.28 (q, J = 17.8 Hz, 2H, H4), 2.19 - 2.05 (m, 2H, H1 and H5), 1.30 (s, 3H, H9), 1.18 (d, J = 8.6 Hz, 1H, H7a), 0.84 (s, 3H, H8); ^{13}C NMR (126 MHz, $CDCl_3$) δ 147.80 (C2), 117.90 (C3), 66.01 (C10), 43.39 (C5), 40.93 (C1), 37.95 (C6), 31.62 (C7), 31.13 (C4), 26.13 (C9), 21.11 (C8).

Data for 4-oxomyrtenyl acetate:
^{1}H NMR (500 MHz, $CDCl_3$) δ 5.91 - 5.85 (m, 1H, H3), 4.77 (dd, J = 16.6, 1.8 Hz, 1H, H10), 4.68 (dd, J = 16.6, 1.8 Hz, 1H, H10), 2.87 (dt, J = 9.5, 5.5 Hz, 1H, H7b), 2.70 (td, J = 6.0, 1.5 Hz, 1H, H5), 2.45 (t, J = 5.4 Hz, 1H, H1), 2.13 (d, J = 7.8 Hz, 4H, H7a and H12), 1.52 (s, 3H, H8), 1.02 (s, 3H, H9); ^{13}C NMR (126 MHz, $CDCl_3$) δ 202.94 (C4), 170.22 (C11), 165.61 (C2), 119.49 (C3), 64.09 (C10), 58.18 (C5), 54.34 (C6), 45.40 (C1), 40.84 (C7), 26.52 (C8), 22.07 (C9), 20.65 (C12).

Data for 4-*cis*-hydroxymyrtenyl acetate:
^{1}H NMR (500 MHz, $CDCl_3$) δ 5.66 (d, J = 1.3 Hz, 1H, H3), 4.59 - 4.43 (m, 3H, *trans* H4 and H10), 2.51 (dt, J = 9.3, 5.8 Hz, 1H, H7b), 2.38 - 2.29 (m, 1H, H5), 2.18 - 2.03 (m, 4H, H1 and H12), 1.41 - 1.32 (m, 4H, H7a and H8), 1.07 (s, 3H, H9); ^{13}C NMR (126 MHz, $CDCl_3$) δ 170.77 (C11), 145.12 (C2), 122.21 (C3), 73.01 (C4), 65.82 (C10), 48.39 (C5), 44.12 (C1), 38.95 (C6), 35.78 (C7), 26.68 (C9), 22.74 (C8), 20.91 (C12).

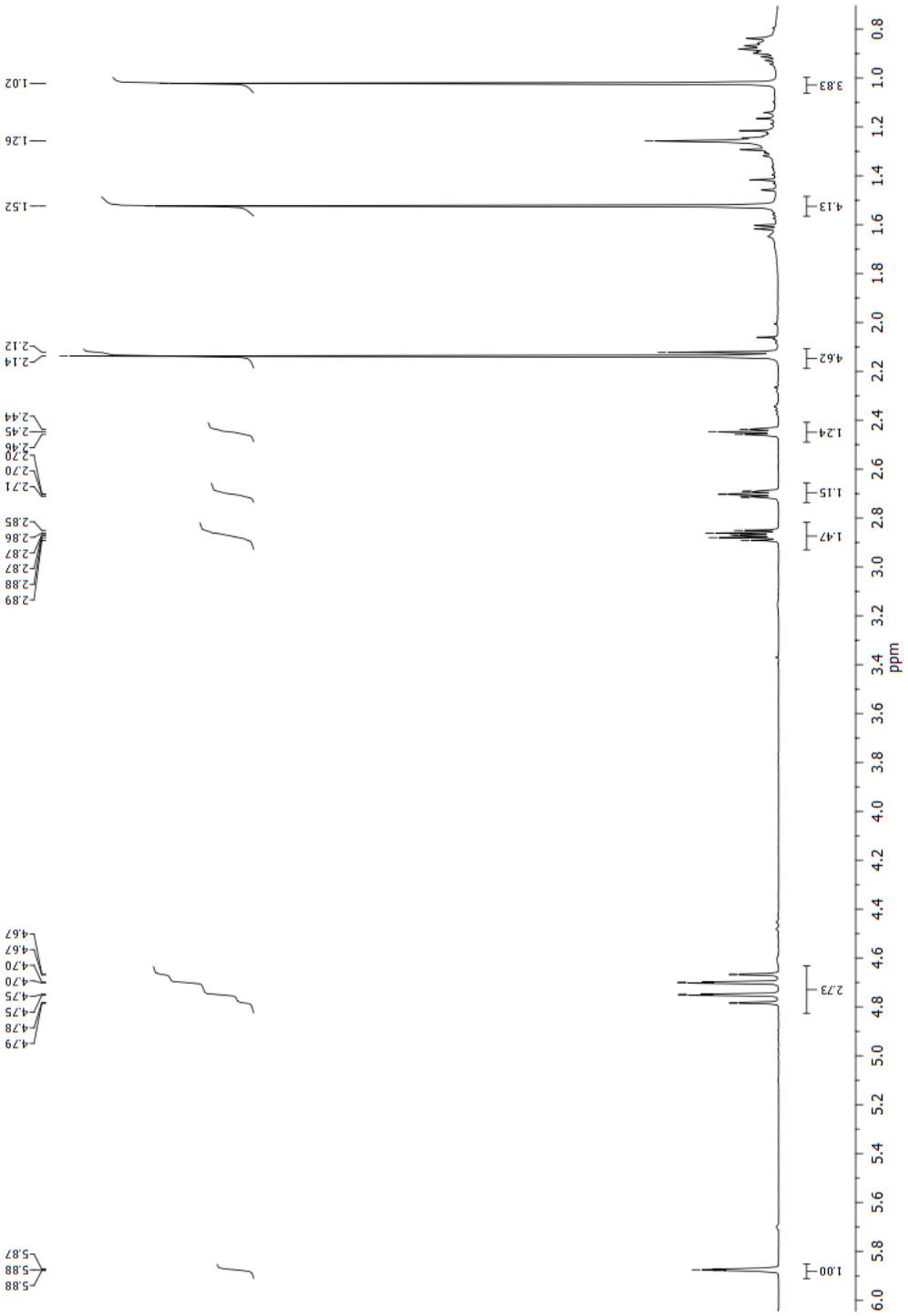

Figure F.89: ^{1}H NMR of 4-oxomyrtenyl acetate

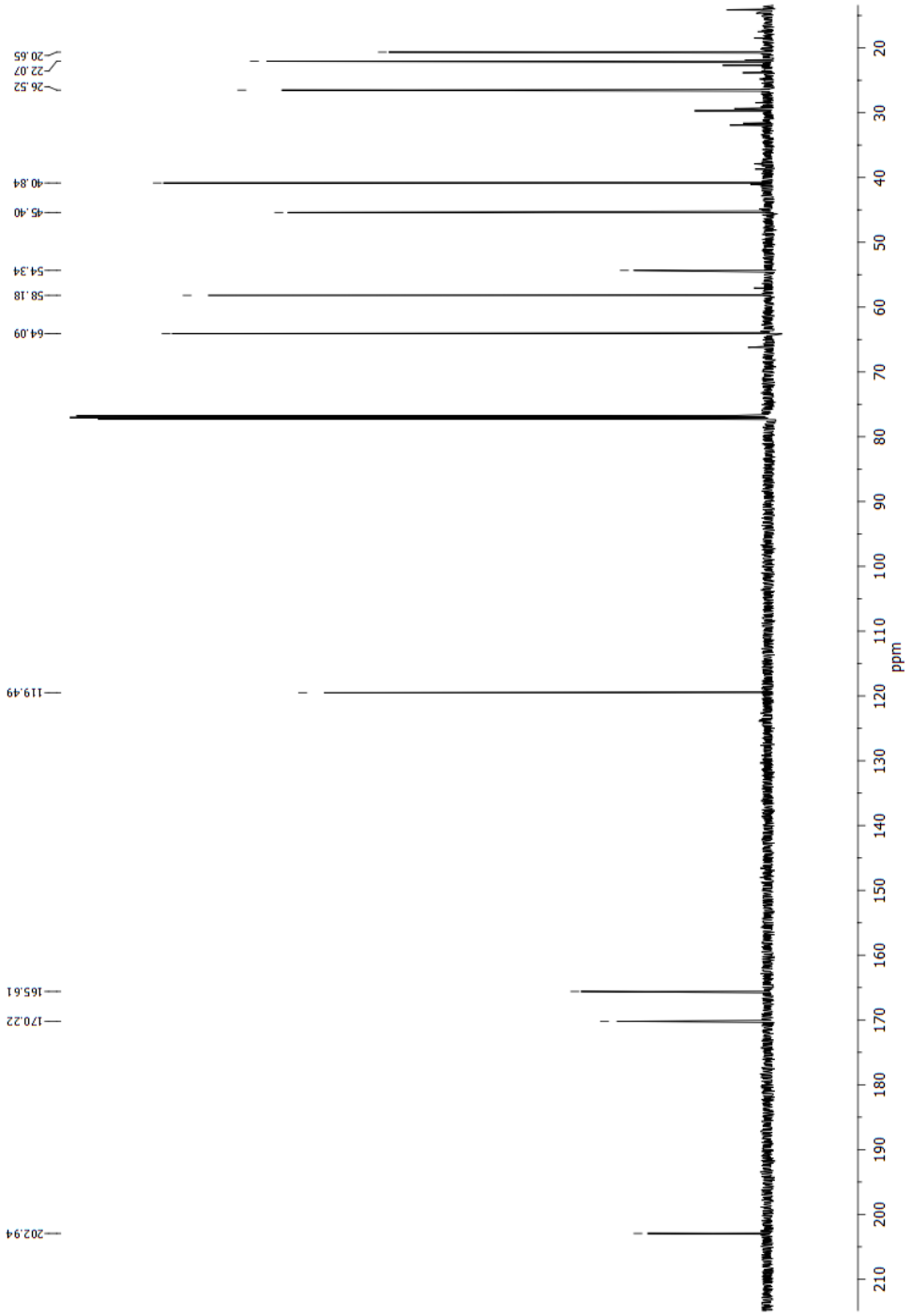

Figure F.90: ^{13}C NMR of 4-oxomyrtenyl acetate

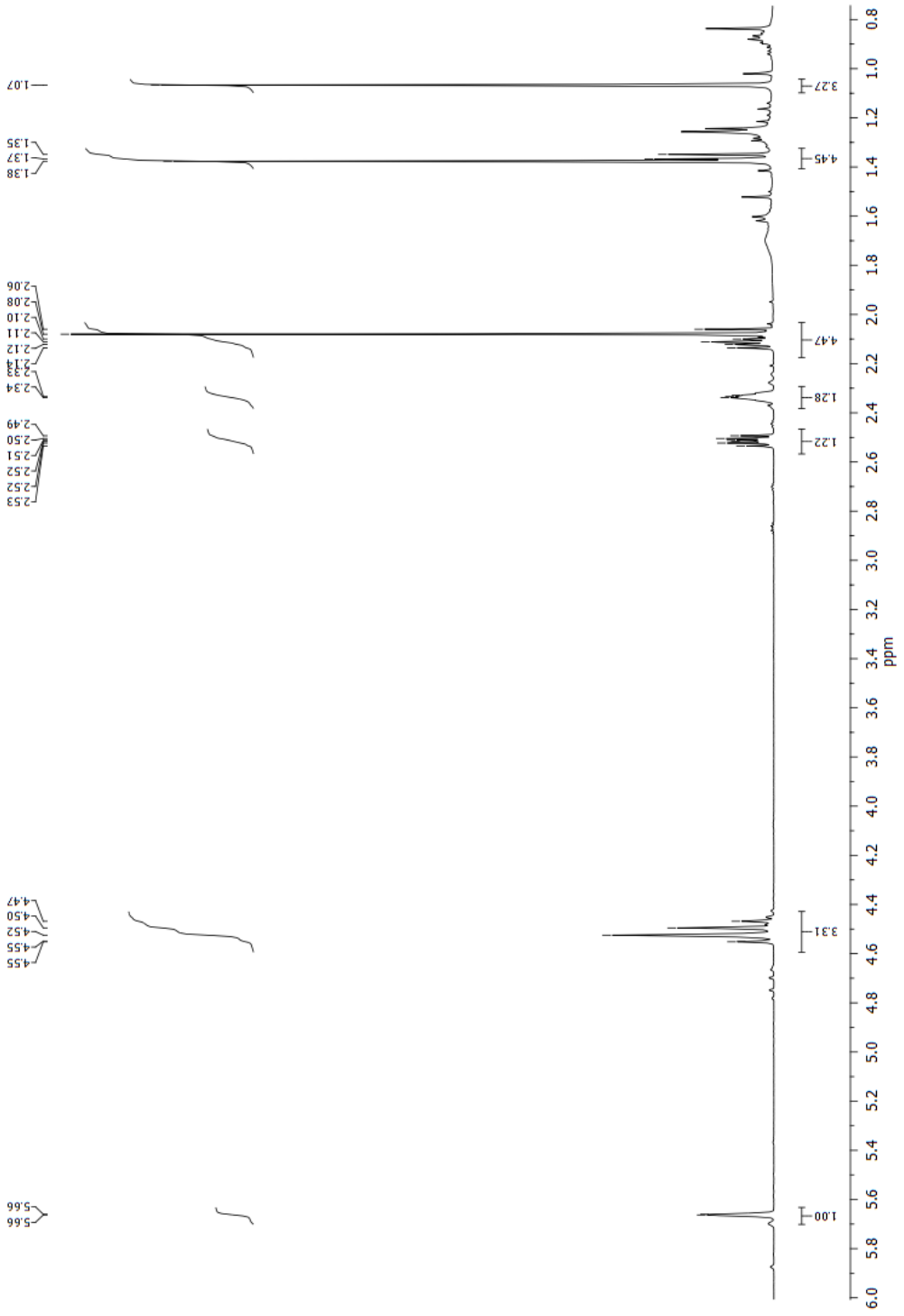

Figure F.91: ^{1}H NMR of 4-*cis*-hydroxymyrtenyl acetate

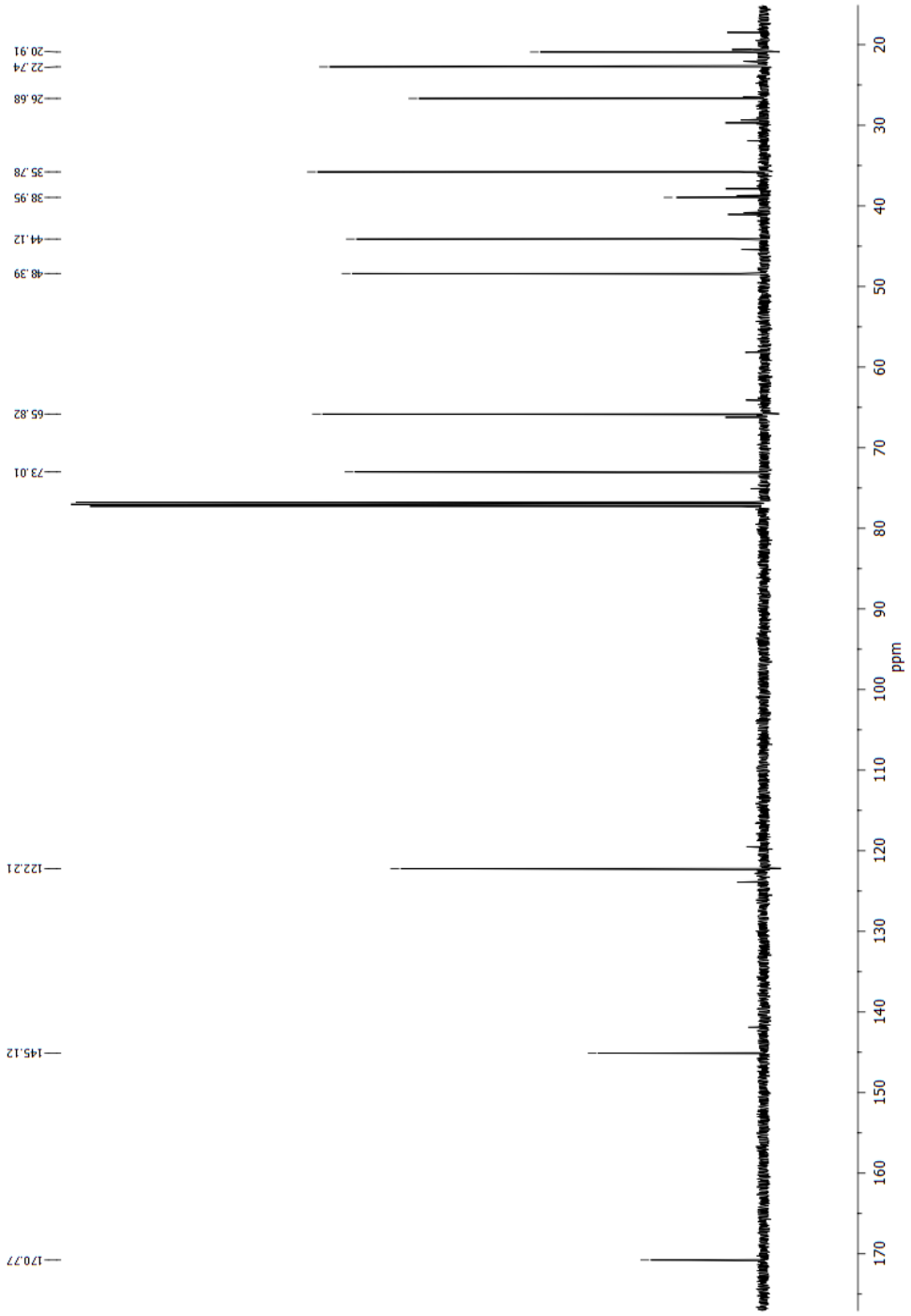

Figure F.92: ^{13}C NMR of 4-*cis*-hydroxymyrtenyl acetate

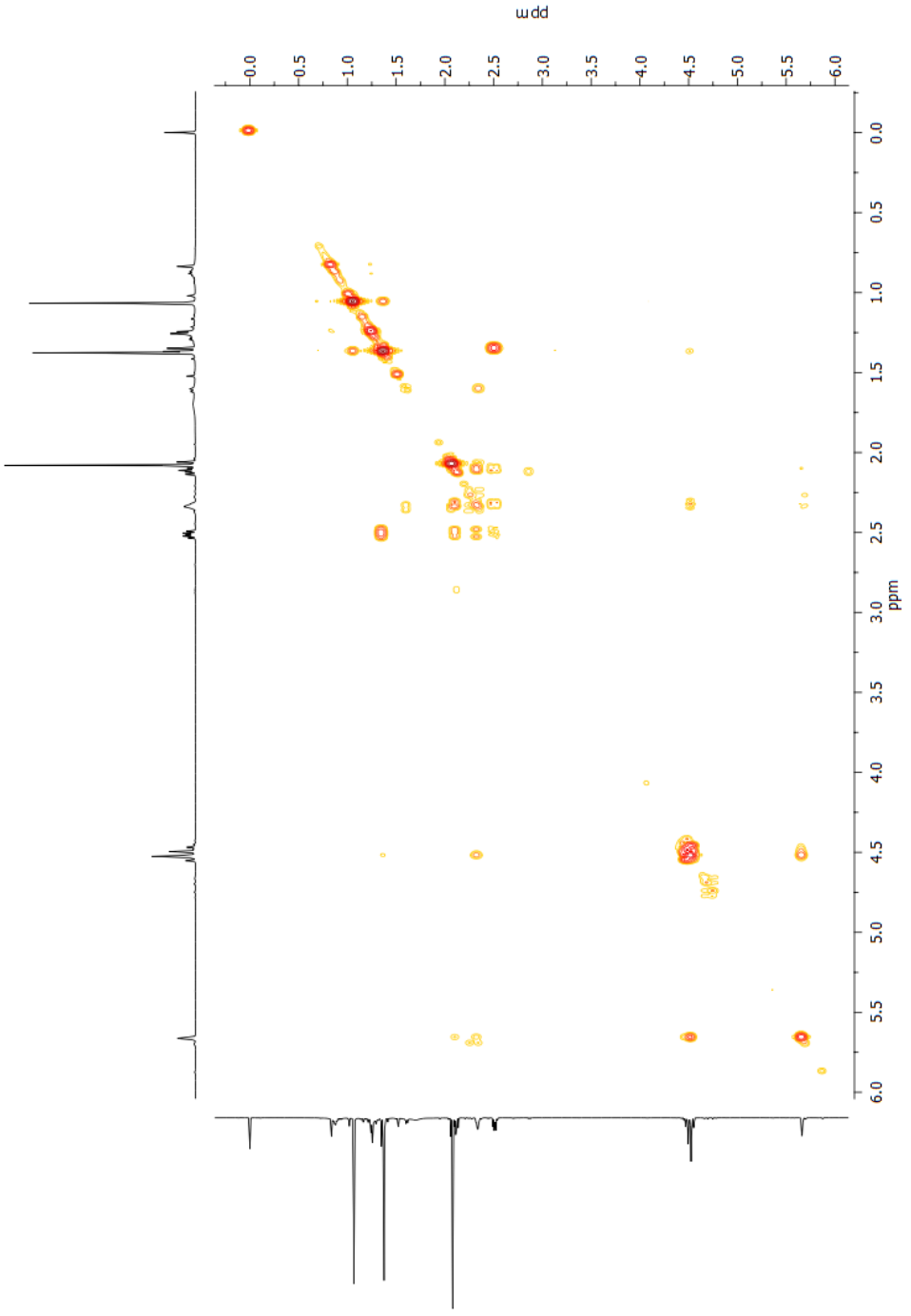

Figure F.93: COSY NMR of 4-*cis*-hydroxymyrtenyl acetate

F.21 (+)-Sclareolide

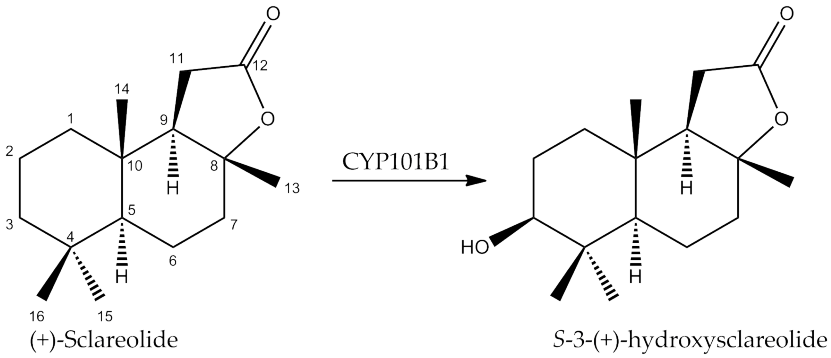

Figure F.94: (+)-Sclareolide

Data for (*S*)-3-(+)-hydroxysclareolide:
^{1}H NMR (600 MHz, $CDCl_3$) δ 3.26 (dd, J = 11.5, 4.8 Hz, 1H, H3), 2.42 (dd, J = 16.2, 14.8 Hz, 1H, H11), 2.24 (dd, J = 16.2, 6.5 Hz, 1H, H11), 2.09 (dt, J = 12.0, 3.3 Hz, 1H, H7), 1.95 - 1.87 (m, 2H, H6 and H9), 1.74 - 1.61 (m, 3H, H2 and H7), 1.49 - 1.42 (m, 2H, H1 and H6), 1.34 (s, 3H, H13), 1.19 (dd, J = 13.3, 9.3 Hz, 1H, H1), 1.04 - 1.00 (m, 4H, H5 and H16), 0.93 (s, 3H, H14), 0.81 (s, 3H, H15); ^{13}C NMR (151 MHz, $CDCl_3$) δ 176.52 (C12), 86.11 (C8), 78.62 (C3), 58.88 (C9), 55.29 (C5), 38.82 (C4), 38.42 (C7), 37.66 (C1), 35.76 (C10), 28.70 (C11), 27.87 (C16), 26.82 (C2), 21.50 (C13), 20.27 (C6), 15.14(C14), 15.04 (C15).

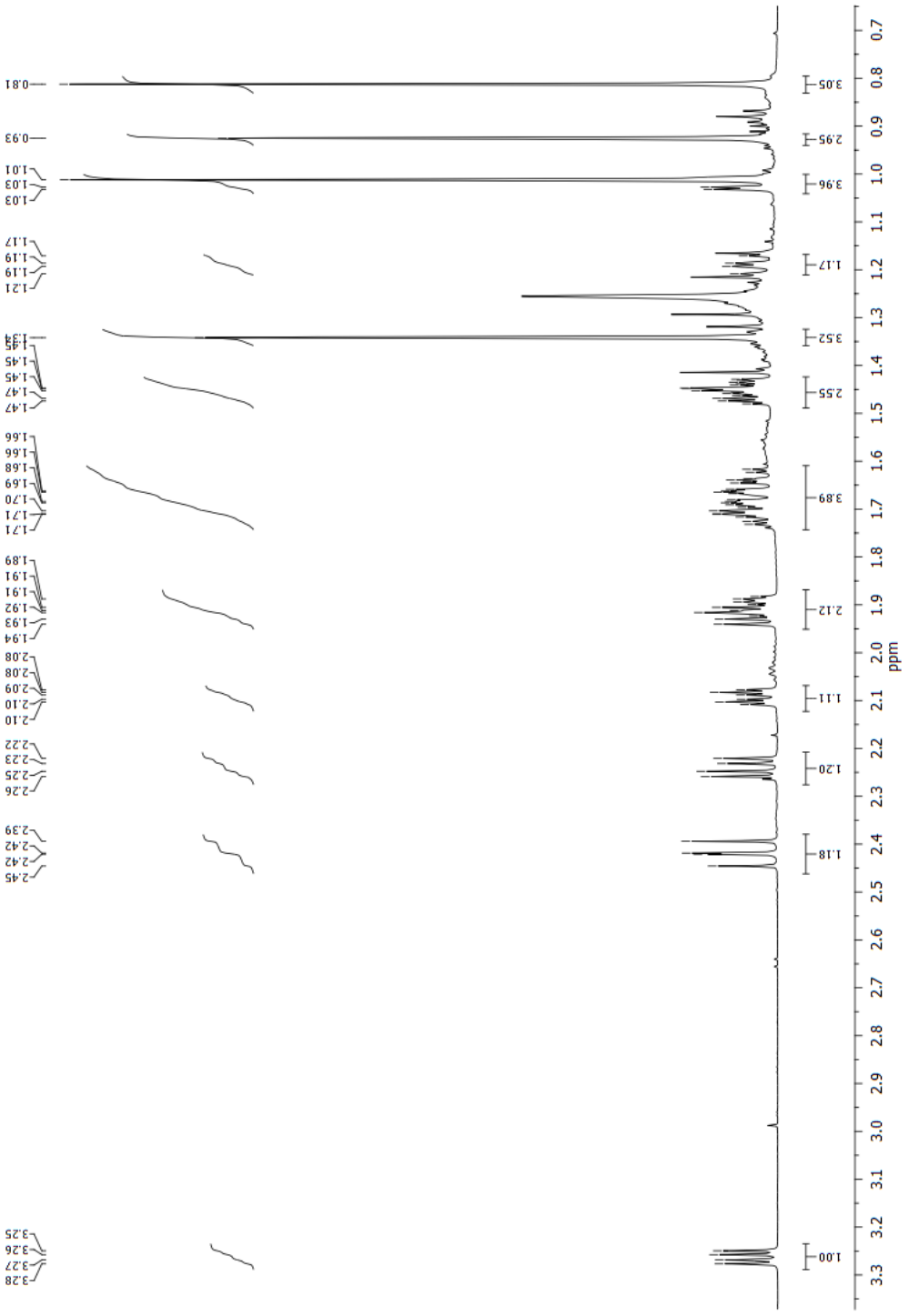

Figure F.95: ^{1}H NMR of (S)-3-(+)-hydroxysclareolide

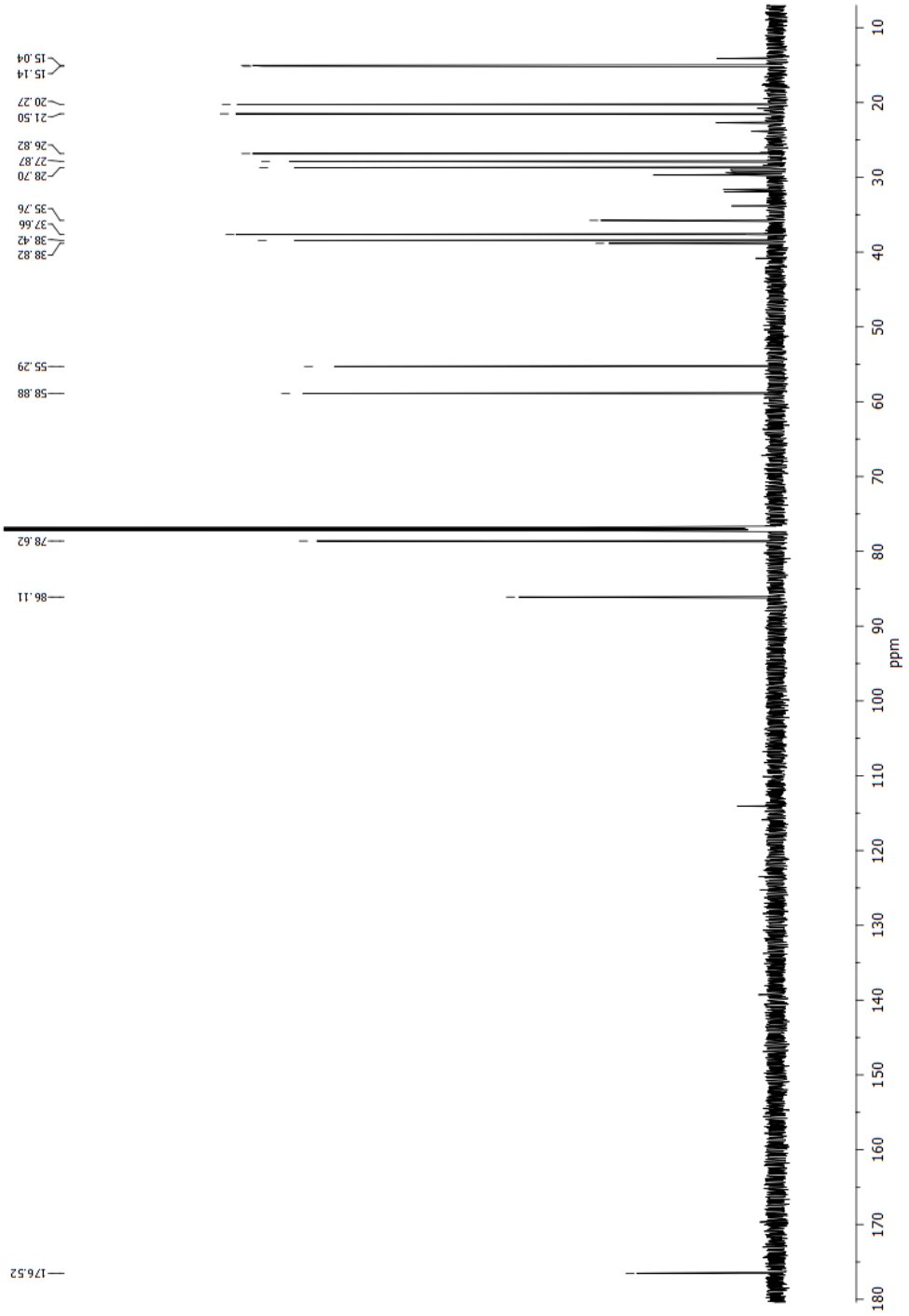

Figure F.96: ^{13}C NMR of (S)-3-(+)-hydroxysclareolide

F.22 2,7-Dimethyl naphthalene

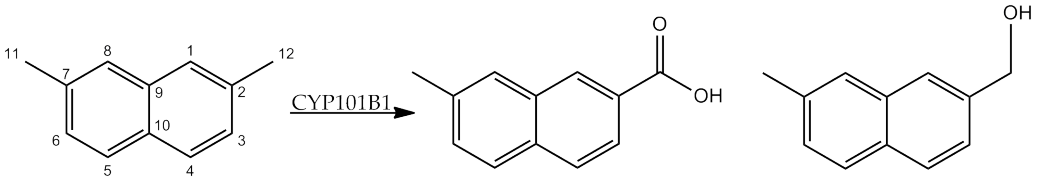

Figure F.97: 2,7-Dimethyl naphthalene products

Data for 2-(7-mehtylnaphthyl)methanol:
^{1}H NMR (500 MHz, d_6-acetone) δ 7.79 (s, 1H, H1), 7.77 (d, J = 2.6 Hz, 1H, H3), 7.75 (d, J = 2.7 Hz, 1H, H5), 7.63 (s, 1H, H4), 7.46 (d, J = 8.4 Hz, 1H, H8), 7.33 (d, J = 8.4 Hz, 1H, H6), 4.77 (s, 2H, H12), 2.48 (s, 3H, H11).

Data for 2-carboxy-7-methylnaphthalene:
^{1}H NMR (500 MHz, d_6-acetone) δ 8.64 (s, 1H, H1), 8.07 (dd, J = 8.6, 1.4 Hz, 1H, H3), 8.02 (d, J = 8.4 Hz, 1H, H5), 7.93 (d, J = 8.6 Hz, 1H, H4), 7.80 (s, 1H, H8), 7.50 (d, J = 7.7 Hz, 1H, H6), 2.57 (s, 3H, H11); ^{13}C NMR (126 MHz, d_6-acetone) δ 168.38 (C12), 139.78 (C9), 137.26 (C10), 132.31 (C7), 132.06 (C1), 130.52 (C5), 130.36 (C6), 128.85 (C4), 128.51 (C2), 128.09 (C8), 126.83 (C3), 22.35 (C11).

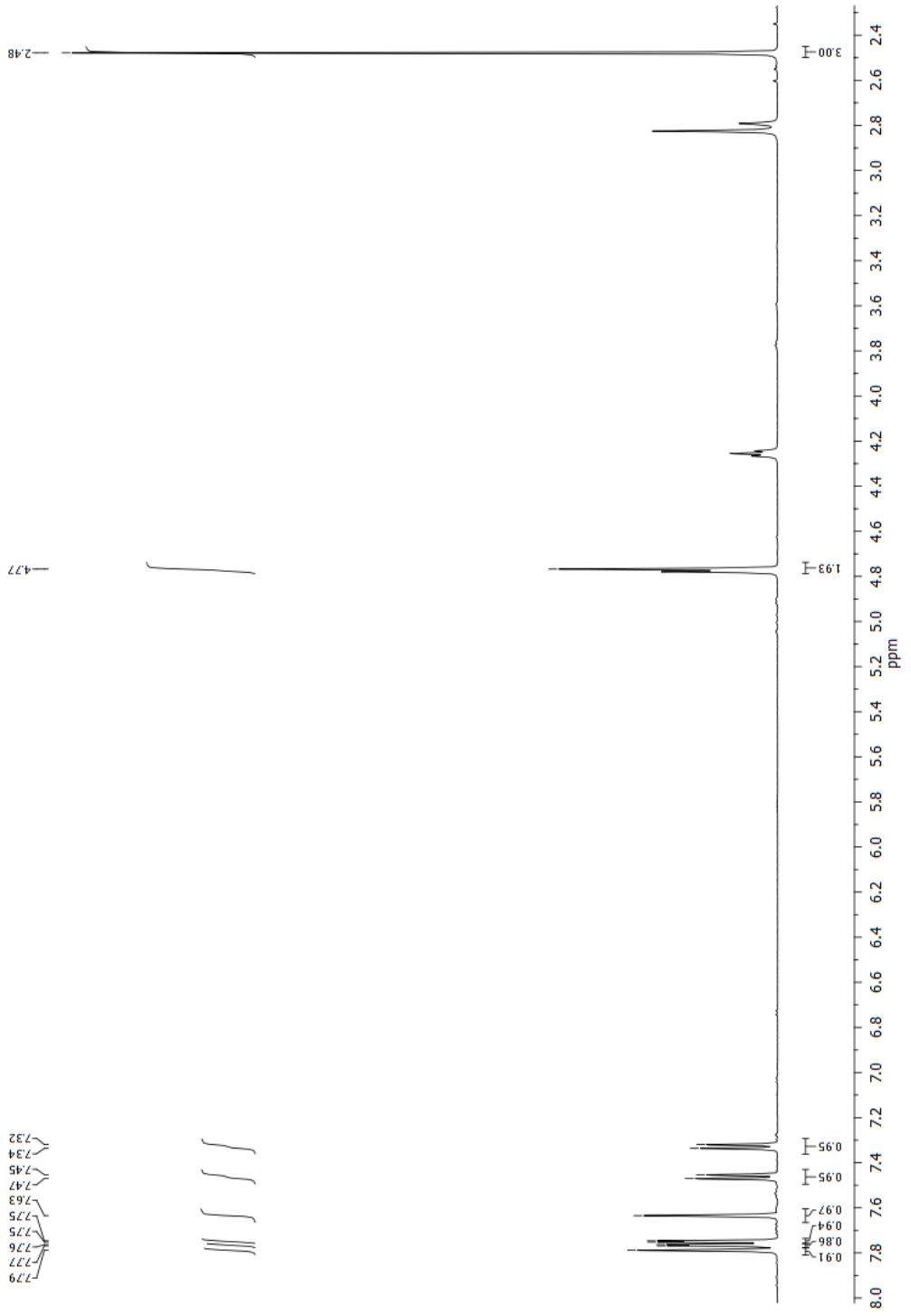

Figure F.98: ^{1}H NMR of 2-(7-mehtylnaphthyl)methanol

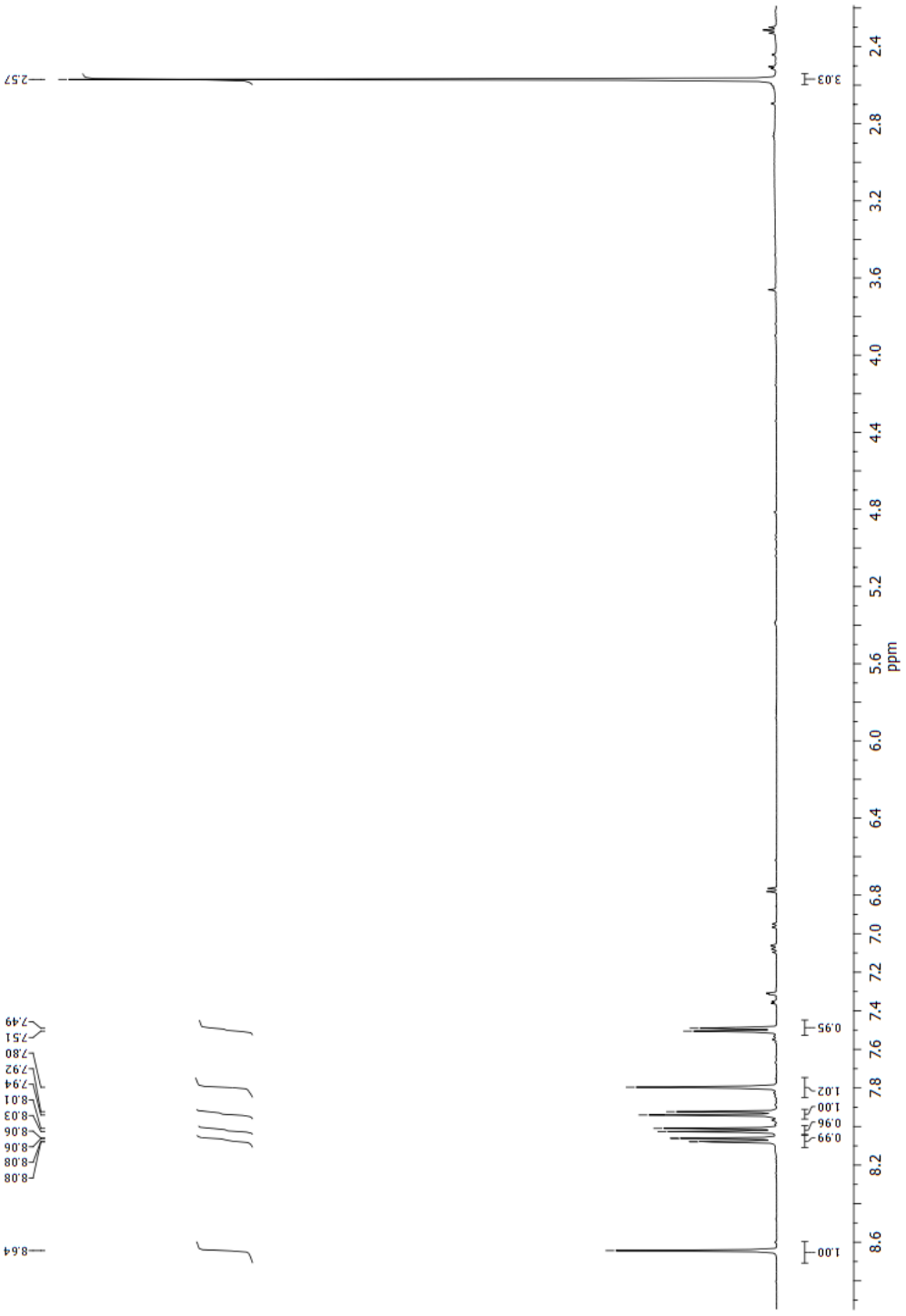

Figure F.99: ^{1}H NMR of 2-carboxy-7-methylnaphthalene

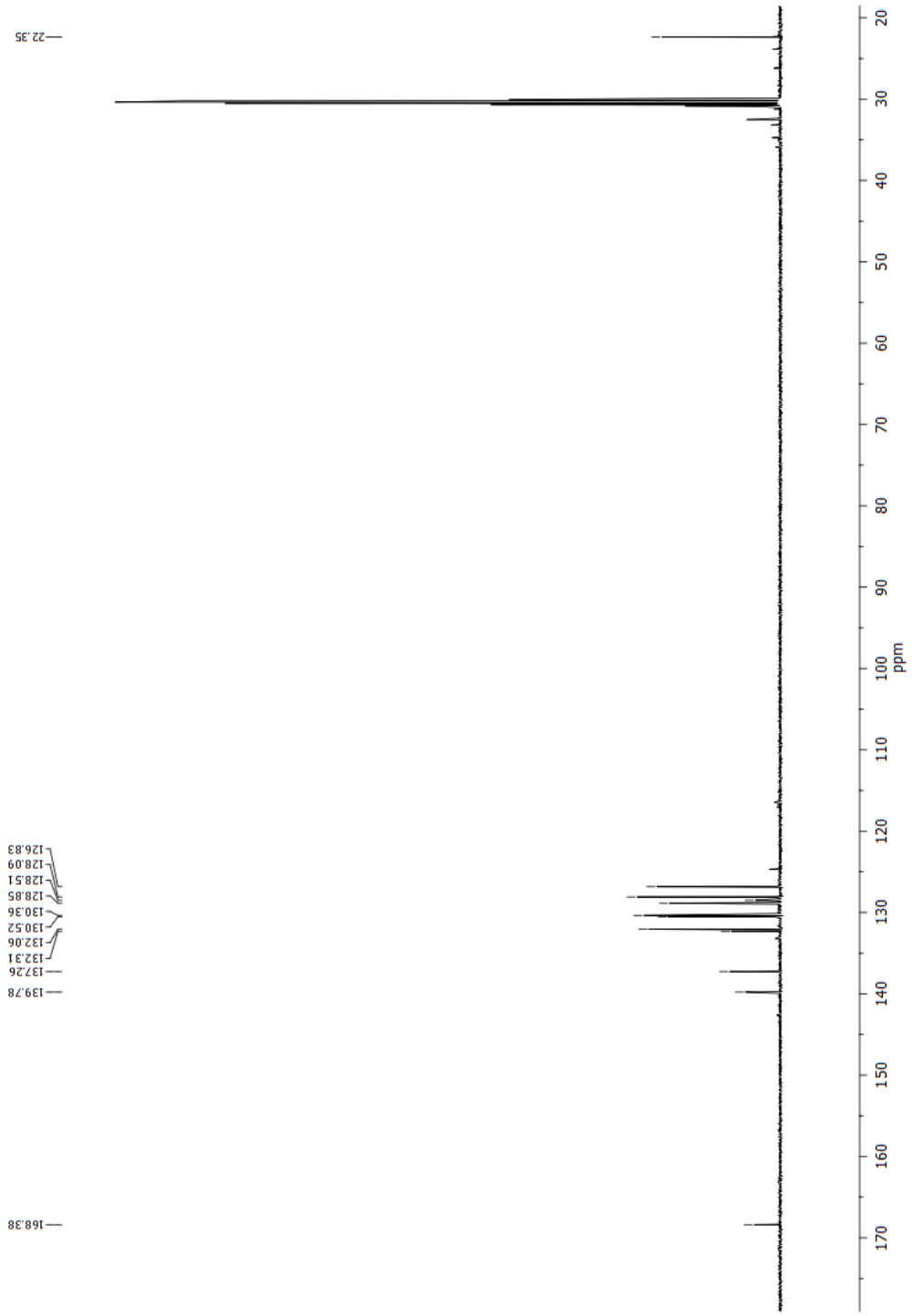

Figure F.100: ^{13}C NMR of 2-carboxy-7-methylnaphthalene

F.23 3-Methyl biphenyl

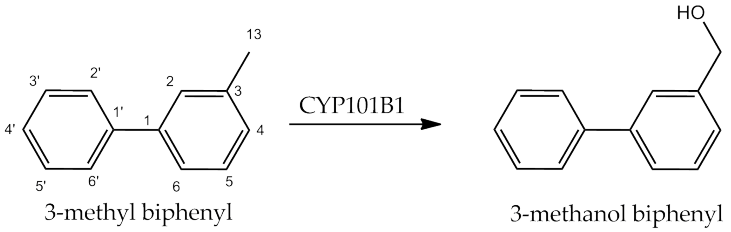

Figure F.101: 3-methyl biphenyl product

Data for 3-methanol biphenyl:
^{1}H NMR (500 MHz, $CDCl_3$) δ 7.64 - 7.57 (m, 3H, H2, H2$'$ and H6$'$), 7.53 (d, J = 7.7 Hz, 1H, H6), 7.64 7.57 (m, 3H, H5, H3$'$ and H5$'$), 7.39 - 7.31 (m, 2H, H4 and H4$'$), 4.77 (s, 2H, H13).

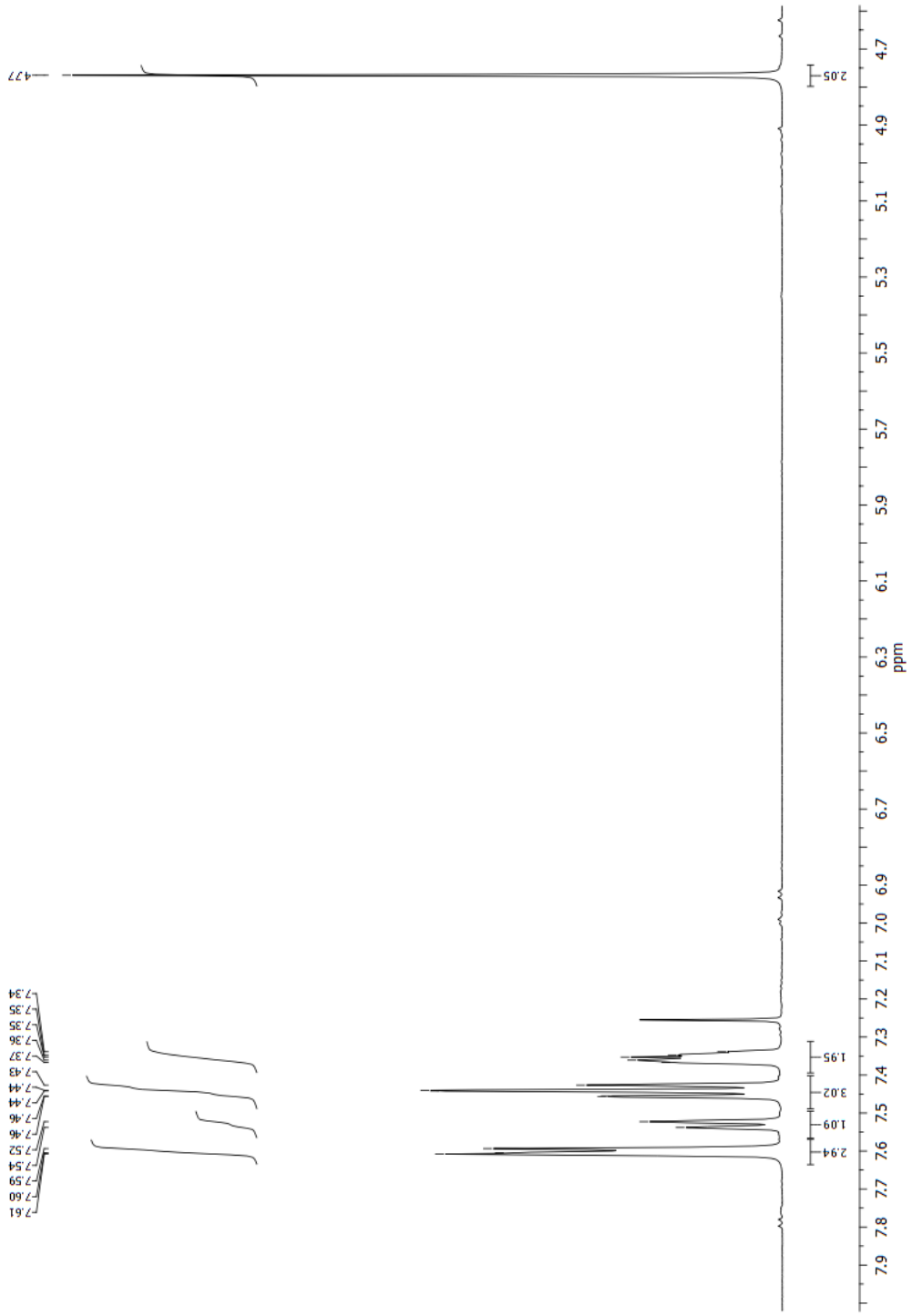

Figure F.102: ^{1}H NMR of 3-methanol biphenyl

F.24 4-Methyl biphenyl

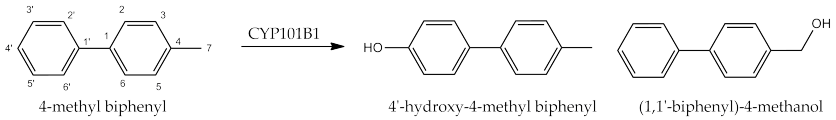

Figure F.103: 4-methyl biphenyl product

Data for 4-hydroxy-4-methylbiphenyl:
^{1}H NMR (500 MHz, $CDCl_3$) δ 7.45 (d, J = 8.3 Hz, 2H, H2' and H6'), 7.43 (d, J = 8.3 Hz, 2H, H2 and H6), 7.22 (d, J = 8.0 Hz, 2H, H3 and H5), 6.88 (d, J = 8.5 Hz, 2H, H3' and H5'), 2.38 (s, 3H, H7).

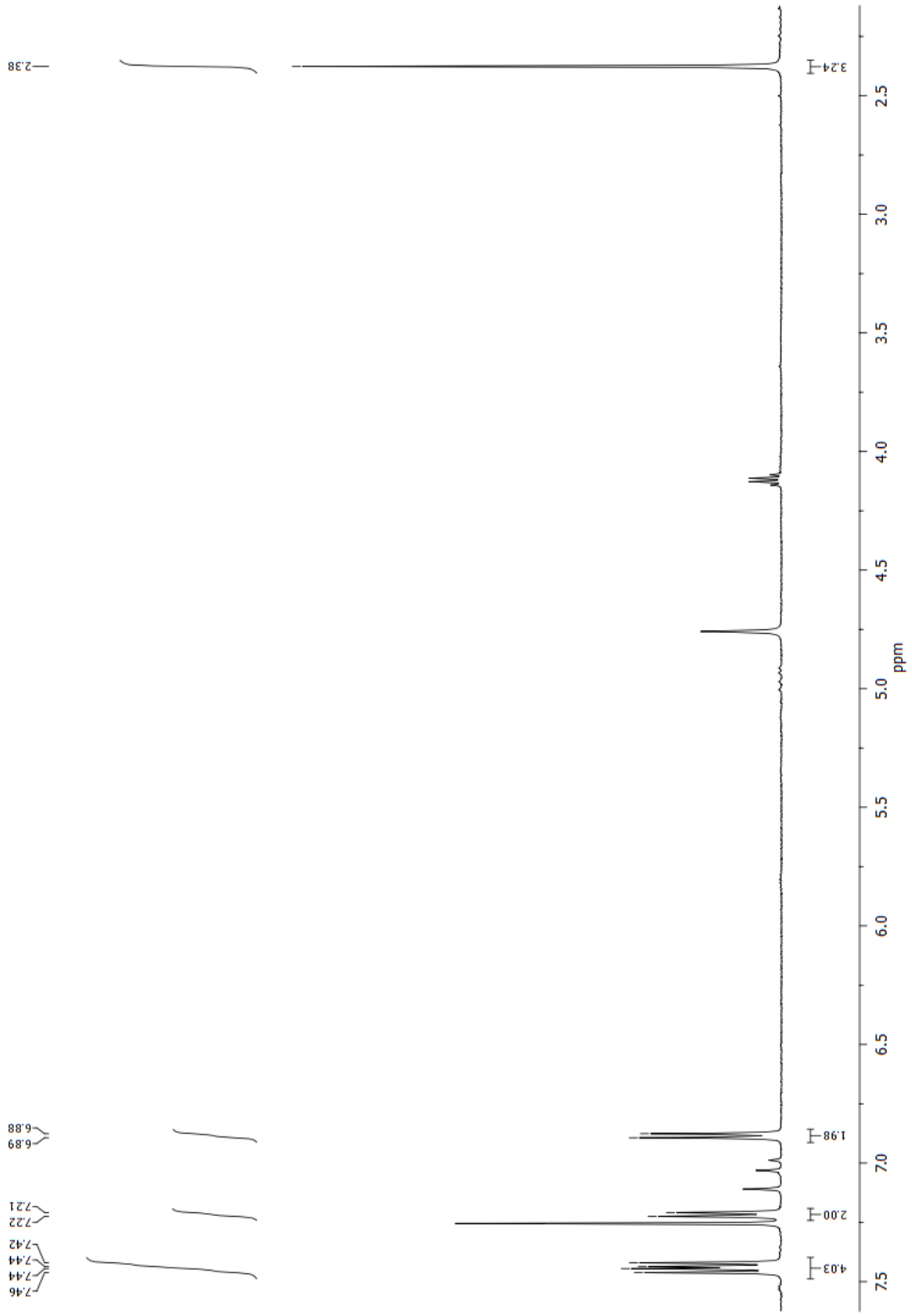

Figure F.104: ^{1}H NMR of 4'-hydroxy-4-methylbiphenyl

F.25 (1,1'-biphenyl)-4-methanol

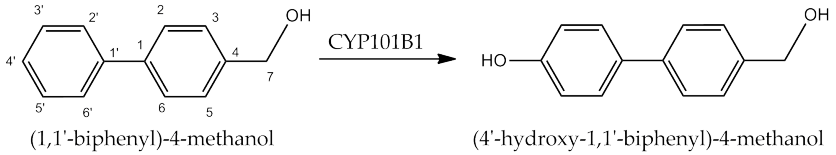

Figure F.105: (1,1'-biphenyl)-4-methanol product

Data for (4'-hydroxy-1,1'-biphenyl)-4-methanol:
^{1}H NMR (500 MHz, d_6-acetone) δ 7.54 (d, J = 8.2 Hz, 2H, H2' and H6'), 7.50 (d, J = 8.6 Hz, 1H, H2 and H6), 7.40 (d, J = 8.1 Hz, 2H, H3 and H5), 6.92 (d, J = 8.6 Hz, 2H, H3' and H5'), 4.65 (s, 2H, H7).

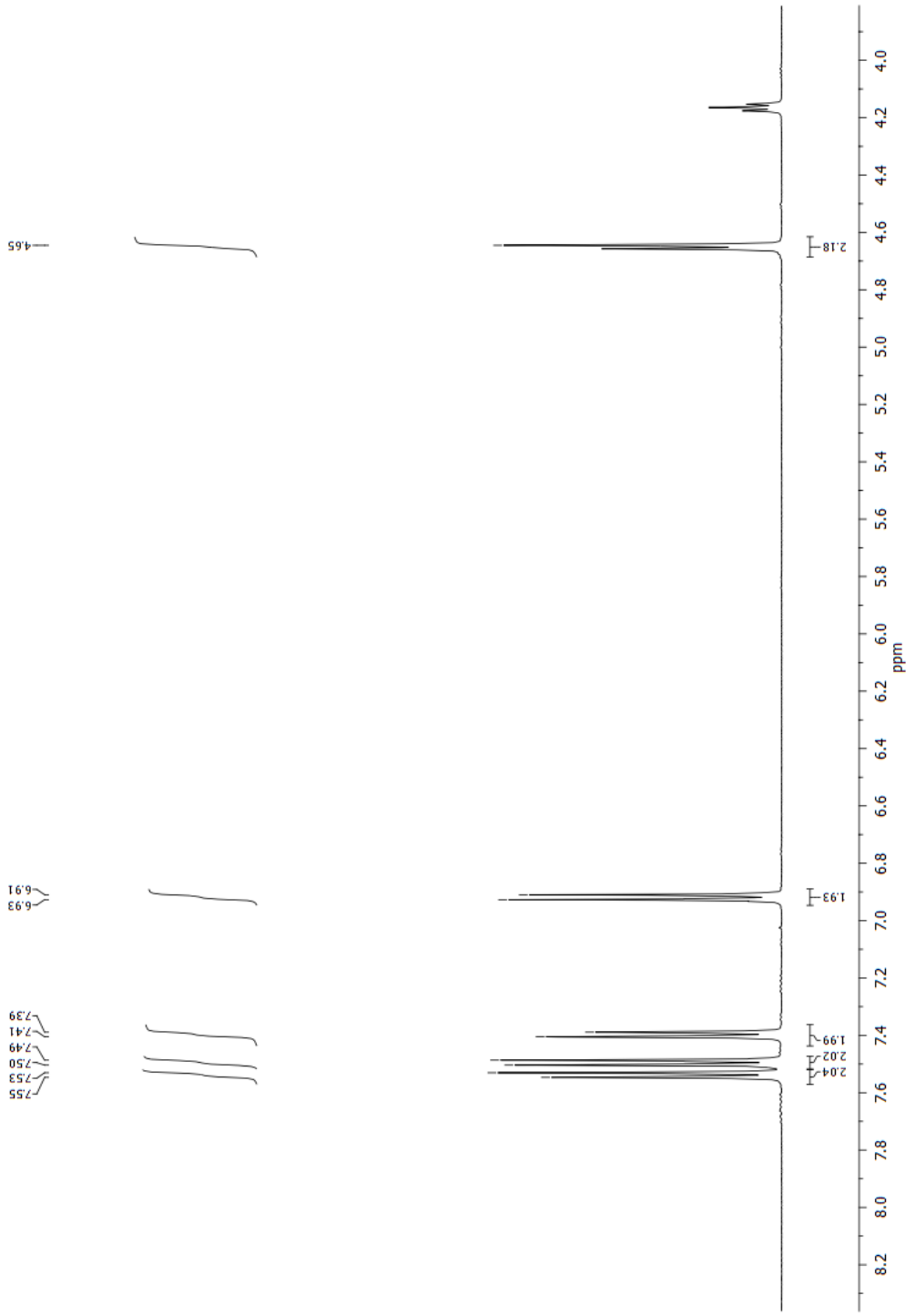

Figure F.106: ^{1}H NMR of (4'-hydroxy-1,1'-biphenyl)-4-methanol

F.26 Diclofenac

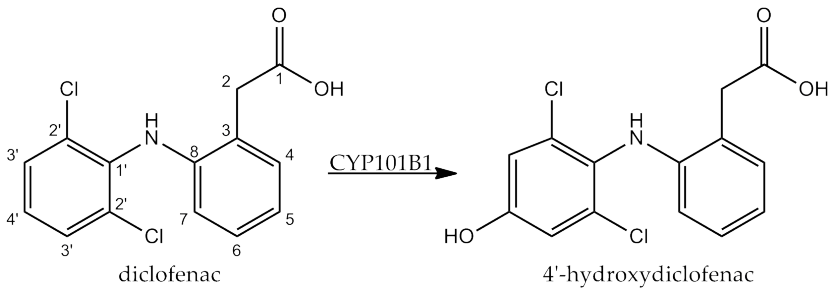

Figure F.107: diclofenac product

Data for 4-hydroxydiclofenac:
^{1}H NMR (600 MHz, DMSO) δ 7.10 (d, J = 7.4 Hz, 1H, H4), 7.00 - 6.96 (m, 1H, H6), 6.93 (s, 2H, 2 x H3'), 6.71 (t, J = 7.4 Hz, 1H, H5), 6.10 (d, J = 8.0 Hz, 1H, H7), 3.6 (s, 2H, H2); ^{13}C NMR (151 MHz, DMSO) δ 176.84 (C1), 155.67 (C4'), 144.68 (C8), 133.08 (C1'), 131.04 (C4), 128.63 (C2'), 127.66 (C6), 123.59 (C3), 119.31 (C5), 116.26 (C3'), 113.97 (C7), 35.98 (C2).

Appendix G

Publications Arising from this Thesis

Chapter 3
Hall, E. A. & Bell, S. G., The efficient and selective biocatalytic oxidation of norisoprenoid and aromatic substrates by CYP101B1 from Novosphingobium aromaticivorans DSM12444, RSC Advances **2015**, *5*, 5762-5773.